Long-Term Atmospheric Measurement and Interpretation of Radiatively Active Trace Gases

September 2019 – August 2020

Detailed Report

Alistair Manning[1], Alison Redington[1], Simon O'Doherty[2], Daniel Say[2], Dickon Young[3], Tim Arnold[4,5], Chris Rennick[4], Matt Rigby[2], Adam Wisher[2], and Peter Simmonds[6]

[1] *Met Office, Fitzroy Road, Exeter, EX1 3PB, United Kingdom*
[2] *Atmospheric Chemistry Research Group, University of Bristol, Cantock's Close, Bristol, BS8 1TS, United Kingdom*
[3] *Terra Modus Consultants Ltd, Bwthyn y Ffynnon, Cwmfelin Boeth, Whitland, SA34 0RS, United Kingdom*
[4] *National Physical Laboratory, Hampton Road, Teddington, TW11 0LW, United Kingdom*
[5] *School of GeoSciences, University of Edinburgh, Edinburgh, EH9 3FE, United Kingdom*
[6] *International Science Consultants, 39 Avon Castle Drive, Ringwood, BH24 2BB, United Kingdom*

October 20, 2020

Photo of Winnats Pass courtesy of @grantrichie/Unsplash

Contents

1 Introduction

Monitoring the atmospheric concentrations of gases is important for policy makers in assessing the impact of national and international policies related to the atmospheric environment. The effects of control measures on the principle greenhouse gases: carbon dioxide (CO_2), methane (CH_4), nitrous oxide (N_2O), hydrofluorocarbons (HFC), perfluorocarbons (PFC), nitrogen trifluoride (NF_3) and sulphur hexafluoride (SF_6), are now observable. Likewise, measures introduced under the Montreal Protocol to protect the stratospheric ozone layer are also being observed in the atmosphere.

This project has two principle aims:

- Estimate the background atmospheric concentrations of the principle greenhouse and ozone-depleting gases from the UK and wider network of observations.
- Estimate the UK emissions of the principle greenhouse gases using the UK network of observations and compare these to the reported inventory.

Since 1987, high frequency, real time measurements of the principal halocarbons and radiatively active trace gases have been made as part of the Global Atmospheric Gases Experiment (GAGE) and Advanced Global Atmospheric Gases Experiment (AGAGE) at Mace Head, County Galway, Ireland. For much of the time, the Mace Head measurement station (MHD), which is situated on the Atlantic coast, monitors clean westerly air that has travelled across the North Atlantic Ocean. However, when the winds are easterly, MHD receives substantial regional scale pollution in air that has travelled from the populated and industrial regions of Europe. The site is therefore uniquely situated to record trace gas concentrations associated with both the Northern Hemisphere background levels and with the more polluted air arising from European emissions.

Building on the success of using the MHD observations in addressing the two principle aims of the project, the UK has developed a network of observation stations called the UK Deriving Emissions related to Climate Change (UK DECC) network. Along with MHD, it consists of four tall tower stations: Ridge Hill (RGL), Herefordshire; Tacolneston (TAC), Norfolk; Bilsdale (BSD), North Yorkshire (originally Angus (TTA), Angus, Scotland); and Heathfield (HFD), West Sussex. RGL became operational in February 2012 and TAC in July 2012. TTA began operating for the network in April 2012 but was decommissioned and replaced with BSD in September 2015 (BSD began operation in January 2014 under the NERC GAUGE programme). HFD began operation in November 2013 under the NERC GAUGE programme but became fully part of the network in September 2018. The expanded network makes it possible to resolve emissions on a higher resolution, both spatially and temporally, across the UK.

The UK DECC network measures, to very high precision, all of the principle greenhouse gases in the inventory as well as many ozone-depleting gases. The Inversion Technique for Emission

Modelling (InTEM) has been developed to use these observations to estimate both mid-latitude Northern Hemisphere concentration trends and UK emissions of each gas. The atmospheric measurements and resulting emission estimates of greenhouse gases provide an important independent cross-check for the national GreenHouse Gas Inventory (GHGI) of emissions submitted annually to the United Nations Framework Convention on Climate Change (UNFCCC). The GHGI are estimated through in-country submissions of Activity Data and Emission Factors that are, in some cases, very uncertain. The comparisons between the GHGI and InTEM estimates enable BEIS to be more informed in their inventory improvement programme and is also considered good practice by the Intergovernmental Panel on Climate Change (IPCC).

The UK is one of only three countries worldwide (Switzerland and Australia are the others) that currently routinely verify their reported inventory emissions as part of their annual UNFCCC submission of emissions. The UK is the only country to do so for all of the principle GHG gases and has done so for longest, since 2003.

The report first describes the instrumentation performance over the last year and then shows the global trends in each of the gases. InTEM is briefly described before an in-depth analysis of the InTEM results compared to the GHGI for each gas in turn; CH_4, N_2O, CO_2, HFCs, PFCs, SF_6 and finally NF_3. The report concludes with a list of the recent publications produced by the group and acknowledgements. The nomenclature at the end describes the acronyms used in the report. The key findings of this report, especially related to UK emissions, are summarised in the companion 'Executive Summary' report.

2 Instrument Performance

A brief summary of site operations is given below.

2.1 Mace Head

General: There have been no major instrumental issues at Mace Head over the past 12-months. Work on the installation of a new chilled water A/C system began on 14^{th} October 2019. Two systems were installed, one each for the AGAGE and CO_2 labs, to replace the two existing split system units both of which are known to leak (HFC-32 and HFC-125). More details of this system are provided in the GCMD section.

Medusa GCMS: The Medusa operated extremely well over the past 12 months with only one significant period of data loss. After a routine valve rotor repair in the Medusa sample module (August 2020), it was discovered that helium was leaking from the main chromatographic GasPro column (in the middle of the column). This is a very unusual fault as it indicated a very small fracture. A new column was ordered and installed on 20^{th} Sept 2019. This resulted in 40 days of data loss. The only stoppages to occur during November 2019 to Feb 2020 were routine maintenance checks such as filament and pump oil changes. On the 4^{th} March it was noted that the Medusa baseplate temperatures were higher than usual and a little unstable. To try an alleviate this issue the Cryotiger was conditioned (heated and cooled to clear any potential oil blockages). The issue was minimised but not fully resolved at this time. A small hole was discovered in the KNF air sampling pump diaphragm on 17th June. A new air sample module was sent from Bristol and was installed on the 25^{th} of June along with a Parker filter to ensure the trapping of oil particles between the Cryotiger and the Medusa cold head. These modifications have ensured that atmospheric sampling has continued and that the Medusa trapping temperatures achieved are now stable.

GCMD: The GCMD operated very well with only a few minor instrumental problems over the past 12 months. The new A/C systems are manufactured by an Italian company, AERMEC and were installed by a local contractor, Porter Cooling Services. The units are identical, each having a cooling capacity of 8.2 kW, slightly more than the existing units. They run off 3-phase electricity which makes them reasonably power efficient (input power is 2.1 kW). The chillers utilise R-410a as refrigerant and a glycol/water mixture to extract heat via the internally mounted fan coil units. In order to minimise the risk of contamination from refrigerant leaks, we have had the chillers mounted as far from the building as is practicable, approximately 5 m on the downwind side (see Figure 1a). The fan coil units are to be mounted in the same locations as the existing internal units. Figure 1b shows the location of the CO_2 fan coil. This entails some lengthy pipework to transport the coolant between the chillers and the fan coils (the black insulated pipework in Figure

1a). This will presumably increase the response time of the system to changing conditions however, as our heat load is fairly constant, we envisage this will not be an issue. The initial works carried out consisted of installation of both external chillers, installation of the CO_2 lab fan coil unit, all electrical and pipework leaving the installation of the AGAGE lab fan coil unit until 2 days before final commissioning to minimise downtime. Following lengthy delays the final commissioning was carried out by AERMEC on 4^{th} December 2019 resulting in a 4-day loss of data.

(a) Outdoor A/C units **(b)** Indoor A/C unit

Figure 1: AERMEC A/C units at Mace Head

The A/C system shut down on 14^{th} Feb 2020 for no obvious reason, it was restarted the same day. The A/C unit failed again on 13^{th} March, whilst Gerry Spain was on holiday, during this period the equipment needed to be shutdown to minimise heat load into the lab. The AERMEC engineer got the A/C started on 23^{rd} March (again with no clear reason for the failure)? The A/C has worked well until debris from a storm fractured the refrigerant pipework on 25^{th} May. The engineer welded a new section of pipework and recharged the refrigerant system on 28^{th} May. The increased heat load caused by the A/C failure on the 13^{th} March caused a few instrumental issues with the MD. Firstly it was noted via a remote connection to the site that the chromatograms for Channel 1 and 2 has disappeared. After running extensive tests it became clear that the Valve 3 actuator was not driving the Valve 3 rotor to load and inject the sample. A spare actuator was fitted and tested and sampling resumed after 8-days of lost data.

Finally, we have an ongoing issue with the CH_4 channel which started in December 2019. The CH_4 data became noisy after the new A/C unit was fitted. The data quality improved after the N_2 carrier gas pressure was optimised and the column heated to bakeout any contaminants (December 19). However, the precision became slowly worse again. In January 2020, the FID tower was purged to remove any possible particles, the column was baked out again and an imbalance in the H_2/air gases that are used to combust the CH_4 were optimised and the precision of the CH_4 data improved for a period of time. It was apparent that the data precision was getting worse again. In March 2020 a series of tests to disable the backflush valve were carried out without any conclusive result. It was apparent that the height data were affected but the area data were not, the CH_4 channel

is now quantified using area data (since June 2020). A full solution to the problem has yet to be found.

2.2 Tacolneston

General: There have been no major issues at Tacolneston over the reporting period. Starting on the 18^{th} November 2019, all instruments were moved from the University of Bristol 'mobile lab' to a new permanent room in the main Arqiva building. A new air-conditioning unit was installed to provide stable laboratory temperatures. 8 days of data were lost on all instruments during this period. Sampling from the new lab began on the 26^{th} November. In January 2020, an ANSTO radon detector was installed and began sampling from a temporary inlet 3 meters above ground level (magl). On the 3^{rd} July, the 100 m line pump failed. Starting on the 4^{th} July, the 185 m sample line suffered a blockage at the inlet. A rigger was able to remove the blockage by trimming the end of the sample line. Closer examination showed that the blockage had occurred due to corrosion of the aluminium layer of the Synflex tubing. On the 6^{th} July, riggers installed the radon sample line to 175 magl and meteorological sensors (wind speed and direction, relative humidity and temperature). Work to relay meteorological data to a central server, located at the University of Bristol, is ongoing.

LGR: The LGR has performed well over the reporting period. On the 12^{th} November 2019, the 2-micron inlet filter was replaced. 8 days of data were lost, starting on the 18^{th} of November, due to the relocation of the laboratory. On the 3^{rd} November, a new target (UoB-62) was installed, replacing the previous target cylinder, UoB-14. On the 17^{th} December, a small leak was discovered on the standard sample line downstream of the Earth Networks box, potentially explaining the long stabilization time observed during previous standard runs. The leak was eliminated upon detection. The instrument software crashed on the 20^{th} January 2020, requiring an instrument reboot. The 100 m line pump failed on the 3^{rd} July, resulting in the loss of 6 days of data. On the 4^{th} July, 3 days of data were lost due to a blockage at the inlet of the 185 m line. On the 18^{th} August, the instrument was rebooted after an apparent loss of precision. A new non-linearity correction was calculated on the 9^{th} September, resulting in adjustments to the standard concentration of 0.026 ppb and 0.016 ppb for N_2O and CO, respectively.

CRDS (G2301): The CRDS has performed fairly well over the reporting period. Starting on the 25^{th} August 2019, 15 days of data were lost due to a failing hotbox fan module which was replaced on the 10^{th} September. Replacement fans gave noticeable improvement days of data were also lost between 18^{th} and 26^{th} November due to the lab relocation. On the 3^{rd} November, a new target (UoB-62) was installed, replacing the previous target cylinder, UoB-14. Target analyses showed a high degree of instability during the first month of analysis but have since stabilized.

Starting on the 3^{rd} July, 6 days of data from the 100 m sample line were lost due to a failed line pump. Water droplet tests were conducted between the 6^{th} and 7^{th} July. A further 5 days of data were lost, starting on the 19^{th} August, due to an instrument error which prevented cavity temperature/pressure stabilization. The software issue was corrected via a manual reboot on the 24^{th} August. On the 28^{th} August, the existing standard (H-321) reached its minimum usable pressure. Due to delays obtaining a replacement, H-321 was replaced by UoB-11, the previous mid-low calibration tank. UoB-11 will remain in place until a replacement standard cylinder is available (anticipated before November 2020). A new non-linearity correction was calculated on the 9^{th} September, resulting in adjustments to the standard concentration of 0.007 ppm and 0.014 ppb for CO_2 and CH_4, respectively.

Medusa GCMS: The Medusa GCMS has performed fairly well over the reporting period. Sporadic 'steps' in the chromatography were observed throughout late 2019 and much of 2020, resulting in spurious data for the effected species. These steps are thought to be linked to a software update, though this has not yet been confirmed – work to identify and correct the issue is ongoing. In the meantime, data effected are flagged on a daily basis. On the 3^{rd} September 2019, the needle valves controlling helium flow to the valve hoods were replaced, reducing helium consumption. Beginning on the 3^{rd} October, 2 days of data were lost due to a failing filament. A further 6 days of data were lost due to contamination of the high energy dynode (HED). The mass spectrometer was vented to allow for cleaning of the HED on the 10^{th} October, after which sampling was restarted. Starting on the 5^{th} of November, 8 days of data were lost due to a failure of the unit providing dry air to the Nafion driers. The fault was attributed to an old piece of internal tube which had become disconnected. On the 18^{th} November, 9 days of data were lost whilst the instrument was moved to the new laboratory. A further 9 days of data were lost from the 13^{th} January 2020 during installation of the ANSTO radon detector, during which various components of the Medusa GCMS were switched off in turn to determine the origin of interference observed by the radon detector. On the 12^{th} March, the base-plate temperature became highly variable, effecting data quality for a number of the more volatile species (e.g. CF_4). Sampling was stopped to condition the Cryotiger unit and the power supply unit for the Valco valves was also replaced. Between 3 and 8 days of data (species dependent) were lost during this period.

2.3 Ridge Hill

General: There have been very few issues at Ridge Hill over the last year. An ANSTO radon detector was brought to site on the 4^{th} November 2019 and installed on its concrete plinth. The instrument began sampling from a temporary inlet 2 magl in late January 2020. Riggers began installation of the radon sample line (inlet at 85 magl) in late June – the instrument began sampling from the tower inlet on the 30^{th} June. Meteorological sensors were also installed during the climb.

Additional cabling was installed to link these sensors to a data-logger located within the University of Bristol cabin. Sensors were tested and began routine operation on the 30^{th} June 2020. Plans to send the meteorological data to a central server located at the University of Bristol are ongoing. Ridge Hill is set to become a category 2 ICOS station, and is currently undergoing phase 2 of the labelling process.

CRDS (G2301): The CRDS has performed well over the reporting period. Annual water droplet tests were conducted on the instrument between the 13^{th} and 14^{th} of February 2020, resulting in the loss of ambient air measurements during this time. 1 day of data was lost on the 3rd of May 2020 due to a loss of temperature control, which reoccurred several times during the following 3 days. On the 7^{th} of May, the instrument was shut down and the hotbox fan module replaced, after which the instrument exhibited excellent temperature control. On the 19^{th} of August, the calibration cylinders (not including the standard and target) were removed from site and sent for re-calibration at the ICOS CAL lab as part of the labelling process. The CRDS will shortly be sent to ICOS MLab for testing (another requirement of the labelling process). During this period, a spare instrument (provided by ICOS) will be installed on site, reducing data loss. A new non-linearity correction was calculated on the 9^{th} September, resulting in adjustments to the standard concentration of 0.003 ppm and 0.022 ppb for CO_2 and CH_4, respectively.

GC-ECD: The GC-ECD has performed well over the reporting period. As noted in the previous report, the sample module heater failed on the 7^{th} July 2019. After an initial period of variability (particularly for N_2O), the instrument has since responded well to fluctuations in ambient temperature. 2 days of data were lost between the 23^{rd} and 24^{th} of January 2020 due to a failed sample module pump. On site diagnostics highlighted a faulty power cable as the cause. A new standard was brought online on the 9^{th} March 2020, replacing the old standard H-299, which is currently at the University of Bristol awaiting analysis and return to Mace Head for refilling.

2.4 Bilsdale

General: There have been no major issues at Bilsdale over the last year. Over the course of winter, the site was given a full service. On the 7^{th} November 2019, all line pumps, line filters and the compressor filter were replaced. On the 26^{th} February 2020, the water traps at the base of the tower were also replaced. On the 30^{th} June, the G2401 outlet valve parameter indicated falling flow rate on all three sample lines. On the 27^{th} July, the 40-micron line filters were replaced, and full flow was restored. The blockages were attributed to the accumulation of soot on the filters as a result of nearby heather burning.

CRDS (G2401): The G2401 has performed well over the reporting period. On the 20^{th} October

2019, the instrument shut down due to a lack of temperature control, resulting in 18 days of data loss. On the 7^{th} November, the hotbox fan module was replaced, and sampling restarted with much improved temperature control. The diaphragm in the MD1 pump downstream of the Picarro was also replaced. Water droplet tests were conducted on the 26^{th} and 27^{th} February 2020. From the 30^{th} June to the 27^{th} of July, the instrument did not sample from the 42 m line due to a blocked line filter. During this period, the instrument sampled an additional 10 minutes each hour from the 248 m line. A new non-linearity correction was calculated on the 9^{th} September, resulting in adjustments to the standard concentration of 0.004 ppm, 0.13 ppb and 0.563 ppb for CO_2, CH_4 and CO, respectively.

CRDS (G5310): The G5310 has performed well over the reporting period. In the months after installation (March 2019), the cycle time (the time taken for each laser pulse to decay) was highly variable and required multiple reboots of the instrument software. However, in late 2019 the cycle time was seen to settle down and the variability observed has not re-occurred. On the 5^{th} November 2019, 2 days of data from the 42 m line were lost due to a failed pump. On the 10^{th} January 2020 the GC-ECD standard was ran on the G5310 to provide a comparison between instruments (the GCECD and G5310 are on different calibration scales). From the 30^{th} June to the 27^{th} July, the instrument did not sample from the 42 m line due to a blocked line filter. During this period, the instrument sampled an additional 10 minutes each hour from the 248 m line. A new non-linearity correction was calculated on the 9^{th} September, resulting in adjustments to the standard concentration of 0.002 ppb and 0.092 ppb for N_2O and CO, respectively.

GC-ECD: The GC-ECD system has had several issues over the last reporting year, particularly for N_2O. However, the installation of the G5310 Picarro means that more precise/higher frequency N_2O measurements continued throughout the problematic periods. On the 27^{th} February 2020, the instrument was shut down whilst the carrier gas plumbing was upgraded. The upgrade allows carrier gas cylinders to be hooked up in pairs, reducing the frequency of site visits. During this visit, a faulty regulator controlling output from the standard cylinder was also replaced. On the 8^{th} April, the N_2O precision worsened considerably. On the 9^{th} of April, the valves contained within the instrument front end were realigned, however this led to a further decrease in precision. Conditioning of the columns did not result in any significant improvement. On the 27^{th} July, the multi-position valve rotor was removed for cleaning, eliminating a suspected cross port leak and resulting in a small improvement in precision. On the 28^{th} of April, the carrier gas cylinders were replaced, resulting in a considerable improvement in precision (comparable to 2019). Investigation into the underlying issue is ongoing.

2.5 Heathfield

General: In November 2019 construction started on a new room at the Heathfield site for expansion and new instrumentation. This space is sectioned from the rest of the Arqiva rooms by a newly constructed stud wall. In January 2020 installation of a radon instrument was completed by Scott Chambers from ANSTO as the first of three installations at DECC sites. This instrument samples from a newly-installed inlet at 100 magl.

In June 2020 two new air conditioning modules were installed in the main instrument room. This is a conventional unit charged with HFC-32, which is fine for this site as no halocarbon measurements are made at Heathfield. This has worked well and kept the room temperature at a constant 21°C where previously the room temperature followed the outdoor temperature. In July 2019 the room temperature reached 40°C necessitating the shutdown of the instruments - no such precaution was required this year. The units are also capable of heating, which will maintain a stable temperature throughout the winter. In August 2020 the 100 magl line pump failed in such a way that the flow indicated on the gauge was in the correct range but the sampling line was not purged. This resulted in the instruments partially sampling laboratory air, but without the usual indications of loss of sampling flow. Checking the raw data shows a pattern of steps in the measurements that was followed back to the most likely failure point on the 4^{th} August 2020. A new pump was installed on 25^{th} August.

CRDS (G2401): While the G2401 has worked well for most of the year, an issue started in July 2020 that caused the instrument to shut down unexpectedly. This was traced to a thermal issue - the hotbox fan module has since been replaced. A new standard gas (H-355) was installed in July following a short period of comparison to the outgoing standard (H-358). The gas remaining in the depleted cylinder will be re-analysed by the central calibration laboratory at EMPA, Switzerland.

CRDS (G5310): The G5310 has performed well throughout the reporting period. The new standard gas (H-355) was also connected to this instrument and run in comparison to the outgoing standard (H-358). The water correction was tested by a droplet test, where a small amount of water is allowed to evaporate into the sample flow and thus humidifying the gas, and the correction has not changed since this was last performed. The de-ionised water used as a coolant for the lasers has been replaced by Koolance propylene glycol solution. This should prevent the growth of mould in the cooling system.

GC-ECD: The GC-ECD system has shown decreasing precision for N_2O over the last year and has not improved after servicing and leak checking the gas fittings and columns and checking the valve rotor alignment. The rotors have been replaced and the precision has increased slightly. The G5310 CRDS has been running well so that high-quality N_2O measurements continued throughout

this period. The precision of SF_6 measurements did not degrade to the same degree.

3 Annual Northern Hemisphere Trends

3.1 Baseline Mole Fractions

For each gas observed at Mace Head a baseline analysis has been performed. ECMWF (ERA-Interim) meteorology is used from 1989 – 2002 inclusive and Met Office meteorology from 2003 – 2020 inclusive. For each gas, monthly and annual Northern Hemisphere (NH) baselines, annual growth rates and the average seasonal cycle seen within the observations are calculated. Table 1 – Table 4 summarises the annual baseline mole fractions for each gas observed.

Table 1: Mid-latitude Northern Hemisphere mole fractions and trends observed at Mace Head for 1990-2019 (ppt, except for CH_4 and N_2O reported in ppb and CO_2 in ppm). AvGr = Average Atmospheric Growth (ppX yr^{-1}) from 2003 (or from when observations started). AvGr12 = Growth rate (ppX yr^{-1}) for last 12 months calculated using a 3-year quadratic fit.

Gas	CH_4	N_2O	CO_2	HFC-125	HFC-134a	HFC-143a	HFC-152a	HFC-23	HFC-32
Unit	ppb	ppb	ppm	ppt	ppt	ppt	ppt	ppt	ppt
1990	1789	309.0							
1991	1807	310.0							
1992	1800	310.0							
1993	1813	311.0	357.0						
1994	1813	312.0	359.0						
1995	1817	312.0	360.0		2.0		1.18		
1996	1821	313.0	363.0		4.0		1.22		
1997	1820	314.0	364.0		6.0		1.36		
1998	1831	315.0	366.0	1.19	10.0		1.79		
1999	1835	315.0	369.0	1.42	13.0		2.18		
2000	1839	317.0	369.0	1.75	17.0		2.48		
2001	1839	317.0	371.0	2.22	21.0		2.87		
2002	1839	318.0	373.0	2.62	25.0		3.37		
2003	1847	319.0	376.0	3.21	30.0		4.09		
2004	1846	319.0	377.0	3.85	35.0	5.47	4.77		1.05
2005	1845	320.0	379.0	4.59	39.0	6.37	5.57		1.57
2006	1844	321.0	382.0	5.39	44.0	7.43	6.70		2.05
2007	1853	322.0	384.0	6.29	48.0	8.39	7.84		2.72
2008	1862	323.0	386.0	7.44	53.0	9.55	8.78	22.54	3.40
2009	1865	323.0	387.0	8.57	58.0	10.66	8.90	23.04	4.09
2010	1868	324.0	390.0	9.98	63.0	11.89	9.36	23.70	5.14
2011	1872	325.0	392.0	11.65	68.0	13.13	9.89	24.65	6.48
2012	1881	326.0	394.0	13.44	73.0	14.51	10.04	25.56	7.72
2013	1885	327.0	397.0	15.46	78.0	15.92	9.98	26.63	9.21
2014	1896	328.0	398.0	17.86	84.0	17.38	9.97	27.85	10.90
2015	1906	329.0	401.0	20.12	89.0	18.75	9.80	28.77	12.66
2016	1918	330.0	404.0	22.62	96.0	20.49	9.92	29.56	15.04
2017	1923	331.0	407.0	25.73	103.0	22.21	9.99	30.67	18.23
2018	1928	332.0	409.0	28.88	108.0	23.73	10.09	31.94	21.45
2019	1938	333.0	411.0	32.23	114.0	25.41	10.58	33.34	25.62
AvAll	5.26	0.81	2.04	1.53	4.71	1.34	0.39	1.00	1.67
Av12m	9.03	0.84	4.30	3.29	5.94	1.63	0.29	1.37	3.91

Table 2: Mid-latitude Northern Hemisphere mole fractions and trends observed at Mace Head for 2004-2019 (ppt). AvGr = Average Atmospheric Growth (ppt yr^{-1}) from 2003 (or from when observations started). AvGr12 = Growth rate (ppt yr^{-1}) for last 12 months calculated using a 3-year quadratic fit.

Gas	HFC-227ea	HFC-4310mee	HFC-365mfc	PFC-14	PFC-116	PFC-218	PFC-318	SF_6	NF_3
Unit	ppt	ppt	ppt	ppt	ppt	ppt	ppt	ppt	ppt
2004				74.90	3.646	0.435		5.57	
2005			0.312	75.45	3.723	0.457		5.80	
2006			0.439	76.17	3.810	0.482		6.06	
2007	0.468		0.524	76.86	3.916	0.498		6.31	
2008	0.544		0.608	77.65	3.996	0.516		6.61	
2009	0.625		0.649	78.10	4.062	0.524		6.90	
2010	0.711		0.688	78.74	4.141	0.550		7.17	
2011	0.791	0.226	0.774	79.53	4.238	0.570	1.334	7.47	
2012	0.885	0.239	0.857	80.28	4.298	0.581	1.376	7.77	
2013	0.993	0.249	0.917	81.08	4.381	0.596	1.429	8.10	
2014	1.095	0.261	1.015	81.79	4.467	0.615	1.484	8.44	1.257
2015	1.184	0.274	1.092	82.59	4.553	0.629	1.536	8.77	1.398
2016	1.323	0.279	1.171	83.47	4.619	0.642	1.592	9.09	1.553
2017	1.450	0.286	1.222	84.33	4.729	0.657	1.662	9.44	1.751
2018	1.583	0.285	1.266	85.28	4.814	0.674	1.732	9.78	1.991
2019	1.726	0.300	1.319	86.12	4.911	0.697	1.795	10.14	2.227
AvAll	0.11	0.01	0.07	0.76	0.08	0.02	0.06	0.31	0.19
Av12m	0.14	0.01	0.04	0.87	0.10	0.02	0.06	0.35	0.23

Table 3: Mid-latitude Northern Hemisphere mole fractions and trends observed at Mace Head for 2004-2019 (ppt). AvGr = Average Atmospheric Growth (ppt yr^{-1}) from 2003 (or from when observations started). AvGr12 = Growth rate (ppt yr^{-1}) for last 12 months calculated using a 3-year quadratic fit.

Gas	CFC-11	CFC-12	CFC-113	HCFC-124	HCFC-141b	HCFC-142b	HCFC-22	HFC-236fa	HFC-245fa	SO_2F_2	CH_3Cl	CH_2Cl_2
Unit	ppt	ppt	ppt	ppt	ppt	ppt	ppt	ppt	ppt	ppt	ppt	ppt
1990	264.0	496.0	75.26									
1991	266.0	506.0	80.91									
1992	268.0	516.0	84.11									
1993	269.0	521.0	84.98									
1994	268.0	527.0	84.27									
1995	267.0	533.0	84.37		5.14	7.99						34.73
1996	266.0	537.0	84.32		7.29	9.26						36.17
1997	265.0	540.0	83.74		9.69	10.60						36.20
1998	263.0	542.0	83.14	1.167	11.28	11.38					536.0	32.93
1999	261.0	543.0	82.61	1.323	13.22	12.43	145.0				535.0	31.26
2000	260.0	546.0	82.22	1.430	15.08	13.60	151.0				517.0	30.00
2001	259.0	546.0	81.41	1.574	16.22	14.58	158.0				513.0	28.73
2002	257.0	546.0	80.64	1.591	17.57	15.05	164.0				514.0	29.03
2003	255.0	546.0	79.96	1.630	18.53	15.52	169.0				526.0	30.62
2004	253.0	545.0	79.28	1.649	19.14	16.27	174.0				524.0	30.45
2005	251.0	544.0	78.71		19.11	16.93	180.0			1.450	528.0	30.20
2006	248.0	543.0	77.85		19.55	18.03	187.0			1.529	520.0	31.88
2007	246.0	541.0	77.09		20.21	19.23	194.0	0.070	1.062	1.552	529.0	34.42
2008	244.0	538.0	76.67		20.88	20.55	204.0	0.079	1.274	1.608	535.0	35.90
2009	242.0	535.0	75.96		21.26	21.41	211.0	0.079	1.390	1.663	531.0	36.01
2010	240.0	533.0	75.21		21.97	21.92	219.0	0.092	1.548	1.737	529.0	39.54
2011	238.0	530.0	74.54		23.05	22.68	226.0	0.107	1.784	1.821	519.0	38.92
2012	236.0	527.0	73.99		24.13	23.02	230.0	0.118	2.007	1.914	527.0	41.13
2013	235.0	524.0	73.33		24.92	23.27	236.0	0.127	2.214	2.024	535.0	49.91
2014	234.0	522.0	72.74		25.29	23.34	241.0	0.140	2.395	2.133	531.0	48.77
2015	232.0	519.0	71.99		25.63	23.33	245.0	0.146	2.565	2.230	539.0	48.24
2016	231.0	515.0	71.49		25.97	23.38	249.0	0.159	2.789	2.325	541.0	50.17
2017	230.0	512.0	70.98		25.92	23.40	252.0	0.172	3.067	2.447	529.0	58.45
2018	229.0	509.0	70.30		25.59	23.26	254.0	0.188	3.229	2.511	525.0	55.07
2019	227.0	505.0	69.83		25.53	23.19	258.0	0.203	3.551	2.628	521.0	55.82
AvAll	-1.19	0.47	-0.11	0.07	0.83	0.62	5.63	0.01	0.21	0.08	-0.87	0.86
Av12m	-1.89	-3.96	-0.51	0.02	-0.05	-0.11	2.83	0.01	0.28	0.10	-2.22	-0.33

Table 4: Mid-latitude Northern Hemisphere mole fractions and trends observed at Mace Head for 2004-2019 (ppt or ppb). AvGr = Average Atmospheric Growth (ppX yr^{-1}) from 2003 (or from when observations started). AvGr12 = Growth rate (ppX yr^{-1}) for last 12 months calculated using a 3-year quadratic fit.

Gas	$CHCl_3$	CCl_4	CH_3CCl_3	C_2Cl_4	CH_3Br	Halon-1211	Halon-1301	Halon-2402	CO	H_2	O_3
Unit	ppt	ppt	ppt	ppt	ppt	ppt	ppt	ppt	ppb	ppb	ppb
1990		108.0	150.0								34.48
1991		105.0	152.0								35.79
1992		105.0	149.0								34.91
1993		104.0	139.0								34.79
1994	11.97	104.0	125.0						110.0	507.0	36.53
1995	12.28	102.0	111.0						113.0	508.0	35.18
1996	12.39	101.0	95.0						125.0	515.0	37.82
1997	11.81	100.0	79.0						114.0	506.0	37.22
1998	11.96	99.0	66.0			4.066	2.694		141.0	519.0	40.22
1999	11.56	98.0	55.0		10.95	4.169	2.833		119.0	520.0	41.99
2000	11.23	97.0	47.0		10.41	4.323	2.958		115.0	511.0	40.36
2001	11.23	96.0	39.0	4.996	9.85	4.373	2.993		111.0	507.0	39.68
2002	11.10	95.0	33.0	4.714	9.14	4.405	3.033		117.0	509.0	40.76
2003	11.22	94.0	27.0	4.627	8.87	4.415	3.075		131.0	513.0	40.95
2004	11.30	93.0	23.0	4.313	9.46	4.497	3.108	0.498	119.0	509.0	40.75
2005	11.38	93.0	19.0	3.799	10.23	4.481	3.164	0.495	120.0	513.0	40.02
2006	11.36	91.0	16.0	3.771	9.39	4.456	3.228	0.490	119.0	516.0	41.44
2007	11.34	90.0	13.0	3.531	9.06	4.418	3.224	0.483	116.0	511.0	39.88
2008	11.58	89.0	11.0	3.410	9.12	4.384	3.261	0.474	119.0	514.0	41.16
2009	10.95	88.0	9.0	2.938	8.58	4.320	3.264	0.466	113.0	510.0	41.06
2010	11.84	87.0	8.0	3.025	8.28	4.242	3.303	0.456	120.0	511.0	39.94
2011	11.65	86.0	7.0	2.674	8.33	4.160	3.303	0.451	114.0	517.0	40.18
2012	11.85	85.0	5.0	2.475	8.22	4.073	3.340	0.446	120.0	517.0	40.07
2013	12.85	84.0	4.0	2.426	8.15	3.968	3.386	0.438	115.0	519.0	41.61
2014	13.93	83.0	4.0	2.381	7.63	3.867	3.401	0.429	114.0	517.0	40.41
2015	14.44	82.0	3.0	2.333	7.55	3.751	3.391	0.423	114.0	516.0	40.57
2016	15.09	80.0	3.0	2.290	7.43	3.639	3.386	0.419	112.0	516.0	39.50
2017	15.77	80.0	2.0	2.359	7.35	3.537	3.378	0.413	110.0	519.0	40.67
2018	15.48	79.0	2.0	2.158	7.18	3.421	3.378	0.403	103.0	523.0	40.44
2019	13.91	78.0	2.0	2.256	7.10	3.327	3.392	0.400	100.0	524.0	40.44
AvAll	0.06	-1.05	-4.94	-0.15	-0.19	-0.04	0.03	-0.01	-0.55	0.66	0.20
Av12m	-1.47	-1.01	-0.26	0.00	-0.07	-0.10	0.01	-0.00	-5.13	1.47	-0.11

4 Regional Emission Estimation

4.1 Introduction

This chapter presents the InTEM inversion results, showing the atmospheric trends and regional emissions of the gases that are measured in the UK DECC network and that are reported to the UNFCCC (United Nations Framework Convention on Climate Change). For each gas, the mid-latitude Northern Hemisphere baselines are presented along with the background mole fractions measured at the five core AGAGE (Advanced Global Atmospheric Gases Experiment) stations that span both hemispheres. UK estimated emissions follow where a comparison is made between the InTEM results and the reported UNFCCC inventory values (April 2020 submission). Finally, for each gas the InTEM estimates for North West Europe (NWEU = IRL + UK + FRA + BEL + NLD + LUX + DEU) are compared to UNFCCC estimates (April 2020 submission).

InTEM is briefly presented but for more information the reader is referred to the Methodology report. The uses, atmospheric lifetimes, and global warming potentials for the different gases reported under the UNFCCC are presented in Table 7.

4.2 Summary of InTEM inverse modelling

Each observation is comprised of two parts; a time-varying Northern Hemisphere baseline concentration and a perturbation above baseline. The perturbations above baseline, observed across the UK DECC network, are driven by emissions on regional scales that have yet to be fully mixed on the hemisphere scale and are the principle information used to estimate surface emissions across north-west Europe. A method for estimating emissions from observations, referred to as 'Inversion Technique for Emission Modelling' (InTEM) (Manning et al. 2011; Arnold et al. 2018), has been developed over many years and is used here to estimate UK and NWEU emissions using the observations from the UK DECC network and other European networks where available.

InTEM links the observation time-series with each 4-hour NAME air history estimate of how surface emissions dilute as they travel to the observation stations. An estimated emission distribution, when combined with the NAME output, can be transformed into a modelled time-series at each of the measurement stations. The modelled and the observed time-series can be compared using statistics (cost function) to produce a skill score for that particular emission distribution. InTEM uses a Bayesian statistical technique with a non-negative least squares solver to find the emission distributions that produces the modelled times-series at each observation station that has the best statistical match to the observations. The Bayesian method requires the use of a prior emission distribution with associated uncertainties as the starting point for the inversion. The prior information

can influence and inform the inversion (posterior) solution. In this work the prior emission information has been chosen to be either land-based but population weighted (HFCs) or spread uniformly across the land (PFCs, SF_6, NF_3) or informed by the NAEI (UK National Atmospheric Emissions Inventory) nested within EDGAR (global prior of emissions) estimate (CH_4 and N_2O). However, to preserve the independence of the inversion results presented here from the prior estimates, the priors were given very large uncertainties thus ensuring the inversion results are dominated by the observations not the prior. For CH_4 and N_2O, where the inversion time window was set to one month, the prior was given more weight but the solutions were still dominated by the observations.

For InTEM to provide robust solutions for every area within the modelled domain, each region needs to significantly contribute to the air concentration at the UK DECC network sites for a reasonable number of time periods. If the signal from an area is only rarely or poorly seen by the network, then its impact on the cost function is minimal and the inversion method will have little skill at determining its true emission. The contributions that different grid boxes make to the air concentration at each station varies from grid to grid. Grid boxes that are distant from the observation site contribute little to the observation, whereas those that are close have a large impact. To balance the contributions from different grid boxes, those that are more distant are grouped together into increasingly larger regions. The grouping cannot extend beyond country or Devolved Administration (DA) boundaries. The country boundaries can extend into the surrounding seas to reflect both emissions from shipping, off-shore installations and river runoff but also because the inversion has geographical uncertainty.

For each greenhouse gas, two sets of inversions are performed, with the inversion time frame being either one calendar year or two calendar years. The 2-year inversions started in the year MHD started observing the gas, the 1-year inversions started in 2012 to coincide with the UK DECC network. Every inversion period is repeated 24 times, each time having 8 randomly chosen blocks of 5-days of observations per year removed from the dataset (equivalent to approximately 10% of the year). Annual emission estimates were made by averaging the inversion results covering the appropriate year. Observations from Jungfraujoch (JFJ, Switzerland) and Monte Cimone (CMN, Italy), Taunus (TOB, Germany), Carnsore Point (CSP, Ireland), Cabauw (CBW, The Netherlands) and Weybourne (WAO, Norfolk, UK) were used where available and complemented those in the UK DECC network. For CH_4, N_2O and SF_6, where observations are available from 5 to 8 sites, the second inversion time frame was set to 1-month rather than 1-year. The repeating of each inversion multiple times with the random removal of $\sim$10% of the observations from each inversion improves the estimates of uncertainty.

There are a range of uncertainties in the emissions that are estimated. Uncertainty arises from many factors: errors in the baseline estimate; emissions that vary over time-scales shorter than the inversion time-window e.g. diurnal, seasonal or intermittent; heterogeneous emissions; errors

in the transport model (NAME) or the underpinning 3-dimensional meteorology; errors in the observations themselves. The potential magnitudes of these uncertainties have been estimated and are incorporated within InTEM to inform the uncertainty of the modelled results.

At RGL, HFD, TAC and BSD, CH_4 is observed at two or more heights. If, during a 4-hour period the observed CH_4 differs significantly across the heights, it is an indication that the meteorology is particularly complex and therefore the modelled meteorology will have significant uncertainty. At the other stations, where measurements are not made at multiple heights, the assessment of poor modelling is made using the modelled boundary layer height, wind speed and atmospheric stability. Such 4-hour periods are identified at each observation station and are excluded from the inverse modelling.

Estimating the model and observation uncertainty is an important part of InTEM. The observation uncertainty is estimated each day by repeatedly measuring the same tank of air. The standard deviation of these measurements is defined as the observation uncertainty for that day's observations of that gas at that station. For the high frequency (1-minute) Picarro observations the variability over each 4-hour period is defined as the observation uncertainty. The model uncertainty is defined as having two components; a baseline uncertainty and a meteorological uncertainty. The baseline uncertainty is estimated during the fitting of the Northern Hemisphere baseline trend to the baseline observations. The meteorological uncertainty is proportional to the magnitude of the pollution event with an imposed minimum of the median pollution event for that gas for that year at that station.

4.3 Improvements to InTEM inverse modelling

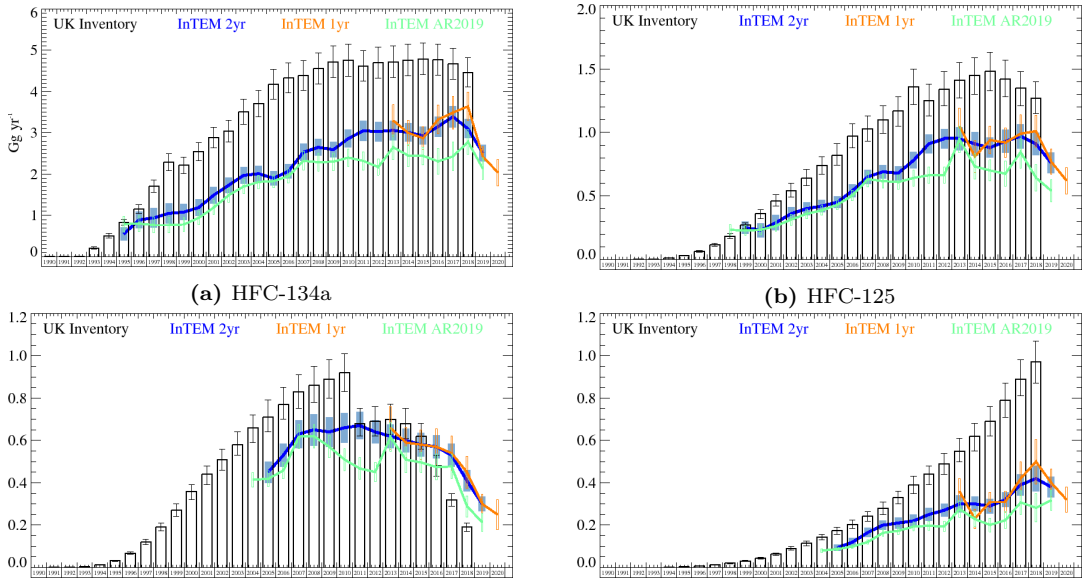

(a) HFC-134a **(b)** HFC-125

(c) HFC-143a **(d)** HFC-32

Figure 2: HFC UK emission estimates (Gg yr^{-1}) from the UNFCCC inventory (black) and InTEM (annually averaged) (a) Annualised 2 year inversion (blue) (b) Annual inversion (orange). (c) Results reported in 2019 Annual report (pale blue) combining 1-, 3- and 4-site InTEM results. The uncertainty bars represent 1-σ.

Figure 2 shows the change in the InTEM estimated emissions for the UK for HFC-134a, HFC-125, HFC-143a and HFC-32 since the annual report in 2019. A significant amount of work has been undertaken to improve InTEM, these are summarised below:

- Improved representation of the model uncertainty per individual measurement point.
- Changing the InTEM averaging period from 2 hours to 4 hours.
- The inclusion of Carnsore Point, Ireland (CSP) and Taunus, Germany (TOB) data where available.
- Improved baseline estimation and uncertainty quantification.
- Improving the prior baseline and increasing the freedom to fit baseline within the inversion.

The fit of the modelled time-series at each of the observation stations and for each gas has improved through the implementation of these changes as shown in Table 5 and Table 6.

Table 5: Correlation coefficient of the comparison of the modelled and observed HFC-134a time-series at each of the observation stations 2013-2018 using two versions of InTEM. The results from the current version of InTEM shown on the left, the results from the version used for the 2019 annual report are shown on the right.

Station	InTEM 2020	InTEM 2019
MHD	0.95	0.92
TAC	0.77	0.71
JFJ	0.77	0.74
CMN	0.69	0.63
TOB	0.50	

Table 6: Correlation coefficient of the comparison of the modelled and observed HFC-125, HFC-143a and HFC-32 time-series at MHD and TAC 2013-2018 using two versions of InTEM. For each gas the results from the current version of InTEM shown on the left, the results from the version used for the 2019 annual report are shown on the right.

Station	HFC-125		HFC-143a		HFC-32	
	InTEM 2020	InTEM 2019	InTEM 2020	InTEM 2019	InTEM 2020	InTEM 2019
MHD	0.92	0.88	0.90	0.84	0.87	0.84
TAC	0.74	0.67	0.73	0.66	0.70	0.67

4.4 Summary of the GHG reported to the UNFCCC

Table 7 describes the principle uses of each of the gases reported to the UNFCCC and observed in the network, their radiative efficiency, atmospheric lifetime and global warming potential in a 100-year framework (GWP_{100}).

Table 7: Principle uses of each of the gases, their radiative efficiency, atmospheric lifetime and global warming potential in a 100-year framework (GWP_{100}) (Chapter 8, Working Group 1, 5th Assessment Report of the IPCC, (Myhre et al. 2013)).

Gas	Chemical Formula	Main Use	Radiative Efficiency ($Wm^{-2}ppb^{-1}$)	Atmospheric lifetime (yr)	GWP_{100}
Methane	CH_4	Landfill, farming, energy, wetlands	0.000363	12.4	28
Nitrous Oxide	N_2O	Nylon manufacture, farming	0.00300	121	265
Carbon Dioxide	CO_2	Combustion	0.0000137	indefinite	1
HFC-125	CHF_2CF_3	Refrigeration blend, fire suppression	0.23	28.2	3,170
HFC-134a	CH_2FCF_3	Mobile air conditioner	0.16	13.4	1,300
HFC-143a	CH_3CF_3	Refrigeration blend	0.16	47.1	4,800
HFC-152a	CH_3CHF_2	Aerosol propellant, foam-blowing agent	0.10	1.5	138
HFC-23	CHF_3	Bi-product of manufacture of HCFC-22	0.18	222	12,400
HFC-32	CH_2F_2	Refrigeration blend	0.11	5.2	677
HFC-227ea	CF_3CHFCF_3	Fire suppression, inhalers, foam blowing	0.26	38.9	3,350
HFC-245fa	$C_3H_3F_5$	Blowing and insulation agent	0.24	7.7	858
HFC-43-10mee	$C_5H_2F_{10}$	Electronics industry	0.42	16.1	1,650
HFC-365mfc	$C_4H_5F_5$	Foam blowing	0.22	8.7	804
PFC-14	CF_4	Bi-product alum. production, electronics	0.09	50,000	6,630
PFC-116	C_2F_6	Electronics, bi-product alum. production	0.25	10,000	11,100
PFC-218	C_3F_8	Electronics, bi-product alum. production	0.28	2,600	8,900
PFC-318	C_4F_8	Semiconductor and electronics industries	0.32	3,200	9,540
Sulphur Hexafluoride	SF_6	Circuit breaker in high voltage switchgear	0.57	3,200	23,500
Nitrogen Trifluoride	NF_3	Semiconductor manufacture	0.20	500	16,100

4.5 Methane (CH_4)

Methane (CH_4) is the second most important anthropogenic greenhouse gas behind carbon dioxide due to its radiative properties and atmospheric abundance. It has a Global Warming Potential over 100 years (GWP_{100}) of 28 and its total global radiative forcing attributable to anthropogenic CH_4 emissions is currently about 0.97 W m^{-2} (Myhre et al. 2013). The global background surface dry air mole fraction of atmospheric CH_4 reached 1857 ppb in 2018, approximately 2.6 times greater than its estimated pre-industrial equilibrium value in the mid 18^{th} century (Saunois et al. 2020). This growth is attributable in large part to increased anthropogenic emissions arising primarily from agriculture (e.g., livestock production, rice cultivation, biomass burning), fossil fuel production and use, waste disposal, and alterations to natural methane fluxes due to increased atmospheric CO_2 concentrations and climate change (Ciais et al. 2013). After a brief plateau period around the turn of the 21^{st}century (Cunnold et al. 2002; Dlugokencky et al. 2003), CH_4 mole fractions began rising again globally in 2007 (Rigby et al. 2008; Dlugokencky et al. 2009; Frankenberg et al. 2011; Nisbet et al. 2016) with some of the strongest growth rates occurring from 2014 onward (Nisbet et al. 2019). This increase in CH_4 growth rate was accompanied by a shift in the δ^{13}C-CH_4 isotopic ratios to more negative values, suggesting a change in the global makeup of sources and/or sinks. The drivers responsible for this shift are presently not well-understood, and possibilities include changes in tropical wetland, biomass burning, agriculture, and fossil fuel emissions or changes in the hydroxyl radical sink (e.g. Monteil et al. 2011; Schaefer et al. 2016; Schwietzke et al. 2016; Nisbet et al. 2016; Rigby et al. 2017; Worden et al. 2017; McNorton et al. 2018; Turner et al. 2019; Nisbet et al. 2019; Hmiel et al. 2020). Quantifying the CH_4 budget and understanding how major sources and sinks have been evolving is key to designing emission pathways that limit global warming due to the importance of CH_4 in meeting global climate targets (Ganesan et al. 2019; Nisbet et al. 2019, 2020).

- Accelerating global trend upwards, currently increasing by ∼9 ppb yr^{-1} (Figure 3).
- Background has a strong seasonal cycle (∼25 ppb).
- UK GHGI and InTEM are in good agreement from 2012.
- InTEM shows little change in emissions from 1990 whereas the GHGI has fallen by more than 50% since 1990 (Figure 5).
- Little evidence of a seasonal cycle in UK emissions although there is year to year variability e.g. suppressed in 2014-15 and 19, more activity 2012 and 2018 (Figure 6).
- UK distribution shows minimal change over the year (Figure 8).

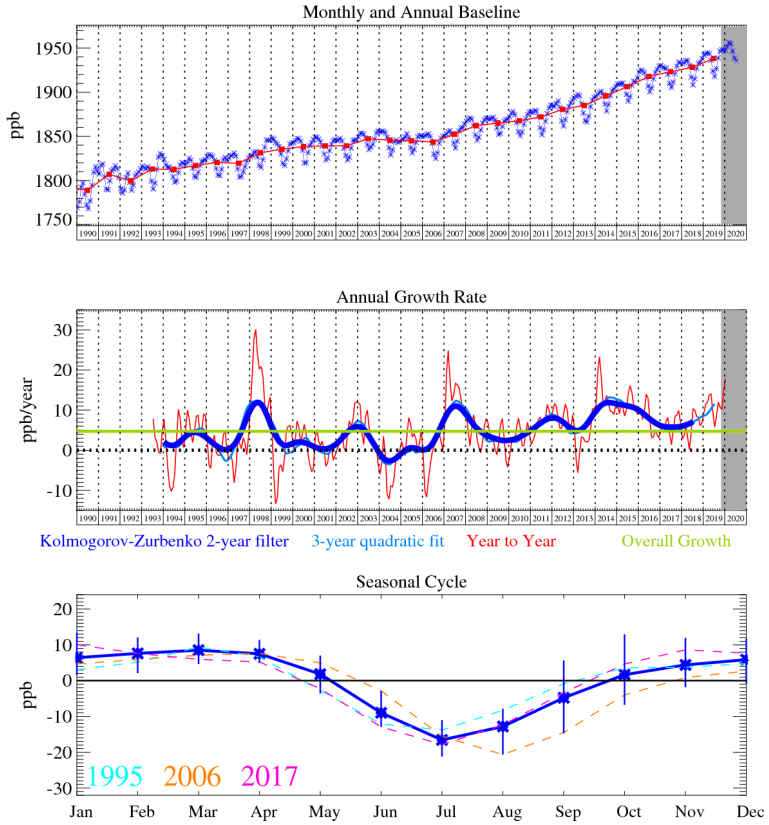

Figure 3: Monthly (blue) and annual (red) Mid-latitude Northern Hemisphere mole fractions (top plot). Annual (blue and red) and overall (green) growth rate (middle plot). Seasonal cycle (de-trended) with year-to-year variability (lower plot). Grey area covers un-ratified provisional data.

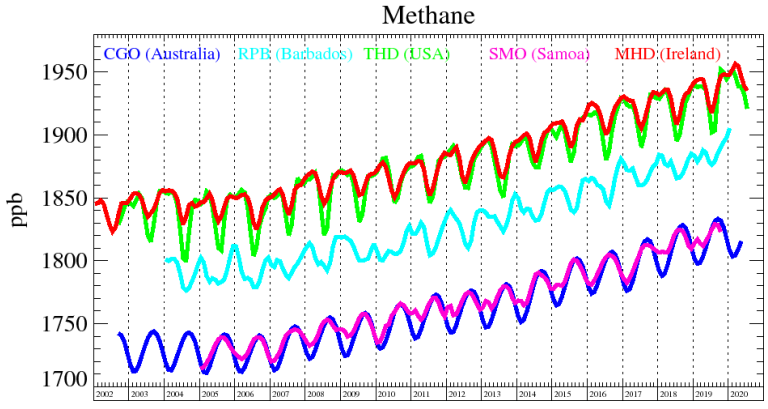

Figure 4: Background mole fractions at 5 AGAGE global stations

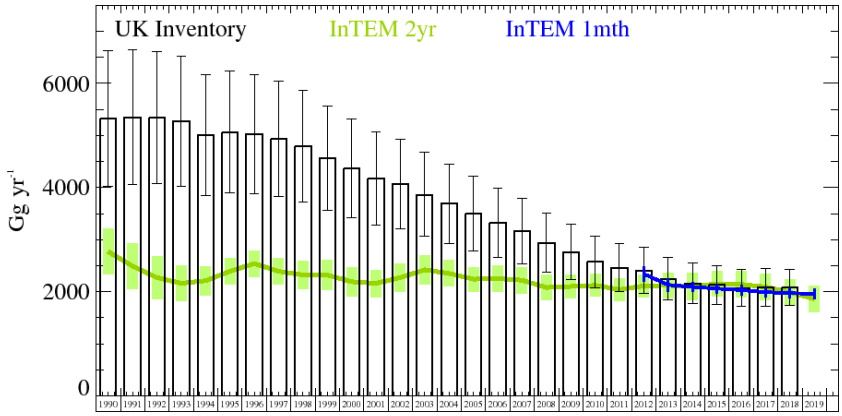

Figure 5: CH_4 UK emission estimates (Gg yr^{-1}) from the UNFCCC GHGI (black) and InTEM (a) Annualised 2 year inversion (green) (b) Annualised 1 month inversion (blue). The uncertainty bars represent 1-σ.

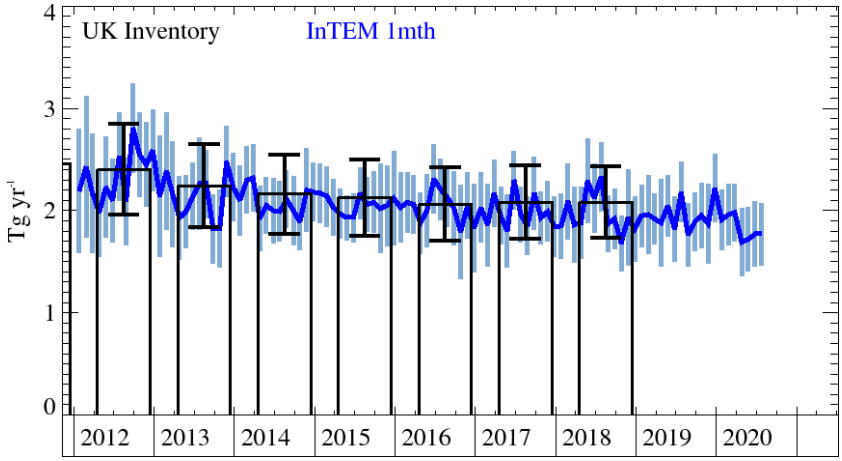

Figure 6: CH_4 UK emission estimates (Gg yr^{-1}) from the UNFCCC GHGI (black) and InTEM (monthly) DECC + CBW + WAO (blue). The uncertainty bars represent 1-σ.

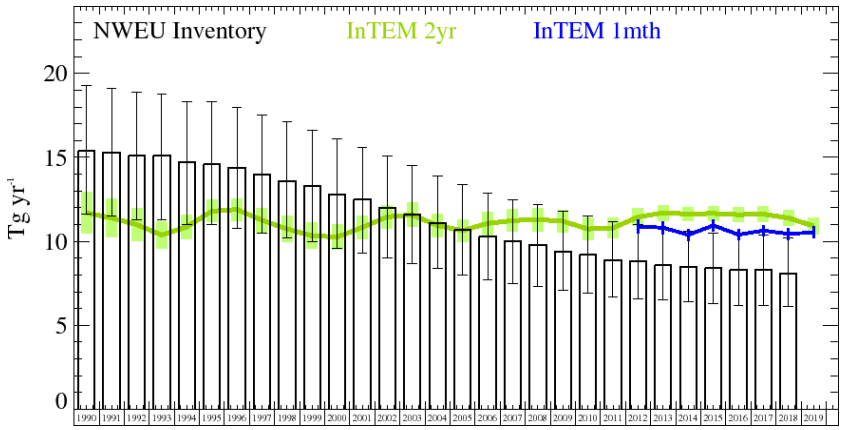

Figure 7: CH_4 NWEU emission estimates (Gg yr^{-1}) from the UNFCCC inventory (black) and InTEM (a) Annualised 2 year inversion (green) (b) Annualised 1 month inversion (blue). The uncertainty bars represent 1-σ.

Table 8: UK and NWEU (Tg yr^{-1}) CH_4 emission estimates with 1-σ uncertainty.

	UK			NWEU		
Years	Inventory	InTEM 2yr	InTEM 1mth	Inventory	InTEM 2yr	InTEM 1mth
1990	5.32 (4.02-6.62)	2.77 (2.33-3.21)		15.4 (11.6-19.3)	11.7 (10.5-13.0)	
1991	5.35 (4.06-6.64)	2.49 (2.05-2.93)		15.3 (11.5-19.1)	11.4 (10.2-12.5)	
1992	5.34 (4.07-6.61)	2.27 (1.86-2.67)		15.1 (11.3-18.9)	11.0 (10.0-12.0)	
1993	5.28 (4.03-6.52)	2.16 (1.81-2.50)		15.1 (11.3-18.8)	10.4 (9.6-11.2)	
1994	5.00 (3.84-6.17)	2.21 (1.93-2.49)		14.7 (11.0-18.3)	10.9 (10.1-11.6)	
1995	5.06 (3.90-6.23)	2.39 (2.14-2.64)		14.6 (11.0-18.3)	11.8 (11.1-12.5)	
1996	5.03 (3.88-6.17)	2.54 (2.29-2.79)		14.4 (10.8-18.0)	11.9 (11.2-12.6)	
1997	4.93 (3.82-6.04)	2.39 (2.14-2.64)		14.0 (10.5-17.5)	11.3 (10.5-12.0)	
1998	4.79 (3.73-5.86)	2.32 (2.05-2.59)		13.6 (10.2-17.1)	10.7 (9.9-11.5)	
1999	4.57 (3.57-5.57)	2.32 (2.02-2.61)		13.3 (10.0-16.6)	10.3 (9.5-11.1)	
2000	4.36 (3.42-5.31)	2.19 (1.91-2.46)		12.8 (9.6-16.1)	10.3 (9.5-11.0)	
2001	4.17 (3.27-5.06)	2.16 (1.90-2.42)		12.5 (9.3-15.6)	10.8 (10.1-11.5)	
2002	4.07 (3.21-4.93)	2.27 (2.00-2.55)		12.0 (9.0-15.1)	11.5 (10.7-12.2)	
2003	3.86 (3.06-4.67)	2.42 (2.13-2.70)		11.6 (8.7-14.5)	11.6 (10.8-12.3)	
2004	3.69 (2.93-4.45)	2.35 (2.10-2.60)		11.1 (8.4-13.9)	10.9 (10.2-11.6)	
2005	3.50 (2.79-4.21)	2.24 (2.00-2.47)		10.7 (8.0-13.4)	10.7 (9.9-11.3)	
2006	3.32 (2.65-3.98)	2.25 (2.00-2.51)		10.3 (7.7-12.9)	11.1 (10.3-11.8)	
2007	3.16 (2.54-3.79)	2.22 (1.97-2.48)		10.0 (7.5-12.5)	11.2 (10.5-11.9)	
2008	2.94 (2.37-3.51)	2.08 (1.84-2.32)		9.8 (7.3-12.2)	11.3 (10.6-12.0)	
2009	2.76 (2.23-3.29)	2.10 (1.87-2.33)		9.4 (7.1-11.8)	11.2 (10.5-11.9)	
2010	2.57 (2.08-3.06)	2.12 (1.91-2.34)		9.2 (6.9-11.5)	10.7 (10.0-11.4)	
2011	2.46 (2.00-2.92)	2.04 (1.83-2.26)		8.9 (6.7-11.2)	10.8 (10.2-11.4)	
2012	2.40 (1.96-2.85)	2.11 (1.89-2.33)	2.34 (2.20-2.48)	8.8 (6.6-11.0)	11.4 (10.9-12.0)	10.9 (10.4-11.3)
2013	2.24 (1.84-2.65)	2.12 (1.88-2.37)	2.13 (2.01-2.26)	8.6 (6.5-10.8)	11.7 (11.2-12.2)	10.8 (10.4-11.2)
2014	2.16 (1.77-2.55)	2.10 (1.85-2.36)	2.09 (2.00-2.18)	8.5 (6.4-10.6)	11.6 (11.2-12.1)	10.4 (10.0-10.7)
2015	2.13 (1.75-2.50)	2.15 (1.91-2.40)	2.06 (1.97-2.15)	8.4 (6.3-10.5)	11.7 (11.2-12.1)	11.0 (10.6-11.3)
2016	2.06 (1.71-2.42)	2.14 (1.89-2.39)	2.03 (1.93-2.13)	8.3 (6.2-10.4)	11.6 (11.1-12.0)	10.4 (10.0-10.7)
2017	2.08 (1.72-2.44)	2.09 (1.83-2.34)	1.99 (1.90-2.08)	8.3 (6.2-10.4)	11.6 (11.1-12.1)	10.6 (10.3-11.0)
2018	2.08 (1.73-2.43)	1.99 (1.74-2.24)	1.97 (1.87-2.07)	8.1 (6.1-10.2)	11.4 (10.9-11.9)	10.4 (10.1-10.8)
2019		1.86 (1.61-2.11)	1.96 (1.86-2.05)		10.9 (10.4-11.4)	10.5 (10.1-10.9)

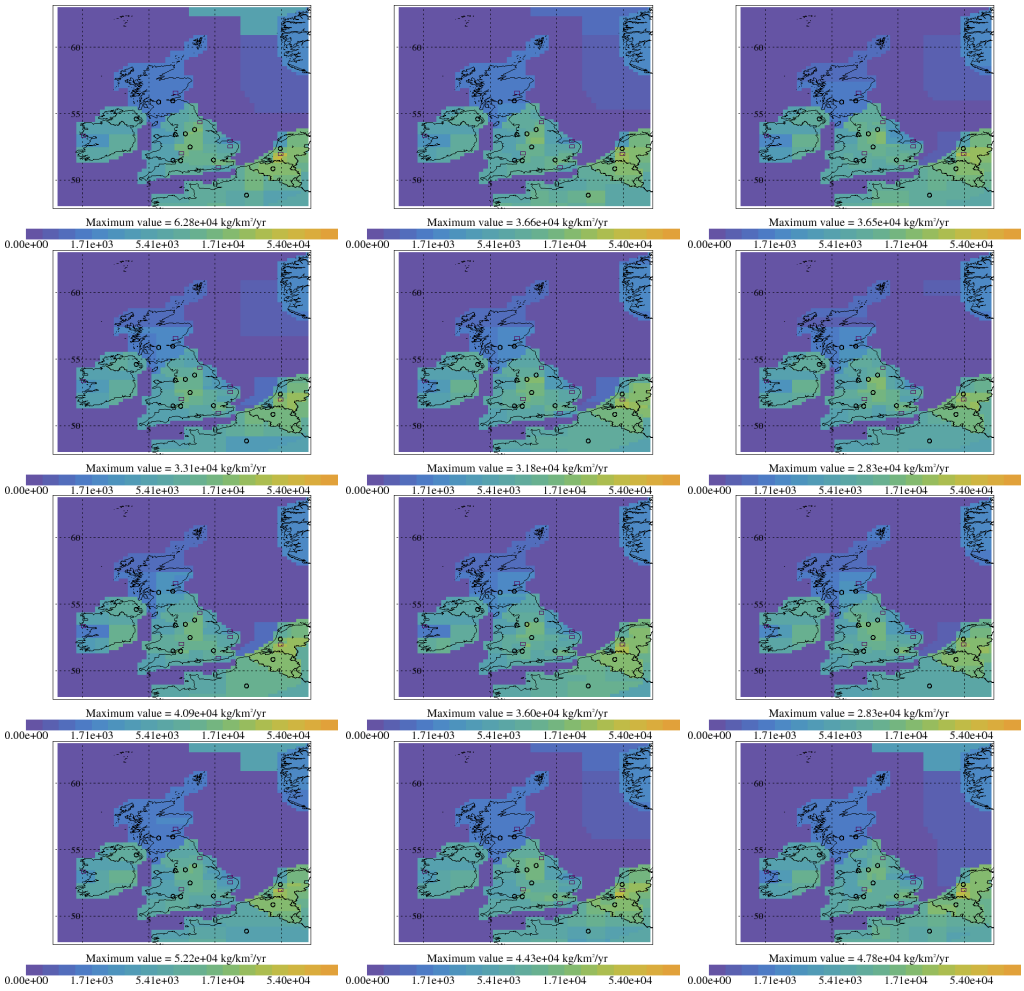

Figure 8: Average monthly InTEM CH_4 emission estimates (kg km^{-2} yr^{-1}) 2012-2019

4.6 Nitrous Oxide (N_2O)

Nitrous oxide (N_2O) is the third most important anthropogenic greenhouse gas after CO_2 and CH_4, it has a GWP_{100} of 265, far exceeding that of CO_2, and its emissions weighted by ozone depletion potential currently exceed those of all other substances (Ravishankara et al. 2009). Atmospheric mixing ratios of N_2O have been rising by approximately 0.93 ppb yr^{-1} (WMO 2018). The long lifetime of this species (∼120 years) results in most emitted N_2O reaching the stratosphere, where photooxidation makes it the primary source of stratospheric NOx ("active nitrogen"). NOx is the main natural catalyst of ozone (O_3) destruction (Crutzen 1970). The main loss mechanism for N_2O is destruction in the stratosphere through photolysis and the reaction with O(1D) (Prather et al. 2015). Anthropogenic sources of N_2O account for ∼40% of all N_2O emissions, with natural sources accounting for the other ∼60% (Ciais et al. 2013). Natural sources of N_2O are from natural soils, oceans, and atmospheric chemistry. Anthropogenic sources are dominated by agriculture, followed by industrial and fossil fuel sources, biomass burning, rivers and estuaries, atmospheric deposition, and human excreta (Ciais et al. 2013). Emissions of N_2O following fertilizer application can exhibit major temporal and spatial variability. This is because microbial nitrification and denitrification processes that give rise to N_2O formation are strongly dependent on soil moisture, temperature, soil type, and fertilizer application timing. It has been reported that indirect N_2O emissions downstream from the site of fertilizer application could be 2.6 - 9 times larger than is presently accounted for in bottom-up estimates (Griffis et al. 2013; Turner et al. 2015), which would imply an underestimate of the importance of agricultural sources for the overall N_2O budget.

- The N_2O global concentration is increasing (∼0.85 ppb yr^{-1}) (Figure 9).
- It has a pronounced background seasonal cycle (amplitude of ∼0.8 ppb)
- UK GHGI estimates are lower than InTEM by ∼15% 2012-2019 (Figure 12).
- UK emissions spread across country. Belgian emissions are consistently high throughout the year (Figure 14).
- UK emissions have a very strong seasonal cycle (amplitude of ∼80 Gg). Peak emissions in May-Aug, minima in Jan-Feb. 2015 has a suppressed summer maximum (Figure 15).
- Estimating annual emission without full 5-site DECC network is difficult and could be biased.
- Improvement in observation instruments has reduced uncertainty.

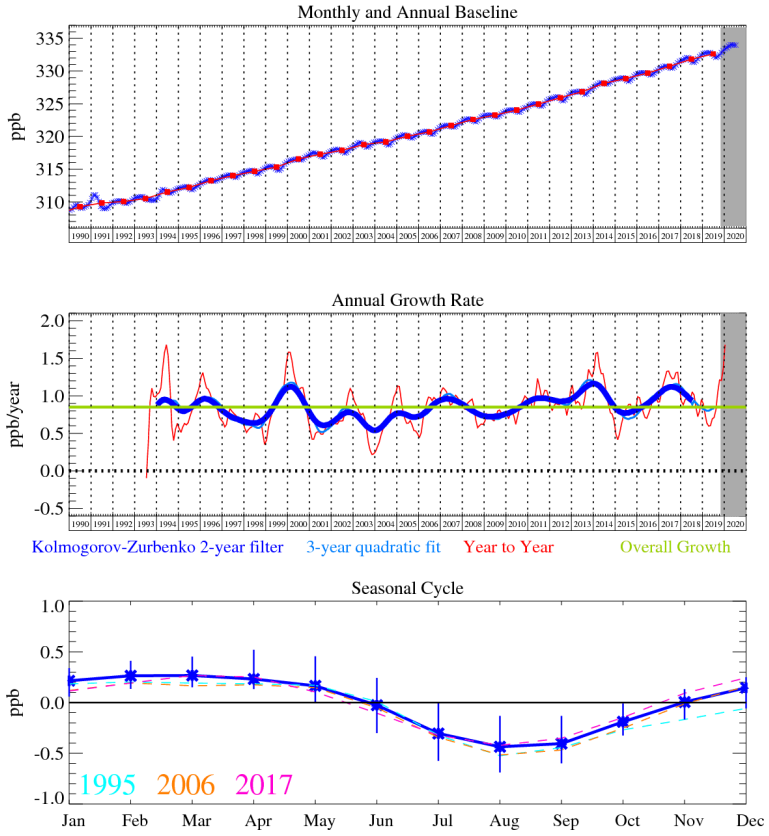

Figure 9: Monthly (blue) and annual (red) Mid-latitude Northern Hemisphere mole fractions (top plot). Annual (blue and red) and overall (green) growth rate (middle plot). Seasonal cycle (de-trended) with year-to-year variability (lower plot). Grey area covers un-ratified provisional data.

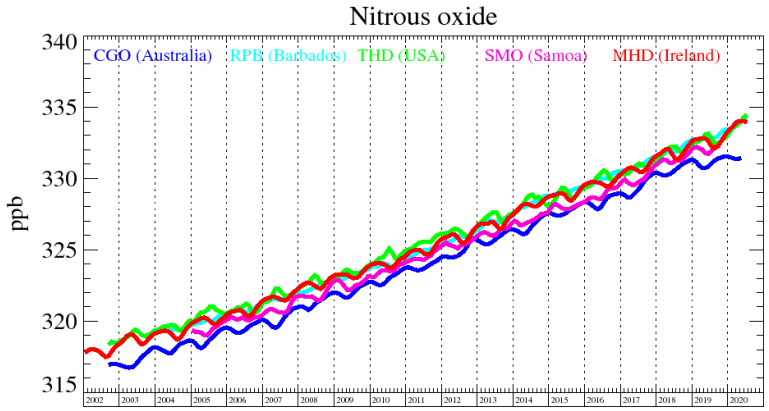

Figure 10: Background mole fractions at 5 AGAGE global stations

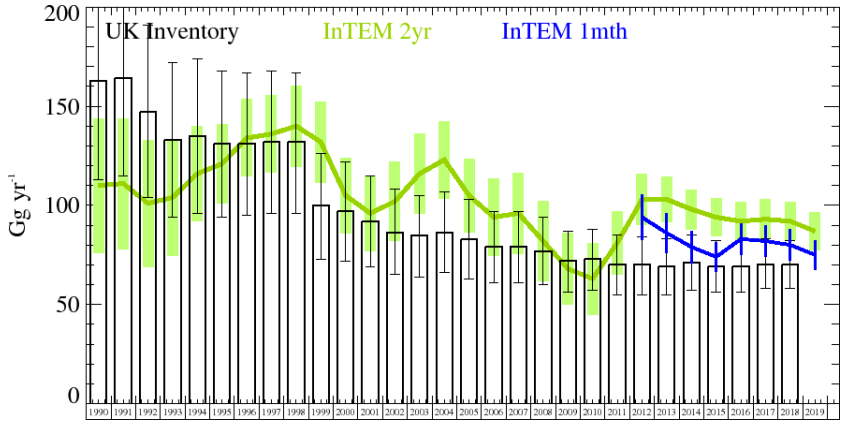

Figure 11: N_2O UK emission estimates (Gg yr^{-1}) from the UNFCCC GHGI (black) and InTEM (a) Annualised 2 year inversion (green) (b) Annualised 1 month inversion (blue). The uncertainty bars represent 1-σ.

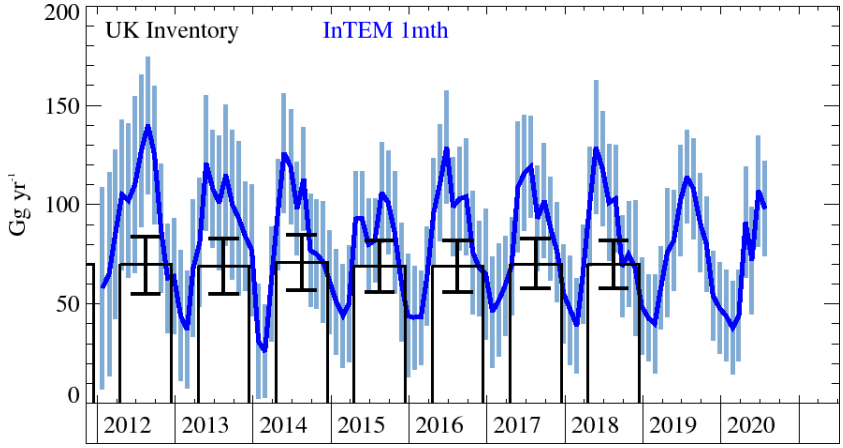

Figure 12: N_2O UK emission estimates (Gg yr^{-1}) from the UNFCCC GHGI (black) and InTEM (monthly) DECC network (blue). The uncertainty bars represent 1-σ.

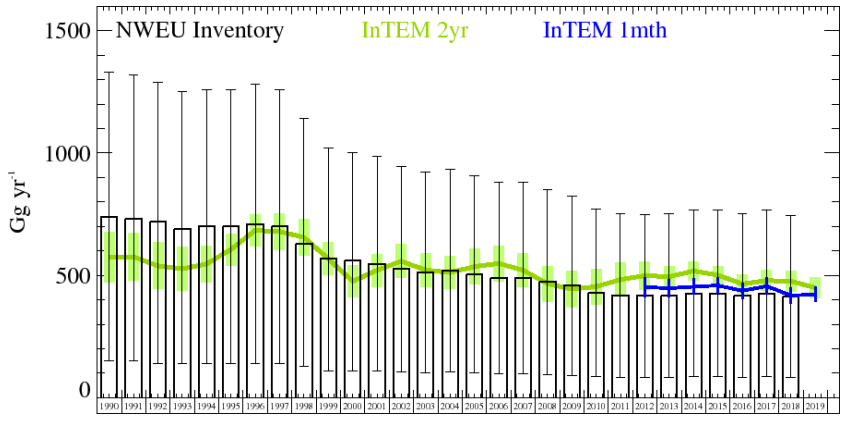

Figure 13: N_2O NWEU emission estimates (Gg yr^{-1}) from the UNFCCC GHGI (black) and InTEM (a) Annualised 2 year inversion (green) (b) Annualised 1 month inversion (blue). The uncertainty bars represent 1-σ.

Table 9: UK N_2O emission (Gg yr^{-1}) estimates with 1-σ uncertainty.

	UK			NWEU		
Years	Inventory	InTEM 2yr	InTEM 1mth	Inventory	InTEM 2yr	InTEM 1mth
1990	163. (33.-294.)	110. (76.-144.)		740. (150.-1330.)	573. (470.-676.)	
1991	164. (33.-295.)	111. (78.-144.)		730. (150.-1320.)	576. (478.-674.)	
1992	147. (29.-265.)	101. (69.-133.)		720. (140.-1290.)	539. (444.-634.)	
1993	133. (27.-240.)	104. (75.-134.)		690. (140.-1250.)	527. (438.-615.)	
1994	135. (27.-243.)	116. (92.-140.)		700. (140.-1260.)	547. (472.-623.)	
1995	131. (26.-236.)	121. (101.-141.)		700. (140.-1260.)	606. (542.-671.)	
1996	131. (26.-236.)	134. (114.-153.)		710. (140.-1280.)	684. (619.-749.)	
1997	132. (26.-237.)	136. (117.-156.)		700. (140.-1260.)	679. (606.-752.)	
1998	132. (26.-237.)	140. (120.-161.)		630. (130.-1140.)	656. (582.-731.)	
1999	100. (20.-179.)	132. (111.-152.)		570. (110.-1020.)	568. (501.-636.)	
2000	97. (19.-175.)	105. (86.-124.)		560. (110.-1000.)	476. (411.-541.)	
2001	92. (18.-165.)	96. (77.-115.)		548. (110.-987.)	521. (455.-588.)	
2002	86. (17.-155.)	102. (82.-122.)		526. (105.-946.)	558. (489.-626.)	
2003	85. (17.-152.)	116. (96.-136.)		513. (103.-923.)	522. (453.-591.)	
2004	86. (17.-155.)	123. (104.-143.)		518. (104.-932.)	512. (443.-580.)	
2005	83. (17.-150.)	105. (87.-124.)		503. (101.-906.)	536. (465.-608.)	
2006	79. (16.-142.)	94. (75.-114.)		490. (98.-881.)	549. (477.-621.)	
2007	79. (16.-142.)	96. (75.-116.)		489. (98.-880.)	521. (451.-590.)	
2008	77. (15.-138.)	82. (62.-102.)		473. (95.-851.)	466. (393.-538.)	
2009	72. (14.-129.)	68. (50.-86.)		459. (92.-826.)	444. (369.-520.)	
2010	73. (15.-131.)	63. (45.-81.)		428. (86.-770.)	454. (382.-525.)	
2011	70. (14.-126.)	81. (65.-97.)		419. (84.-754.)	483. (415.-552.)	
2012	70. (14.-125.)	103. (90.-116.)	94. (83.-106.)	416. (83.-749.)	499. (442.-557.)	452. (412.-491.)
2013	69. (14.-125.)	103. (91.-114.)	86. (76.-96.)	418. (84.-753.)	495. (453.-537.)	448. (412.-483.)
2014	71. (14.-128.)	98. (88.-108.)	79. (71.-87.)	426. (85.-767.)	518. (480.-555.)	454. (421.-487.)
2015	69. (14.-125.)	94. (84.-103.)	74. (67.-82.)	426. (85.-767.)	501. (463.-539.)	459. (426.-492.)
2016	69. (14.-124.)	92. (82.-101.)	83. (75.-91.)	418. (84.-752.)	465. (425.-505.)	437. (405.-469.)
2017	70. (14.-126.)	93. (83.-103.)	82. (74.-90.)	426. (85.-767.)	479. (437.-521.)	456. (421.-491.)
2018	70. (14.-126.)	92. (83.-102.)	80. (72.-88.)	413. (83.-744.)	476. (435.-518.)	418. (385.-452.)
2019		87. (77.-96.)	75. (67.-82.)		450. (409.-492.)	422. (391.-453.)

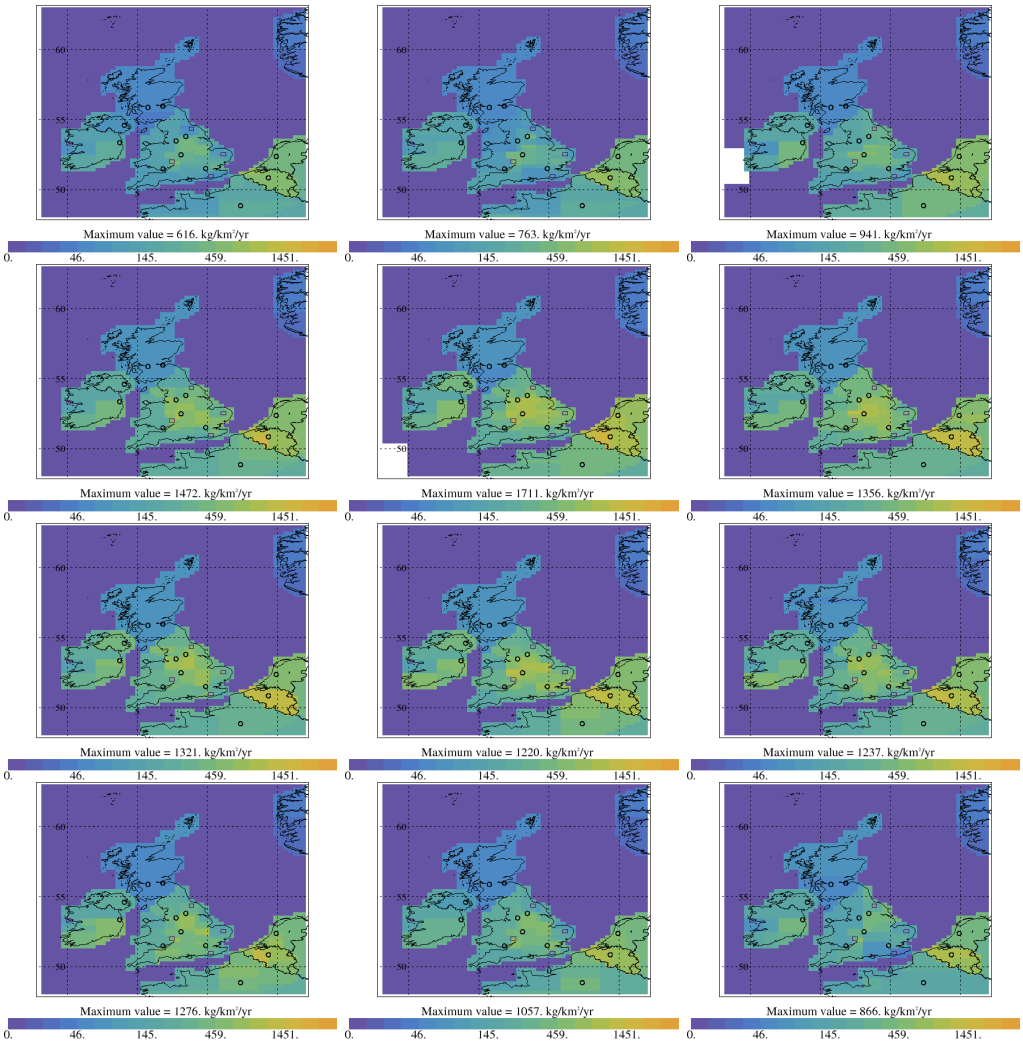

Figure 14: Average monthly InTEM N_2O emission estimates (kg km^{-2} yr^{-1}) 2012-2019

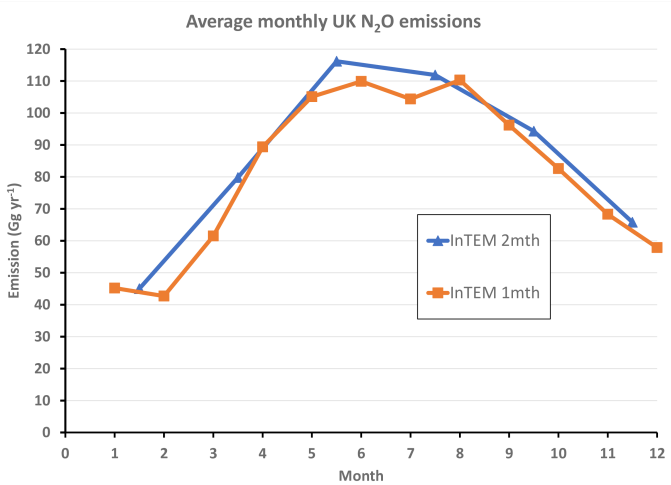

Figure 15: Average Seasonal Cycle in InTEM N_2O emission estimates (Gg yr^{-1}) 2014-2019

4.7 Carbon Dioxide (CO_2)

CO_2 is the most important greenhouse gas due to its abundance in the atmosphere. Since 1992, its Northern Hemispheric background surface dry air mole fraction has increased at an average rate of ~2 ppm yr^{-1}, but this rate has increased slightly since 2012.

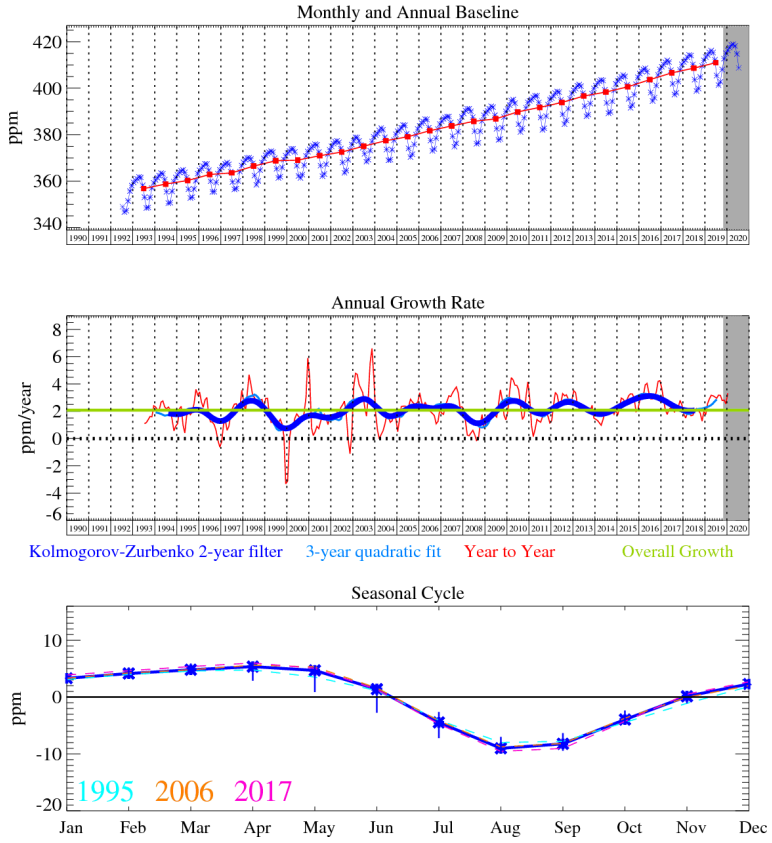

Figure 16: Monthly (blue) and annual (red) Mid-latitude Northern Hemisphere mole fractions (top plot). Annual (blue and red) and overall (green) growth rate (middle plot). Seasonal cycle (de-trended) with year-to-year variability (lower plot). Grey area covers un-ratified provisional data.

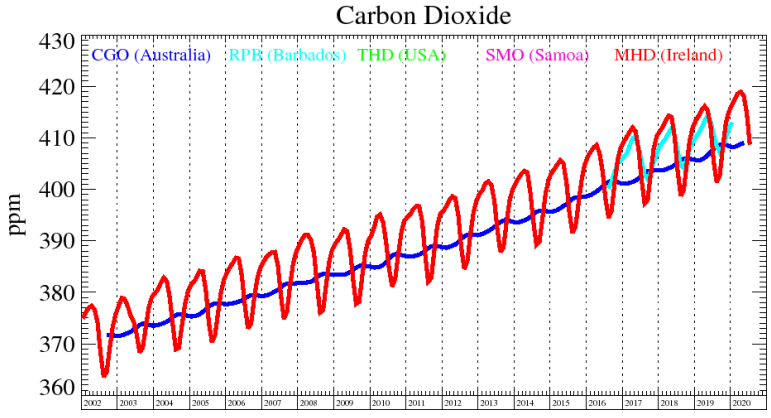

Figure 17: Background mole fractions at 5 AGAGE global stations

4.8 HFC Summary

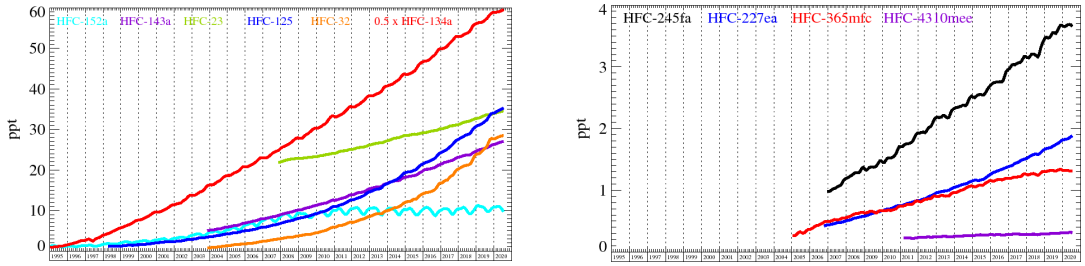

Figure 18: Northern Hemisphere Atmospheric Background Levels of HFCs as observed at the Mace Head observing station. Note the change in scale from the left to the right plot. For scale purposes the atmospheric mole fractions of HFC-134a have been halved.

The atmospheric concentrations of all the HFC's reported here (HFC-125, HFC-134a, HFC-143a, HFC-152a, HFC-23, HFC-32, HFC-227ea, HFC-245fa, HFC-43-10mee and HFC-365) are growing in the Northern Hemisphere as can been seen in Figure 18 and this is replicated in the Southern Hemisphere albeit with a time lag of 1-2 years. These plots show the background mid-latitude Northern Hemisphere mole fractions of each of the HFCs measured at Mace Head, Ireland. Some of the gases, notably HFC-134a, HFC-125, HFC-32 and HFC-227ea, are growing very rapidly in the atmosphere. Others are growing much more slowly e.g. HFC-152a, HFC-43-10mee, HFC-365. It is important to recognise that HFC-23 is the most important in terms of its impact on the climate as its GWP_{100} is by far the highest at over 12,000, the next most important gases, with GWP_{100}s of 3,000-5,000, are HFC-125, HFC-143a and HFC-227ea and then HFC-134a with a GWP_{100} of 1,300 (Table 7).

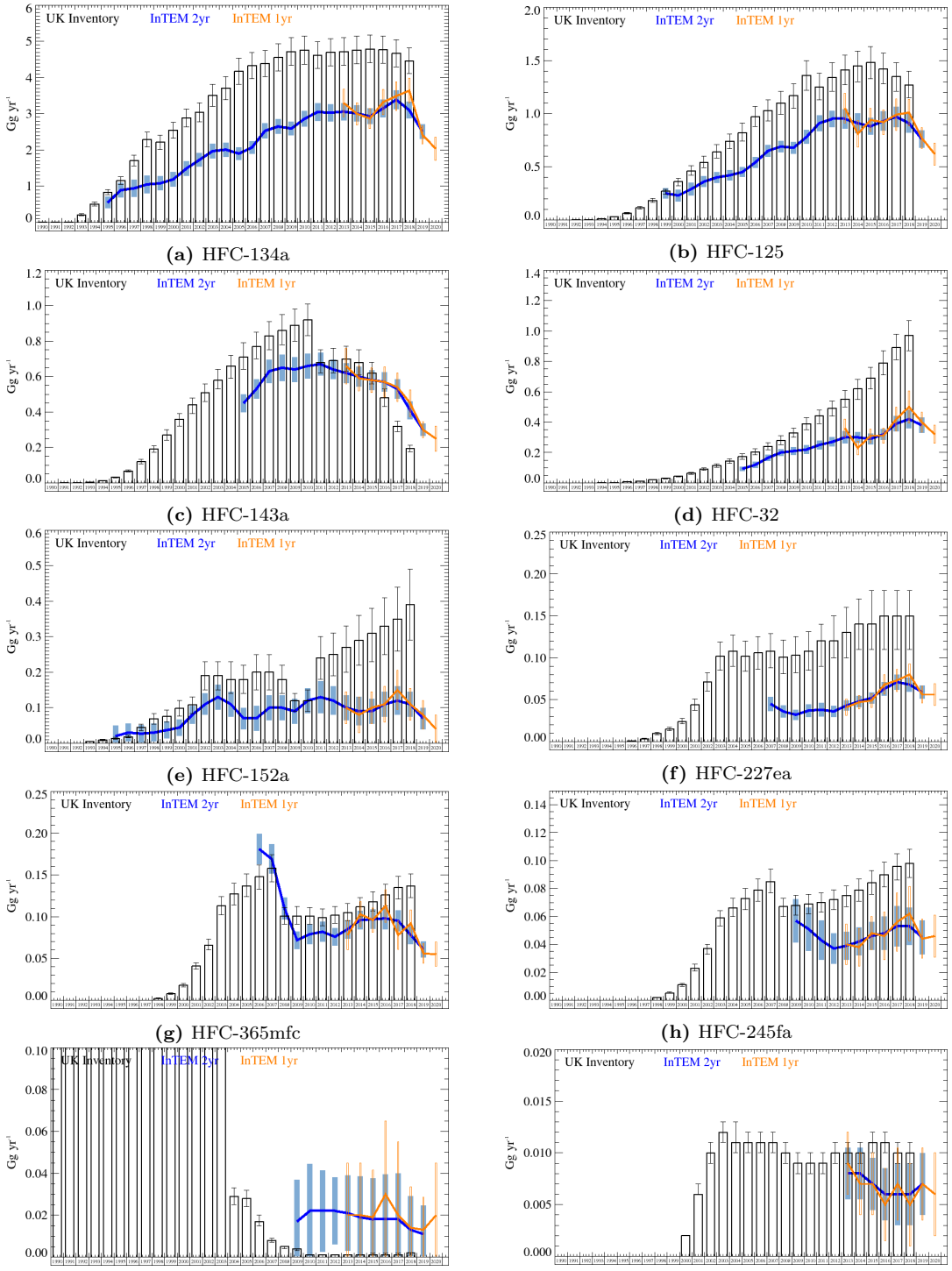

(a) HFC-134a **(b)** HFC-125

(c) HFC-143a **(d)** HFC-32

(e) HFC-152a **(f)** HFC-227ea

(g) HFC-365mfc **(h)** HFC-245fa

(i) HFC-23 **(j)** HFC-43-10mee

Figure 19: HFC UK emission estimates (Gg yr^{-1}) from the UNFCCC inventory (black) and InTEM (a) Annualised 2-year inversion (blue) (b) Annual inversion (orange). The uncertainty bars represent 1-σ.

Figure 19 shows the UK InTEM and the UK Inventory (GHGI submitted April 2020) estimated annual emissions up to and including 2020. With the exception of HFC-23 and HFC-43-10mee which are flat, InTEM estimates that all of the UK HFC emissions have decreased over the last

2 years from 2018. Please note that data for 2020 should be treated as provisional as it is based on only 7 months of measurement data. The InTEM estimate is plotted against the UK UNFCCC submission estimate whose latest data year is for 2018. For HFC-134a, HFC-125 and HFC-143a the 2018 GHGI inventory has decreased compared with that estimated for 2017, for HFC-32, HFC-152a and HFC-365mfc the inventory has increased, and for the other gases they are broadly unchanged. The InTEM decline in UK HFC-143a emissions is slower than the GHGI predicts. For HFC-32, HFC-152a, HFC-365mfc and HFC-245fa the recent estimates are diverging when InTEM and the GHGI are compared, with the GHGI increasing and InTEM decreasing. It is also noticable that, with the exception of HFC-143a and HFC-23, the InTEM estimates of UK emissions are smaller than those reported in the GHGI, sometimes strikingly so for example HFC-32, HFC-152a and HFC-227ea.

Figures 29, 24 and 34 show 3 year average emission maps and indicate that the model predicts the largest emission sources for HFC-125, HFC-134a and HFC-143a to be from Belgium, the Netherlands and central and southern regions of the UK. They also show evidence of emissions from the region around Paris which is considerably more pronounced for HFC-143a. The maps show generally increasing emissions over the 3 year time averaged periods presented, until a decrease is evident in 2017-2019 for HFC-143a. The downward trend in emissions seen in the annual timeseries for HFC-125 and HFC-134a is not easily apparent in the maps however, probably because the downturn is more recent than for HFC-143a and also less strong in the larger North West Europe region compared with the UK. In contrast, Figure 44 has a different spatial pattern than for Figures 29, 24 and 34, showing the largest modelled HFC-152a emissions are coming from Belgium, with a lesser emission source in the southern part of the UK. This gas is also showing strong evidence of a decrease over time in North West Europe when comparing the 3 year average maps.

Figures 59 and 54 for HFC-245fa and HFC-365mfc respectively, show very similar spatial distributions, with the dominant emissions coming from Belgium. Lesser magnitude emissions are also predicted to come from central and southern UK,the Paris region and the Netherlands. Figures 49 and 71 for HFC-227ea and HFC-4310mee have similar spatial distributions to each other with similarly elevated regions in central and southern UK, Paris, Belgium and the Netherlands.

4.9 HFC-134a

Globally, the atmospheric concentration of HFC-134a continues to grow at an accelerating rate. In 2018, the Northern Hemispheric baseline mole fraction grew at a rate of ∼6 ppt yr^{-1}, a significant increase on the ∼2 ppt yr^{-1} observed at the start of the record. UK emissions grew steadily until 2017, but fell considerably in the three years to 2020. A significant discrepancy still exists between InTEM and UK GHGI estimates - the inventory is larger in all reporting years. A similar trend is observed across NWEU. Across the UK and NWEU, populated areas are the most significant sources. In the UK, the largest emissions are from south east England.

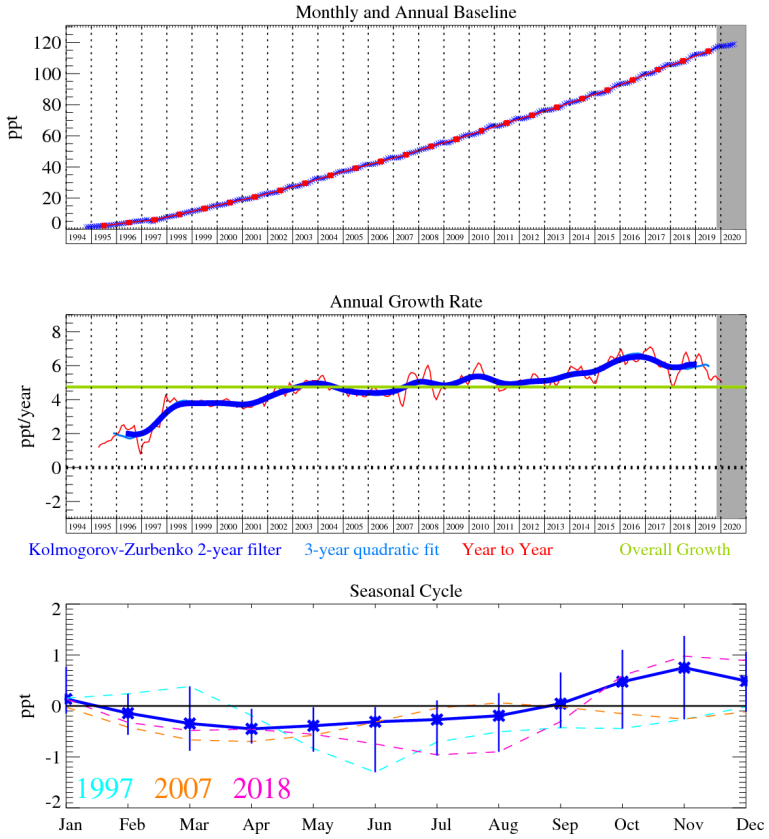

Figure 20: Monthly (blue) and annual (red) Mid-latitude Northern Hemisphere mole fractions (top plot). Annual (blue and red) and overall (green) growth rate (middle plot). Seasonal cycle (de-trended) with year-to-year variability (lower plot). Grey area covers un-ratified provisional data.

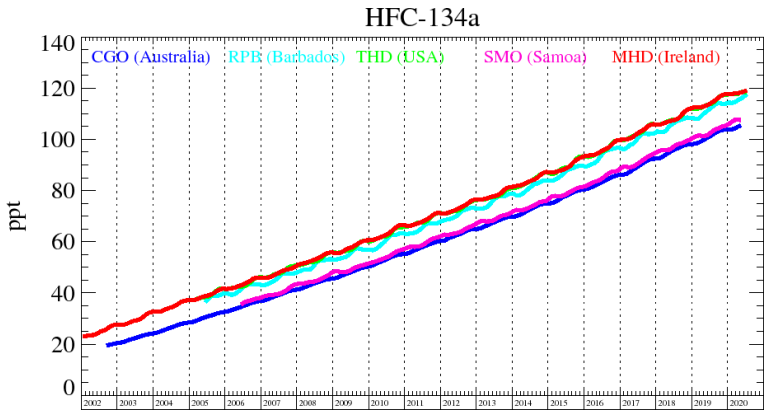

Figure 21: Background mole fractions at 5 AGAGE global stations

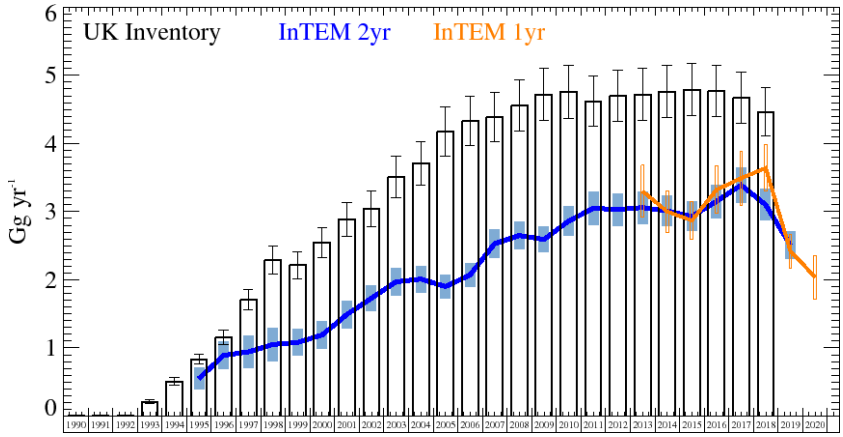

Figure 22: HFC-134a UK emission estimates (Gg yr^{-1}) from the UNFCCC GHGI (black) and InTEM (a) Annualised 2-year inversion (blue) (b) Annual inversion (orange). The uncertainty bars represent 1-σ.

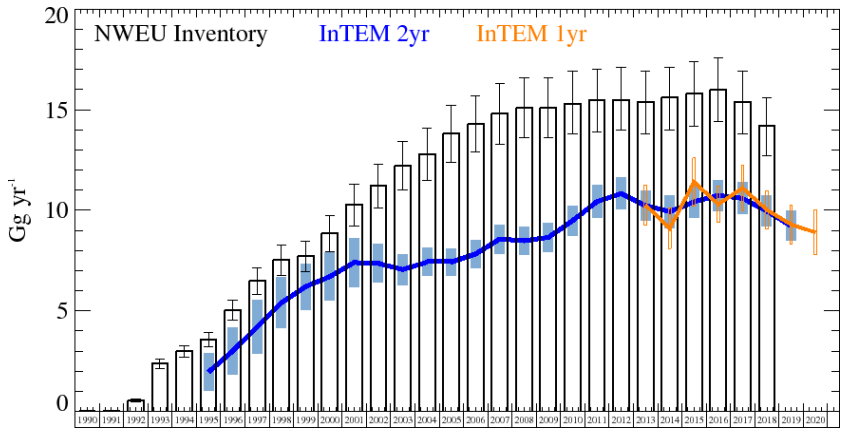

Figure 23: HFC-134a NWEU emission estimates (Gg yr^{-1}) from the UNFCCC GHGI (black) and InTEM (a) Annualised 2-year inversion (blue) (b) Annual inversion (orange). The uncertainty bars represent 1-σ.

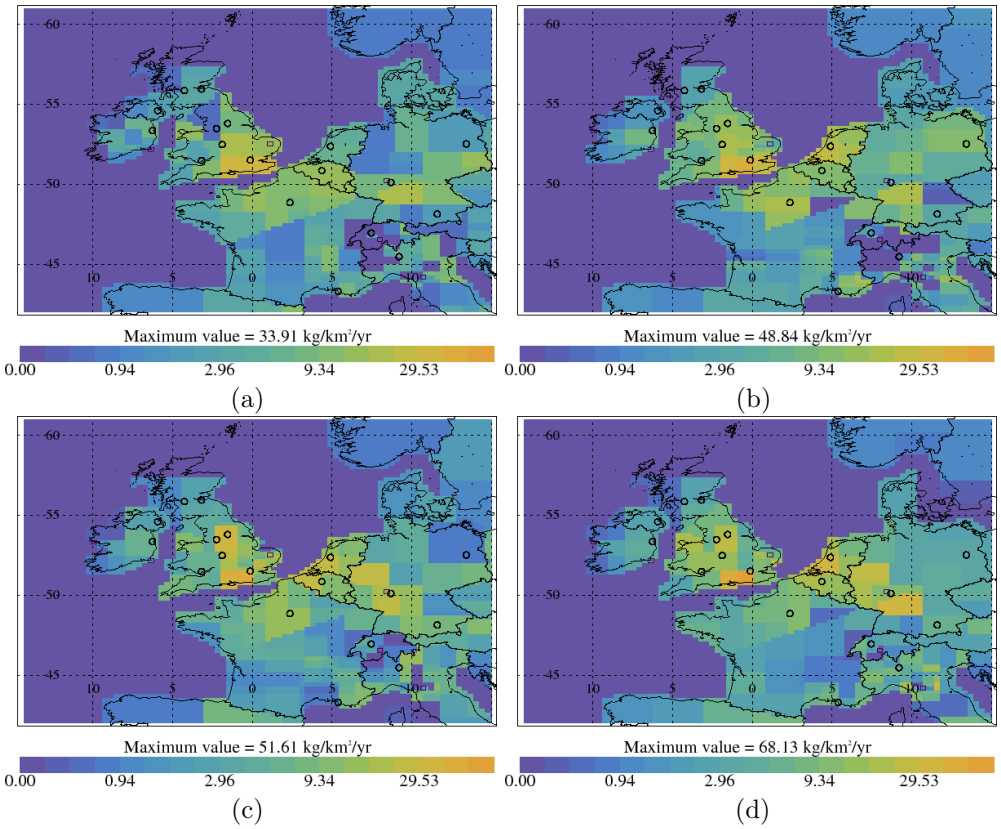

Figure 24: HFC-134a InTEM emission estimates (kg km^{-2} yr^{-1}) (a) 2008-2010 (b) 2011-2013 (c) 2014-2016 (d) 2017-2019

Table 10: UK and NWEU HFC-134a emission (Gg yr^{-1}) estimates with 1-σ uncertainty.

	UK			NWEU		
Years	Inventory	InTEM 2yr	InTEM 1yr	Inventory	InTEM 2yr	InTEM 1yr
1990	0.00 (0.00-0.00)			0.00 (0.00-0.01)		
1991	0.00 (0.00-0.00)			0.01 (0.00-0.02)		
1992	0.01 (0.00-0.01)			0.55 (0.49-0.60)		
1993	0.21 (0.19-0.24)			2.37 (2.14-2.61)		
1994	0.51 (0.46-0.57)			2.98 (2.68-3.27)		
1995	0.83 (0.76-0.91)	0.55 (0.39-0.71)		3.56 (3.20-3.92)	1.95 (1.00-2.89)	
1996	1.15 (1.05-1.26)	0.89 (0.69-1.09)		5.04 (4.54-5.54)	3.00 (1.90-4.20)	
1997	1.71 (1.56-1.86)	0.94 (0.70-1.18)		6.48 (5.83-7.13)	4.20 (2.80-5.50)	
1998	2.29 (2.09-2.49)	1.05 (0.81-1.29)		7.52 (6.77-8.27)	5.40 (4.10-6.60)	
1999	2.22 (2.02-2.41)	1.08 (0.89-1.28)		7.71 (6.94-8.48)	6.20 (5.10-7.40)	
2000	2.55 (2.32-2.77)	1.19 (0.99-1.38)		8.85 (7.96-9.73)	6.70 (5.50-7.90)	
2001	2.89 (2.64-3.14)	1.49 (1.28-1.69)		10.3 (9.2-11.3)	7.40 (6.20-8.60)	
2002	3.04 (2.78-3.30)	1.73 (1.54-1.92)		11.2 (10.1-12.3)	7.36 (6.40-8.33)	
2003	3.51 (3.21-3.81)	1.97 (1.77-2.17)		12.2 (11.0-13.4)	7.05 (6.28-7.83)	
2004	3.71 (3.39-4.02)	2.01 (1.82-2.21)		12.8 (11.5-14.1)	7.42 (6.72-8.11)	
2005	4.17 (3.82-4.53)	1.90 (1.73-2.08)		13.8 (12.4-15.2)	7.42 (6.76-8.08)	
2006	4.33 (3.97-4.70)	2.07 (1.90-2.24)		14.3 (12.9-15.7)	7.82 (7.12-8.52)	
2007	4.39 (4.03-4.75)	2.53 (2.33-2.74)		14.8 (13.3-16.3)	8.57 (7.86-9.29)	
2008	4.56 (4.18-4.94)	2.65 (2.45-2.86)		15.1 (13.6-16.6)	8.48 (7.80-9.16)	
2009	4.72 (4.34-5.11)	2.59 (2.41-2.78)		15.1 (13.6-16.6)	8.65 (7.95-9.35)	
2010	4.76 (4.37-5.15)	2.86 (2.64-3.07)		15.3 (13.8-16.9)	9.48 (8.73-10.23)	
2011	4.62 (4.25-4.99)	3.05 (2.81-3.29)		15.5 (13.9-17.0)	10.43 (9.62-11.24)	
2012	4.70 (4.32-5.08)	3.03 (2.80-3.27)		15.5 (14.0-17.1)	10.83 (10.04-11.62)	
2013	4.72 (4.34-5.10)	3.06 (2.82-3.29)	3.30 (2.92-3.68)	15.4 (13.8-16.9)	10.23 (9.49-10.97)	10.26 (9.26-11.25)
2014	4.76 (4.38-5.14)	3.01 (2.79-3.24)	3.00 (2.69-3.31)	15.6 (14.0-17.1)	9.93 (9.13-10.73)	9.10 (8.10-10.10)
2015	4.79 (4.41-5.17)	2.93 (2.72-3.15)	2.87 (2.59-3.15)	15.8 (14.2-17.4)	10.42 (9.61-11.22)	11.40 (10.20-12.60)
2016	4.77 (4.39-5.15)	3.15 (2.91-3.39)	3.32 (2.97-3.67)	16.0 (14.4-17.6)	10.74 (9.97-11.52)	10.30 (9.39-11.22)
2017	4.67 (4.30-5.05)	3.39 (3.13-3.65)	3.49 (3.10-3.89)	15.4 (13.8-16.9)	10.59 (9.79-11.38)	11.10 (10.00-12.30)
2018	4.46 (4.11-4.82)	3.10 (2.87-3.33)	3.64 (3.30-3.98)	14.2 (12.7-15.6)	9.96 (9.20-10.72)	10.02 (9.06-10.97)
2019		2.51 (2.31-2.71)	2.42 (2.17-2.67)		9.22 (8.48-9.96)	9.29 (8.34-10.24)
2020			2.04 (1.72-2.36)			8.9 (7.8-10.0)

4.10 HFC-125

The atmospheric concentration of HFC-125 is increasing globally. UK emissions increased through 2012, were roughly flat until 2017 and then fell dramatically. A similar pattern is seen across NWEU but the recent decrease is less sharp. Both in the UK and on the continent, populated areas are the most significant sources. The InTEM estimated emissions of HFC-125, both for the UK and NWEU (figures 27, 28) have risen considerably as a result of the improvements made to the modelling system, compared to those reported last year. The agreement between the model results and the inventory estimates are much closer, with the InTEM emissions now increasing at a similar rate to the inventory.

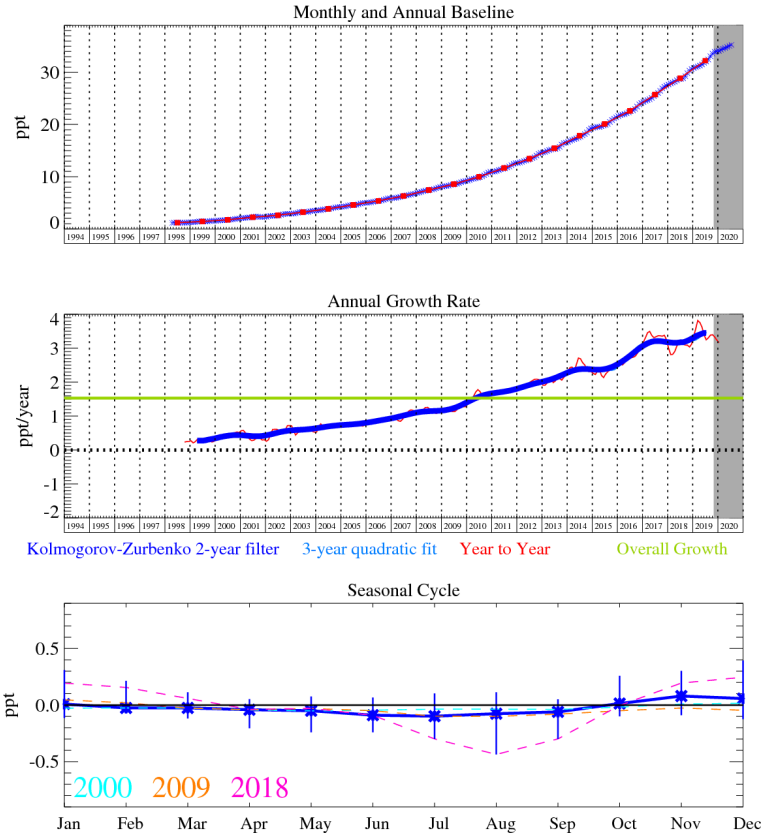

Figure 25: Monthly (blue) and annual (red) Mid-latitude Northern Hemisphere mole fractions (top plot). Annual (blue and red) and overall (green) growth rate (middle plot). Seasonal cycle (de-trended) with year-to-year variability (lower plot). Grey area covers un-ratified provisional data.

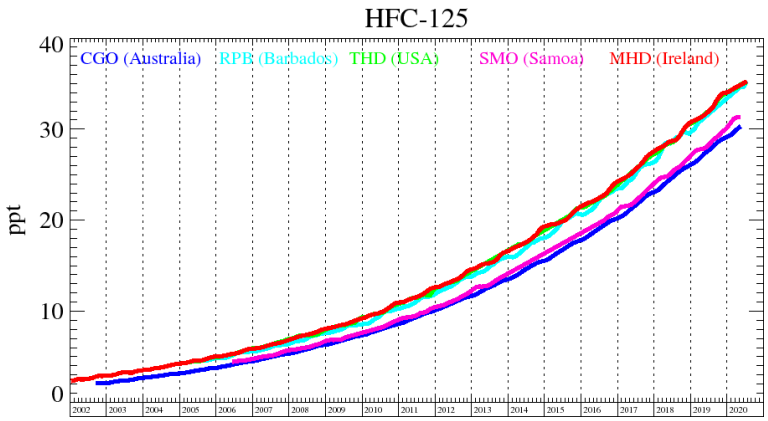

Figure 26: Background mole fractions at 5 AGAGE global stations

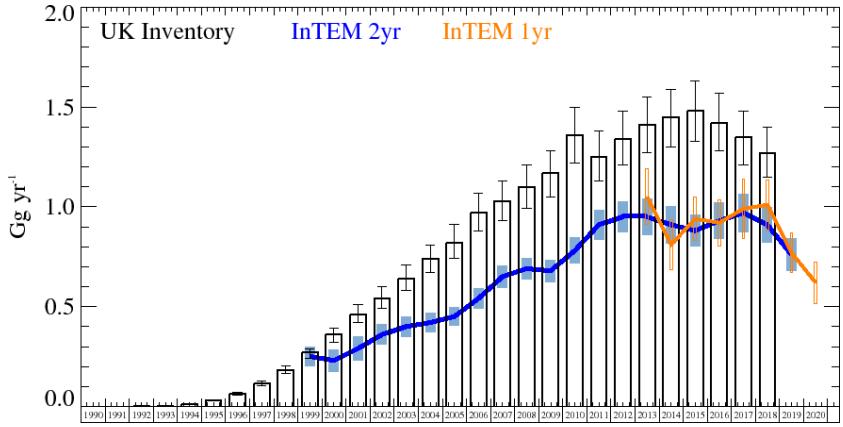

Figure 27: HFC-125 UK emission estimates (Gg yr^{-1}) from the UNFCCC GHGI (black) and InTEM (a) Annualised 2-year inversion (blue) (b) Annual inversion (orange). The uncertainty bars represent 1-σ.

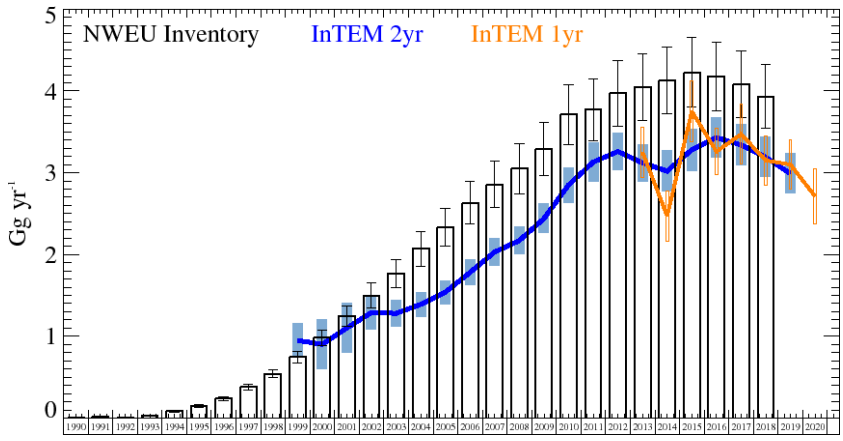

Figure 28: HFC-125 NWEU emission estimates (Gg yr^{-1}) from the UNFCCC GHGI (black) and InTEM (a) Annualised 2-year inversion (blue) (b) Annual inversion (orange). The uncertainty bars represent 1-σ.

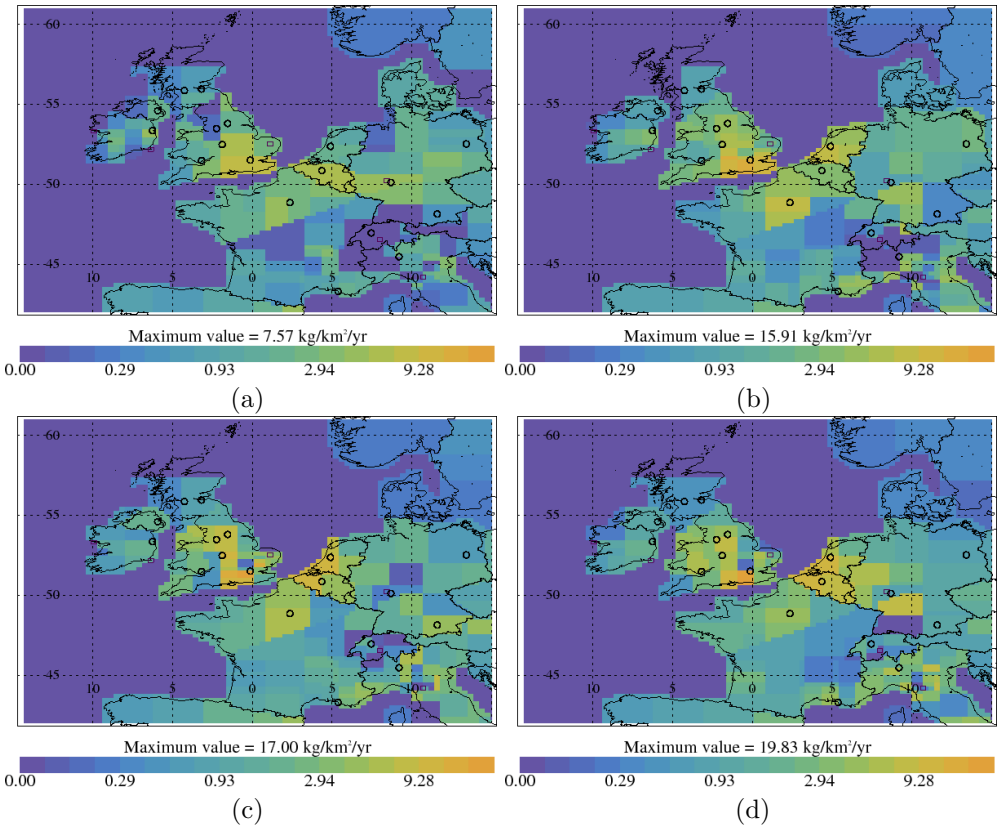

Figure 29: HFC-125 InTEM emission estimates (kg km^{-2} yr^{-1}) (a) 2008-2010 (b) 2011-2013 (c) 2014-2016 (d) 2017-2019

Table 11: UK HFC-125 emission (Gg yr^{-1}) estimates with 1-σ uncertainty.

	UK			NWEU		
Years	Inventory	InTEM 2yr	InTEM 1yr	Inventory	InTEM 2yr	InTEM 1yr
1990	0.00 (0.00-0.00)			0.01 (0.00-0.02)		
1991	0.00 (0.00-0.00)			0.01 (0.00-0.02)		
1992	0.00 (0.00-0.00)			0.01 (0.00-0.02)		
1993	0.00 (0.00-0.00)			0.03 (0.02-0.04)		
1994	0.01 (0.01-0.01)			0.08 (0.07-0.09)		
1995	0.03 (0.03-0.03)			0.15 (0.13-0.16)		
1996	0.06 (0.06-0.07)			0.24 (0.22-0.27)		
1997	0.12 (0.10-0.13)			0.38 (0.34-0.41)		
1998	0.18 (0.17-0.20)			0.54 (0.49-0.59)		
1999	0.27 (0.24-0.29)	0.25 (0.20-0.30)		0.75 (0.67-0.82)	0.95 (0.74-1.16)	
2000	0.36 (0.32-0.39)	0.23 (0.17-0.28)		0.98 (0.88-1.08)	0.90 (0.60-1.21)	
2001	0.46 (0.42-0.51)	0.29 (0.23-0.35)		1.25 (1.12-1.37)	1.10 (0.80-1.41)	
2002	0.54 (0.49-0.60)	0.36 (0.31-0.41)		1.50 (1.35-1.65)	1.29 (1.09-1.49)	
2003	0.64 (0.58-0.71)	0.40 (0.35-0.45)		1.77 (1.59-1.94)	1.28 (1.11-1.44)	
2004	0.74 (0.67-0.81)	0.42 (0.37-0.47)		2.07 (1.86-2.28)	1.39 (1.24-1.54)	
2005	0.82 (0.74-0.91)	0.45 (0.41-0.50)		2.33 (2.10-2.56)	1.54 (1.39-1.68)	
2006	0.97 (0.88-1.07)	0.54 (0.49-0.59)		2.63 (2.37-2.89)	1.78 (1.62-1.93)	
2007	1.03 (0.93-1.13)	0.65 (0.60-0.71)		2.85 (2.57-3.14)	2.03 (1.87-2.20)	
2008	1.10 (0.99-1.21)	0.69 (0.63-0.74)		3.05 (2.74-3.35)	2.17 (2.00-2.34)	
2009	1.17 (1.05-1.28)	0.68 (0.63-0.74)		3.29 (2.96-3.62)	2.44 (2.26-2.62)	
2010	1.36 (1.22-1.50)	0.78 (0.72-0.85)		3.71 (3.34-4.08)	2.85 (2.64-3.07)	
2011	1.25 (1.13-1.38)	0.91 (0.84-0.99)		3.77 (3.39-4.15)	3.13 (2.89-3.36)	
2012	1.34 (1.21-1.48)	0.95 (0.88-1.03)		3.97 (3.57-4.37)	3.26 (3.03-3.49)	
2013	1.41 (1.27-1.55)	0.95 (0.86-1.04)	1.05 (0.91-1.19)	4.05 (3.64-4.45)	3.12 (2.89-3.35)	3.25 (2.94-3.56)
2014	1.45 (1.30-1.59)	0.91 (0.81-1.00)	0.81 (0.68-0.93)	4.13 (3.72-4.54)	3.02 (2.77-3.27)	2.47 (2.16-2.78)
2015	1.48 (1.33-1.63)	0.88 (0.80-0.96)	0.94 (0.83-1.05)	4.22 (3.80-4.65)	3.28 (3.03-3.54)	3.75 (3.38-4.12)
2016	1.42 (1.28-1.57)	0.93 (0.84-1.02)	0.92 (0.81-1.04)	4.18 (3.76-4.60)	3.43 (3.19-3.68)	3.26 (2.97-3.54)
2017	1.35 (1.21-1.48)	0.97 (0.88-1.07)	0.99 (0.84-1.14)	4.08 (3.67-4.49)	3.34 (3.09-3.59)	3.47 (3.10-3.83)
2018	1.27 (1.15-1.40)	0.91 (0.82-1.00)	1.01 (0.88-1.13)	3.93 (3.54-4.32)	3.19 (2.94-3.43)	3.15 (2.85-3.45)
2019		0.76 (0.68-0.84)	0.77 (0.67-0.87)		2.99 (2.74-3.23)	3.10 (2.80-3.40)
2020			0.62 (0.51-0.72)			2.71 (2.37-3.05)

4.11 HFC-143a

The atmospheric concentration of HFC-143a is increasing globally, however the rate of increase has now been constant since 2016. InTEM UK emissions increased rapidly between 2005-2007 followed by a period of stability until 2012, after which emissions began to decline. In recent years the rate of decline has increased. The UK GHGI has a dramatic decline in 2011 that is not mirrored by InTEM. However, this step-change brings the inventory within good agreement with InTEM until 2016. From 2017 onwards, the rate of decline in the UK GHGI is far greater than that predicted by InTEM. For NWEU, there is very good agreement between the GHGI and InTEM from 2012 onwards. The largest UK sources of HFC-143a are associated with populated regions, particularly in the south east.

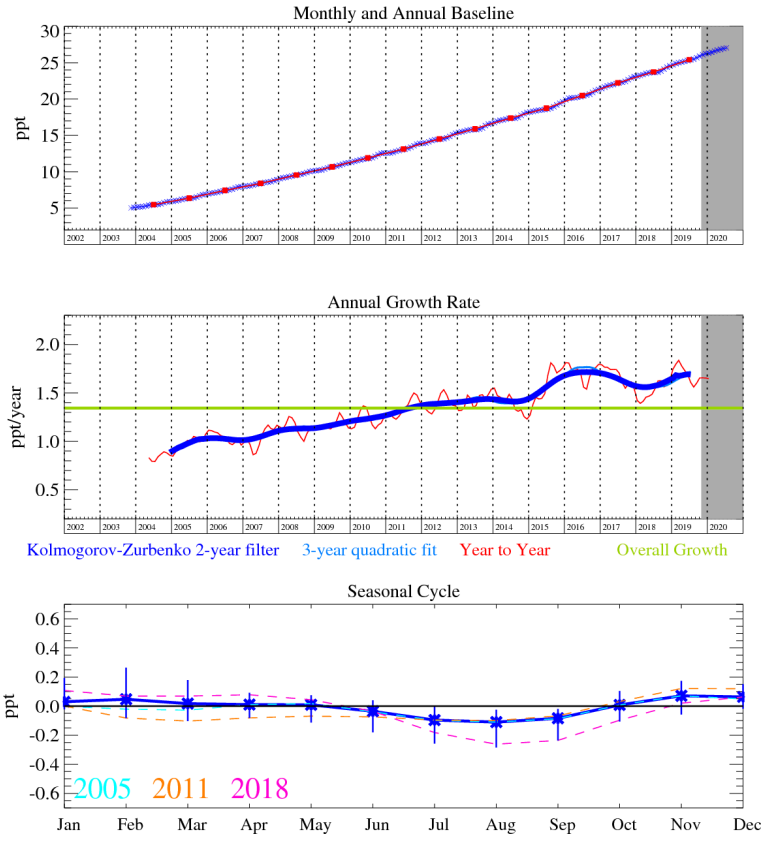

Figure 30: Monthly (blue) and annual (red) Mid-latitude Northern Hemisphere mole fractions (top plot). Annual (blue and red) and overall (green) growth rate (middle plot). Seasonal cycle (de-trended) with year-to-year variability (lower plot). Grey area covers un-ratified provisional data.

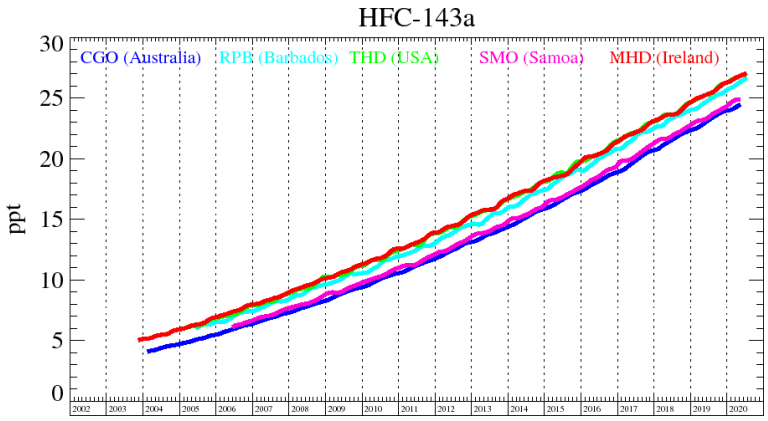

Figure 31: Background mole fractions at 5 AGAGE global stations

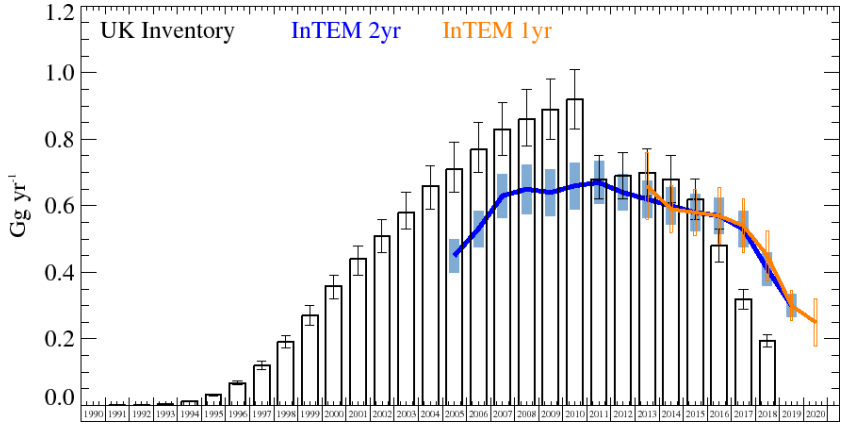

Figure 32: HFC-143a UK emission estimates (Gg yr^{-1}) from the UNFCCC GHGI (black) and InTEM (a) Annualised 2-year inversion (blue) (b) Annual inversion (orange). The uncertainty bars represent 1-σ.

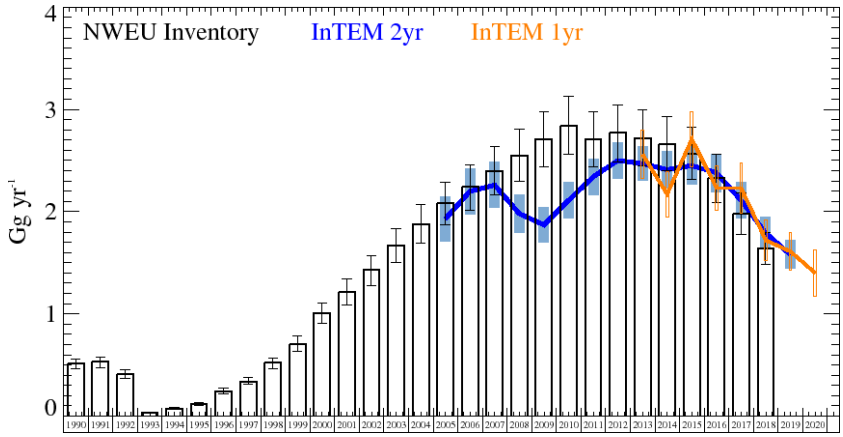

Figure 33: HFC-143a NWEU emission estimates (Gg yr^{-1}) from the UNFCCC GHGI (black) and InTEM (a) Annualised 2-year inversion (blue) (b) Annual inversion (orange). The uncertainty bars represent 1-σ.

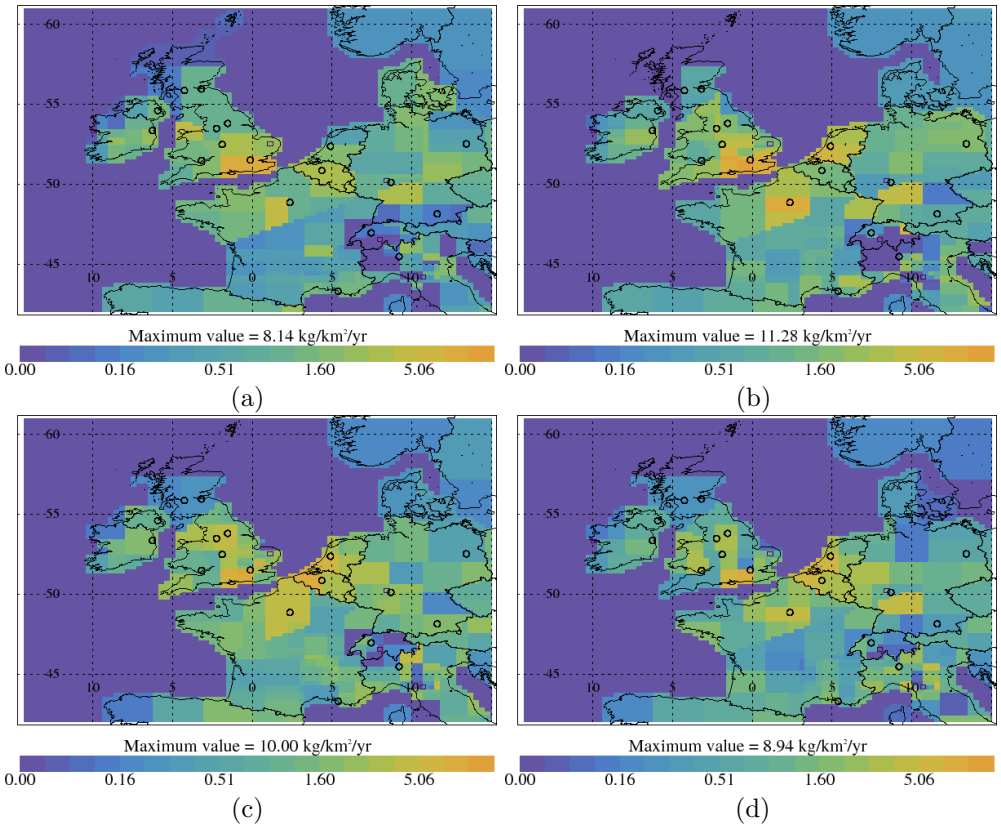

Figure 34: HFC-143a InTEM emission estimates (kg km^{-2} yr^{-1}) (a) 2008-2010 (b) 2011-2013 (c) 2014-2016 (d) 2017-2019

Table 12: UK and NWEU HFC-143a emission (Gg yr^{-1}) estimates with 1-σ uncertainty.

	UK			NWEU		
Years	Inventory	InTEM 2yr	InTEM 1yr	Inventory	InTEM 2yr	InTEM 1yr
1990	0.00 (0.00-0.01)			0.51 (0.46-0.56)		
1991	0.00 (0.00-0.01)			0.53 (0.47-0.58)		
1992	0.00 (0.00-0.01)			0.41 (0.37-0.45)		
1993	0.00 (0.00-0.01)			0.03 (0.02-0.04)		
1994	0.01 (0.01-0.02)			0.07 (0.06-0.08)		
1995	0.03 (0.02-0.04)			0.12 (0.10-0.13)		
1996	0.07 (0.06-0.08)			0.25 (0.22-0.27)		
1997	0.12 (0.10-0.13)			0.34 (0.31-0.38)		
1998	0.19 (0.17-0.21)			0.52 (0.46-0.57)		
1999	0.27 (0.24-0.30)			0.70 (0.63-0.78)		
2000	0.36 (0.32-0.39)			1.01 (0.91-1.11)		
2001	0.44 (0.39-0.48)			1.21 (1.09-1.34)		
2002	0.51 (0.46-0.56)			1.43 (1.28-1.57)		
2003	0.58 (0.53-0.64)			1.67 (1.50-1.83)		
2004	0.66 (0.59-0.72)			1.88 (1.69-2.07)		
2005	0.71 (0.64-0.79)	0.45 (0.40-0.50)		2.08 (1.87-2.29)	1.93 (1.71-2.15)	
2006	0.77 (0.70-0.85)	0.53 (0.48-0.59)		2.24 (2.01-2.46)	2.20 (1.97-2.42)	
2007	0.83 (0.75-0.91)	0.63 (0.56-0.69)		2.40 (2.16-2.64)	2.26 (2.03-2.48)	
2008	0.86 (0.78-0.95)	0.65 (0.57-0.72)		2.55 (2.30-2.81)	1.98 (1.79-2.17)	
2009	0.89 (0.80-0.98)	0.64 (0.57-0.71)		2.71 (2.44-2.98)	1.87 (1.69-2.04)	
2010	0.92 (0.83-1.01)	0.66 (0.59-0.73)		2.84 (2.56-3.13)	2.11 (1.93-2.28)	
2011	0.68 (0.62-0.75)	0.67 (0.60-0.73)		2.71 (2.44-2.98)	2.34 (2.16-2.52)	
2012	0.69 (0.62-0.76)	0.64 (0.59-0.70)		2.77 (2.49-3.04)	2.50 (2.32-2.68)	
2013	0.70 (0.63-0.77)	0.62 (0.57-0.68)	0.66 (0.56-0.76)	2.72 (2.45-3.00)	2.47 (2.30-2.64)	2.56 (2.33-2.80)
2014	0.68 (0.61-0.75)	0.60 (0.55-0.66)	0.59 (0.52-0.66)	2.66 (2.40-2.93)	2.41 (2.23-2.59)	2.17 (1.95-2.40)
2015	0.62 (0.56-0.68)	0.58 (0.52-0.63)	0.58 (0.51-0.65)	2.57 (2.32-2.83)	2.45 (2.27-2.64)	2.71 (2.44-2.98)
2016	0.48 (0.43-0.53)	0.57 (0.52-0.63)	0.57 (0.49-0.66)	2.33 (2.09-2.56)	2.38 (2.19-2.56)	2.23 (2.01-2.45)
2017	0.32 (0.29-0.35)	0.53 (0.47-0.58)	0.54 (0.46-0.62)	1.98 (1.78-2.18)	2.11 (1.94-2.29)	2.23 (1.99-2.48)
2018	0.19 (0.18-0.21)	0.41 (0.36-0.46)	0.45 (0.38-0.53)	1.64 (1.48-1.80)	1.79 (1.64-1.95)	1.72 (1.52-1.91)
2019		0.30 (0.27-0.34)	0.30 (0.25-0.34)		1.58 (1.44-1.72)	1.61 (1.43-1.80)
2020			0.25 (0.18-0.32)			1.40 (1.18-1.63)

4.12 HFC-32

The global atmospheric concentration of HFC-32 is increasing at an accelerating rate, and the hemispheric gradient is growing. The UK GHGI shows a rapid increase in emissions over the reporting period, in contrast to InTEM which shows a roughly linear increase from 2005 until 2018 and a small decrease thereafter. The UK GHGI is considerably greater than InTEM in all reporting years. A similar picture is seen across NWEU, but the UK accounts for ∼40% of the NWEU estimates. While the InTEM estimates indicate a decline in emissions in recent years, the emissions maps shown in Figure 39 show a persistent source in south east England that has increased in strength across the reporting period. Further years of data will be required to see if this source continues to grow whilst UK emissions as a whole decline.

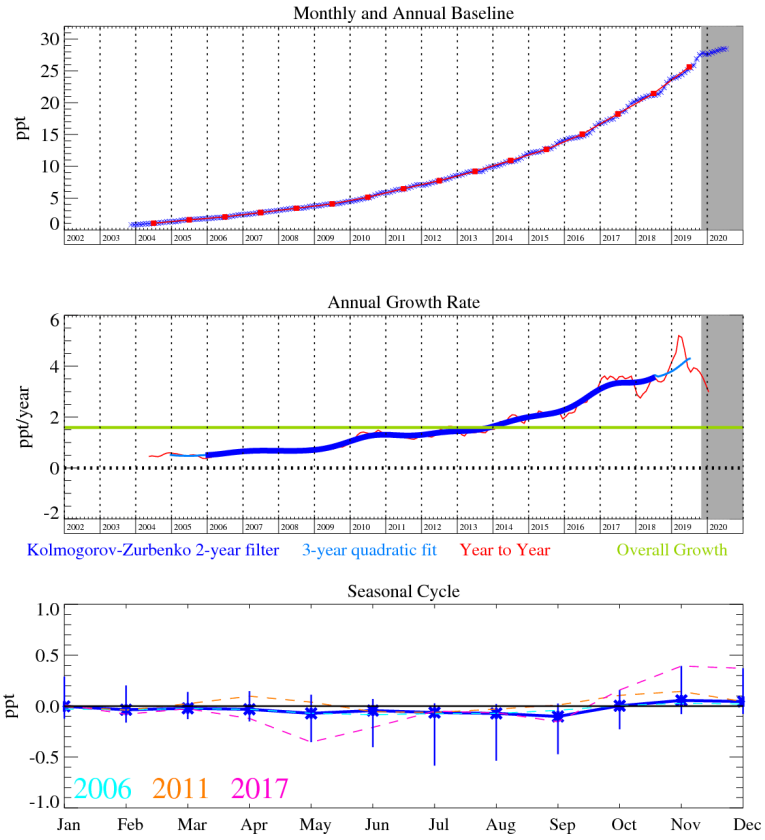

Figure 35: Monthly (blue) and annual (red) Mid-latitude Northern Hemisphere mole fractions (top plot). Annual (blue and red) and overall (green) growth rate (middle plot). Seasonal cycle (de-trended) with year-to-year variability (lower plot). Grey area covers un-ratified provisional data.

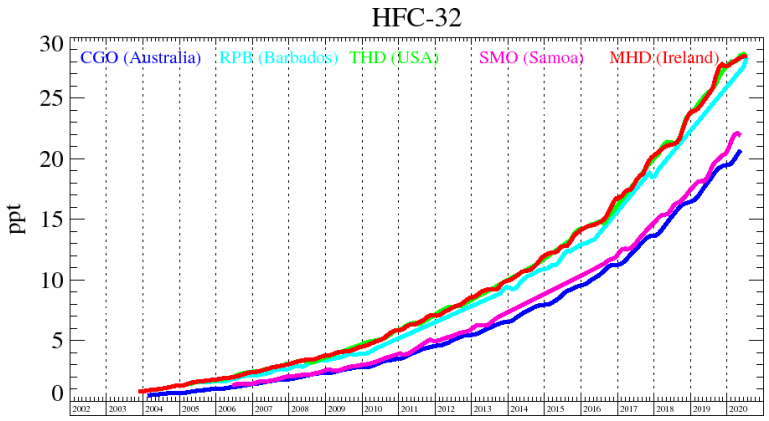

Figure 36: Background mole fractions at 5 AGAGE global stations

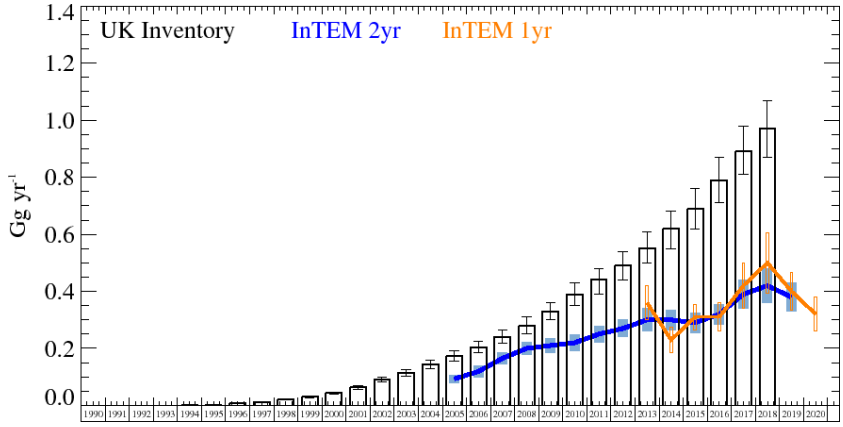

Figure 37: HFC-32 UK emission estimates (Gg yr^{-1}) from the UNFCCC GHGI (black) and InTEM (a) Annualised 2-year inversion (blue) (b) Annual inversion (orange). The uncertainty bars represent 1-σ.

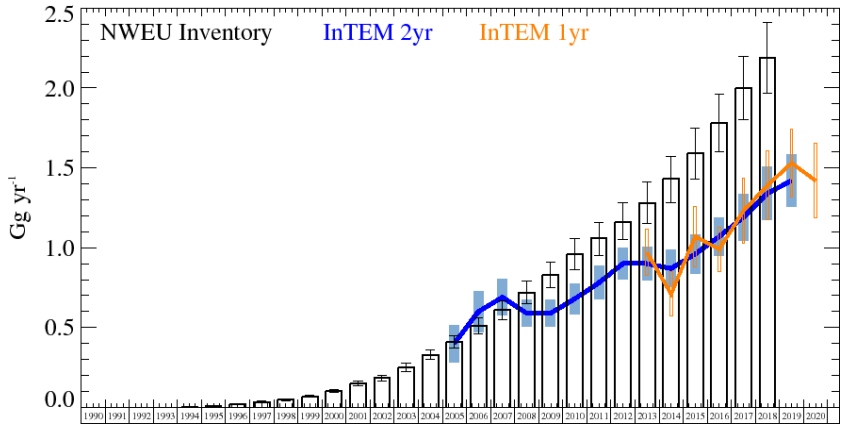

Figure 38: HFC-32 NWEU emission estimates (Gg yr^{-1}) from the UNFCCC GHGI (black) and InTEM (a) Annualised 2-year inversion (blue) (b) Annual inversion (orange). The uncertainty bars represent 1-σ.

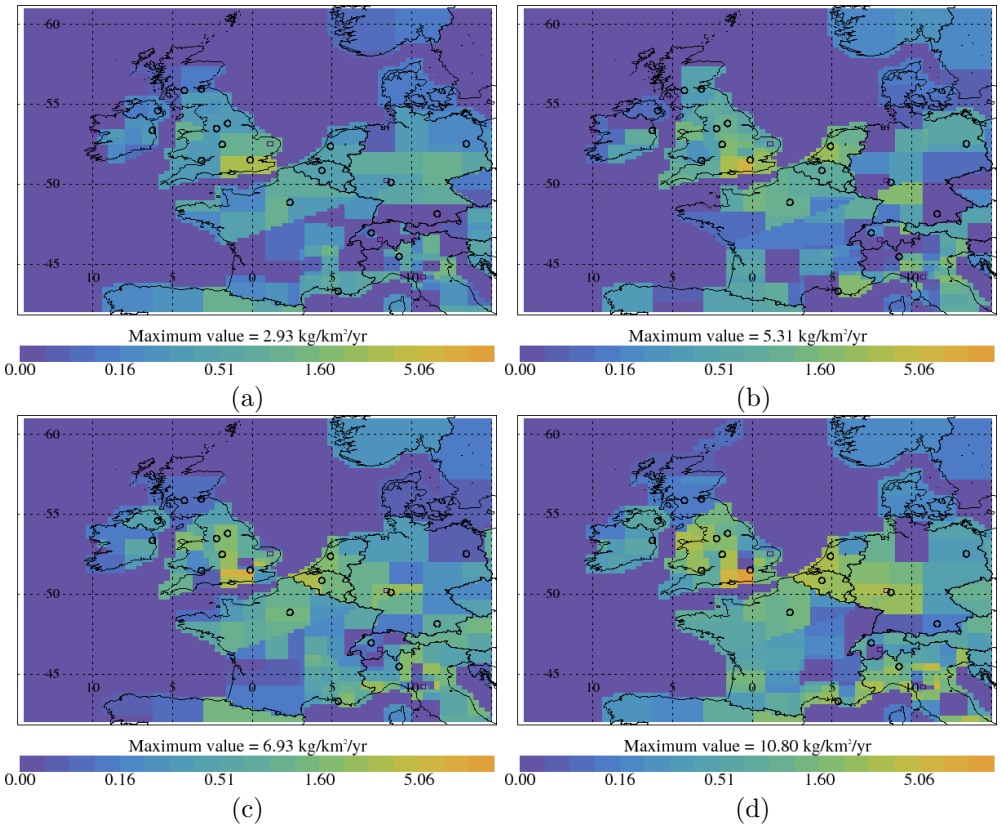

Figure 39: HFC-32 InTEM emission estimates (kg km^{-2} yr^{-1}) (a) 2008-2010 (b) 2011-2013 (c) 2014-2016 (d) 2017-2019

Table 13: UK and NWEU HFC-32 emission (Gg yr^{-1}) estimates with 1-σ uncertainty.

	UK			NWEU		
Years	Inventory	InTEM 2yr	InTEM 1yr	Inventory	InTEM 2yr	InTEM 1yr
1990	0.00 (0.00-0.01)			0.00 (0.00-0.01)		
1991	0.00 (0.00-0.01)			0.00 (0.00-0.01)		
1992	0.00 (0.00-0.01)			0.00 (0.00-0.01)		
1993	0.00 (0.00-0.01)			0.00 (0.00-0.01)		
1994	0.00 (0.00-0.01)			0.00 (0.00-0.01)		
1995	0.00 (0.00-0.01)			0.01 (0.00-0.02)		
1996	0.01 (0.00-0.02)			0.02 (0.01-0.03)		
1997	0.01 (0.00-0.02)			0.04 (0.03-0.05)		
1998	0.02 (0.01-0.03)			0.05 (0.04-0.06)		
1999	0.03 (0.02-0.04)			0.07 (0.06-0.08)		
2000	0.04 (0.03-0.05)			0.10 (0.09-0.11)		
2001	0.06 (0.05-0.07)			0.15 (0.13-0.17)		
2002	0.09 (0.08-0.10)			0.18 (0.16-0.20)		
2003	0.12 (0.10-0.13)			0.25 (0.22-0.28)		
2004	0.14 (0.13-0.16)			0.33 (0.30-0.36)		
2005	0.17 (0.16-0.19)	0.09 (0.08-0.11)		0.41 (0.37-0.45)	0.40 (0.28-0.51)	
2006	0.20 (0.18-0.23)	0.12 (0.10-0.14)		0.51 (0.46-0.56)	0.60 (0.47-0.73)	
2007	0.24 (0.22-0.27)	0.17 (0.14-0.19)		0.61 (0.55-0.67)	0.69 (0.57-0.80)	
2008	0.28 (0.25-0.31)	0.20 (0.18-0.22)		0.72 (0.65-0.79)	0.59 (0.51-0.68)	
2009	0.33 (0.30-0.36)	0.21 (0.18-0.23)		0.83 (0.75-0.91)	0.59 (0.50-0.67)	
2010	0.39 (0.35-0.43)	0.22 (0.19-0.25)		0.96 (0.86-1.06)	0.68 (0.58-0.77)	
2011	0.44 (0.39-0.48)	0.25 (0.22-0.28)		1.06 (0.95-1.16)	0.78 (0.67-0.88)	
2012	0.49 (0.44-0.54)	0.27 (0.24-0.30)		1.16 (1.05-1.28)	0.90 (0.80-1.00)	
2013	0.55 (0.50-0.61)	0.30 (0.26-0.34)	0.36 (0.30-0.42)	1.28 (1.15-1.41)	0.90 (0.79-1.00)	0.97 (0.82-1.11)
2014	0.62 (0.55-0.68)	0.30 (0.26-0.33)	0.23 (0.19-0.28)	1.43 (1.28-1.57)	0.87 (0.75-0.98)	0.71 (0.57-0.85)
2015	0.69 (0.62-0.76)	0.29 (0.25-0.32)	0.31 (0.26-0.35)	1.59 (1.43-1.75)	0.96 (0.84-1.08)	1.07 (0.88-1.26)
2016	0.79 (0.71-0.87)	0.32 (0.29-0.36)	0.31 (0.26-0.36)	1.78 (1.60-1.96)	1.07 (0.95-1.19)	0.99 (0.85-1.13)
2017	0.89 (0.81-0.98)	0.39 (0.34-0.44)	0.42 (0.34-0.50)	2.00 (1.80-2.20)	1.19 (1.04-1.33)	1.23 (1.03-1.44)
2018	0.97 (0.87-1.07)	0.42 (0.36-0.48)	0.50 (0.40-0.61)	2.19 (1.97-2.41)	1.34 (1.17-1.50)	1.39 (1.18-1.61)
2019		0.38 (0.33-0.43)	0.40 (0.33-0.46)		1.42 (1.25-1.58)	1.53 (1.32-1.74)
2020			0.32 (0.26-0.38)			1.42 (1.19-1.66)

4.13 HFC-152a

The atmospheric concentration has been flat since 2012 but there are signs of a rise in the last 2 years. HFC-152a has a strong seasonal cycle and a large inter-hemispheric gradient due to its short lifetime. UK InTEM emissions have been relatively flat, and falling from 2018. The UK InTEM emissions are very different when compared with the GHGI estimates. InTEM is largely flat from 2013 to 2017 at around 0.1 Gg /yr, then falling rapidly from 2017. The GHGI however is rising steadily from 2010. Figure 44 indicates that Southern England and Belgium are the most significant sources.

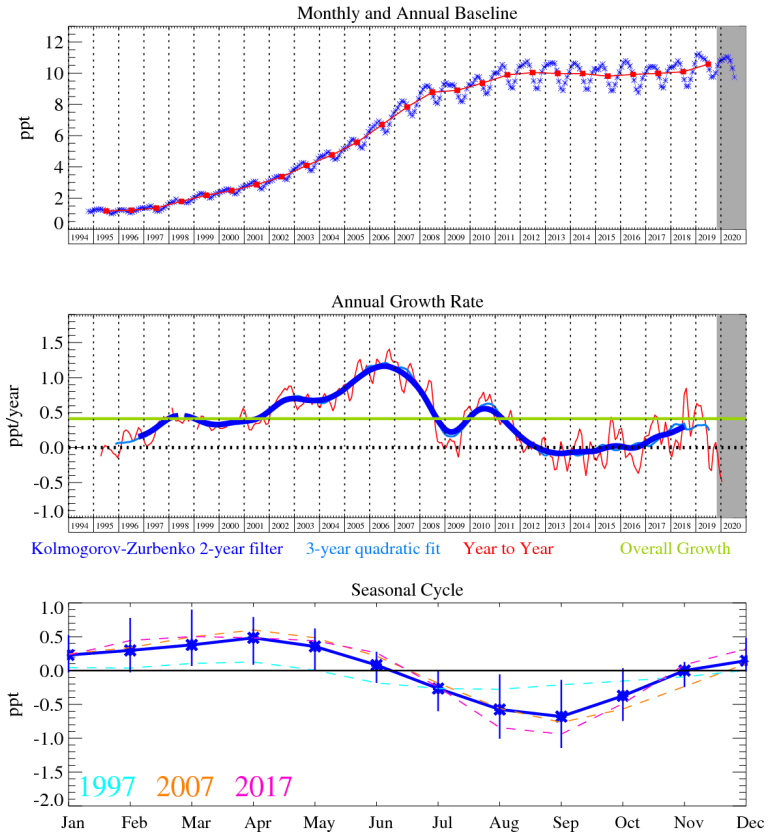

Figure 40: Monthly (blue) and annual (red) Mid-latitude Northern Hemisphere mole fractions (top plot). Annual (blue and red) and overall (green) growth rate (middle plot). Seasonal cycle (de-trended) with year-to-year variability (lower plot). Grey area covers un-ratified provisional data.

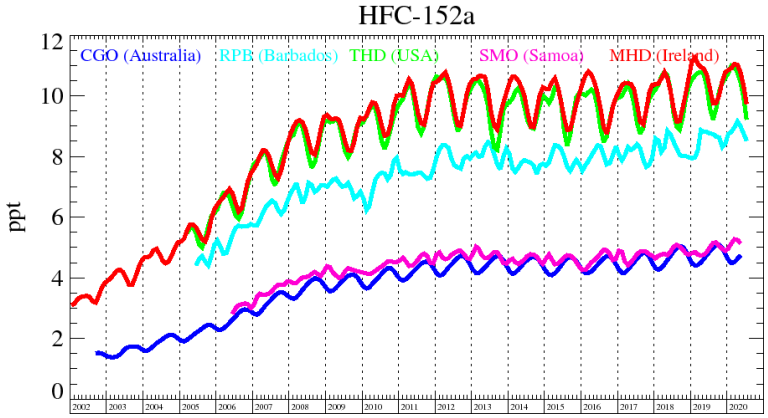

Figure 41: Background mole fractions at 5 AGAGE global stations

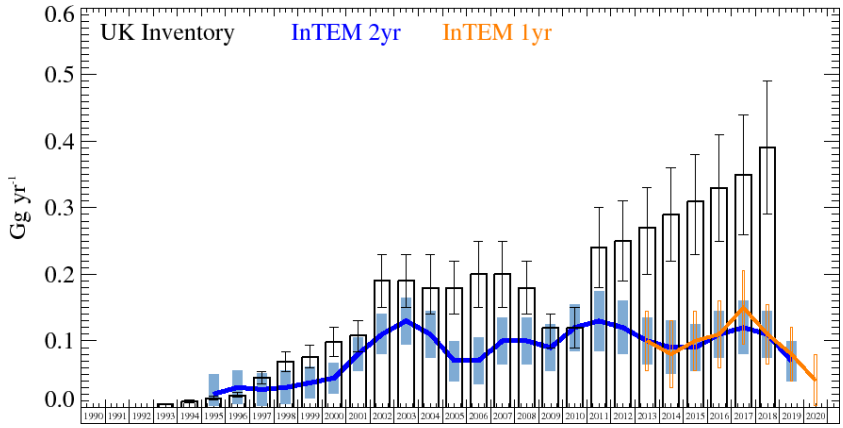

Figure 42: HFC-152a UK emission estimates (Gg yr^{-1}) from the UNFCCC GHGI (black) and InTEM (a) Annualised 2-year inversion (blue) (b) Annual inversion (orange). The uncertainty bars represent 1-σ.

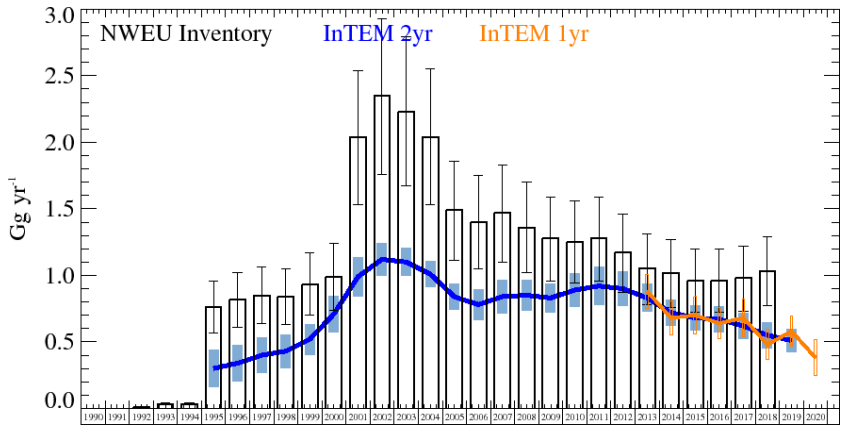

Figure 43: HFC-152a NWEU emission estimates (Gg yr^{-1}) from the UNFCCC GHGI (black) and InTEM (a) Annualised 2-year inversion (blue) (b) Annual inversion (orange). The uncertainty bars represent 1-σ.

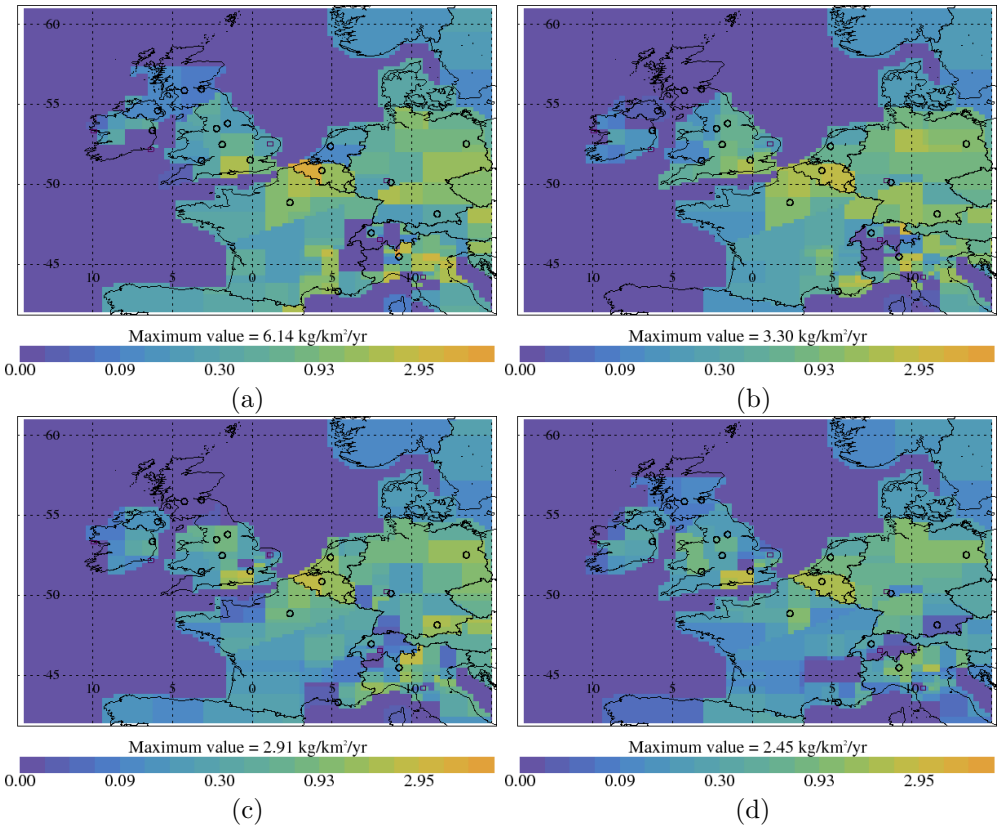

Figure 44: HFC-152a InTEM emission estimates (kg km^{-2} yr^{-1}) (a) 2008-2010 (b) 2011-2013 (c) 2014-2016 (d) 2017-2019

Table 14: UK and NWEU HFC-152a emission (Gg yr^{-1}) estimates with 1-σ uncertainty.

	UK			NWEU		
Years	Inventory	InTEM 2yr	InTEM 1yr	Inventory	InTEM 2yr	InTEM 1yr
1990	0.00 (0.00-0.00)			0.00 (0.00-0.01)		
1991	0.00 (0.00-0.00)			0.00 (0.00-0.01)		
1992	0.00 (0.00-0.00)			0.01 (0.00-0.02)		
1993	0.01 (0.00-0.01)			0.03 (0.02-0.04)		
1994	0.01 (0.00-0.01)			0.03 (0.02-0.04)		
1995	0.01 (0.01-0.02)	0.02 (0.00-0.06)		0.76 (0.57-0.96)	0.30 (0.16-0.44)	
1996	0.01 (0.01-0.02)	0.03 (0.01-0.06)		0.82 (0.61-1.02)	0.34 (0.21-0.48)	
1997	0.05 (0.04-0.05)	0.03 (0.00-0.05)		0.85 (0.64-1.06)	0.40 (0.26-0.53)	
1998	0.07 (0.05-0.08)	0.03 (0.01-0.06)		0.84 (0.63-1.05)	0.43 (0.31-0.56)	
1999	0.08 (0.06-0.09)	0.04 (0.01-0.06)		0.93 (0.70-1.17)	0.52 (0.41-0.64)	
2000	0.10 (0.08-0.12)	0.04 (0.02-0.07)		0.99 (0.74-1.24)	0.71 (0.58-0.85)	
2001	0.11 (0.08-0.13)	0.08 (0.05-0.10)		2.04 (1.53-2.54)	0.99 (0.84-1.13)	
2002	0.19 (0.15-0.23)	0.11 (0.08-0.14)		2.35 (1.76-2.93)	1.12 (0.99-1.24)	
2003	0.19 (0.15-0.23)	0.13 (0.09-0.16)		2.23 (1.67-2.79)	1.10 (1.00-1.21)	
2004	0.18 (0.14-0.23)	0.11 (0.07-0.14)		2.04 (1.53-2.55)	1.01 (0.91-1.11)	
2005	0.18 (0.14-0.22)	0.07 (0.04-0.10)		1.49 (1.11-1.86)	0.84 (0.74-0.94)	
2006	0.20 (0.15-0.25)	0.07 (0.04-0.11)		1.40 (1.05-1.75)	0.78 (0.66-0.89)	
2007	0.20 (0.15-0.25)	0.10 (0.06-0.13)		1.47 (1.10-1.83)	0.84 (0.71-0.96)	
2008	0.18 (0.14-0.22)	0.10 (0.06-0.13)		1.36 (1.02-1.70)	0.85 (0.73-0.96)	
2009	0.12 (0.09-0.14)	0.09 (0.06-0.13)		1.28 (0.96-1.59)	0.83 (0.72-0.94)	
2010	0.12 (0.09-0.15)	0.12 (0.08-0.15)		1.25 (0.94-1.56)	0.89 (0.77-1.02)	
2011	0.24 (0.18-0.30)	0.13 (0.09-0.18)		1.28 (0.96-1.59)	0.92 (0.78-1.07)	
2012	0.25 (0.19-0.31)	0.12 (0.08-0.16)		1.17 (0.87-1.46)	0.90 (0.77-1.03)	
2013	0.27 (0.20-0.33)	0.10 (0.06-0.13)	0.10 (0.06-0.15)	1.05 (0.78-1.31)	0.83 (0.72-0.93)	0.88 (0.75-1.01)
2014	0.29 (0.22-0.36)	0.09 (0.05-0.13)	0.08 (0.03-0.13)	1.02 (0.76-1.27)	0.72 (0.62-0.82)	0.68 (0.55-0.81)
2015	0.31 (0.23-0.38)	0.09 (0.06-0.13)	0.10 (0.06-0.15)	0.96 (0.72-1.20)	0.68 (0.58-0.77)	0.70 (0.56-0.84)
2016	0.33 (0.25-0.41)	0.11 (0.07-0.14)	0.11 (0.06-0.16)	0.96 (0.72-1.20)	0.67 (0.58-0.77)	0.64 (0.53-0.76)
2017	0.35 (0.26-0.44)	0.12 (0.08-0.16)	0.15 (0.10-0.21)	0.98 (0.73-1.22)	0.62 (0.52-0.71)	0.68 (0.54-0.82)
2018	0.39 (0.29-0.49)	0.11 (0.07-0.14)	0.11 (0.07-0.16)	1.03 (0.77-1.29)	0.55 (0.45-0.64)	0.48 (0.37-0.60)
2019		0.07 (0.04-0.10)	0.08 (0.04-0.12)		0.51 (0.42-0.60)	0.58 (0.46-0.69)
2020			0.04 (0.00-0.08)			0.38 (0.24-0.51)

4.14 HFC-227ea

The atmospheric concentration is increasing globally and accelerating with a widening hemispheric gradient. The UK GHGI emission estimates more than twice those estimated by InTEM. InTEM looks to be showing a decline after 2018. The UK emissions are about half of the NWEU emissions in both estimates. The spatial pattern of the InTEM estimates (Figure 49) largely follows population, with high emissions also observed from the Benelux countries.

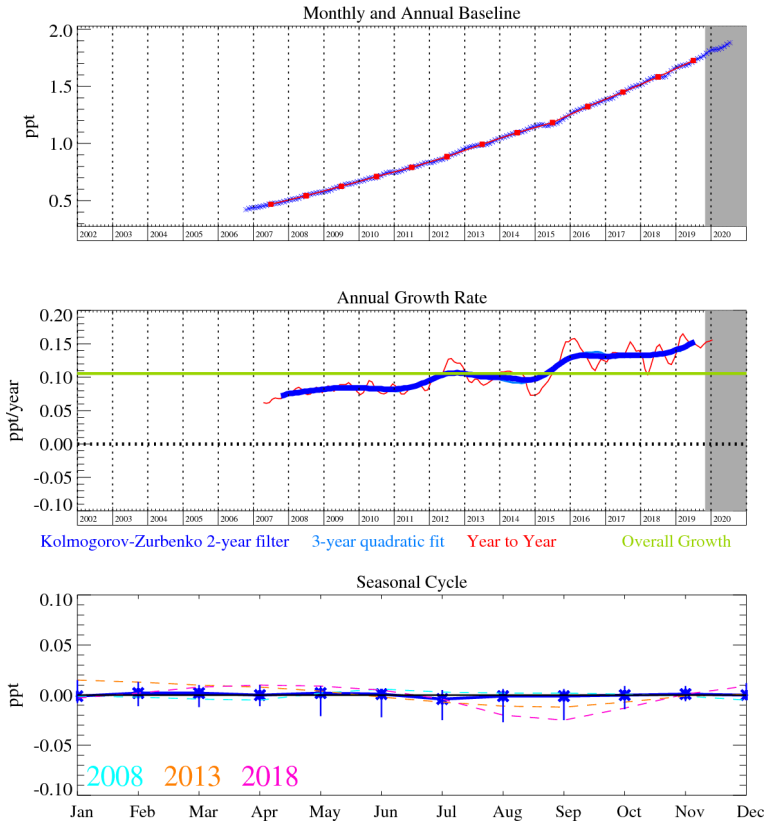

Figure 45: Monthly (blue) and annual (red) Mid-latitude Northern Hemisphere mole fractions (top plot). Annual (blue and red) and overall (green) growth rate (middle plot). Seasonal cycle (de-trended) with year-to-year variability (lower plot). Grey area covers un-ratified provisional data.

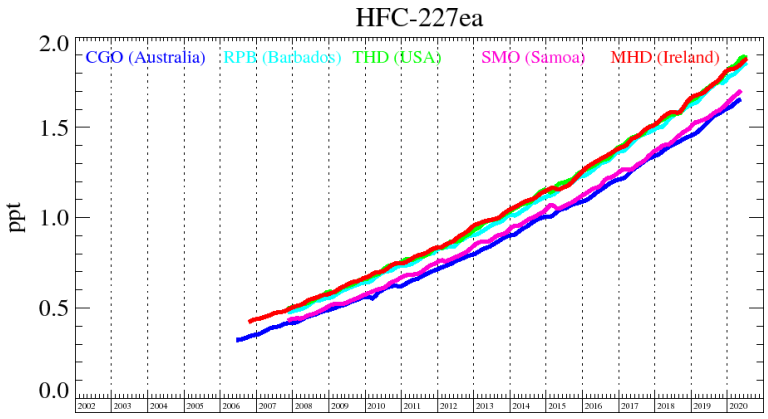

Figure 46: Background mole fractions at 5 AGAGE global stations

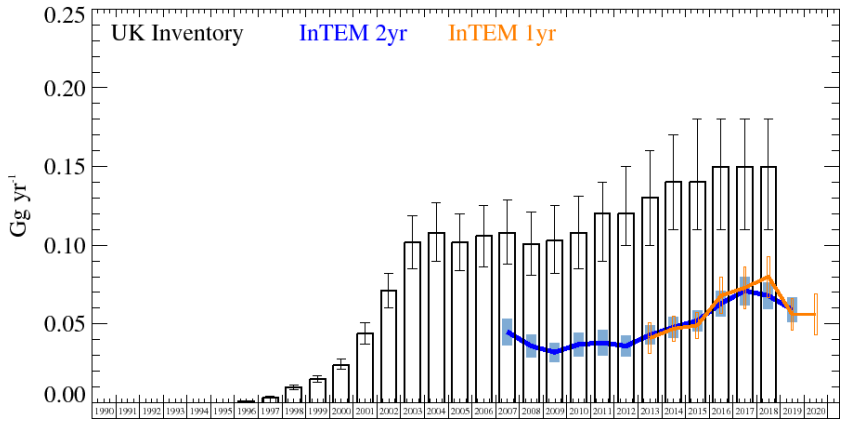

Figure 47: HFC-227ea UK emission estimates (Gg yr^{-1}) from the UNFCCC GHGI (black) and InTEM (a) Annualised 2-year inversion (blue) (b) Annual inversion (orange). The uncertainty bars represent 1-σ.

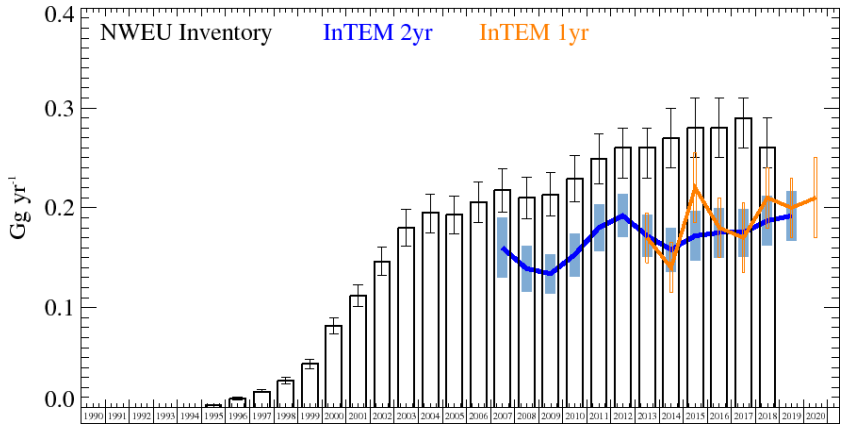

Figure 48: HFC-227ea NWEU emission estimates (Gg yr^{-1}) from the UNFCCC GHGI (black) and InTEM (a) Annualised 2-year inversion (blue) (b) Annual inversion (orange). The uncertainty bars represent 1-σ.

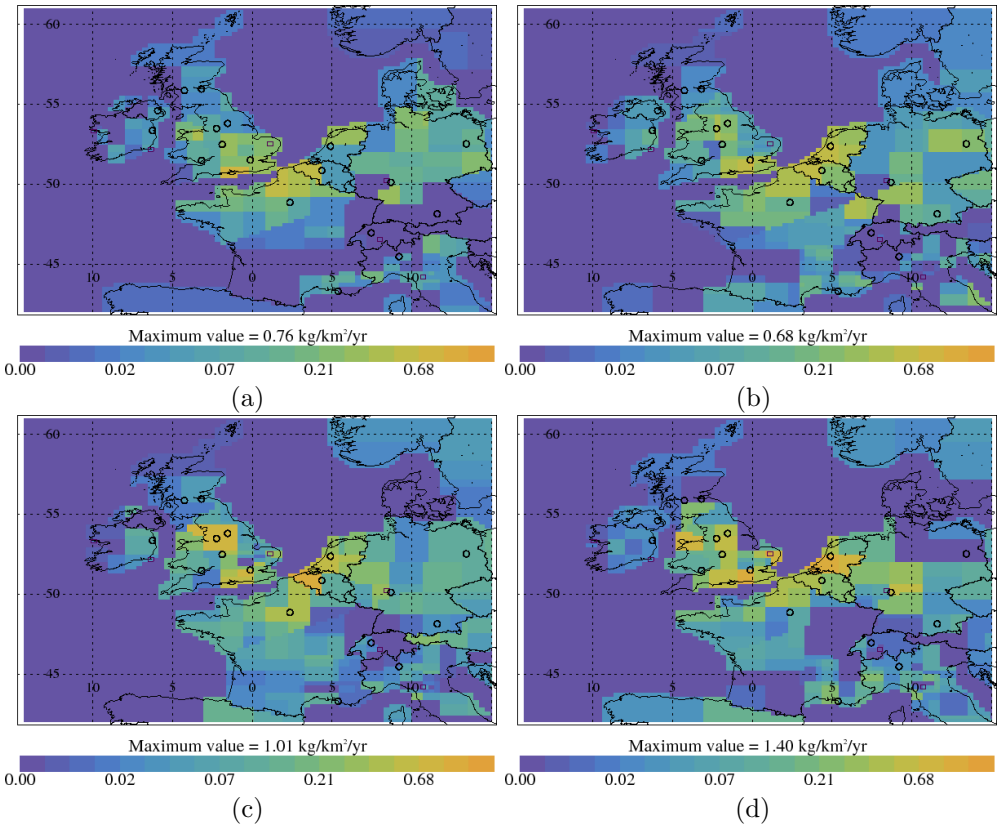

Figure 49: HFC-227ea InTEM emission estimates (kg km^{-2} yr^{-1}) (a) 2008-2010 (b) 2011-2013 (c) 2014-2016 (d) 2017-2019

Table 15: UK and NWEU HFC-227ea emission (Gg yr^{-1}) estimates with 1-σ uncertainty.

	UK			NWEU		
Years	Inventory	InTEM 2yr	InTEM 1yr	Inventory	InTEM 2yr	InTEM 1yr
1995	0.000 (0.00-0.01)			0.00 (0.00-0.01)		
1996	0.001 (0.00-0.01)			0.01 (0.00-0.02)		
1997	0.003 (0.00-0.01)			0.02 (0.01-0.03)		
1998	0.010 (0.00-0.02)			0.03 (0.02-0.04)		
1999	0.015 (0.00-0.02)			0.04 (0.03-0.05)		
2000	0.024 (0.01-0.03)			0.08 (0.07-0.09)		
2001	0.044 (0.03-0.05)			0.11 (0.10-0.12)		
2002	0.071 (0.06-0.08)			0.15 (0.13-0.16)		
2003	0.102 (0.09-0.12)			0.18 (0.16-0.20)		
2004	0.108 (0.09-0.13)			0.20 (0.17-0.21)		
2005	0.102 (0.08-0.12)			0.19 (0.17-0.21)		
2006	0.106 (0.09-0.13)			0.21 (0.18-0.23)		
2007	0.108 (0.09-0.13)	0.045 (0.04-0.05)		0.22 (0.19-0.24)	0.16 (0.13-0.19)	
2008	0.101 (0.08-0.12)	0.036 (0.03-0.04)		0.21 (0.18-0.23)	0.14 (0.11-0.16)	
2009	0.103 (0.08-0.13)	0.032 (0.03-0.04)		0.21 (0.19-0.24)	0.13 (0.11-0.15)	
2010	0.108 (0.09-0.13)	0.037 (0.03-0.05)		0.23 (0.20-0.25)	0.15 (0.13-0.18)	
2011	0.120 (0.09-0.14)	0.038 (0.03-0.05)		0.25 (0.22-0.27)	0.18 (0.15-0.20)	
2012	0.120 (0.10-0.15)	0.036 (0.03-0.04)		0.26 (0.23-0.28)	0.19 (0.17-0.21)	
2013	0.130 (0.10-0.16)	0.043 (0.04-0.05)	0.041 (0.03-0.05)	0.26 (0.23-0.28)	0.17 (0.15-0.19)	0.17 (0.15-0.20)
2014	0.140 (0.11-0.17)	0.048 (0.04-0.06)	0.047 (0.04-0.06)	0.27 (0.24-0.30)	0.16 (0.13-0.18)	0.14 (0.12-0.17)
2015	0.140 (0.11-0.18)	0.052 (0.05-0.06)	0.049 (0.04-0.06)	0.28 (0.25-0.31)	0.17 (0.14-0.20)	0.22 (0.18-0.25)
2016	0.150 (0.11-0.18)	0.063 (0.06-0.07)	0.068 (0.06-0.08)	0.28 (0.25-0.31)	0.18 (0.15-0.20)	0.18 (0.15-0.21)
2017	0.150 (0.11-0.18)	0.071 (0.06-0.08)	0.073 (0.06-0.09)	0.29 (0.26-0.31)	0.18 (0.15-0.20)	0.17 (0.13-0.20)
2018	0.150 (0.11-0.18)	0.068 (0.06-0.08)	0.080 (0.07-0.09)	0.26 (0.24-0.29)	0.19 (0.16-0.21)	0.21 (0.18-0.24)
2019		0.059 (0.05-0.07)	0.056 (0.05-0.07)		0.19 (0.16-0.22)	0.20 (0.17-0.23)
2020			0.056 (0.04-0.07)			0.21 (0.17-0.25)

4.15 HFC-365mfc

The atmospheric concentration globally appears to have reached a plateau at 1.4 ppt. The UK GHGI emission estimates are in very good agreement with InTEM except that InTEM shows a decline after 2016 not seen in the GHGI. In NWEU the InTEM estimates are higher than GHGI but modestly so, showing good agreement from 2017 with both now declining. InTEM estimates significant emissions from Belgium, Figure 54.

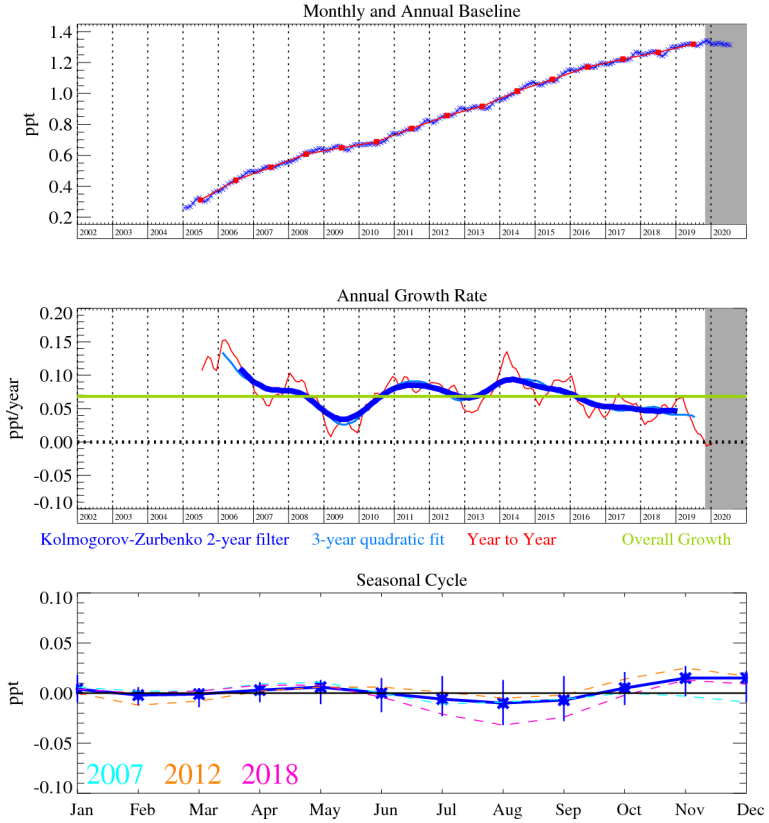

Figure 50: Monthly (blue) and annual (red) Mid-latitude Northern Hemisphere mole fractions (top plot). Annual (blue and red) and overall (green) growth rate (middle plot). Seasonal cycle (de-trended) with year-to-year variability (lower plot). Grey area covers un-ratified provisional data.

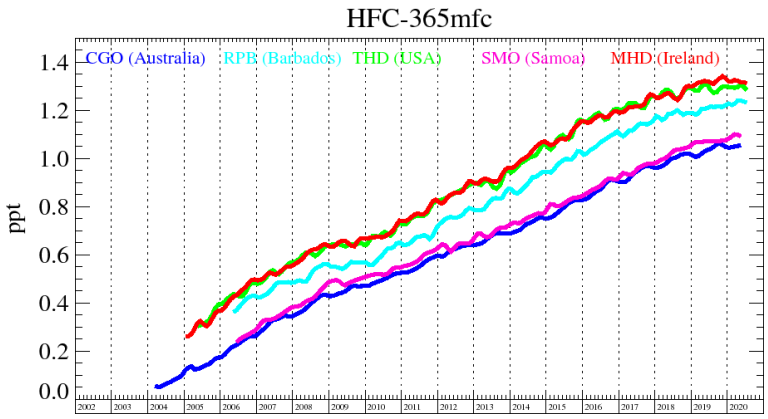

Figure 51: Background mole fractions at 5 AGAGE global stations

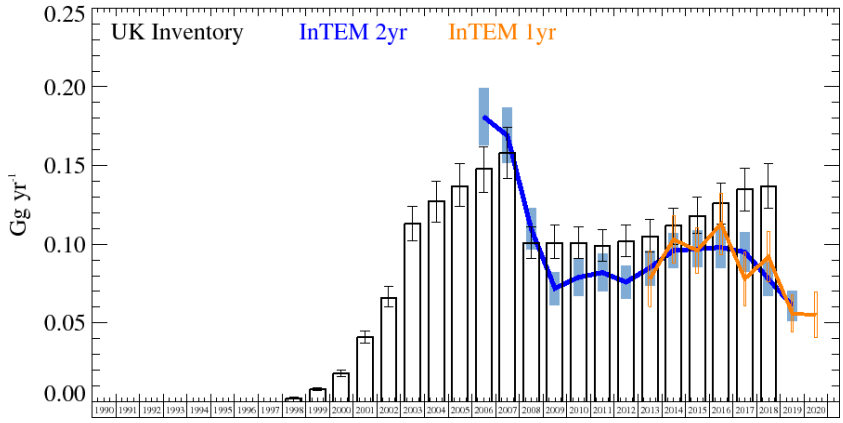

Figure 52: HFC-365mfc UK emission estimates (Gg yr^{-1}) from the UNFCCC GHGI (black) and InTEM (a) Annualised 2-year inversion (blue) (b) Annual inversion (orange). The uncertainty bars represent 1-σ.

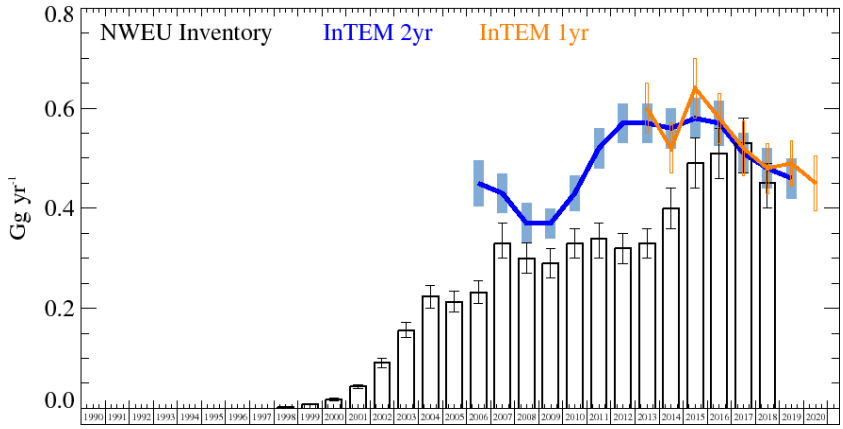

Figure 53: HFC-365mfc NWEU emission estimates (Gg yr^{-1}) from the UNFCCC GHGI (black) and InTEM (a) Annualised 2-year inversion (blue) (b) Annual inversion (orange). The uncertainty bars represent 1-σ.

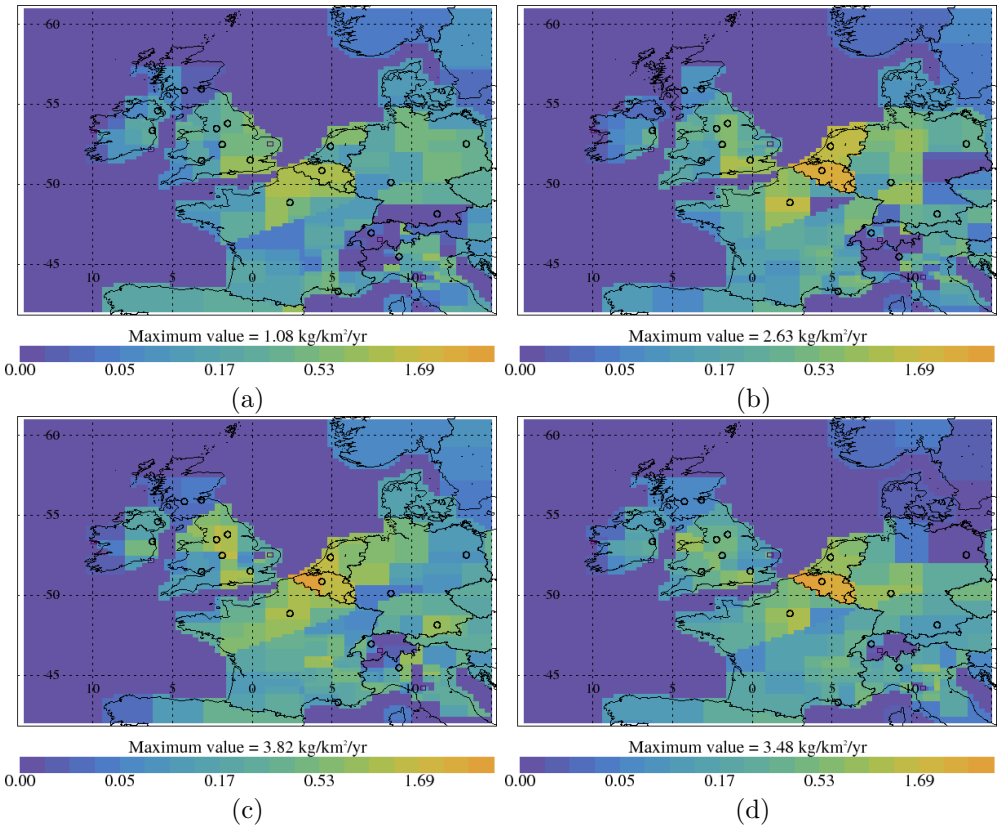

Figure 54: HFC-365mfc InTEM emission estimates (kg km^{-2} yr^{-1}) (a) 2008-2010 (b) 2011-2013 (c) 2014-2016 (d) 2017-2019

Table 16: UK and NWEU HFC-365mfc emission (Gg yr^{-1}) estimates with 1-σ uncertainty.

Years	UK Inventory	UK InTEM 2yr	UK InTEM 1yr	NWEU Inventory	NWEU InTEM 2yr	NWEU InTEM 1yr
1998	0.002 (0.00-0.00)			0.00 (0.00-0.01)		
1999	0.008 (0.00-0.01)			0.01 (0.00-0.02)		
2000	0.018 (0.02-0.02)			0.02 (0.01-0.03)		
2001	0.041 (0.04-0.05)			0.04 (0.03-0.05)		
2002	0.066 (0.06-0.07)			0.09 (0.08-0.10)		
2003	0.113 (0.10-0.12)			0.16 (0.14-0.17)		
2004	0.127 (0.11-0.14)			0.22 (0.20-0.25)		
2005	0.137 (0.12-0.15)			0.21 (0.19-0.23)		
2006	0.148 (0.13-0.16)	0.181 (0.16-0.20)		0.23 (0.20-0.26)	0.45 (0.40-0.49)	
2007	0.158 (0.14-0.17)	0.169 (0.15-0.19)		0.33 (0.30-0.37)	0.43 (0.39-0.47)	
2008	0.101 (0.09-0.11)	0.110 (0.10-0.12)		0.30 (0.27-0.33)	0.37 (0.33-0.41)	
2009	0.101 (0.09-0.11)	0.072 (0.06-0.08)		0.29 (0.26-0.32)	0.37 (0.34-0.40)	
2010	0.101 (0.09-0.11)	0.079 (0.07-0.09)		0.33 (0.30-0.36)	0.43 (0.40-0.47)	
2011	0.099 (0.09-0.11)	0.082 (0.07-0.09)		0.34 (0.30-0.37)	0.52 (0.48-0.56)	
2012	0.102 (0.09-0.11)	0.076 (0.06-0.09)		0.32 (0.29-0.35)	0.57 (0.53-0.61)	
2013	0.105 (0.09-0.12)	0.085 (0.07-0.10)	0.078 (0.06-0.10)	0.33 (0.30-0.36)	0.57 (0.53-0.61)	0.60 (0.55-0.65)
2014	0.112 (0.10-0.12)	0.096 (0.08-0.11)	0.103 (0.09-0.12)	0.40 (0.36-0.44)	0.56 (0.52-0.60)	0.52 (0.47-0.57)
2015	0.118 (0.11-0.13)	0.097 (0.09-0.11)	0.096 (0.08-0.11)	0.49 (0.44-0.54)	0.58 (0.54-0.62)	0.64 (0.58-0.70)
2016	0.126 (0.11-0.14)	0.098 (0.08-0.11)	0.113 (0.09-0.13)	0.51 (0.46-0.56)	0.57 (0.52-0.61)	0.58 (0.53-0.63)
2017	0.135 (0.12-0.15)	0.095 (0.08-0.11)	0.078 (0.06-0.10)	0.53 (0.47-0.58)	0.51 (0.47-0.55)	0.52 (0.46-0.57)
2018	0.137 (0.12-0.15)	0.078 (0.07-0.09)	0.092 (0.08-0.11)	0.45 (0.40-0.49)	0.48 (0.44-0.52)	0.48 (0.43-0.53)
2019		0.061 (0.05-0.07)	0.056 (0.04-0.07)		0.46 (0.42-0.50)	0.49 (0.44-0.53)
2020			0.055 (0.04-0.07)			0.45 (0.40-0.51)

4.16 HFC-245fa

The atmospheric concentration of HFC-245fa is increasing globally and the hemispheric gradient is widening. The UK GHGI emission estimate is higher than InTEM. InTEM is showing a slight decline after 2018. In NWEU there is a very good match between annual estimates except for 2018, where InTEM shows a very steep decline in emissions as the inventory continues to rise. InTEM estimates show significant emissions from Benelux countries especially Belgium (Figure 59).

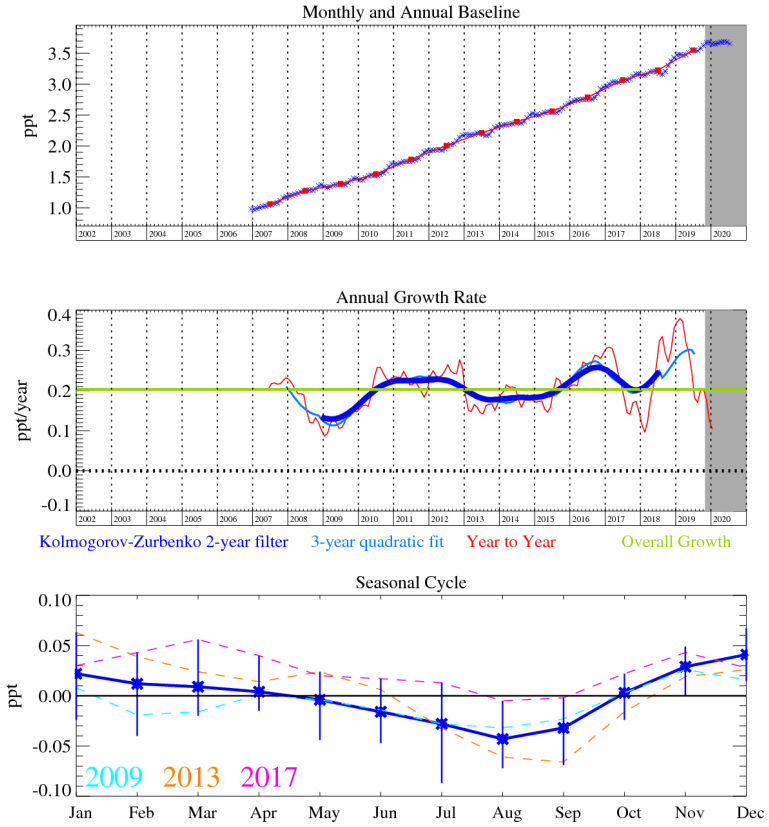

Figure 55: Monthly (blue) and annual (red) Mid-latitude Northern Hemisphere mole fractions (top plot). Annual (blue and red) and overall (green) growth rate (middle plot). Seasonal cycle (de-trended) with year-to-year variability (lower plot). Grey area covers un-ratified provisional data.

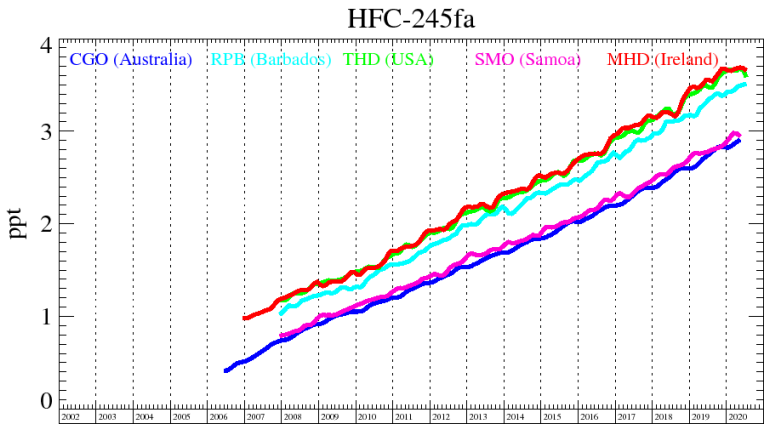

Figure 56: Background mole fractions at 5 AGAGE global stations

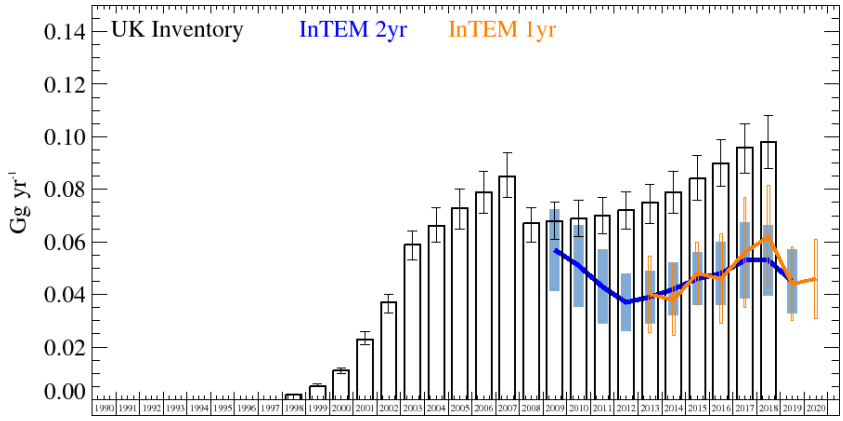

Figure 57: HFC-245fa UK emission estimates (Gg yr^{-1}) from the UNFCCC GHGI (black) and InTEM (a) Annualised 2-year inversion (blue) (b) Annual inversion (orange). The uncertainty bars represent 1-σ.

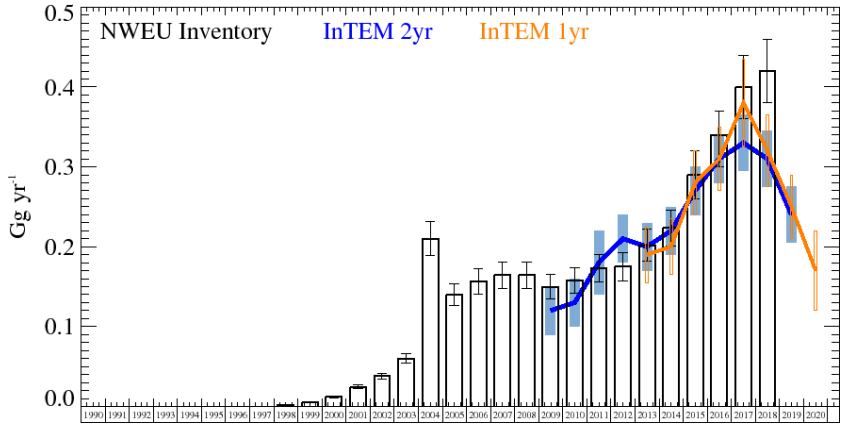

Figure 58: HFC-245fa NWEU emission estimates (Gg yr^{-1}) from the UNFCCC GHGI (black) and InTEM (a) Annualised 2-year inversion (blue) (b) Annual inversion (orange). The uncertainty bars represent 1-σ.

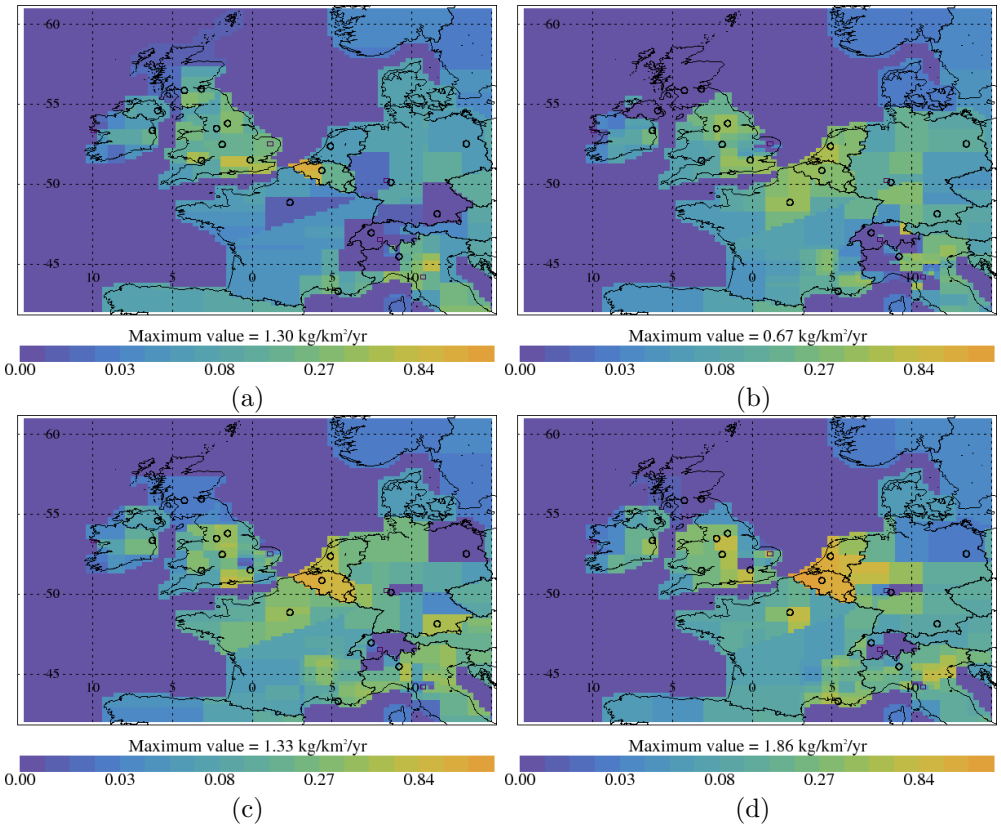

Figure 59: HFC-245fa InTEM emission estimates (kg km^{-2} yr^{-1}) (a) 2008-2010 (b) 2011-2013 (c) 2014-2016 (d) 2017-2019

Table 17: UK and NWEU HFC-245fa emission (Gg yr^{-1}) estimates with 1-σ uncertainty.

	UK			NWEU		
Years	Inventory	InTEM 2yr	InTEM 1yr	Inventory	InTEM 2yr	InTEM 1yr
1998	0.002 (0.00-0.01)			0.00 (0.00-0.01)		
1999	0.005 (0.00-0.01)			0.01 (0.00-0.02)		
2000	0.011 (0.01-0.02)			0.01 (0.01-0.02)		
2001	0.023 (0.02-0.03)			0.02 (0.02-0.03)		
2002	0.037 (0.03-0.04)			0.04 (0.03-0.05)		
2003	0.059 (0.05-0.06)			0.06 (0.05-0.07)		
2004	0.066 (0.06-0.07)			0.21 (0.18-0.23)		
2005	0.073 (0.06-0.08)			0.14 (0.12-0.15)		
2006	0.079 (0.07-0.09)			0.16 (0.14-0.17)		
2007	0.085 (0.07-0.09)			0.17 (0.14-0.18)		
2008	0.067 (0.06-0.07)			0.17 (0.14-0.18)		
2009	0.068 (0.06-0.08)	0.057 (0.04-0.07)		0.15 (0.13-0.17)	0.12 (0.09-0.15)	
2010	0.069 (0.06-0.08)	0.051 (0.03-0.07)		0.16 (0.14-0.17)	0.13 (0.10-0.16)	
2011	0.070 (0.06-0.08)	0.043 (0.02-0.06)		0.17 (0.15-0.19)	0.18 (0.14-0.22)	
2012	0.072 (0.06-0.08)	0.037 (0.02-0.05)		0.18 (0.15-0.19)	0.21 (0.18-0.24)	
2013	0.075 (0.06-0.08)	0.039 (0.02-0.05)	0.040 (0.02-0.05)	0.20 (0.18-0.22)	0.20 (0.17-0.23)	0.19 (0.15-0.22)
2014	0.079 (0.07-0.09)	0.042 (0.03-0.05)	0.038 (0.02-0.05)	0.22 (0.20-0.25)	0.22 (0.19-0.25)	0.20 (0.17-0.24)
2015	0.084 (0.07-0.09)	0.046 (0.03-0.06)	0.048 (0.03-0.06)	0.29 (0.26-0.32)	0.27 (0.24-0.30)	0.28 (0.24-0.32)
2016	0.090 (0.08-0.10)	0.048 (0.03-0.06)	0.046 (0.02-0.06)	0.34 (0.30-0.37)	0.31 (0.28-0.34)	0.31 (0.27-0.35)
2017	0.096 (0.08-0.11)	0.053 (0.03-0.07)	0.056 (0.03-0.08)	0.40 (0.36-0.44)	0.33 (0.30-0.37)	0.38 (0.33-0.44)
2018	0.098 (0.08-0.11)	0.053 (0.04-0.07)	0.062 (0.04-0.08)	0.42 (0.38-0.46)	0.31 (0.27-0.34)	0.32 (0.28-0.37)
2019		0.045 (0.03-0.06)	0.044 (0.03-0.06)		0.24 (0.21-0.28)	0.25 (0.21-0.29)
2020			0.046 (0.03-0.06)			0.17 (0.12-0.22)

4.17 HFC-23

The atmospheric concentration is increasing globally with UK emissions negligible in the GHGI after 2009 - although intermittent pollution events are still seen in observations. InTEM and the GHGI are in good agreement. Germany and Italy are estimated to have the most significant emissions according to InTEM. Emissions of HFC-23 have greatly reduced in Europe since the 1990's and remained flat since 2004, as seen in the unremarkable 3 year average emission maps in Figure 66.

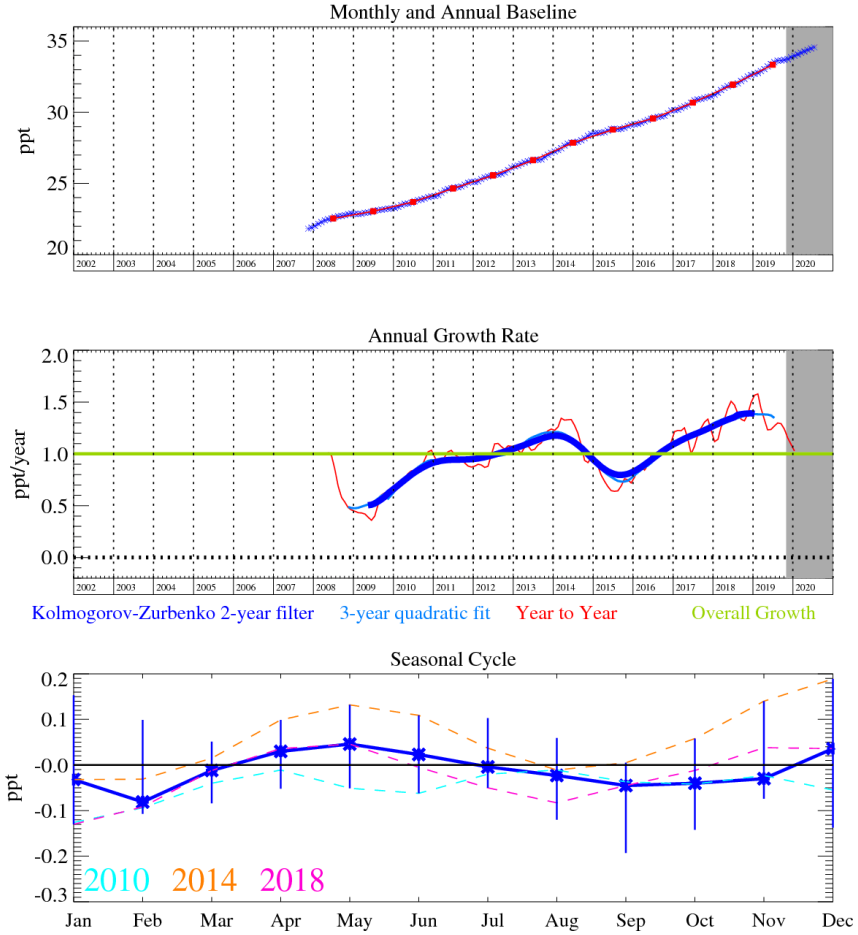

Figure 60: Monthly (blue) and annual (red) Mid-latitude Northern Hemisphere mole fractions (top plot). Annual (blue and red) and overall (green) growth rate (middle plot). Seasonal cycle (de-trended) with year-to-year variability (lower plot). Grey area covers un-ratified provisional data.

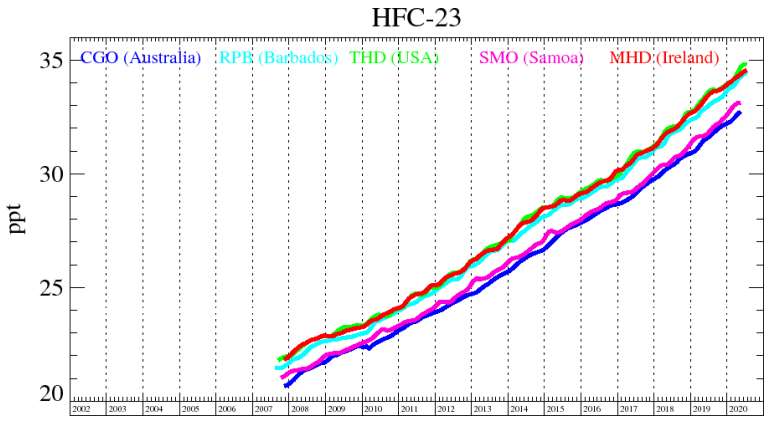

Figure 61: Background mole fractions at 5 AGAGE global stations

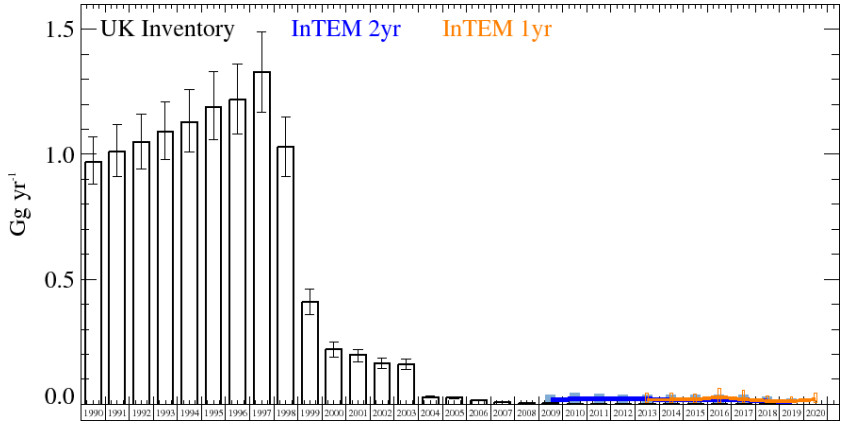

Figure 62: HFC-23 UK emission estimates (Gg yr^{-1}) from the UNFCCC inventory (black) and InTEM (a) Annualised 2-year inversion (blue) (b) Annual inversion (orange). The uncertainty bars represent 1-σ.

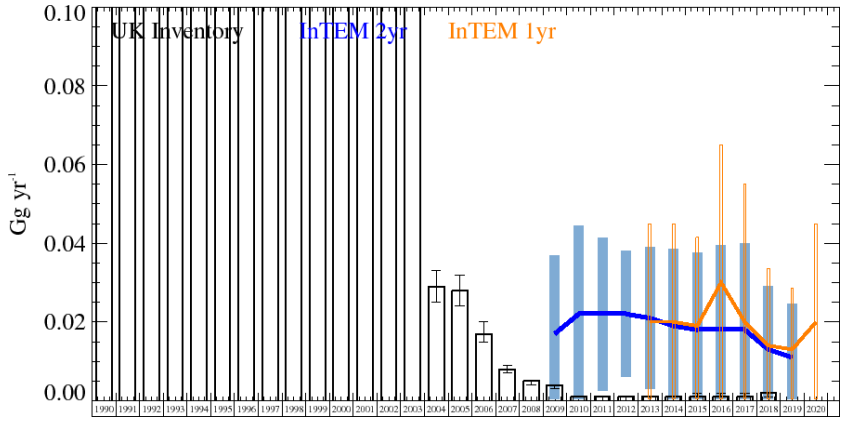

Figure 63: Expanded Y-axis: HFC-23 UK emission estimates (Gg yr^{-1}) from the UNFCCC GHGI (black) and InTEM (a) Annualised 2-year inversion (blue) (b) Annual inversion (orange). The uncertainty bars represent 1-σ.

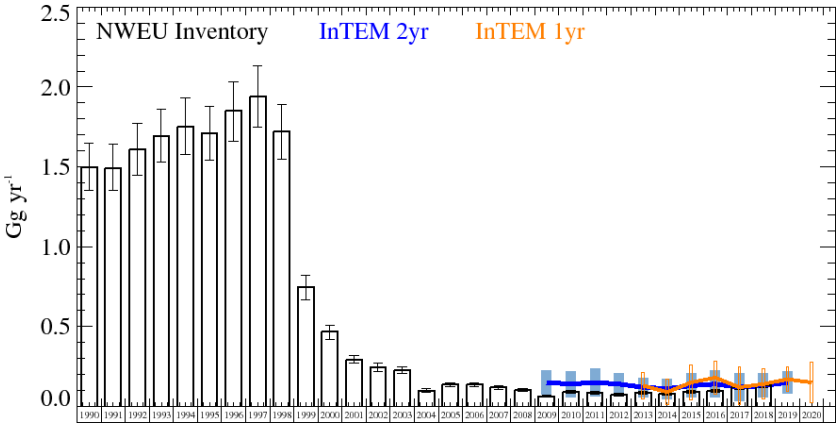

Figure 64: HFC-23 NWEU emission estimates (Gg yr^{-1}) from the UNFCCC GHGI (black) and InTEM (a) Annualised 2-year inversion (blue) (b) Annual inversion (orange). The uncertainty bars represent 1-σ.

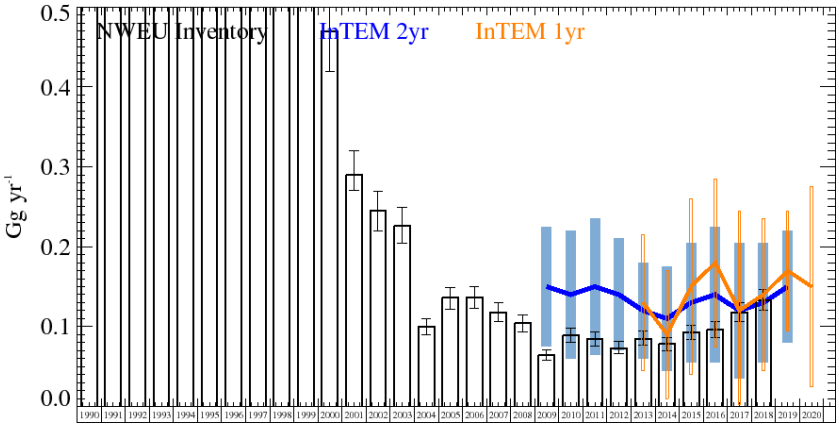

Figure 65: Extended Y-axis HFC-23 NWEU emission estimates (Gg yr^{-1}) from the UNFCCC GHGI (black) and InTEM (a) Annualised 2-year inversion (blue) (b) Annual inversion (orange). The uncertainty bars represent 1-σ.

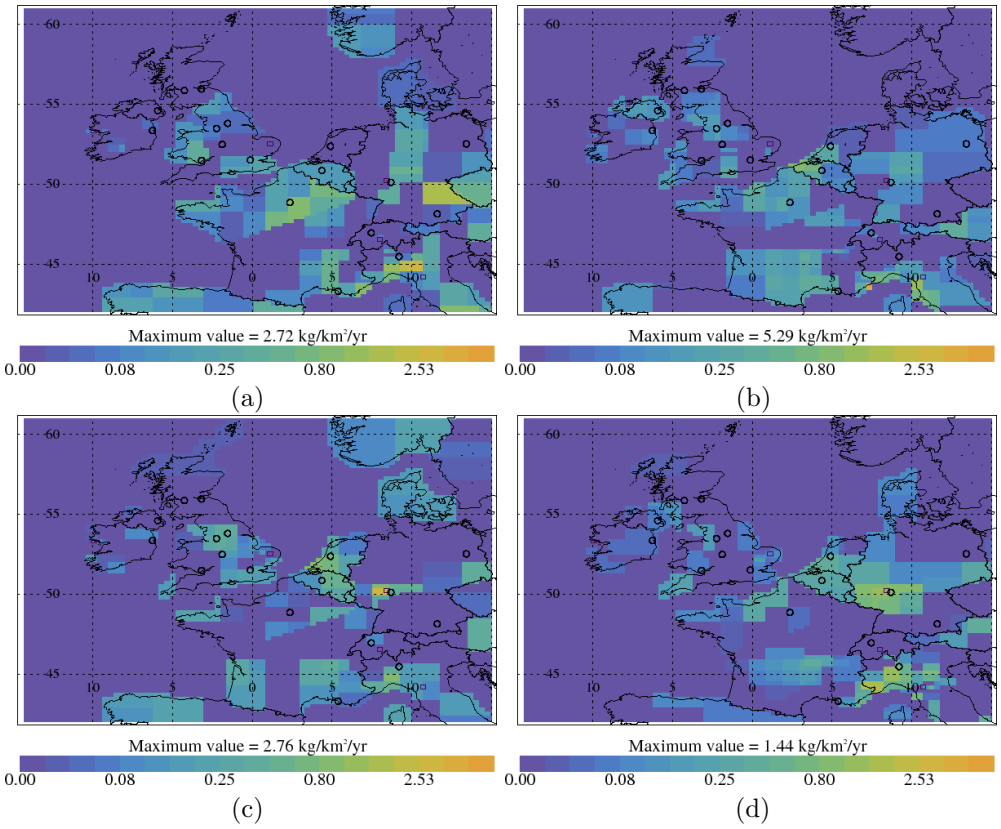

Figure 66: HFC-23 InTEM emission estimates (kg km^{-2} yr^{-1}) (a) 2008-2010 (b) 2011-2013 (c) 2014-2016 (d) 2017-2019

Table 18: UK and NWEU HFC-23 emission (Gg yr^{-1}) estimates with 1-σ uncertainty.

	UK			NWEU		
Years	Inventory	InTEM 2yr	InTEM 1yr	Inventory	InTEM 2yr	InTEM 1yr
1990	0.97 (0.88-1.07)			1.50 (1.35-1.65)		
1991	1.01 (0.91-1.12)			1.49 (1.35-1.64)		
1992	1.05 (0.94-1.16)			1.61 (1.45-1.77)		
1993	1.09 (0.98-1.21)			1.69 (1.53-1.86)		
1994	1.13 (1.01-1.26)			1.75 (1.58-1.93)		
1995	1.19 (1.06-1.33)			1.71 (1.54-1.88)		
1996	1.22 (1.08-1.36)			1.85 (1.66-2.03)		
1997	1.33 (1.17-1.49)			1.94 (1.75-2.13)		
1998	1.03 (0.91-1.15)			1.72 (1.55-1.89)		
1999	0.41 (0.36-0.46)			0.75 (0.67-0.82)		
2000	0.22 (0.19-0.25)			0.47 (0.42-0.51)		
2001	0.20 (0.17-0.22)			0.29 (0.27-0.32)		
2002	0.17 (0.14-0.19)			0.24 (0.22-0.27)		
2003	0.16 (0.14-0.18)			0.23 (0.20-0.25)		
2004	0.029 (0.025-0.033)			0.10 (0.09-0.11)		
2005	0.028 (0.024-0.032)			0.14 (0.12-0.15)		
2006	0.017 (0.015-0.020)			0.14 (0.12-0.15)		
2007	0.008 (0.007-0.009)			0.12 (0.10-0.13)		
2008	0.005 (0.004-0.005)			0.10 (0.09-0.11)		
2009	0.004 (0.003-0.004)	0.02 (0.00-0.04)		0.06 (0.05-0.07)	0.15 (0.07-0.22)	
2010	0.001 (0.001-0.001)	0.02 (0.00-0.04)		0.09 (0.08-0.10)	0.14 (0.06-0.22)	
2011	0.001 (0.001-0.001)	0.02 (0.00-0.04)		0.08 (0.07-0.09)	0.15 (0.07-0.24)	
2012	0.001 (0.001-0.001)	0.02 (0.00-0.04)		0.07 (0.06-0.08)	0.14 (0.07-0.21)	
2013	0.001 (0.001-0.001)	0.02 (0.00-0.04)	0.02 (0.00-0.05)	0.09 (0.07-0.09)	0.12 (0.06-0.18)	0.13 (0.05-0.22)
2014	0.001 (0.001-0.001)	0.02 (0.00-0.04)	0.02 (0.00-0.05)	0.08 (0.07-0.09)	0.11 (0.04-0.17)	0.09 (0.01-0.17)
2015	0.001 (0.001-0.002)	0.02 (0.00-0.04)	0.02 (0.00-0.04)	0.09 (0.08-0.10)	0.13 (0.06-0.21)	0.15 (0.04-0.26)
2016	0.001 (0.001-0.002)	0.02 (0.00-0.04)	0.03 (0.00-0.07)	0.10 (0.08-0.11)	0.14 (0.05-0.22)	0.18 (0.07-0.28)
2017	0.001 (0.001-0.002)	0.02 (0.00-0.04)	0.02 (0.00-0.07)	0.12 (0.10-0.13)	0.12 (0.03-0.20)	0.12 (0.00-0.25)
2018	0.002 (0.001-0.002)	0.01 (0.00-0.03)	0.01 (0.00-0.04)	0.13 (0.12-0.15)	0.13 (0.06-0.21)	0.14 (0.05-0.24)
2019		0.01 (0.00-0.03)	0.01 (0.00-0.03)		0.15 (0.08-0.22)	0.17 (0.09-0.24)
2020			0.02 (0.00-0.05)			0.15 (0.02-0.27)

4.18 HFC-43-10mee

The atmospheric concentration is slowly increasing globally. Given the uncertainties, the UK GHGI emission estimates are similar to InTEM. It is clear from Figure 70 that currently only the UK is reporting emission numbers for this gas. The spatial distribution that InTEM estimates is broadly inline with population.

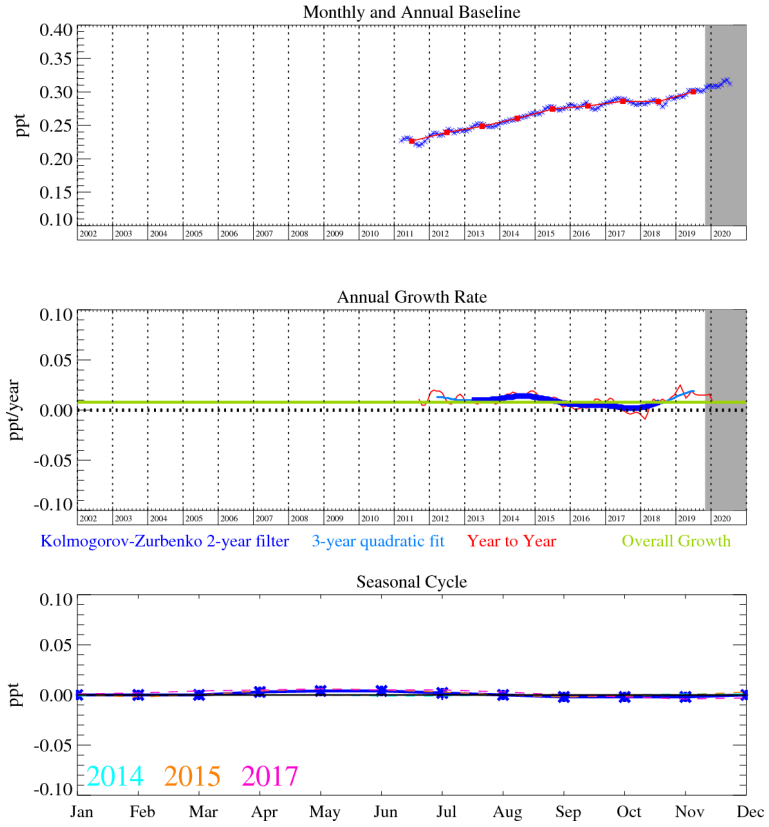

Figure 67: Monthly (blue) and annual (red) Mid-latitude Northern Hemisphere mole fractions (top plot). Annual (blue and red) and overall (green) growth rate (middle plot). Seasonal cycle (de-trended) with year-to-year variability (lower plot). Grey area covers un-ratified provisional data.

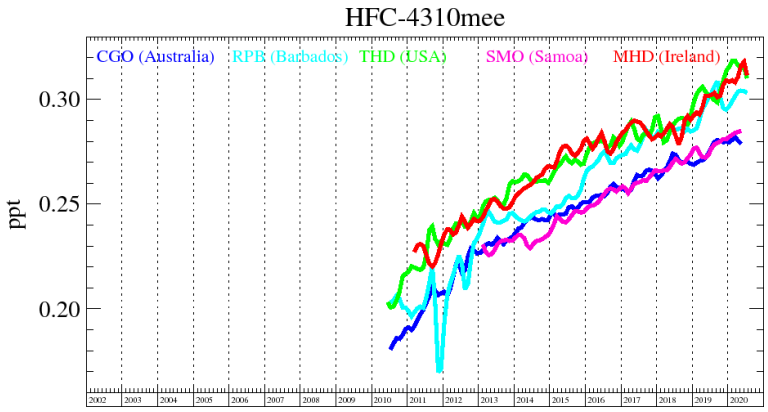

Figure 68: Background mole fractions at 5 AGAGE global stations

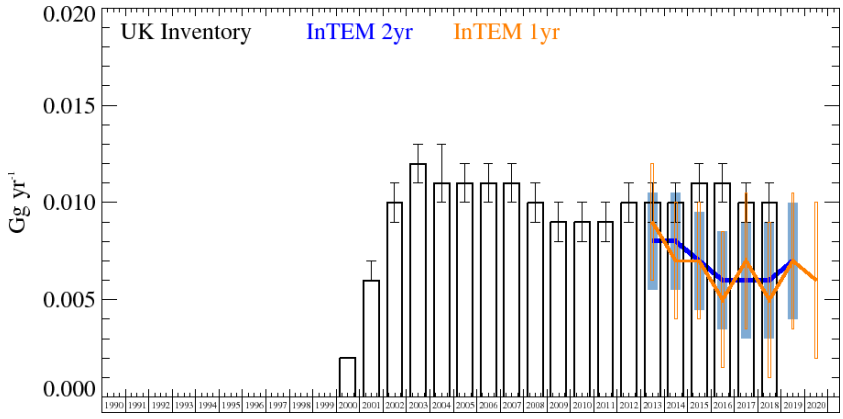

Figure 69: HFC-43-10mee UK emission estimates (Gg yr^{-1}) from the UNFCCC GHGI (black) and InTEM (a) Annualised 2-year inversion (blue) (b) Annual inversion (orange). The uncertainty bars represent 1-σ.

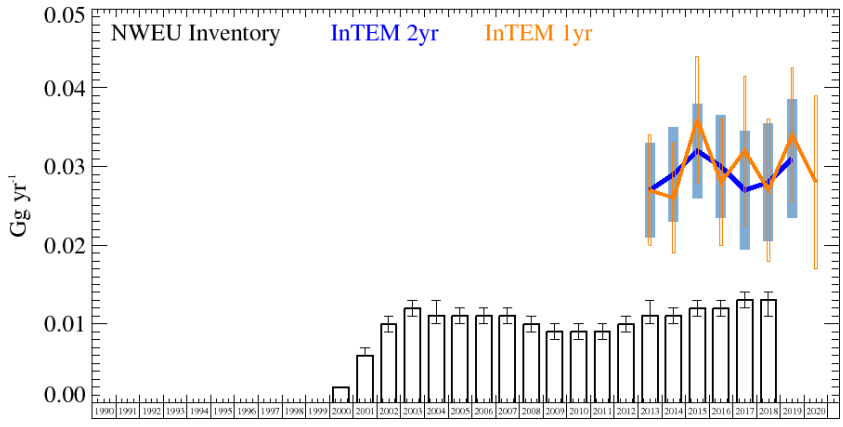

Figure 70: HFC-43-10mee NWEU emission estimates (Gg yr^{-1}) from the UNFCCC GHGI (black) and InTEM (a) Annualised 2-year inversion (blue) (b) Annual inversion (orange). The uncertainty bars represent 1-σ.

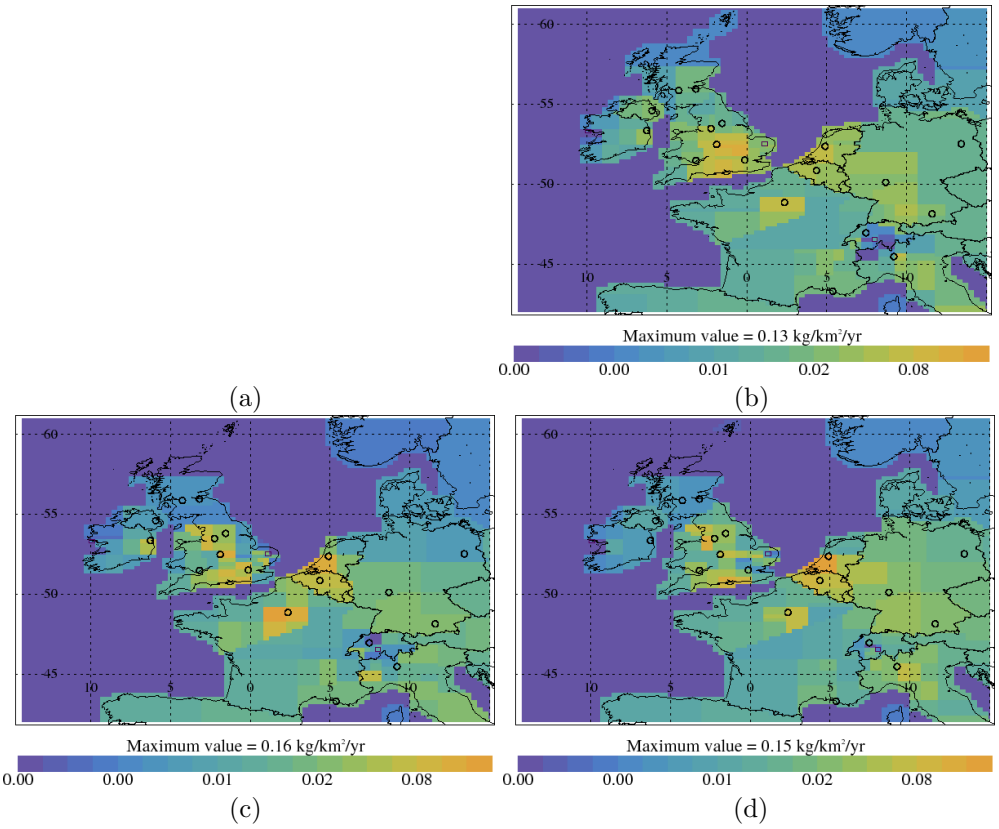

Figure 71: HFC-43-10mee InTEM emission estimates (kg km^{-2} yr^{-1}) (a) No Data (b) 2011-2013 (c) 2014-2016 (d) 2017-2019

Table 19: UK and NWEU HFC-43-10mee emission (Mg yr^{-1}) estimates with 1-σ uncertainty.

	UK			NWEU		
Years	Inventory	InTEM 2yr	InTEM 1yr	Inventory	InTEM 2yr	InTEM 1yr
2000	2 (2-02)			2 (1-3)		
2001	6 (6-07)			6 (5-7)		
2002	10 (9-11)			10 (9-11)		
2003	12 (11-13)			12 (11-13)		
2004	11 (10-13)			11 (10-13)		
2005	11 (10-12)			11 (10-12)		
2006	11 (10-12)			11 (10-12)		
2007	11 (10-12)			11 (10-12)		
2008	10 (9-11)			10 (9-11)		
2009	9 (8-10)			9 (8-10)		
2010	9 (8-10)			9 (8-10)		
2011	9 (8-10)			9 (8-10)		
2012	10 (9-11)			10 (9-11)		
2013	10 (9-11)	8 (6-11)	9 (6-12)	11 (10-13)	27 (21-33)	27 (20-34)
2014	10 (9-11)	8 (5-10)	7 (4-10)	11 (10-12)	29 (23-35)	26 (19-33)
2015	11 (10-12)	7 (4-09)	7 (4-10)	12 (11-13)	32 (26-38)	36 (28-44)
2016	11 (10-12)	6 (4-09)	5 (2-9)	12 (11-13)	30 (24-37)	28 (20-36)
2017	10 (9-11)	6 (3-09)	7 (3-10)	13 (12-14)	27 (20-35)	32 (23-42)
2018	10 (9-11)	6 (3-09)	5 (1-9)	13 (11-14)	28 (21-36)	27 (18-36)
2019		7 (4-10)	7 (4-11)		31 (23-38)	34 (25-42)
2020			6 (2-10)			28 (17-39)

4.19 PFC Summary

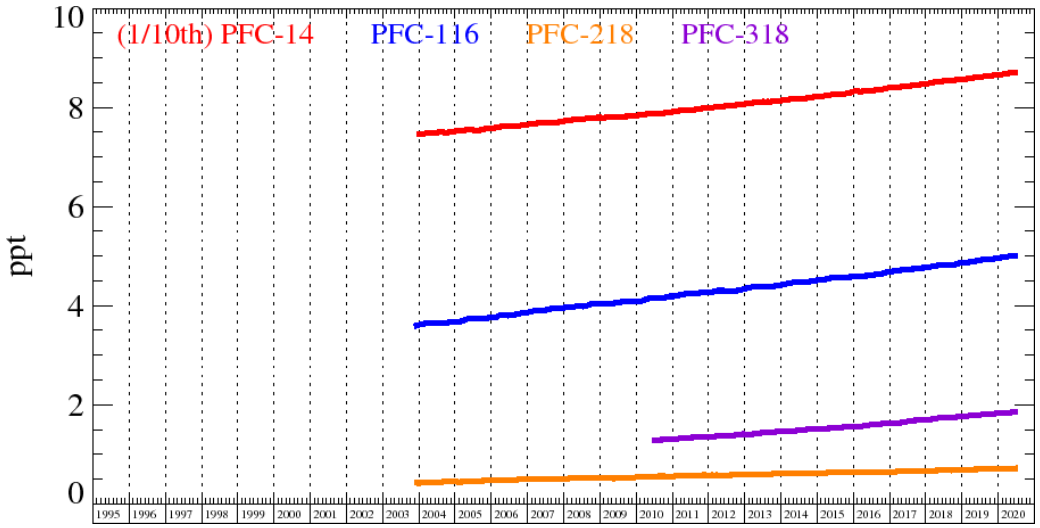

Figure 72: Northern Hemisphere Atmospheric Background Levels of PFCs as observed at the Mace Head observing station. Note that for scale purposes the atmospheric mole fractions of PFC-14 have been divided by 10.

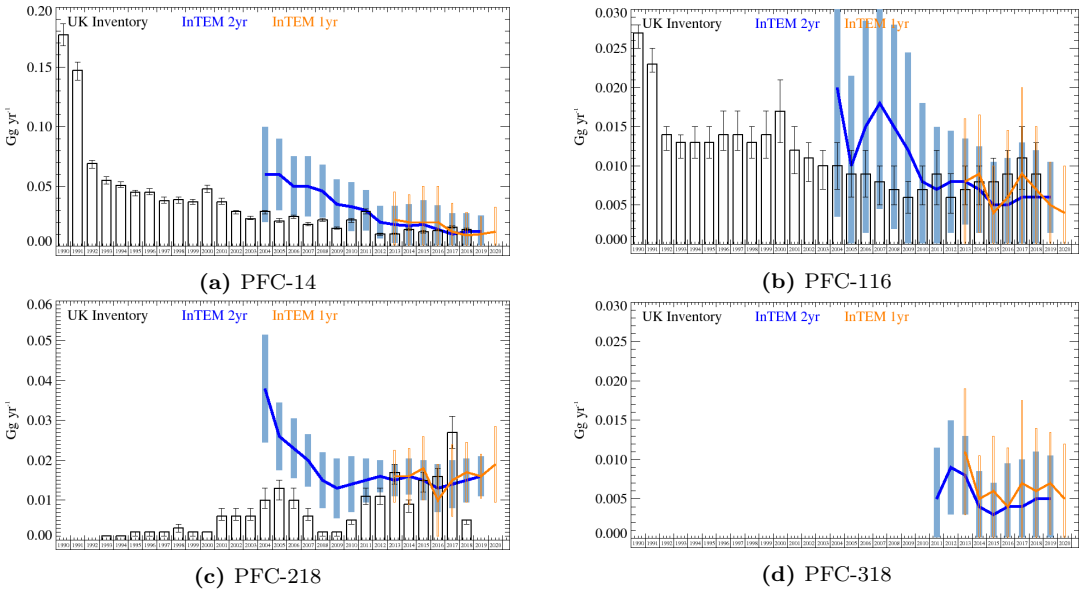

(a) PFC-14

(b) PFC-116

(c) PFC-218

(d) PFC-318

Figure 73: PFC UK emission estimates (Gg yr^{-1}) from the UNFCCC inventory (black) and InTEM (a) Annualised 2-year inversion (blue) (b) Annual inversion (orange). The uncertainty bars represent 1-σ.

Globally, atmospheric concentrations of all the PFC's are growing. They all have long atmospheric lifetimes and high GWP100's (Table 7). They originate as by-products from the production of aluminium and from the electronic and semi-conductor industries. Over the UK the emissions of these gases has been quite stable at low levels for the last few years, however there is now some evidence from InTEM estimates that PFC-218 emissions may have increased in the last 2 years.

Within the area of north west Europe modelled by InTEM there are also emerging indications of slight increases in PFC-14, PFC-116 and PFC-218.

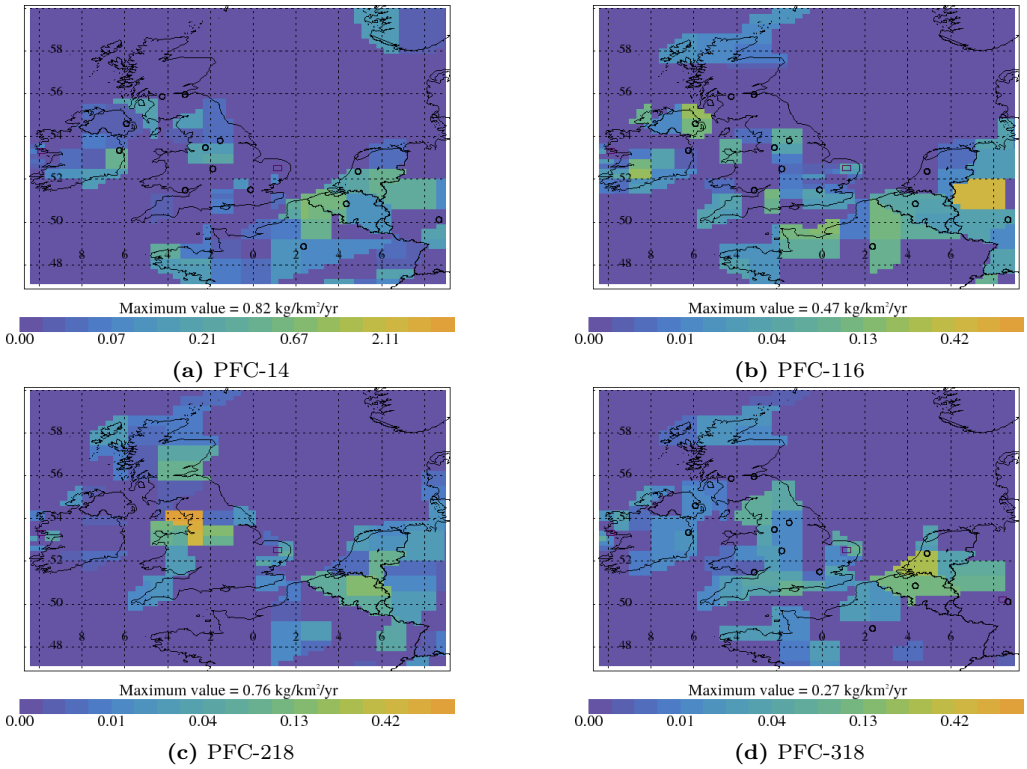

(a) PFC-14 **(b)** PFC-116

(c) PFC-218 **(d)** PFC-318

Figure 74: InTEM PFC emission estimates (kg km^{-2} yr^{-1}). Note each plot has its own scale.

4.20 PFC-14

The atmospheric concentration is increasing globally with the Northern Hemisphere concentration increasing at an average rate of 0.75 ppt yr^{-1}, but increasing after 2014. There is evidence of a significant drop in growth rate after the 2008 financial crisis. InTEM estimates larger emissions than the GHGI for the UK from 2004-2009, but with good agreement thereafter. NWEU results show a similar pattern. Both InTEM and UK GHGI show declining UK emissions across reporting period, however NWEU InTEM results show a possible increase in annual emissions in 2019 and 2020 (provisional). The 3-year average InTEM maps show that north west Italy shows a strong source of PFC-14.

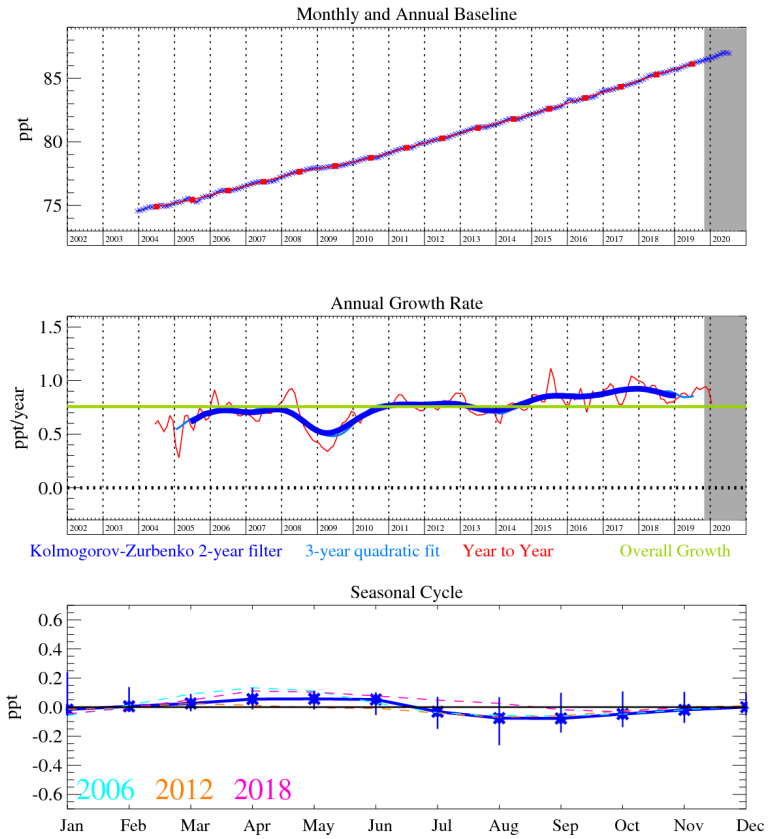

Figure 75: Monthly (blue) and annual (red) Mid-latitude Northern Hemisphere mole fractions (top plot). Annual (blue and red) and overall (green) growth rate (middle plot). Seasonal cycle (de-trended) with year-to-year variability (lower plot). Grey area covers un-ratified provisional data.

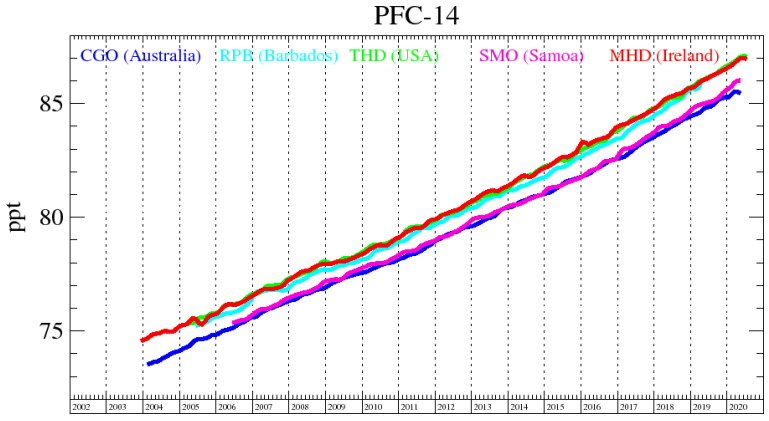

Figure 76: Background mole fractions at 5 AGAGE global stations

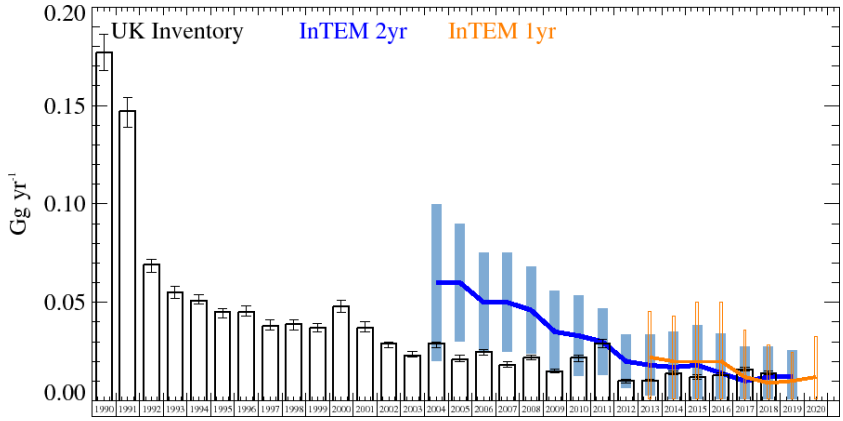

Figure 77: PFC-14 UK emission estimates (Gg yr^{-1}) from the UNFCCC GHGI (black) and InTEM (a) Annualised 2-year inversion (blue) (b) Annual inversion (orange). The uncertainty bars represent 1-σ.

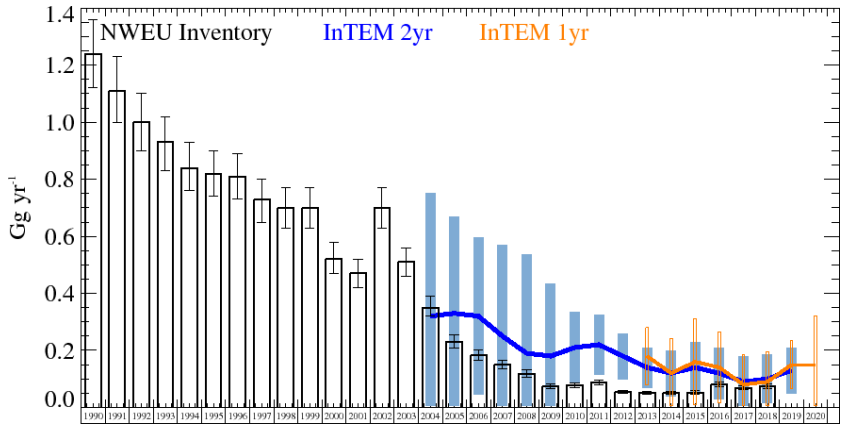

Figure 78: PFC-14 NWEU emission estimates (Gg yr^{-1}) from the UNFCCC GHGI (black) and InTEM (a) Annualised 2-year inversion (blue) (b) Annual inversion (orange). The uncertainty bars represent 1-σ.

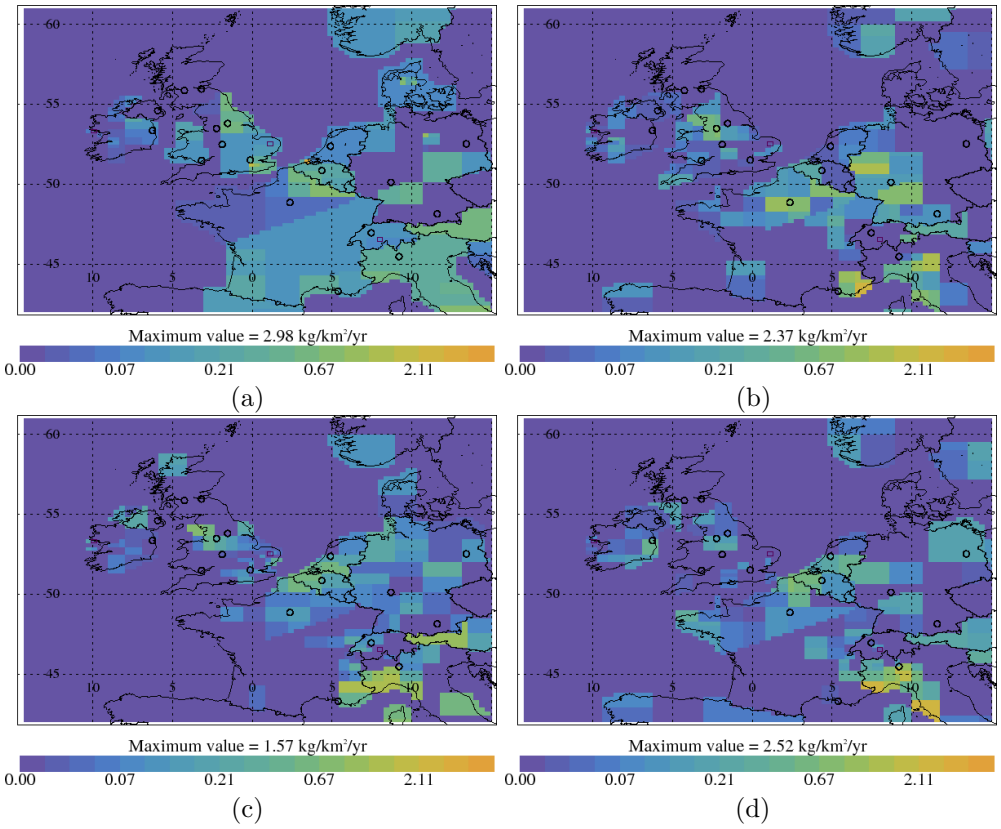

Figure 79: PFC-14 InTEM emission estimates (kg km^{-2} yr^{-1}) (a) 2008-2010 (b) 2011-2013 (c) 2014-2016 (d) 2017-2019

Table 20: UK and NWEU PFC-14 emission (Gg yr^{-1}) estimates with 1-σ uncertainty.

	UK			NWEU		
Years	Inventory	InTEM 2yr	InTEM 1yr	Inventory	InTEM 2yr	InTEM 1yr
1990	0.177 (0.168-0.186)			1.24 (1.12-1.36)		
1991	0.147 (0.139-0.154)			1.11 (1.00-1.23)		
1992	0.069 (0.065-0.072)			1.00 (0.90-1.10)		
1993	0.055 (0.052-0.058)			0.93 (0.83-1.02)		
1994	0.051 (0.049-0.054)			0.84 (0.76-0.93)		
1995	0.045 (0.042-0.047)			0.82 (0.74-0.90)		
1996	0.045 (0.043-0.048)			0.81 (0.73-0.89)		
1997	0.038 (0.036-0.041)			0.73 (0.65-0.80)		
1998	0.039 (0.036-0.041)			0.70 (0.63-0.77)		
1999	0.037 (0.035-0.039)			0.70 (0.63-0.77)		
2000	0.048 (0.045-0.051)			0.52 (0.47-0.58)		
2001	0.037 (0.035-0.040)			0.47 (0.42-0.52)		
2002	0.029 (0.027-0.030)			0.70 (0.63-0.77)		
2003	0.023 (0.022-0.025)			0.51 (0.46-0.56)		
2004	0.029 (0.027-0.030)	0.060 (0.02-0.10)		0.35 (0.32-0.39)	0.32 (0.00-0.86)	
2005	0.021 (0.020-0.023)	0.060 (0.03-0.09)		0.23 (0.20-0.25)	0.33 (0.00-0.68)	
2006	0.025 (0.023-0.026)	0.050 (0.03-0.08)		0.18 (0.16-0.20)	0.32 (0.05-0.60)	
2007	0.018 (0.017-0.020)	0.050 (0.02-0.07)		0.15 (0.13-0.17)	0.25 (0.00-0.64)	
2008	0.022 (0.021-0.023)	0.046 (0.02-0.07)		0.12 (0.10-0.13)	0.19 (0.00-0.69)	
2009	0.015 (0.014-0.016)	0.035 (0.01-0.06)		0.07 (0.06-0.08)	0.18 (0.00-0.51)	
2010	0.022 (0.020-0.023)	0.033 (0.01-0.05)		0.08 (0.07-0.09)	0.21 (0.09-0.34)	
2011	0.029 (0.027-0.031)	0.030 (0.01-0.05)		0.09 (0.07-0.10)	0.22 (0.11-0.32)	
2012	0.010 (0.009-0.011)	0.020 (0.00-0.03)		0.06 (0.04-0.06)	0.18 (0.10-0.26)	
2013	0.010 (0.010-0.011)	0.018 (0.00-0.03)	0.022 (0.00-0.05)	0.05 (0.04-0.06)	0.14 (0.07-0.21)	0.18 (0.08-0.28)
2014	0.014 (0.013-0.015)	0.017 (0.00-0.04)	0.020 (0.00-0.05)	0.05 (0.04-0.06)	0.12 (0.04-0.20)	0.12 (0.00-0.24)
2015	0.012 (0.011-0.013)	0.018 (0.00-0.04)	0.020 (0.00-0.06)	0.05 (0.04-0.06)	0.14 (0.05-0.23)	0.16 (0.01-0.31)
2016	0.013 (0.013-0.014)	0.014 (0.00-0.04)	0.020 (0.00-0.06)	0.08 (0.07-0.09)	0.12 (0.03-0.21)	0.14 (0.01-0.26)
2017	0.016 (0.015-0.017)	0.010 (0.00-0.03)	0.012 (0.00-0.05)	0.07 (0.06-0.08)	0.09 (0.00-0.18)	0.08 (0.00-0.21)
2018	0.014 (0.013-0.015)	0.012 (0.00-0.03)	0.009 (0.00-0.04)	0.07 (0.06-0.08)	0.10 (0.02-0.19)	0.09 (0.00-0.21)
2019		0.012 (0.00-0.03)	0.010 (0.00-0.03)		0.13 (0.05-0.21)	0.15 (0.07-0.24)
2020			0.012 (0.00-0.04)			0.15 (0.00-0.34)

4.21 PFC-116

The global atmospheric concentration is increasing at an approximate rate of 0.08 ppt yr^{-1}. The InTEM uncertainties encapsulate UK GHGI estimates in all reporting years. Agreement is particularly good after 2009. InTEM shows no significant decline in UK emissions post-2010, mirrored by the UK GHGI. NWEU GHGI emissions decreased significantly between 1990 and 2009, thereafter they have remained largely constant. InTEM is in good agreement, note that the 1-year InTEM results for 2019 and 2020 indicate a possible upturn. The largest source of emissions in the 2008-2010 average are from Leixlip, Ireland, an area west of Dublin. This is consistent with the location of Intel's fabrication plant. The average 2017-2019 map shows large emissions from the Ruhr Valley, Germany.

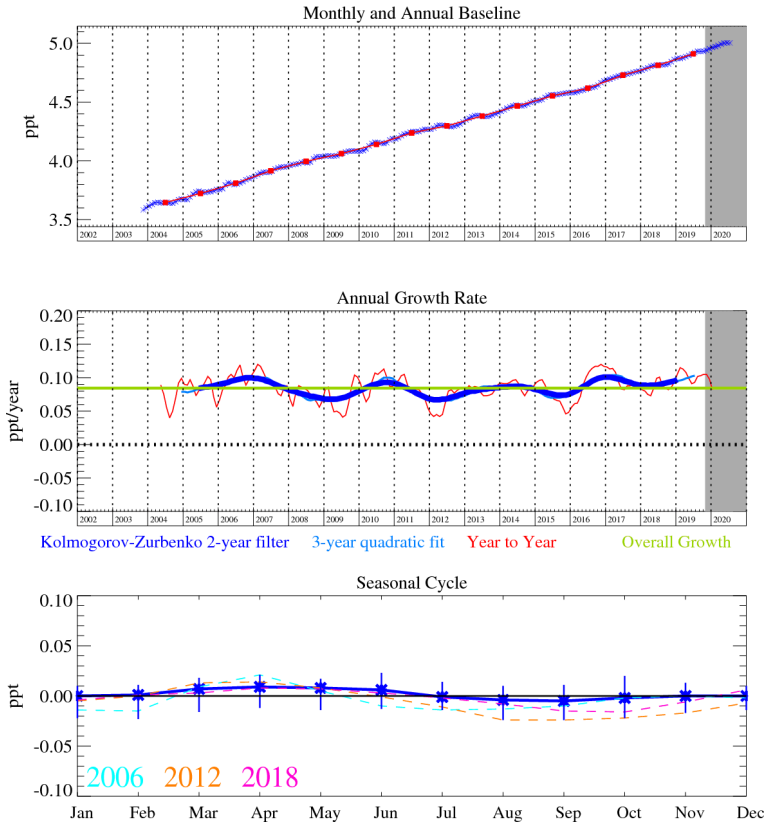

Figure 80: Monthly (blue) and annual (red) Mid-latitude Northern Hemisphere mole fractions (top plot). Annual (blue and red) and overall (green) growth rate (middle plot). Seasonal cycle (de-trended) with year-to-year variability (lower plot). Grey area covers un-ratified provisional data.

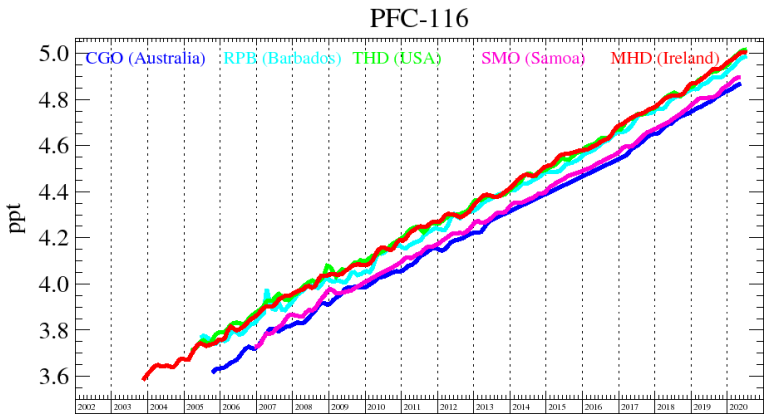

Figure 81: Background mole fractions at 5 AGAGE global stations

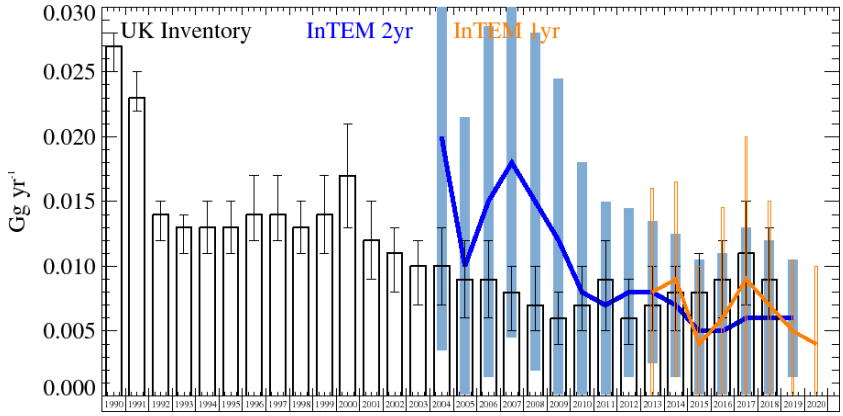

Figure 82: PFC-116 UK emission estimates (Gg yr^{-1}) from the UNFCCC GHGI (black) and InTEM (a) Annualised 2-year inversion (blue) (b) Annual inversion (orange). The uncertainty bars represent 1-σ.

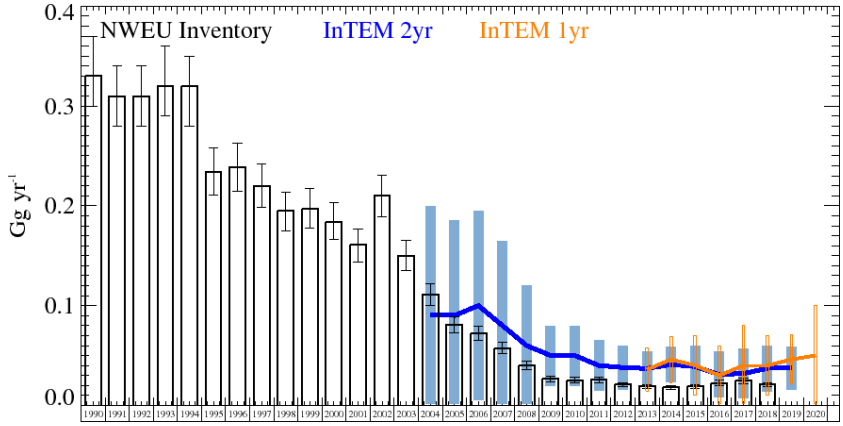

Figure 83: PFC-116 NWEU emission estimates (Gg yr^{-1}) from the UNFCCC GHGI (black) and InTEM (a) Annualised 2-year inversion (blue) (b) Annual inversion (orange). The uncertainty bars represent 1-σ.

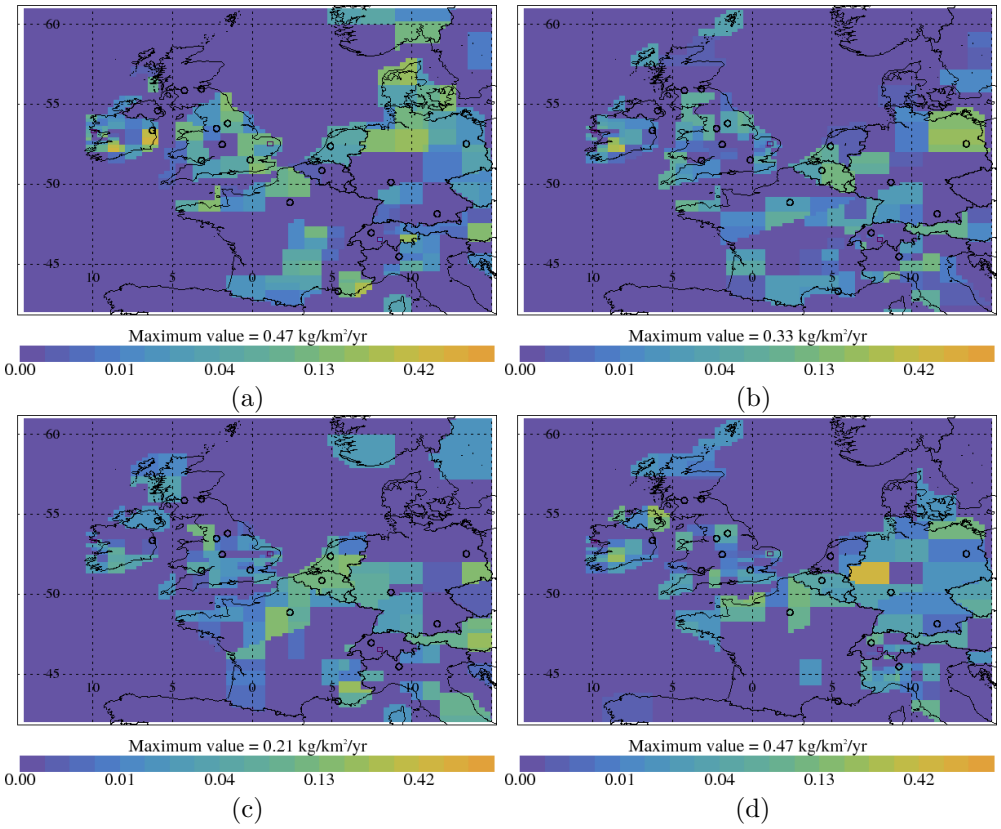

Figure 84: PFC-116 InTEM emission estimates (kg km^{-2} yr^{-1}) (a) 2008-2010 (b) 2011-2013 (c) 2014-2016 (d) 2017-2019

Table 21: UK and NWEU PFC-116 emission (Gg yr^{-1}) estimates with 1-σ uncertainty.

	UK			NWEU		
Years	Inventory	InTEM 2yr	InTEM 1yr	Inventory	InTEM 2yr	InTEM 1yr
1990	0.027 (0.025-0.028)			0.330 (0.30-0.37)		
1991	0.023 (0.022-0.025)			0.310 (0.28-0.34)		
1992	0.014 (0.012-0.015)			0.310 (0.28-0.34)		
1993	0.013 (0.011-0.014)			0.320 (0.29-0.36)		
1994	0.013 (0.011-0.015)			0.320 (0.28-0.35)		
1995	0.013 (0.011-0.015)			0.234 (0.21-0.26)		
1996	0.014 (0.012-0.017)			0.239 (0.21-0.26)		
1997	0.014 (0.012-0.017)			0.220 (0.20-0.24)		
1998	0.013 (0.011-0.015)			0.195 (0.17-0.21)		
1999	0.014 (0.011-0.017)			0.197 (0.18-0.22)		
2000	0.017 (0.013-0.021)			0.184 (0.16-0.20)		
2001	0.012 (0.009-0.015)			0.161 (0.14-0.18)		
2002	0.011 (0.008-0.013)			0.210 (0.19-0.23)		
2003	0.010 (0.007-0.012)			0.150 (0.13-0.16)		
2004	0.010 (0.007-0.013)	0.020 (0.004-0.037)		0.111 (0.10-0.12)	0.09 (0.00-0.22)	
2005	0.009 (0.006-0.012)	0.010 (0.000-0.023)		0.081 (0.07-0.09)	0.09 (0.00-0.19)	
2006	0.009 (0.006-0.012)	0.015 (0.002-0.029)		0.072 (0.06-0.08)	0.10 (0.00-0.19)	
2007	0.008 (0.005-0.010)	0.018 (0.005-0.032)		0.057 (0.05-0.06)	0.08 (0.00-0.17)	
2008	0.007 (0.005-0.010)	0.015 (0.002-0.028)		0.040 (0.03-0.04)	0.06 (0.00-0.12)	
2009	0.006 (0.004-0.008)	0.012 (0.000-0.025)		0.027 (0.02-0.03)	0.05 (0.02-0.08)	
2010	0.007 (0.005-0.010)	0.008 (0.000-0.020)		0.025 (0.02-0.03)	0.05 (0.02-0.08)	
2011	0.009 (0.005-0.012)	0.007 (0.000-0.016)		0.026 (0.02-0.03)	0.04 (0.02-0.07)	
2012	0.006 (0.004-0.009)	0.008 (0.001-0.014)		0.021 (0.02-0.02)	0.04 (0.02-0.06)	
2013	0.007 (0.005-0.010)	0.008 (0.002-0.013)	0.008 (0.000-0.016)	0.019 (0.02-0.02)	0.04 (0.02-0.05)	0.04 (0.01-0.06)
2014	0.008 (0.005-0.010)	0.007 (0.001-0.012)	0.009 (0.001-0.016)	0.018 (0.01-0.02)	0.04 (0.02-0.06)	0.05 (0.02-0.07)
2015	0.008 (0.005-0.011)	0.005 (0.000-0.011)	0.004 (0.000-0.012)	0.019 (0.02-0.02)	0.04 (0.02-0.06)	0.04 (0.01-0.07)
2016	0.009 (0.006-0.012)	0.005 (0.000-0.012)	0.006 (0.000-0.017)	0.022 (0.02-0.02)	0.03 (0.01-0.05)	0.03 (0.00-0.06)
2017	0.011 (0.007-0.015)	0.006 (0.000-0.014)	0.009 (0.000-0.022)	0.025 (0.02-0.03)	0.03 (0.01-0.06)	0.04 (0.00-0.08)
2018	0.009 (0.006-0.013)	0.006 (0.000-0.012)	0.007 (0.000-0.016)	0.021 (0.02-0.02)	0.04 (0.01-0.06)	0.04 (0.01-0.07)
2019		0.006 (0.001-0.010)	0.005 (0.000-0.011)		0.04 (0.01-0.06)	0.05 (0.02-0.07)
2020			0.004 (0.000-0.012)			0.05 (0.00-0.10)

4.22 PFC-218

The atmospheric concentration is growing globally, increasing at a rate of approximately 0.018 ppt yr^{-1}. InTEM estimates significantly larger emissions than the UK GHGI between 2004 - 2010 with reasonable agreement thereafter, but a large discrepancy again in 2018 where the modelled value is nearly double the inventory. The InTEM 2019 and 2020 model results indicate a possible increase in UK emissions. Over the NWEU region InTEM estimates are typically higher but the uncertainties overlap in most years. F2 Chemicals in the north west of England is the stand out source across the north west European domain modelled, in all years.

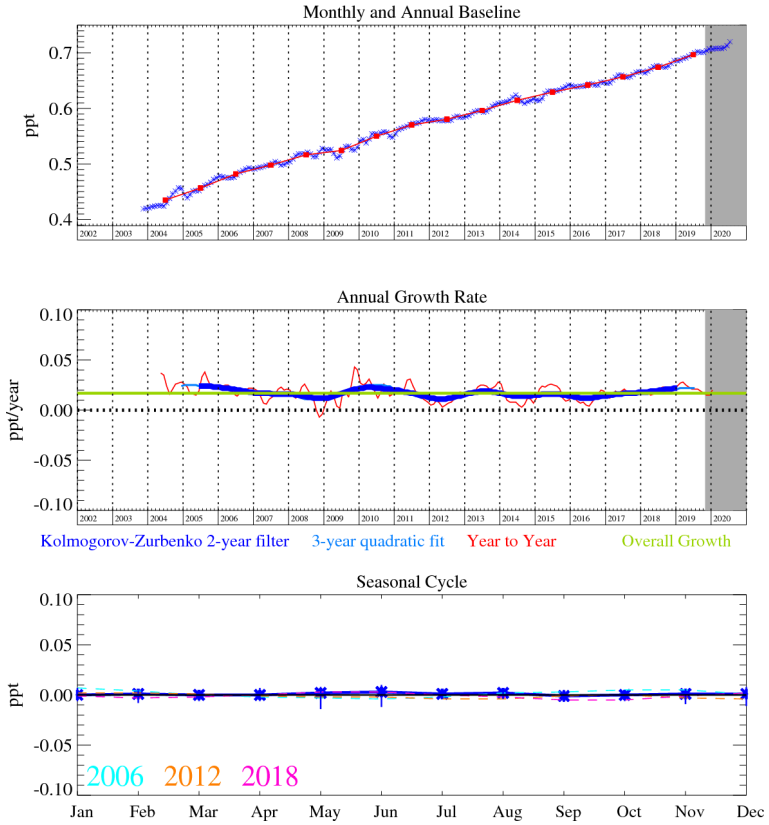

Figure 85: Monthly (blue) and annual (red) Mid-latitude Northern Hemisphere mole fractions (top plot). Annual (blue and red) and overall (green) growth rate (middle plot). Seasonal cycle (de-trended) with year-to-year variability (lower plot). Grey area covers un-ratified provisional data.

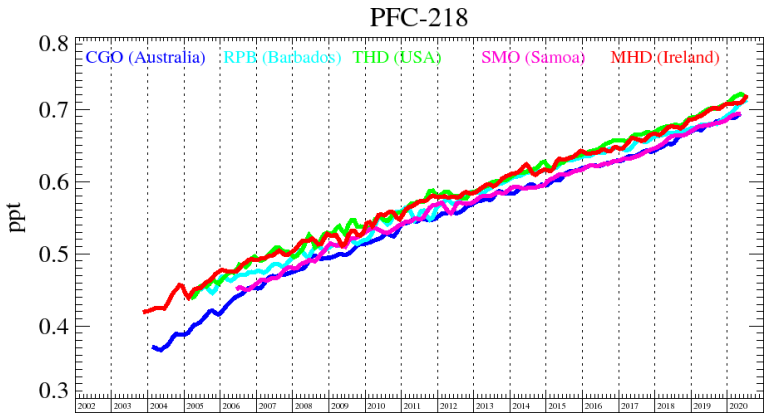

Figure 86: Background mole fractions at 5 AGAGE global stations

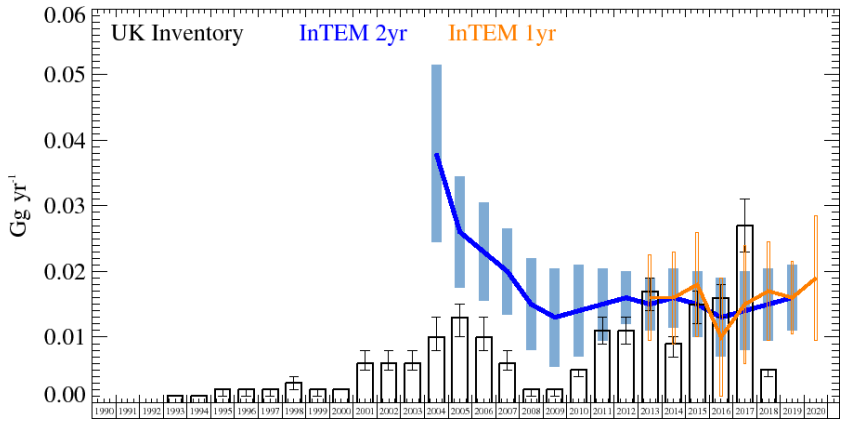

Figure 87: PFC-218 UK emission estimates (Gg yr^{-1}) from the UNFCCC GHGI (black) and InTEM (a) Annualised 2-year inversion (blue) (b) Annual inversion (orange). The uncertainty bars represent 1-σ.

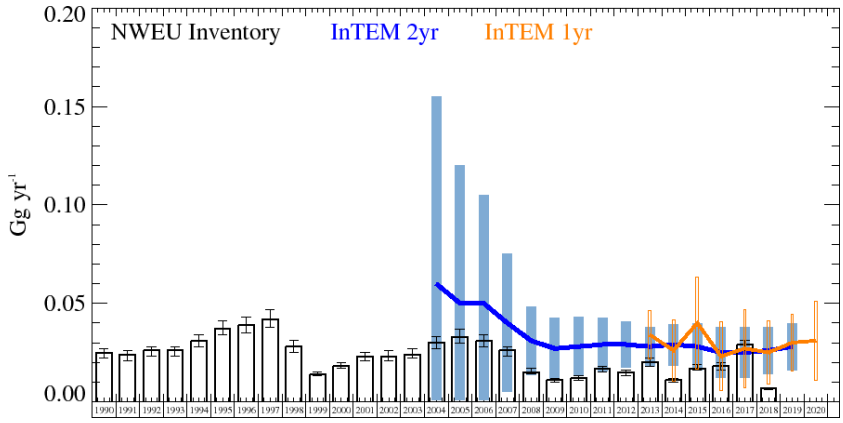

Figure 88: PFC-218 NWEU emission estimates (Gg yr^{-1}) from the UNFCCC GHGI (black) and InTEM (a) Annualised 2-year inversion (blue) (b) Annual inversion (orange). The uncertainty bars represent 1-σ.

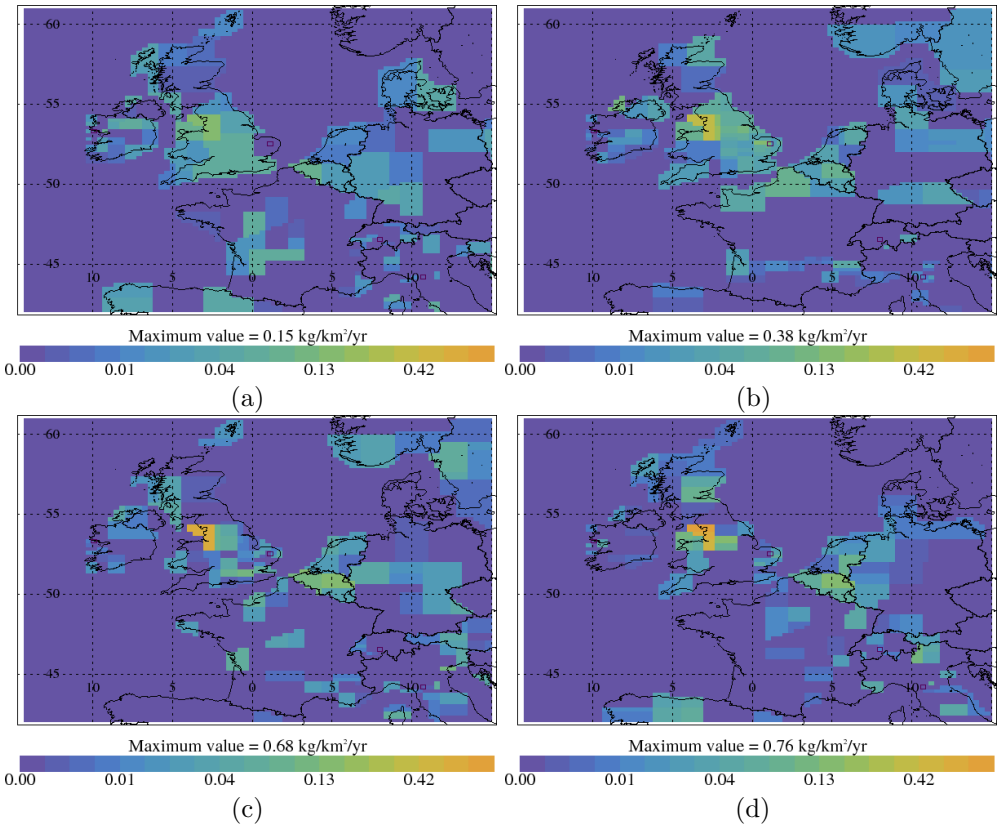

Figure 89: PFC-218 InTEM emission estimates (kg km^{-2} yr^{-1}) (a) 2008-2010 (b) 2011-2013 (c) 2014-2016 (d) 2017-2019

Table 22: UK and NWEU PFC-218 emission (Gg yr^{-1}) estimates with 1-σ uncertainty.

	UK			NWEU		
Years	Inventory	InTEM 2yr	InTEM 1yr	Inventory	InTEM 2yr	InTEM 1yr
1990	0.000 (0.00-0.01)			0.025 (0.02-0.03)		
1991	0.000 (0.00-0.01)			0.024 (0.02-0.03)		
1992	0.000 (0.00-0.01)			0.026 (0.02-0.03)		
1993	0.001 (0.00-0.01)			0.026 (0.02-0.03)		
1994	0.001 (0.00-0.01)			0.031 (0.02-0.03)		
1995	0.002 (0.00-0.01)			0.037 (0.03-0.04)		
1996	0.002 (0.00-0.01)			0.039 (0.03-0.04)		
1997	0.002 (0.00-0.01)			0.042 (0.03-0.05)		
1998	0.003 (0.00-0.01)			0.028 (0.02-0.03)		
1999	0.002 (0.00-0.01)			0.014 (0.01-0.02)		
2000	0.002 (0.00-0.01)			0.018 (0.01-0.02)		
2001	0.006 (0.00-0.01)			0.023 (0.02-0.03)		
2002	0.006 (0.00-0.01)			0.023 (0.02-0.03)		
2003	0.006 (0.00-0.01)			0.024 (0.02-0.03)		
2004	0.010 (0.00-0.02)	0.038 (0.02-0.05)		0.030 (0.02-0.03)	0.060 (0.00-0.19)	
2005	0.013 (0.01-0.02)	0.026 (0.01-0.03)		0.033 (0.03-0.04)	0.050 (0.00-0.14)	
2006	0.010 (0.00-0.02)	0.023 (0.01-0.03)		0.031 (0.02-0.03)	0.050 (0.00-0.11)	
2007	0.006 (0.00-0.01)	0.020 (0.01-0.03)		0.026 (0.02-0.03)	0.040 (0.01-0.08)	
2008	0.002 (0.00-0.01)	0.015 (0.00-0.02)		0.015 (0.01-0.02)	0.031 (0.01-0.05)	
2009	0.002 (0.00-0.01)	0.013 (0.00-0.02)		0.011 (0.01-0.01)	0.027 (0.01-0.04)	
2010	0.005 (0.00-0.01)	0.014 (0.00-0.02)		0.012 (0.01-0.01)	0.028 (0.01-0.04)	
2011	0.011 (0.00-0.02)	0.015 (0.01-0.02)		0.017 (0.01-0.02)	0.029 (0.01-0.04)	
2012	0.011 (0.00-0.02)	0.016 (0.01-0.02)		0.015 (0.01-0.02)	0.029 (0.02-0.04)	
2013	0.017 (0.01-0.02)	0.015 (0.01-0.02)	0.016 (0.01-0.02)	0.020 (0.01-0.02)	0.028 (0.02-0.04)	0.034 (0.02-0.05)
2014	0.009 (0.00-0.01)	0.016 (0.01-0.02)	0.016 (0.01-0.02)	0.011 (0.01-0.01)	0.029 (0.02-0.04)	0.026 (0.01-0.04)
2015	0.015 (0.01-0.02)	0.015 (0.01-0.02)	0.018 (0.01-0.03)	0.017 (0.01-0.02)	0.028 (0.01-0.04)	0.040 (0.02-0.06)
2016	0.016 (0.01-0.02)	0.013 (0.00-0.02)	0.010 (0.00-0.03)	0.018 (0.01-0.02)	0.025 (0.01-0.04)	0.023 (0.01-0.04)
2017	0.027 (0.02-0.03)	0.014 (0.00-0.02)	0.015 (0.01-0.02)	0.029 (0.02-0.03)	0.025 (0.01-0.04)	0.027 (0.01-0.05)
2018	0.005 (0.00-0.01)	0.015 (0.01-0.02)	0.017 (0.01-0.02)	0.007 (0.00-0.01)	0.026 (0.01-0.04)	0.025 (0.01-0.04)
2019		0.016 (0.01-0.02)	0.016 (0.01-0.02)		0.028 (0.01-0.04)	0.030 (0.01-0.04)
2020			0.019 (0.01-0.03)			0.031 (0.01-0.05)

4.23 PFC-318

The global atmospheric concentration is increasing at an average rate of 0.059 ppt yr^{-1}. The UK GHGI doesn't reports any emissions of PFC-318. The InTEM estimates are not statistically greater than 0 in most years. The NWEU GHGI has not varied significantly since 2003. The InTEM estimates for NWEU are greater than the inventory but the uncertainties are large. The strongest source can be seen in the Benelux region.

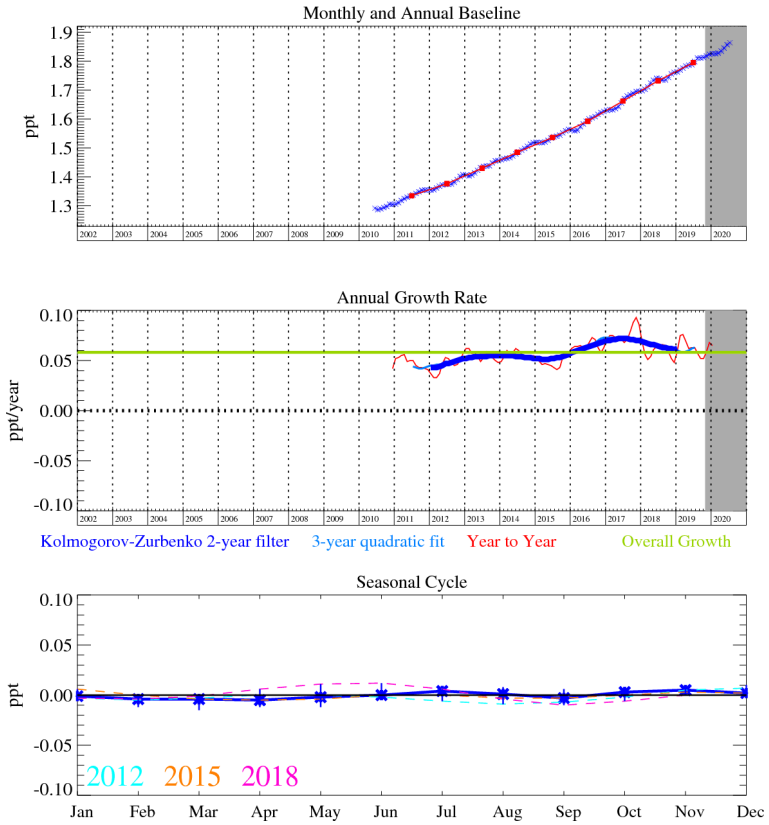

Figure 90: Monthly (blue) and annual (red) Mid-latitude Northern Hemisphere mole fractions (top plot). Annual (blue and red) and overall (green) growth rate (middle plot). Seasonal cycle (de-trended) with year-to-year variability (lower plot). Grey area covers un-ratified provisional data.

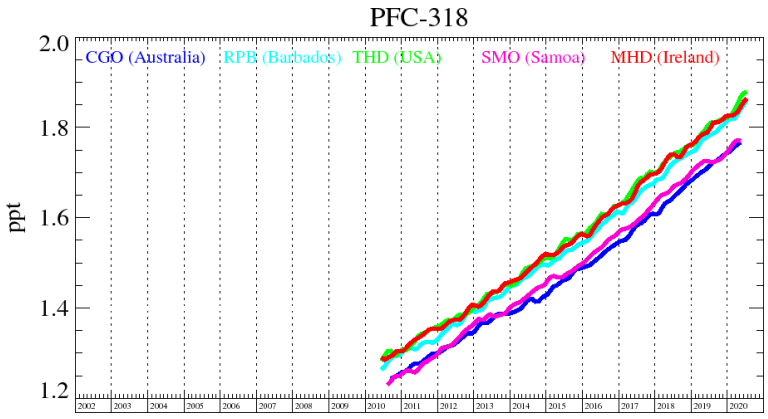

Figure 91: Background mole fractions at 5 AGAGE global stations

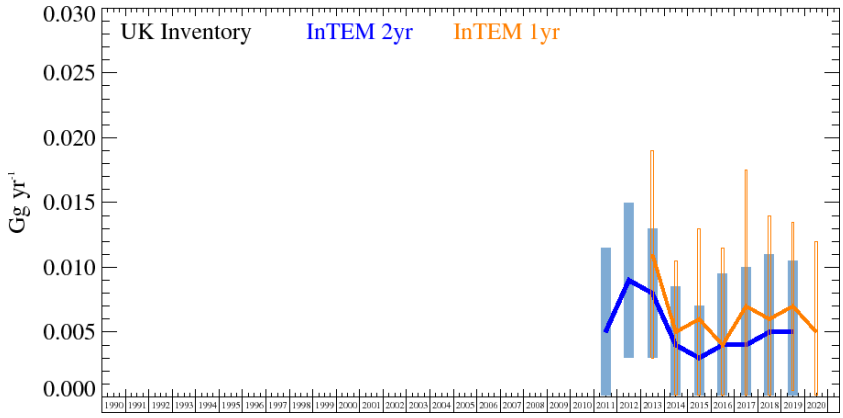

Figure 92: PFC-318 UK emission estimates (Gg yr^{-1}) from the UNFCCC GHGI (black) and InTEM (a) Annualised 2-year inversion (blue) (b) Annual inversion (orange). The uncertainty bars represent 1-σ.

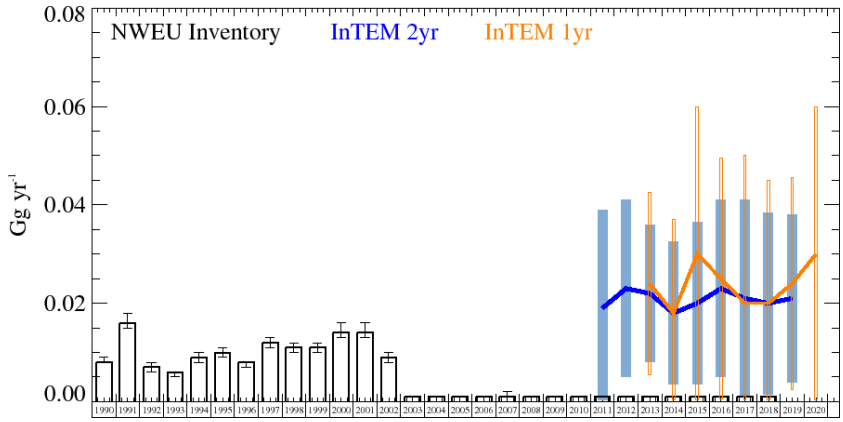

Figure 93: PFC-318 NWEU emission estimates (Gg yr^{-1}) from the UNFCCC GHGI (black) and InTEM (a) Annualised 2-year inversion (blue) (b) Annual inversion (orange). The uncertainty bars represent 1-σ.

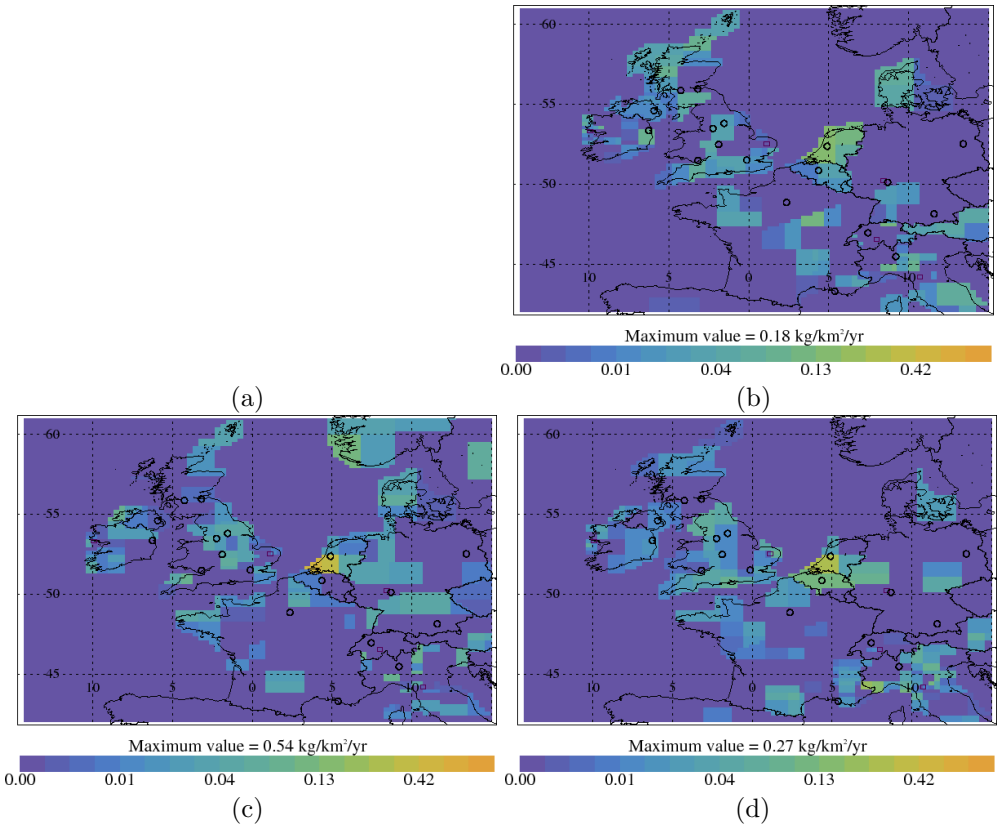

Figure 94: PFC-318 InTEM emission estimates (kg km^{-2} yr^{-1}) (a) No Data (b) 2011-2013 (c) 2014-2016 (d) 2017-2019

Table 23: UK and NWEU PFC-318 emission (Gg yr^{-1}) estimates with 1-σ uncertainty.

	UK			NWEU		
Years	Inventory	InTEM 2yr	InTEM 1yr	Inventory	InTEM 2yr	InTEM 1yr
1990	0.000 (0.00-0.01)			0.008 (0.008-0.009)		
1991	0.000 (0.00-0.01)			0.016 (0.015-0.018)		
1992	0.000 (0.00-0.01)			0.007 (0.006-0.008)		
1993	0.000 (0.00-0.01)			0.006 (0.005-0.006)		
1994	0.000 (0.00-0.01)			0.009 (0.008-0.010)		
1995	0.000 (0.00-0.01)			0.010 (0.009-0.011)		
1996	0.000 (0.00-0.01)			0.008 (0.007-0.008)		
1997	0.000 (0.00-0.01)			0.012 (0.011-0.013)		
1998	0.000 (0.00-0.01)			0.011 (0.010-0.012)		
1999	0.000 (0.00-0.01)			0.011 (0.010-0.012)		
2000	0.000 (0.00-0.01)			0.014 (0.013-0.016)		
2001	0.000 (0.00-0.01)			0.014 (0.013-0.016)		
2002	0.000 (0.00-0.01)			0.009 (0.008-0.010)		
2003	0.000 (0.00-0.01)			0.001 (0.001-0.001)		
2004	0.000 (0.00-0.01)			0.001 (0.001-0.001)		
2005	0.000 (0.00-0.01)			0.001 (0.001-0.001)		
2006	0.000 (0.00-0.01)			0.001 (0.001-0.001)		
2007	0.000 (0.00-0.01)			0.001 (0.001-0.002)		
2008	0.000 (0.00-0.01)			0.001 (0.001-0.001)		
2009	0.000 (0.00-0.01)			0.001 (0.001-0.001)		
2010	0.000 (0.00-0.01)			0.001 (0.001-0.001)		
2011	0.000 (0.00-0.01)	0.005 (0.000-0.013)		0.001 (0.001-0.001)	0.02 (0.00-0.04)	
2012	0.000 (0.00-0.01)	0.009 (0.003-0.015)		0.001 (0.001-0.001)	0.02 (0.01-0.04)	
2013	0.000 (0.00-0.01)	0.008 (0.003-0.013)	0.011 (0.003-0.019)	0.001 (0.001-0.001)	0.02 (0.01-0.04)	0.02 (0.01-0.04)
2014	0.000 (0.00-0.01)	0.004 (0.000-0.009)	0.005 (0.000-0.011)	0.001 (0.001-0.001)	0.02 (0.00-0.03)	0.02 (0.00-0.04)
2015	0.000 (0.00-0.01)	0.003 (0.000-0.008)	0.006 (0.000-0.014)	0.001 (0.001-0.001)	0.02 (0.00-0.04)	0.03 (0.00-0.06)
2016	0.000 (0.00-0.01)	0.004 (0.000-0.011)	0.004 (0.000-0.015)	0.001 (0.001-0.001)	0.02 (0.01-0.04)	0.03 (0.00-0.05)
2017	0.000 (0.00-0.01)	0.004 (0.000-0.012)	0.007 (0.000-0.021)	0.001 (0.001-0.001)	0.02 (0.00-0.04)	0.02 (0.00-0.06)
2018	0.000 (0.00-0.01)	0.005 (0.000-0.012)	0.006 (0.000-0.016)	0.001 (0.001-0.001)	0.02 (0.00-0.04)	0.02 (0.00-0.05)
2019		0.005 (0.000-0.011)	0.007 (0.000-0.013)		0.02 (0.00-0.04)	0.02 (0.00-0.05)
2020			0.005 (0.000-0.014)			0.03 (0.00-0.06)

4.24 Sulphur Hexafluoride (SF_6)

SF_6 is the most potent GHG of the reported gases in terms of GWP_{100} (Table 7). The global mole fraction is increasing at an accelerating rate. The growth rate is now 0.35 ppt yr^{-1}, up from 0.25 ppt yr^{-1} in 2005. SF_6 is predominantly used in electrical circuit breakers, heavy-duty gas-insulated switchgear for systems with voltages from 5 - 38 kV, and other switchgear used in the electrical transmission systems to manage high voltages (>38 kV). The electrical power industry uses ∼80% of all SF_6 produced worldwide. Although the units themselves are hermetically sealed and pressurised, aging equipment, breakdown and disposal, alongside leakage from wear-and-tear will cause this sector to emit SF_6. A minor use of this gas is as a blanketing (i.e. oxygen inhibiting inert gas) agent during magnesium production. Hence there are many sources of SF_6, some of which are quite diffuse.

The UK GHGI shows a steady decrease in emissions after 2001. The InTEM 2-year inversions show increasing emissions from 2005-2008 and then a decline thereafter, also matched by the 1-year inversions (Figure 97). There is good agreement with the inventory after 2015. The InTEM 1-month estimates, Figure 98, shows periodic spikes in emissions. InTEM 2-year and the annualised 1-month estimates agree well with NWEU GHGI across all years. There is evidence of strong emissions from SW Germany, Figure 100.

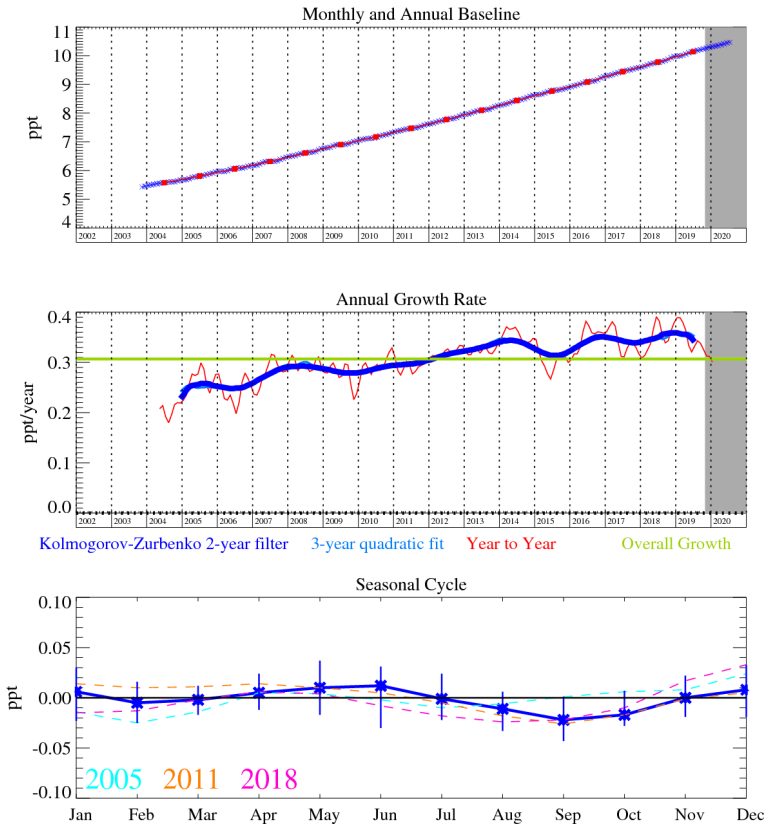

Figure 95: Monthly (blue) and annual (red) Mid-latitude Northern Hemisphere mole fractions (top plot). Annual (blue and red) and overall (green) growth rate (middle plot). Seasonal cycle (de-trended) with year-to-year variability (lower plot). Grey area covers un-ratified provisional data.

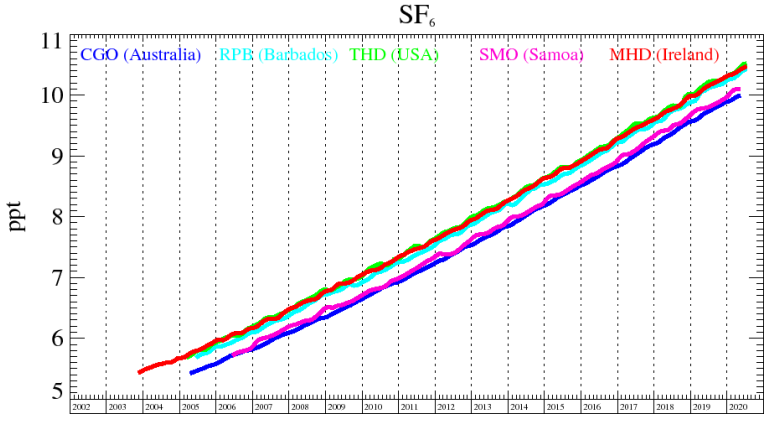

Figure 96: Background mole fractions at 5 AGAGE global stations

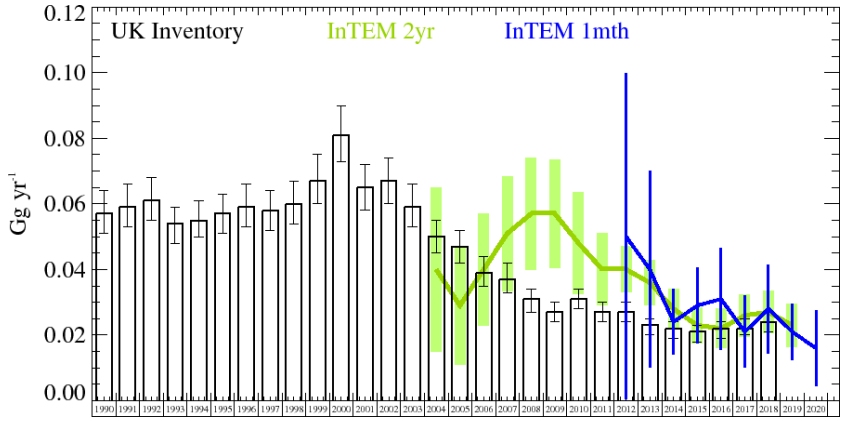

Figure 97: SF_6 UK emission estimates (Gg yr^{-1}) from the UNFCCC GHGI (black) and InTEM (a) Annualised 2 year inversion (green) (b) Annualised 1 month inversion (blue). The uncertainty bars represent 1-σ.

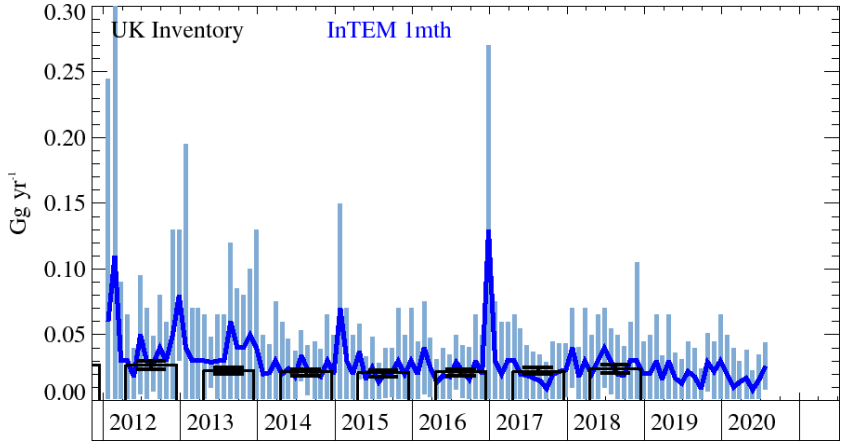

Figure 98: SF_6 UK emission estimates (Gg yr^{-1}) from the UNFCCC GHGI (black) and InTEM (monthly) DECC network (blue). The uncertainty bars represent 1-σ.

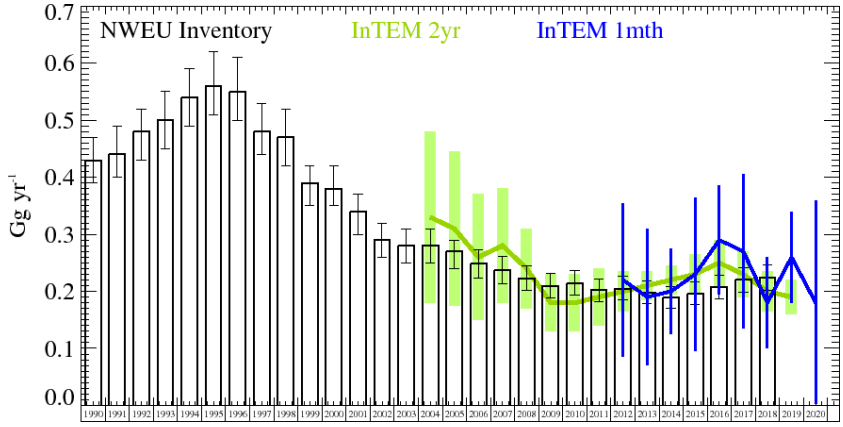

Figure 99: SF_6 NWEU emission estimates (Gg yr^{-1}) from the UNFCCC GHGI (black) and InTEM (a) Annualised 2 year inversion (green) (b) Annualised 1 month inversion (blue). The uncertainty bars represent 1-σ.

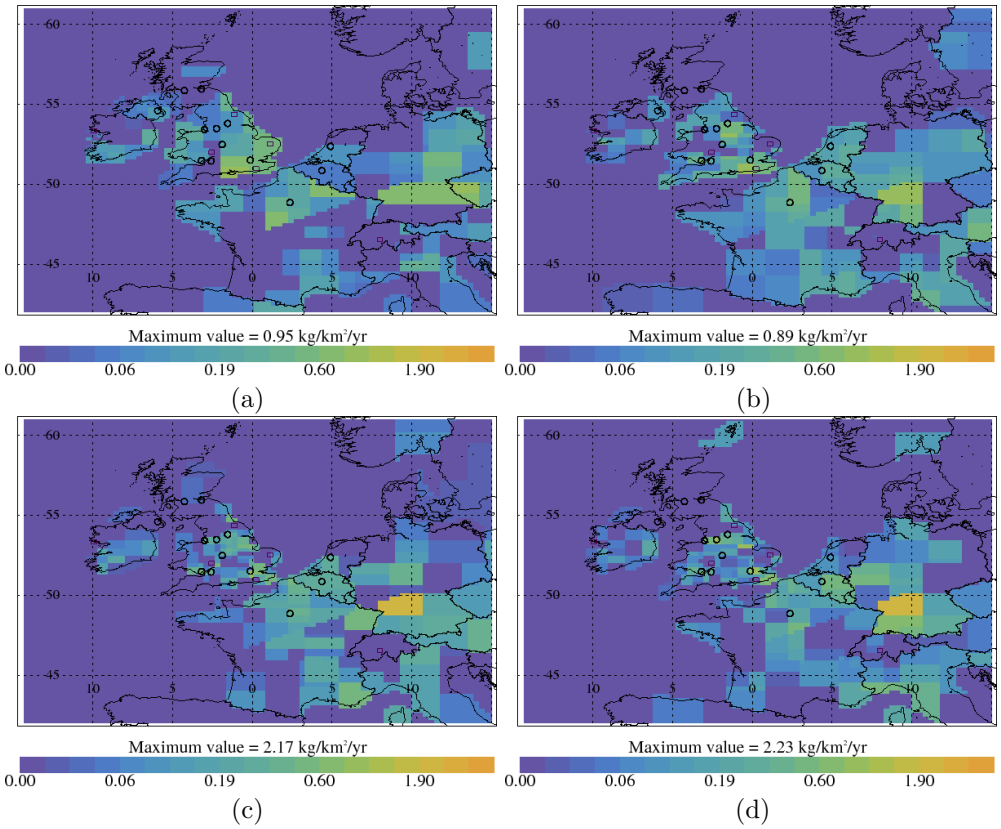

Figure 100: SF_6 InTEM emission estimates (kg km^{-2} yr^{-1}) (a) 2008-2010 (b) 2011-2013 (c) 2014-2016 (d) 2017-2019

Table 24: UK SF_6 emission (Gg yr^{-1}) estimates with 1-σ uncertainty.

	UK			NWEU		
Years	Inventory	InTEM 2yr	InTEM 1mth	Inventory	InTEM 2yr	InTEM 1mth
1990	0.057 (0.051-0.064)			0.43 (0.39-0.47)		
1991	0.059 (0.053-0.066)			0.44 (0.40-0.49)		
1992	0.061 (0.055-0.068)			0.48 (0.43-0.52)		
1993	0.054 (0.048-0.059)			0.50 (0.45-0.55)		
1994	0.055 (0.050-0.061)			0.54 (0.49-0.59)		
1995	0.057 (0.051-0.063)			0.56 (0.51-0.62)		
1996	0.059 (0.053-0.066)			0.55 (0.50-0.61)		
1997	0.058 (0.052-0.064)			0.48 (0.44-0.53)		
1998	0.060 (0.054-0.067)			0.47 (0.42-0.52)		
1999	0.067 (0.060-0.075)			0.39 (0.35-0.42)		
2000	0.081 (0.073-0.090)			0.38 (0.35-0.42)		
2001	0.065 (0.058-0.072)			0.34 (0.30-0.37)		
2002	0.067 (0.060-0.074)			0.29 (0.26-0.32)		
2003	0.059 (0.053-0.066)			0.28 (0.25-0.31)		
2004	0.050 (0.045-0.055)	0.040 (0.020-0.070)		0.28 (0.25-0.31)	0.33 (0.18-0.48)	
2005	0.047 (0.042-0.052)	0.029 (0.011-0.047)		0.27 (0.24-0.29)	0.31 (0.17-0.44)	
2006	0.039 (0.035-0.044)	0.040 (0.023-0.057)		0.25 (0.22-0.27)	0.26 (0.15-0.37)	
2007	0.037 (0.033-0.042)	0.051 (0.034-0.069)		0.24 (0.21-0.26)	0.28 (0.18-0.38)	
2008	0.031 (0.027-0.034)	0.057 (0.040-0.074)		0.22 (0.20-0.24)	0.24 (0.17-0.31)	
2009	0.027 (0.024-0.030)	0.057 (0.041-0.074)		0.21 (0.19-0.23)	0.18 (0.13-0.23)	
2010	0.031 (0.028-0.034)	0.048 (0.032-0.063)		0.21 (0.19-0.24)	0.18 (0.13-0.23)	
2011	0.027 (0.024-0.030)	0.040 (0.029-0.051)		0.20 (0.18-0.22)	0.19 (0.14-0.24)	
2012	0.027 (0.024-0.030)	0.040 (0.033-0.047)	0.050 (0.000-0.100)	0.20 (0.18-0.23)	0.20 (0.17-0.24)	0.22 (0.08-0.35)
2013	0.023 (0.020-0.025)	0.036 (0.029-0.043)	0.040 (0.010-0.070)	0.20 (0.18-0.22)	0.21 (0.19-0.24)	0.19 (0.07-0.31)
2014	0.022 (0.019-0.024)	0.028 (0.022-0.034)	0.024 (0.014-0.034)	0.19 (0.17-0.21)	0.22 (0.20-0.25)	0.20 (0.13-0.28)
2015	0.021 (0.018-0.023)	0.023 (0.018-0.029)	0.029 (0.017-0.040)	0.20 (0.18-0.22)	0.23 (0.20-0.27)	0.23 (0.09-0.36)
2016	0.022 (0.019-0.024)	0.022 (0.016-0.028)	0.031 (0.016-0.047)	0.21 (0.19-0.23)	0.25 (0.21-0.29)	0.29 (0.20-0.39)
2017	0.022 (0.020-0.025)	0.026 (0.019-0.032)	0.021 (0.010-0.032)	0.22 (0.20-0.24)	0.23 (0.19-0.27)	0.27 (0.14-0.41)
2018	0.024 (0.021-0.027)	0.027 (0.021-0.034)	0.028 (0.015-0.042)	0.22 (0.20-0.25)	0.20 (0.16-0.23)	0.18 (0.10-0.26)
2019		0.023 (0.017-0.030)	0.021 (0.013-0.030)		0.19 (0.16-0.22)	0.26 (0.18-0.34)
2020			0.016 (0.004-0.027)			0.18 (0.00-0.36)

4.25 Nitrogen trifluoride (NF_3)

NF_3 is used in the manufacture of semiconductors, flat panel displays and photovoltaic cells. Although the current contribution of NF_3 to radiative forcing is small, its potential to impact the climate is significant (see Table 7). NF_3 is rapidly increasing in the atmosphere. Its atmospheric growth rate appears to have stabilised after a period of rapid growth (2015-2017). UK emissions as reported through the GHGI are very small and this is in line with what is observed in the atmosphere. The InTEM results for both the UK and NWEU are very small and uncertain.

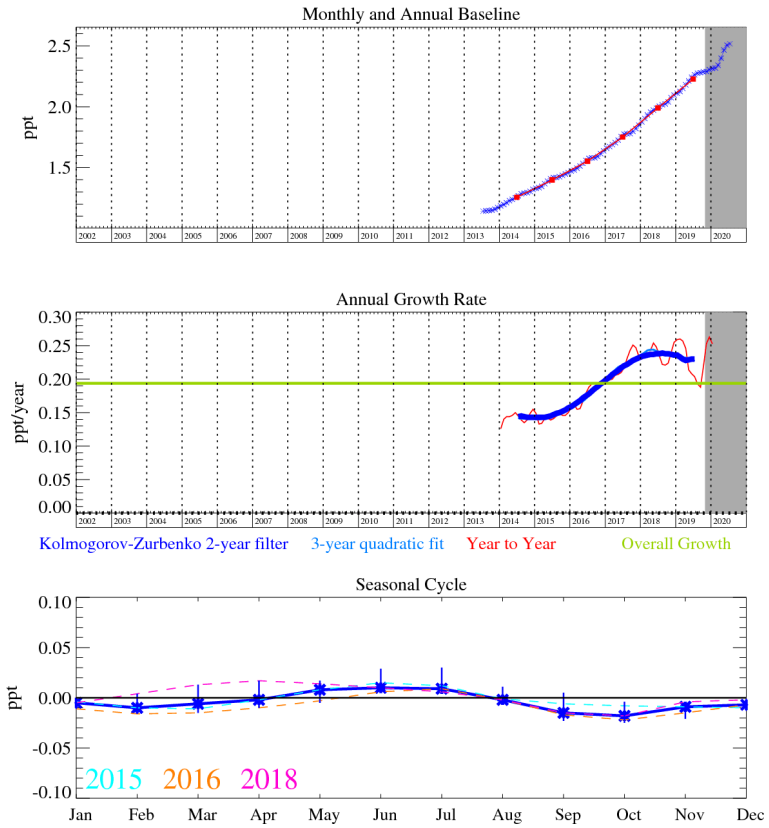

Figure 101: Monthly (blue) and annual (red) Mid-latitude Northern Hemisphere mole fractions (top plot). Annual (blue and red) and overall (green) growth rate (middle plot). Seasonal cycle (de-trended) with year-to-year variability (lower plot). Grey area covers un-ratified provisional data.

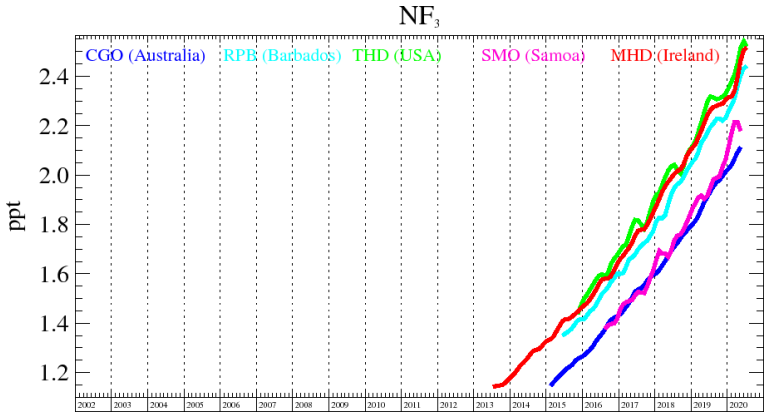

Figure 102: Background mole fractions at 5 AGAGE global stations

4.26 CFC Summary

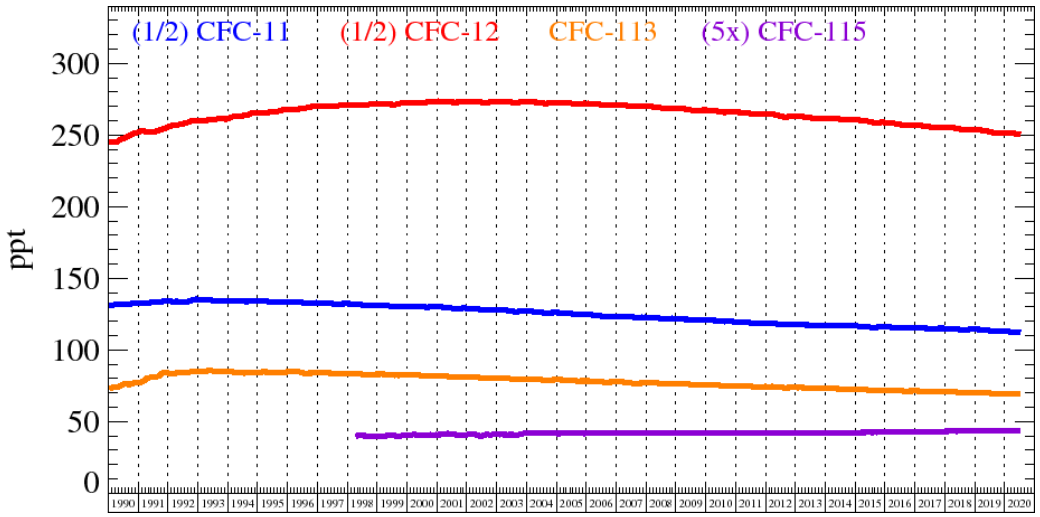

Figure 103: Northern Hemisphere Atmospheric Background Levels of CFCs as observed at the Mace Head observing station. Note that for scale purposes the atmospheric mole fractions of CFC-11 and CFC-12 have been divided by 2. and CFC-115 multiplied by 5

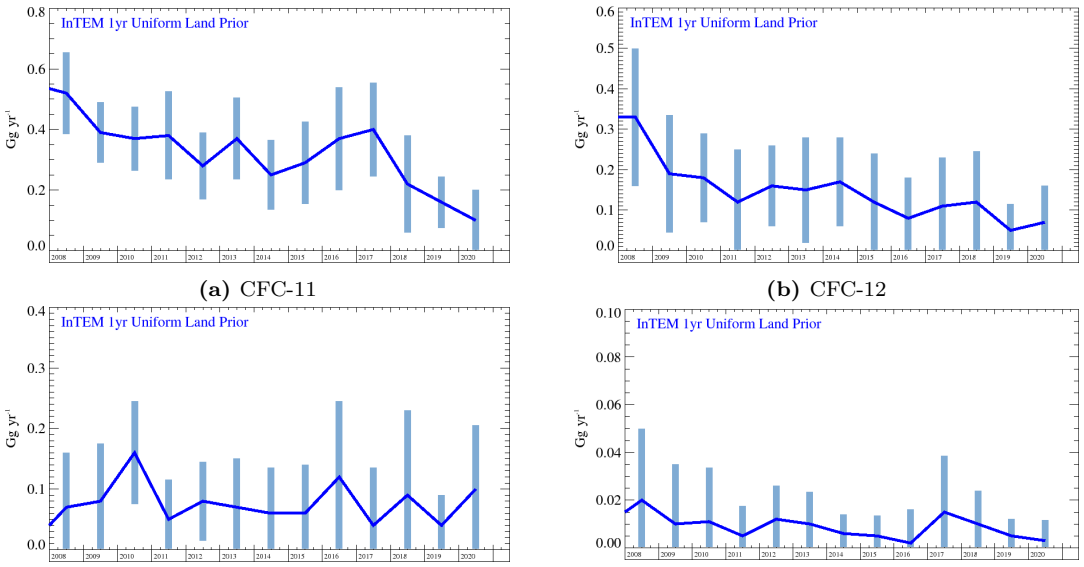

(a) CFC-11

(b) CFC-12

(c) CFC-113

(d) CFC-115

Figure 104: CFC UK emission estimates (Gg yr^{-1}) from InTEM annual inversion (blue). The uncertainty bars represent 1-σ.

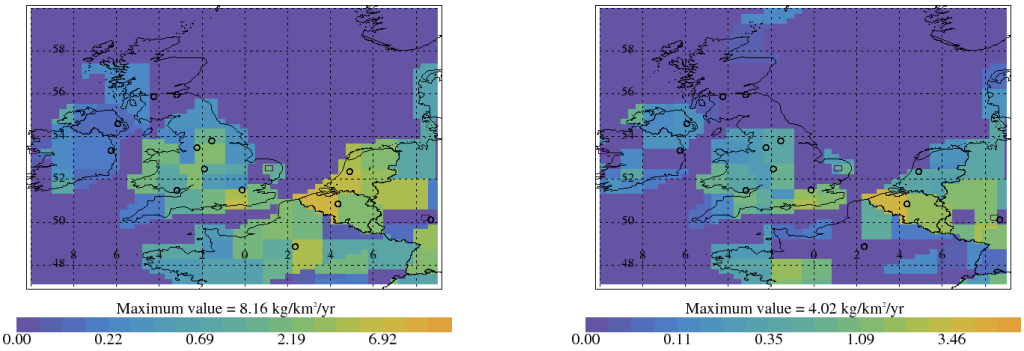

(a) CFC-11

(b) CFC-12

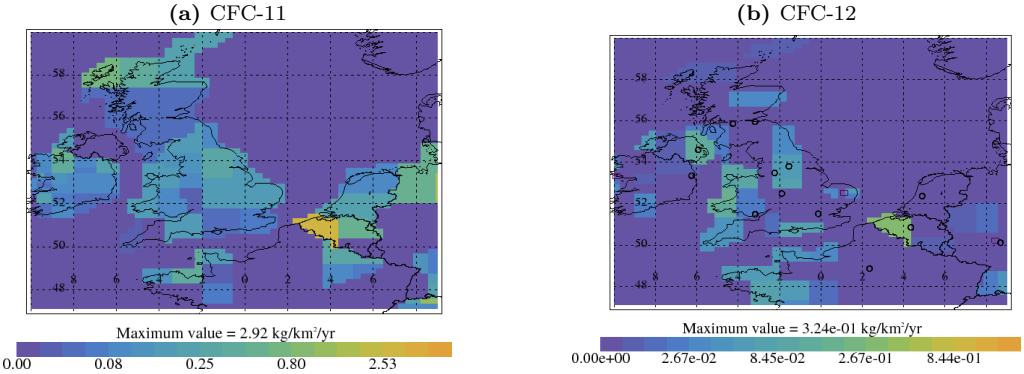

(c) CFC-113

(d) CFC-115

Figure 105: InTEM CFC emission estimates (kg km^{-2} yr^{-1}). Note each plot has its own scale.

4.27 CFC-11

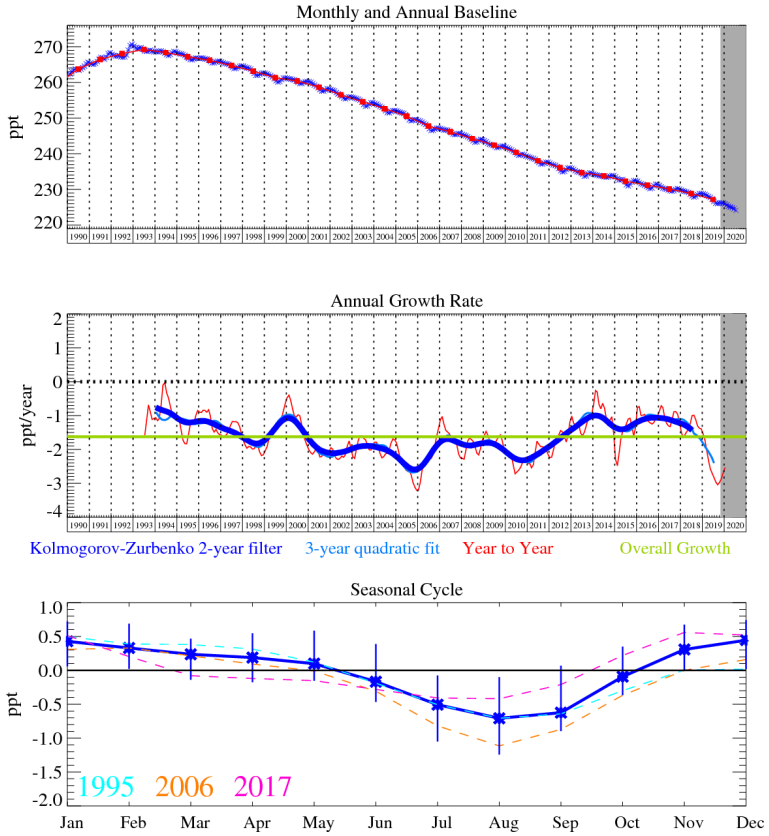

Figure 106: Monthly (blue) and annual (red) Mid-latitude Northern Hemisphere mole fractions (top plot). Annual (blue and red) and overall (green) growth rate (middle plot). Seasonal cycle (de-trended) with year-to-year variability (lower plot). Grey area covers un-ratified provisional data.

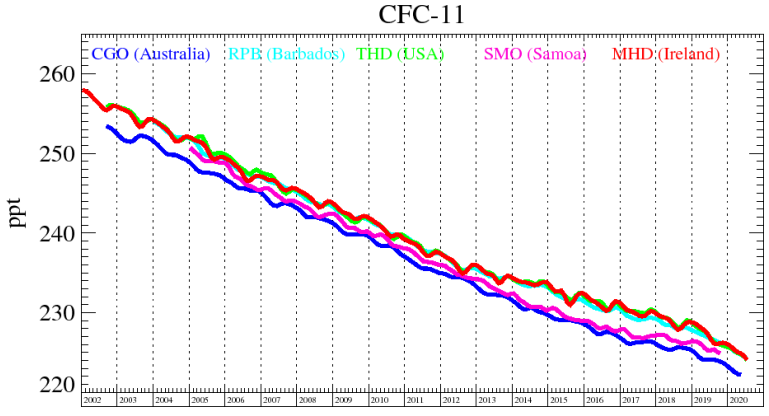

Figure 107: Background mole fractions at 5 AGAGE global stations

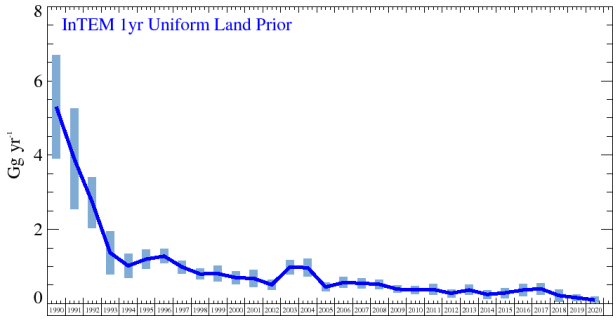

Figure 108: CFC-11 UK emission estimates (Gg yr^{-1}) from InTEM annual inversion (blue). The uncertainty bars represent 1-σ.

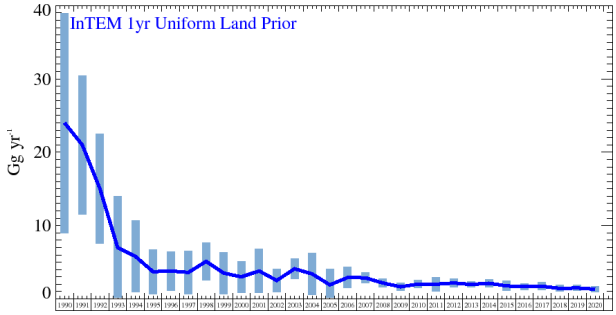

Figure 109: CFC-11 NWEU emission estimates (Gg yr^{-1}) from InTEM annual inversion (blue). The uncertainty bars represent 1-σ.

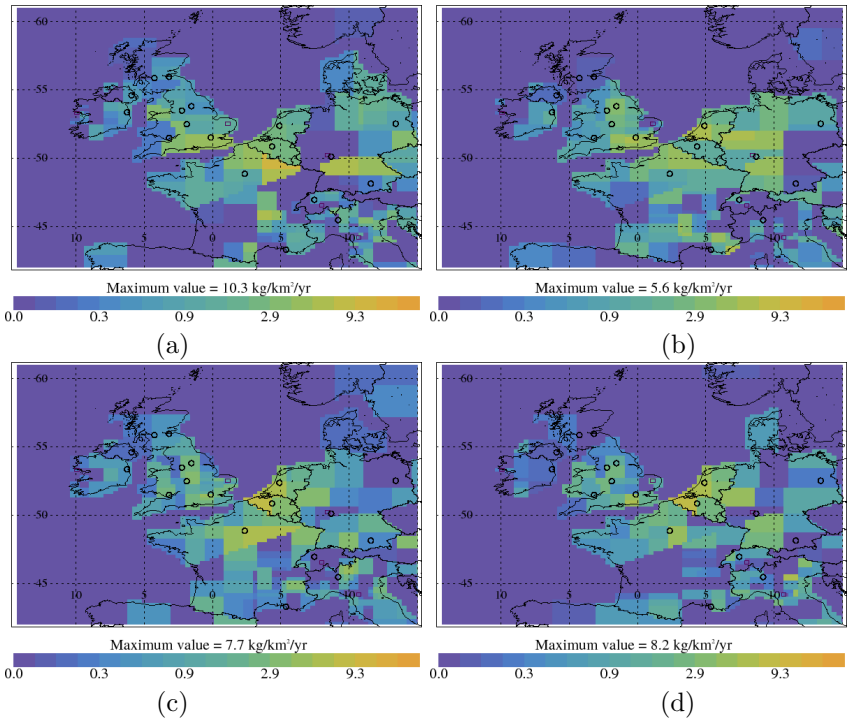

Figure 110: CFC-11 InTEM emission estimates (kg km^{-2} yr^{-1}) (a) 2008-2010 (b) 2011-2013 (c) 2014-2016 (d) 2017-2019

Table 25: UK and NWEU CFC-11 emission (Gg yr^{-1}) estimates with 1-σ uncertainty.

Years	UK InTEM 1yr	NWEU InTEM 1yr
1990	5.30 (3.90-6.70)	24.0 (9.-39.)
1991	3.90 (2.60-5.30)	21.0 (11.-30.)
1992	2.73 (2.04-3.41)	15.0 (7.-22.)
1993	1.37 (0.80-1.95)	7.00 (0.-14.)
1994	1.02 (0.70-1.35)	5.80 (0.9-10.7)
1995	1.20 (0.95-1.46)	3.70 (0.7-6.8)
1996	1.28 (1.09-1.48)	3.80 (1.1-6.4)
1997	0.99 (0.81-1.16)	3.60 (0.7-6.6)
1998	0.80 (0.65-0.94)	5.10 (2.5-7.6)
1999	0.81 (0.60-1.02)	3.50 (0.6-6.3)
2000	0.70 (0.52-0.88)	3.00 (0.9-5.2)
2001	0.68 (0.44-0.91)	3.80 (0.8-6.8)
2002	0.51 (0.38-0.64)	2.50 (0.9-4.1)
2003	0.98 (0.78-1.17)	4.10 (2.8-5.5)
2004	0.97 (0.73-1.20)	3.40 (0.6-6.3)
2005	0.45 (0.33-0.57)	1.90 (0.0-4.4)
2006	0.57 (0.42-0.71)	2.90 (1.4-4.3)
2007	0.55 (0.41-0.68)	2.87 (2.12-3.62)
2008	0.52 (0.39-0.66)	2.16 (1.57-2.76)
2009	0.39 (0.29-0.49)	1.64 (1.07-2.22)
2010	0.37 (0.26-0.47)	2.01 (1.47-2.55)
2011	0.38 (0.24-0.53)	1.99 (1.06-2.93)
2012	0.28 (0.17-0.39)	2.16 (1.59-2.73)
2013	0.37 (0.23-0.50)	1.96 (1.55-2.36)
2014	0.25 (0.14-0.37)	2.12 (1.62-2.62)
2015	0.29 (0.16-0.43)	1.76 (1.09-2.44)
2016	0.37 (0.20-0.54)	1.65 (1.18-2.11)
2017	0.40 (0.24-0.55)	1.72 (1.18-2.27)
2018	0.22 (0.06-0.38)	1.42 (0.98-1.86)
2019	0.16 (0.07-0.24)	1.48 (1.10-1.86)
2020	0.10 (0.00-0.20)	1.32 (0.90-1.75)

4.28 CFC-12

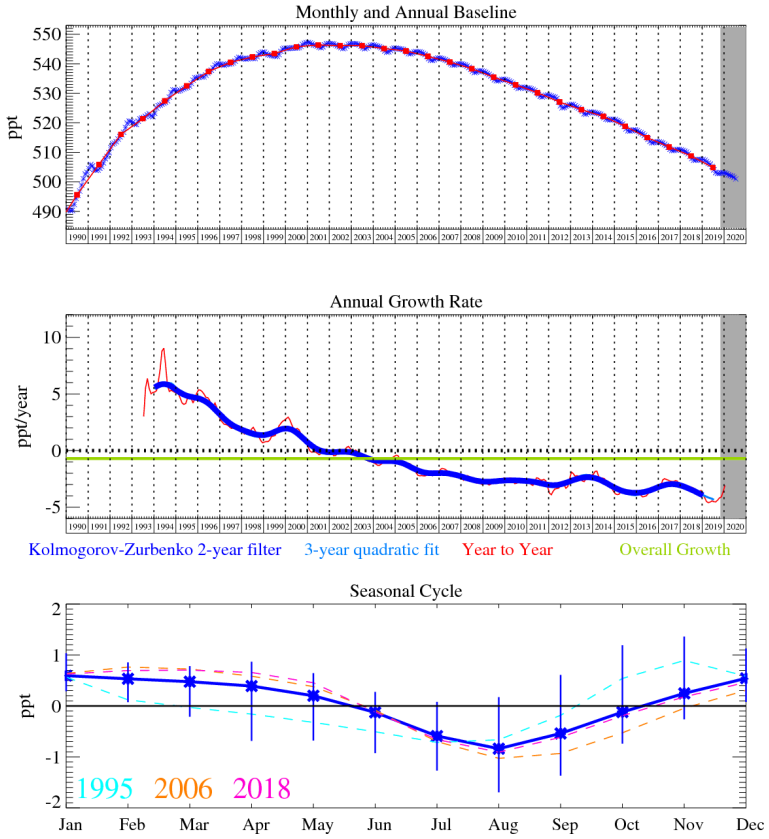

Figure 111: Monthly (blue) and annual (red) Mid-latitude Northern Hemisphere mole fractions (top plot). Annual (blue and red) and overall (green) growth rate (middle plot). Seasonal cycle (de-trended) with year-to-year variability (lower plot). Grey area covers un-ratified provisional data.

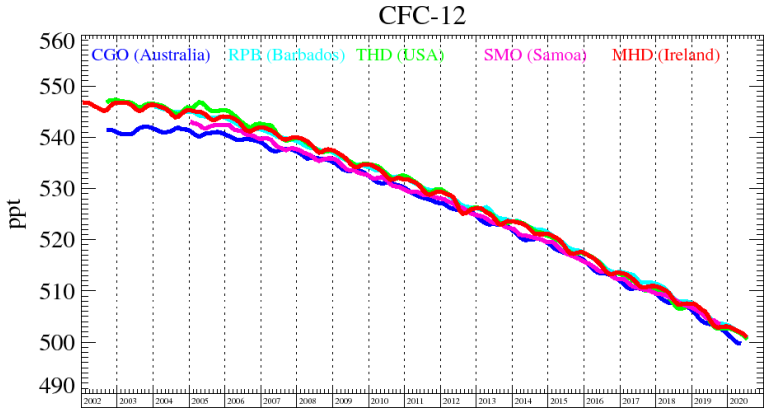

Figure 112: Background mole fractions at 5 AGAGE global stations

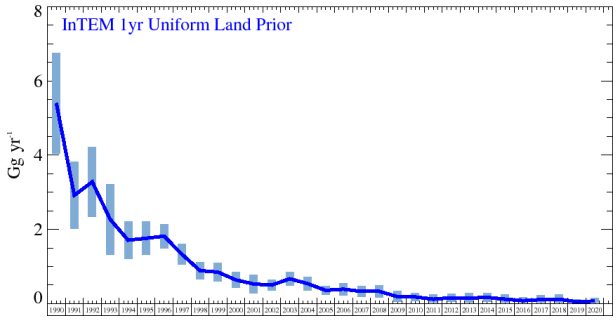

Figure 113: CFC-12 UK emission estimates (Gg yr^{-1}) from InTEM annual inversion (blue). The uncertainty bars represent 1-σ.

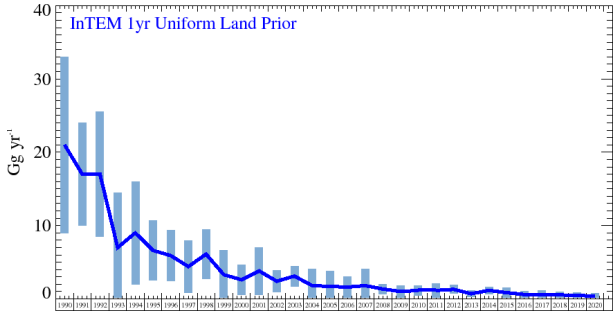

Figure 114: CFC-12 NWEU emission estimates (Gg yr^{-1}) from InTEM annual inversion (blue). The uncertainty bars represent 1-σ.

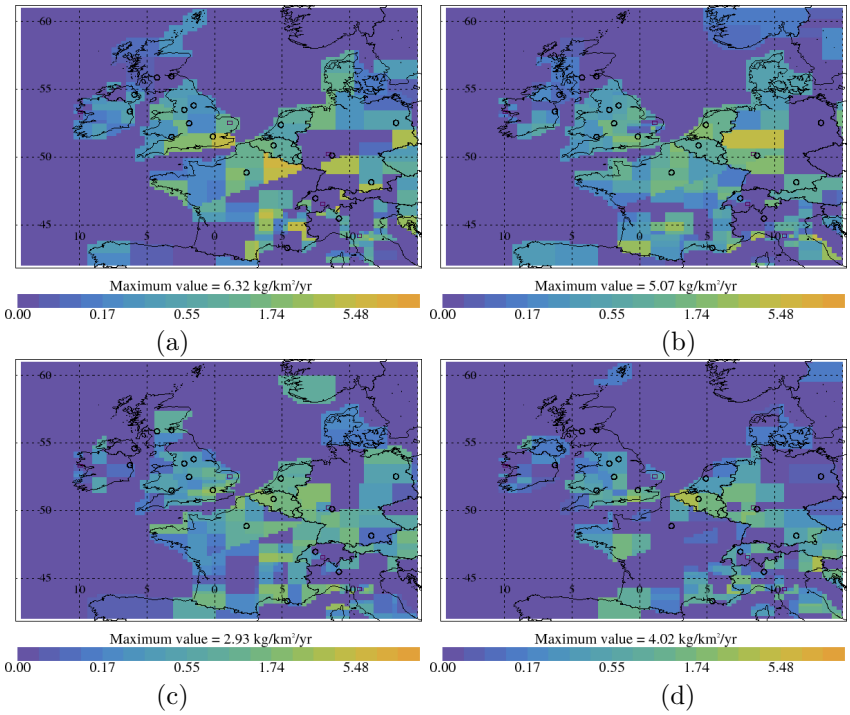

Figure 115: CFC-12 InTEM emission estimates (kg km^{-2} yr^{-1}) (a) 2008-2010 (b) 2011-2013 (c) 2014-2016 (d) 2017-2019

Table 26: UK and NWEU CFC-12 emission (Gg yr^{-1}) estimates with 1-σ uncertainty.

Years	UK InTEM 1yr	NWEU InTEM 1yr
1990	5.4 (4.1-6.8)	21. (1.-40.)
1991	2.92 (2.02-3.82)	17. (10.-24.)
1992	3.28 (2.34-4.22)	17. (8.-25.)
1993	2.27 (1.32-3.22)	7. (0.-15.)
1994	1.71 (1.21-2.22)	9. (2.-16.)
1995	1.76 (1.31-2.21)	6.6 (2.5-10.7)
1996	1.82 (1.50-2.15)	5.9 (2.4-9.4)
1997	1.33 (1.05-1.61)	4.4 (0.9-8.0)
1998	0.89 (0.66-1.12)	6.1 (2.7-9.5)
1999	0.85 (0.60-1.10)	3.3 (0.0-6.6)
2000	0.64 (0.43-0.84)	2.6 (0.6-4.7)
2001	0.53 (0.29-0.78)	3.8 (0.5-7.0)
2002	0.50 (0.35-0.65)	2.4 (0.9-3.9)
2003	0.67 (0.49-0.84)	3.1 (1.7-4.5)
2004	0.54 (0.35-0.73)	1.8 (0.0-4.6)
2005	0.36 (0.23-0.48)	1.7 (0.0-4.1)
2006	0.39 (0.23-0.55)	1.6 (0.2-3.0)
2007	0.33 (0.17-0.48)	1.8 (0.0-4.6)
2008	0.33 (0.16-0.50)	1.34 (0.65-2.04)
2009	0.19 (0.05-0.34)	1.00 (0.19-1.81)
2010	0.18 (0.07-0.29)	1.14 (0.45-1.84)
2011	0.12 (0.00-0.26)	1.14 (0.17-2.11)
2012	0.16 (0.06-0.26)	1.29 (0.72-1.86)
2013	0.15 (0.02-0.28)	0.70 (0.30-1.11)
2014	0.17 (0.06-0.28)	1.15 (0.64-1.66)
2015	0.12 (0.00-0.24)	0.84 (0.15-1.53)
2016	0.08 (0.00-0.20)	0.59 (0.11-1.07)
2017	0.11 (0.00-0.24)	0.54 (0.00-1.14)
2018	0.12 (0.00-0.25)	0.53 (0.10-0.95)
2019	0.05 (0.00-0.13)	0.46 (0.05-0.86)
2020	0.07 (0.00-0.18)	0.37 (0.00-0.86)

4.29 CFC-113

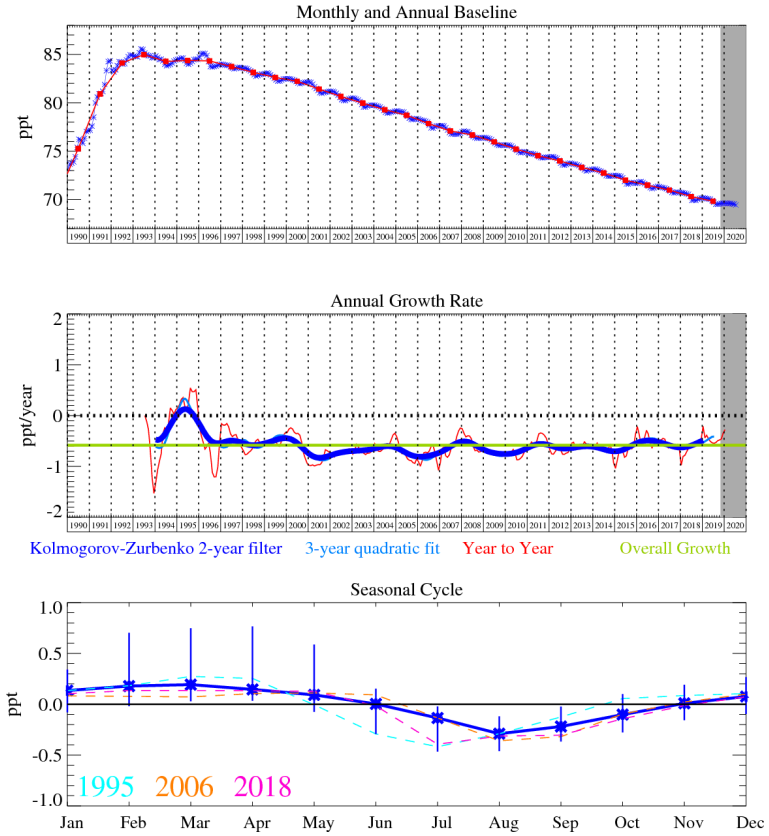

Figure 116: Monthly (blue) and annual (red) Mid-latitude Northern Hemisphere mole fractions (top plot). Annual (blue and red) and overall (green) growth rate (middle plot). Seasonal cycle (de-trended) with year-to-year variability (lower plot). Grey area covers un-ratified provisional data.

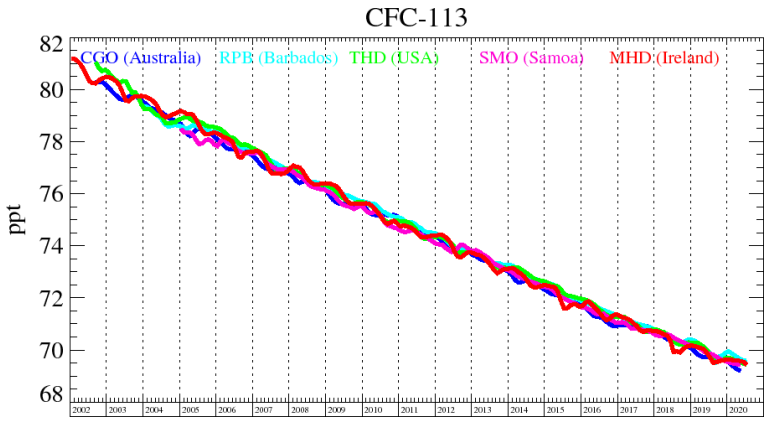

Figure 117: Background mole fractions at 5 AGAGE global stations

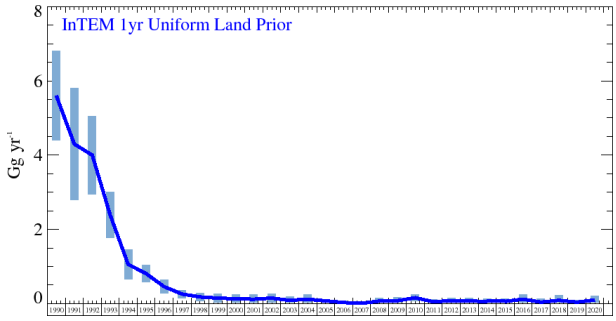

Figure 118: CFC-113 UK emission estimates (Gg yr^{-1}) from InTEM annual inversion (blue). The uncertainty bars represent 1-σ.

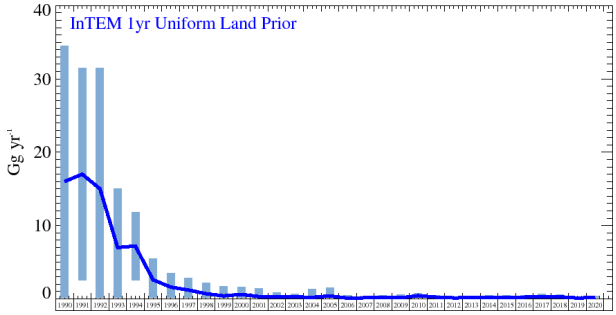

Figure 119: CFC-113 NWEU emission estimates (Gg yr^{-1}) from InTEM annual inversion (blue). The uncertainty bars represent 1-σ.

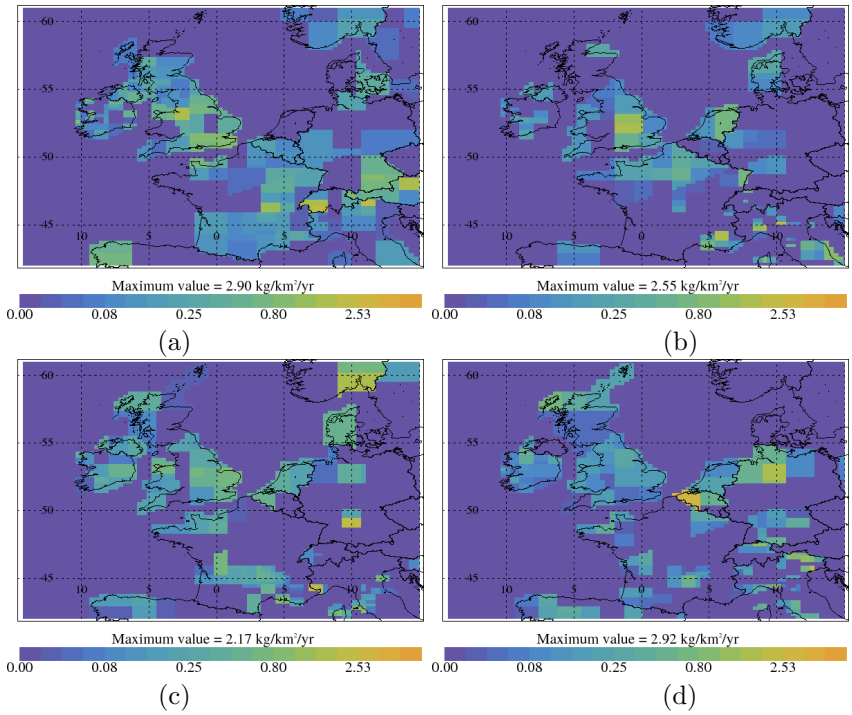

Figure 120: CFC-113 InTEM emission estimates (kg km^{-2} yr^{-1}) (a) 2008-2010 (b) 2011-2013 (c) 2014-2016 (d) 2017-2019

Table 27: UK and NWEU CFC-113 emission (Gg yr^{-1}) estimates with 1-σ uncertainty.

Years	UK InTEM 1yr	NWEU InTEM 1yr
1990	5.6 (4.4-6.8)	16. (0.-37.)
1991	4.3 (2.8-5.8)	17. (2.-31.)
1992	4.0 (3.0-5.1)	15. (0.-33.)
1993	2.39 (1.78-3.01)	7. (0.-16.)
1994	1.06 (0.67-1.46)	7.2 (2.6-11.9)
1995	0.81 (0.57-1.04)	2.6 (0.0-5.8)
1996	0.46 (0.28-0.64)	1.6 (0.0-3.9)
1997	0.26 (0.16-0.37)	1.2 (0.0-3.3)
1998	0.18 (0.06-0.29)	0.7 (0.0-2.9)
1999	0.15 (0.02-0.27)	0.4 (0.0-2.7)
2000	0.13 (0.02-0.24)	0.6 (0.0-2.1)
2001	0.12 (0.00-0.25)	0.3 (0.0-2.3)
2002	0.15 (0.03-0.28)	0.27 (0.00-1.19)
2003	0.09 (0.00-0.20)	0.26 (0.00-0.90)
2004	0.12 (0.00-0.24)	0.2 (0.0-2.2)
2005	0.00 (0.00-0.10)	0.4 (0.0-2.3)
2006	0.03 (0.00-0.11)	0.09 (0.00-0.79)
2007	0.01 (0.00-0.11)	0.0 (0.0-2.4)
2008	0.07 (0.00-0.18)	0.20 (0.00-0.56)
2009	0.08 (0.00-0.19)	0.14 (0.00-0.95)
2010	0.16 (0.08-0.25)	0.43 (0.09-0.77)
2011	0.05 (0.00-0.13)	0.23 (0.00-0.56)
2012	0.08 (0.02-0.15)	0.13 (0.00-0.38)
2013	0.07 (0.00-0.16)	0.15 (0.00-0.39)
2014	0.06 (0.00-0.15)	0.23 (0.00-0.57)
2015	0.06 (0.00-0.16)	0.20 (0.00-0.58)
2016	0.12 (0.00-0.25)	0.23 (0.00-0.51)
2017	0.04 (0.00-0.19)	0.29 (0.00-0.69)
2018	0.09 (0.00-0.28)	0.27 (0.00-0.56)
2019	0.04 (0.00-0.10)	0.11 (0.00-0.32)
2020	0.10 (0.00-0.21)	0.19 (0.00-0.49)

4.30 CFC-115

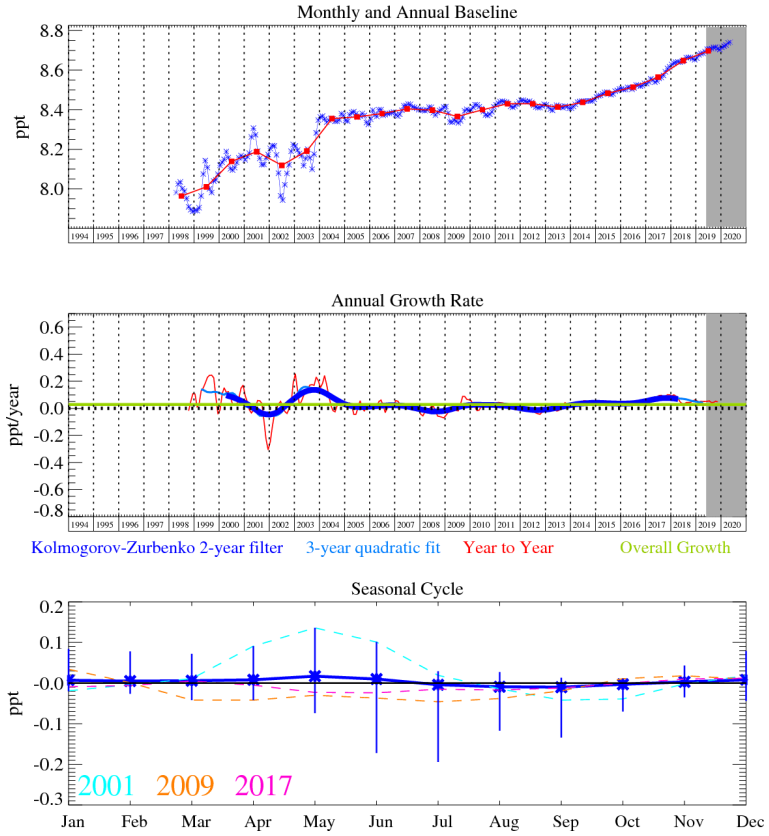

Figure 121: Monthly (blue) and annual (red) Mid-latitude Northern Hemisphere mole fractions (top plot). Annual (blue and red) and overall (green) growth rate (middle plot). Seasonal cycle (de-trended) with year-to-year variability (lower plot). Grey area covers un-ratified provisional data.

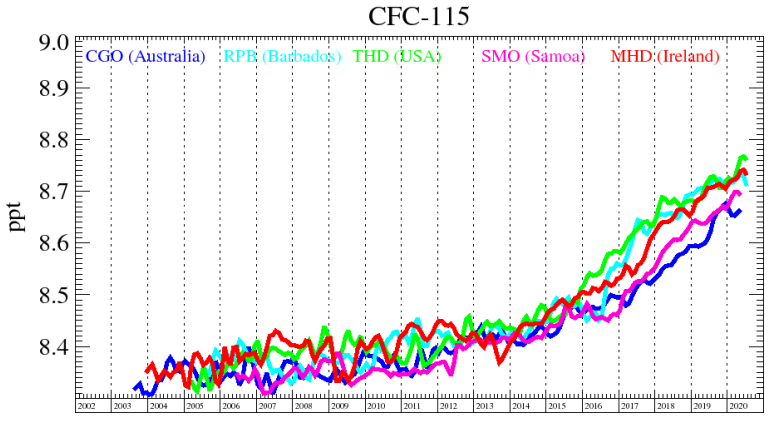

Figure 122: Background mole fractions at 5 AGAGE global stations

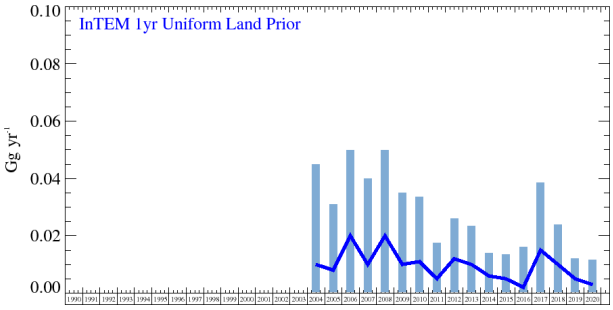

Figure 123: CFC-115 UK emission estimates (Gg yr^{-1}) from InTEM annual inversion (blue). The uncertainty bars represent 1-σ.

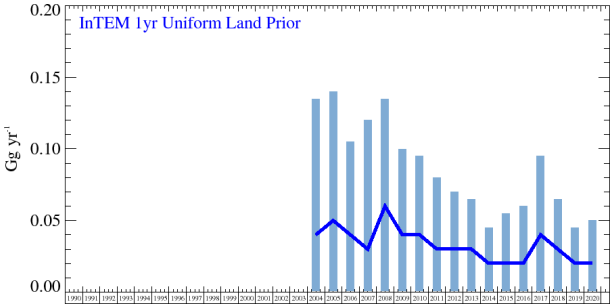

Figure 124: CFC-115 NWEU emission estimates (Gg yr^{-1}) from InTEM annual inversion (blue). The uncertainty bars represent 1-σ.

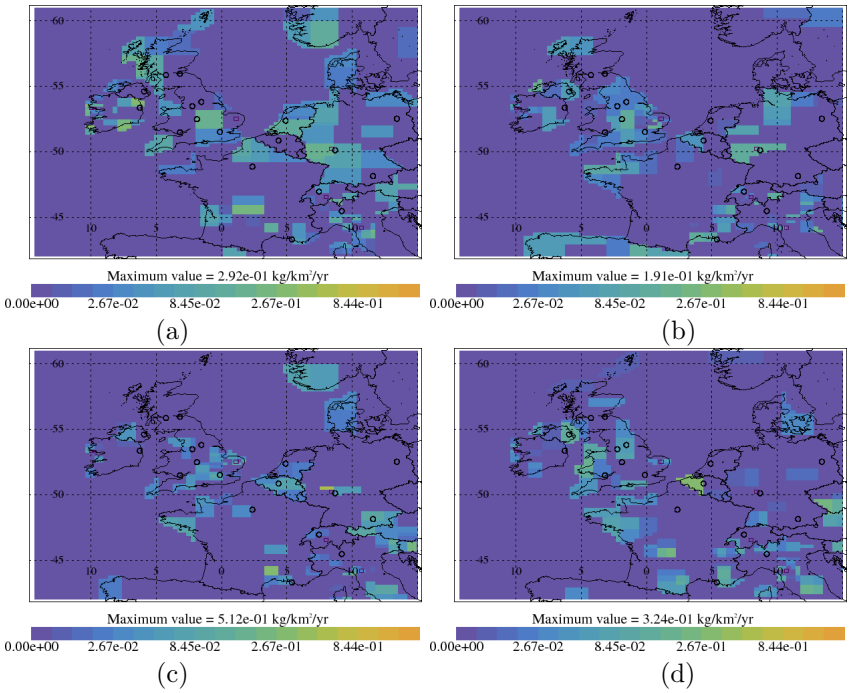

Figure 125: CFC-115 InTEM emission estimates (kg km^{-2} yr^{-1}) (a) 2008-2010 (b) 2011-2013 (c) 2014-2016 (d) 2017-2019

Table 28: UK and NWEU CFC-115 emission (Gg yr^{-1}) estimates with 1-σ uncertainty.

Years	UK InTEM 1yr	NWEU InTEM 1yr
2004	0.01 (0.00-0.07)	0.04 (0.00-0.19)
2005	0.008 (0.000-0.046)	0.05 (0.00-0.18)
2006	0.02 (0.00-0.06)	0.04 (0.00-0.13)
2007	0.01 (0.00-0.06)	0.03 (0.00-0.18)
2008	0.02 (0.00-0.06)	0.06 (0.00-0.15)
2009	0.01 (0.00-0.05)	0.04 (0.00-0.12)
2010	0.011 (0.000-0.045)	0.04 (0.00-0.11)
2011	0.005 (0.000-0.025)	0.03 (0.00-0.10)
2012	0.012 (0.000-0.028)	0.03 (0.00-0.08)
2013	0.010 (0.000-0.027)	0.03 (0.00-0.07)
2014	0.006 (0.000-0.016)	0.02 (0.00-0.05)
2015	0.005 (0.000-0.017)	0.02 (0.00-0.07)
2016	0.002 (0.000-0.028)	0.02 (0.00-0.08)
2017	0.015 (0.000-0.047)	0.04 (0.00-0.11)
2018	0.010 (0.000-0.028)	0.03 (0.00-0.07)
2019	0.005 (0.000-0.014)	0.02 (0.00-0.05)
2020	0.003 (0.000-0.017)	0.02 (0.00-0.06)

4.31 HCFC Summary

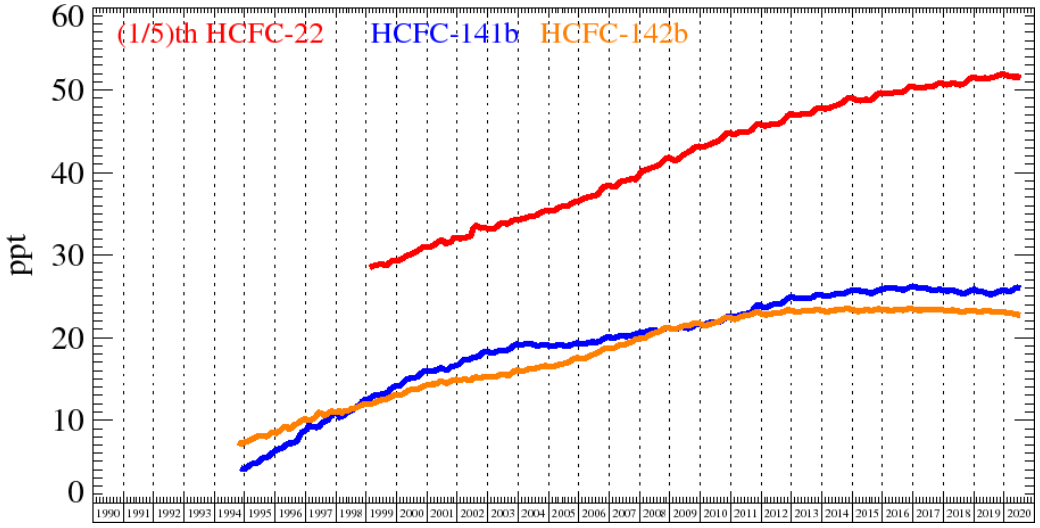

Figure 126: Northern Hemisphere Atmospheric Background Levels of HCFCs as observed at the Mace Head observing station. Note that for scale purposes the atmospheric mole fractions of HCFC-22 has been divided by 5

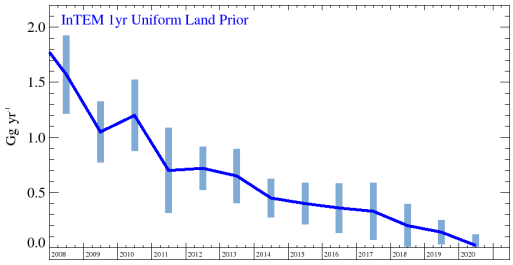

(a) HCFC-22

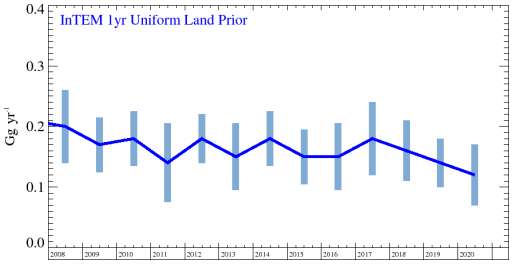

(b) HCFC-141b

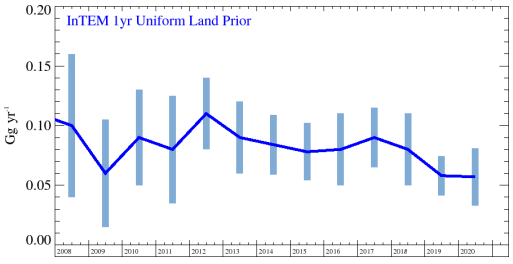

(c) HCFC-142b

Figure 127: HCFC UK emission estimates (Gg yr^{-1}) from InTEM annual inversion (blue). The uncertainty bars represent 1-σ.

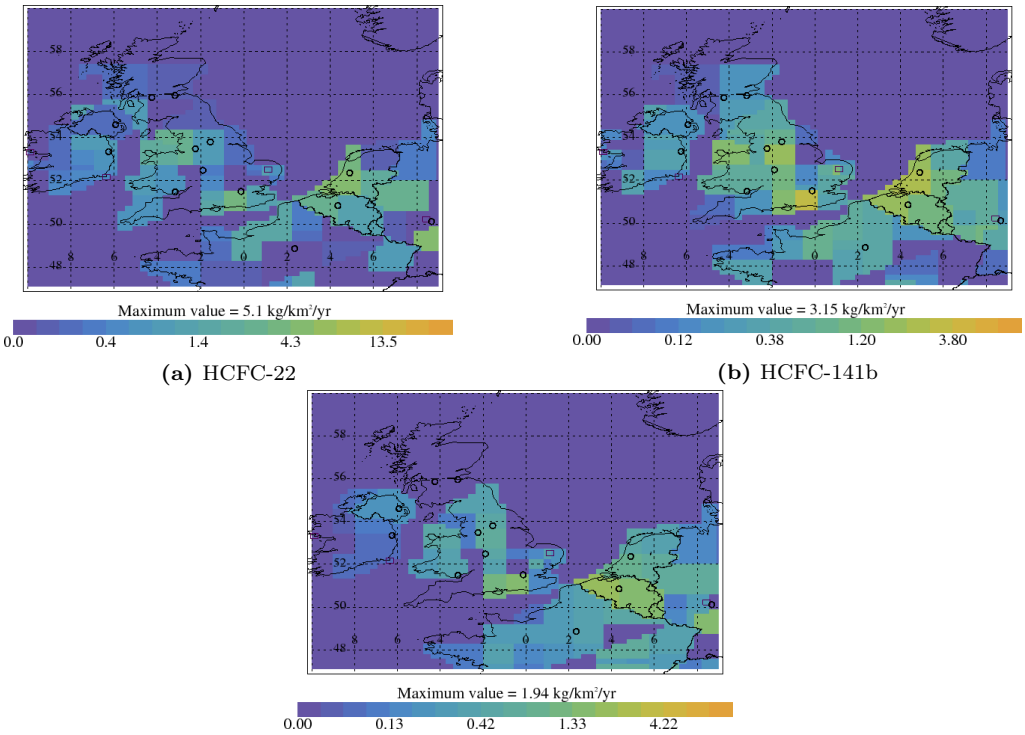

(a) HCFC-22

(b) HCFC-141b

(c) HCFC-142b

Figure 128: InTEM HCFC emission estimates (kg km^{-2} yr^{-1}). Note each plot has its own scale.

4.32 HCFC-22

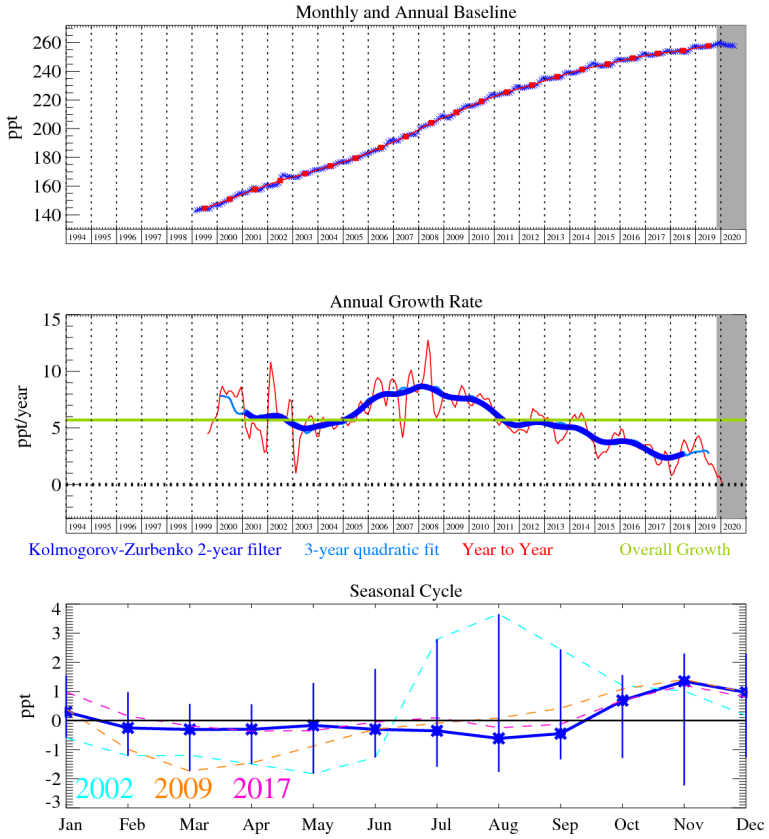

Figure 129: Monthly (blue) and annual (red) Mid-latitude Northern Hemisphere mole fractions (top plot). Annual (blue and red) and overall (green) growth rate (middle plot). Seasonal cycle (de-trended) with year-to-year variability (lower plot). Grey area covers un-ratified provisional data.

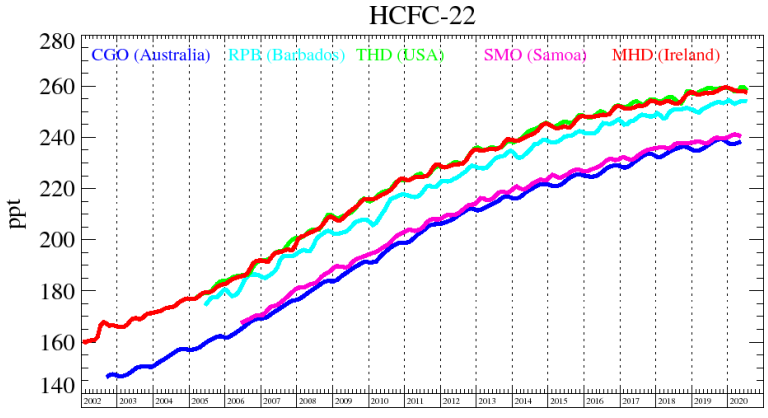

Figure 130: Background mole fractions at 5 AGAGE global stations

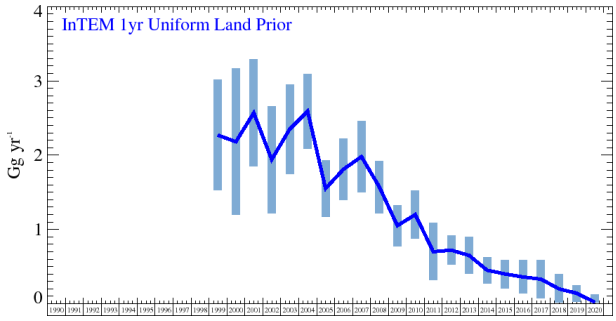

Figure 131: HCFC-22 UK emission estimates (Gg yr^{-1}) from InTEM annual inversion (blue). The uncertainty bars represent 1-σ.

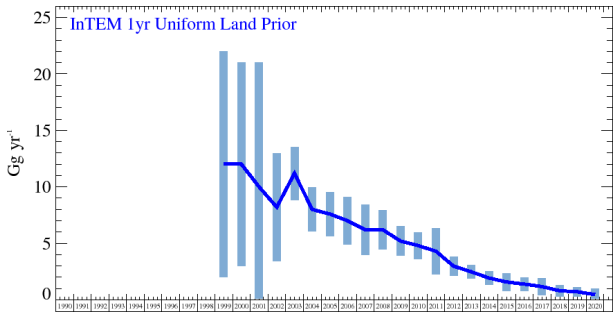

Figure 132: HCFC-22 NWEU emission estimates (Gg yr^{-1}) from InTEM annual inversion (blue). The uncertainty bars represent 1-σ.

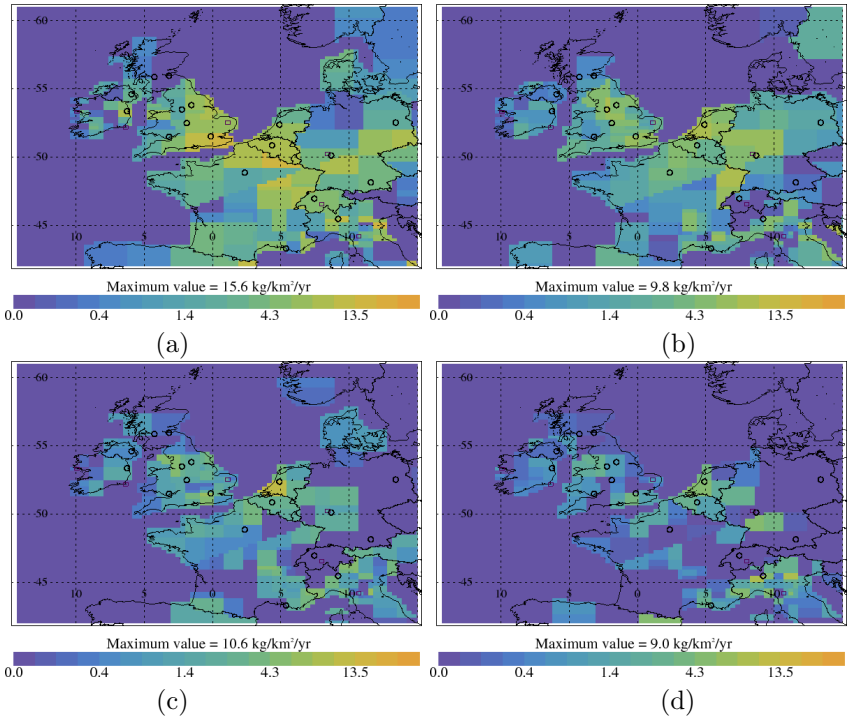

Figure 133: HCFC-22 InTEM emission estimates (kg km^{-2} yr^{-1}) (a) 2008-2010 (b) 2011-2013 (c) 2014-2016 (d) 2017-2019

Table 29: UK and NWEU HCFC-22 emission (Gg yr^{-1}) estimates with 1-σ uncertainty.

Years	UK InTEM 1yr	NWEU InTEM 1yr
1999	2.27 (1.53-3.02)	12. (2.-22.)
2000	2.18 (1.20-3.17)	12. (3.-21.)
2001	2.57 (1.85-3.29)	10. (0.-22.)
2002	1.94 (1.22-2.66)	8.2 (3.4-13.0)
2003	2.35 (1.75-2.95)	11.2 (8.9-13.6)
2004	2.59 (2.09-3.10)	8.0 (6.0-9.9)
2005	1.55 (1.17-1.93)	7.6 (5.6-9.5)
2006	1.81 (1.40-2.22)	7.0 (4.9-9.1)
2007	1.98 (1.50-2.46)	6.2 (4.0-8.4)
2008	1.57 (1.22-1.93)	6.2 (4.5-8.0)
2009	1.05 (0.78-1.33)	5.2 (3.9-6.5)
2010	1.20 (0.88-1.53)	4.8 (3.6-6.0)
2011	0.70 (0.32-1.09)	4.3 (2.2-6.3)
2012	0.72 (0.53-0.92)	2.98 (2.16-3.80)
2013	0.65 (0.41-0.90)	2.48 (1.89-3.06)
2014	0.45 (0.27-0.62)	1.93 (1.31-2.55)
2015	0.40 (0.21-0.59)	1.58 (0.80-2.36)
2016	0.36 (0.13-0.58)	1.39 (0.81-1.98)
2017	0.33 (0.07-0.59)	1.17 (0.42-1.92)
2018	0.20 (0.01-0.40)	0.80 (0.31-1.30)
2019	0.14 (0.03-0.25)	0.71 (0.28-1.15)
2020	0.02 (0.00-0.20)	0.46 (0.00-1.05)

4.33 HCFC-141b

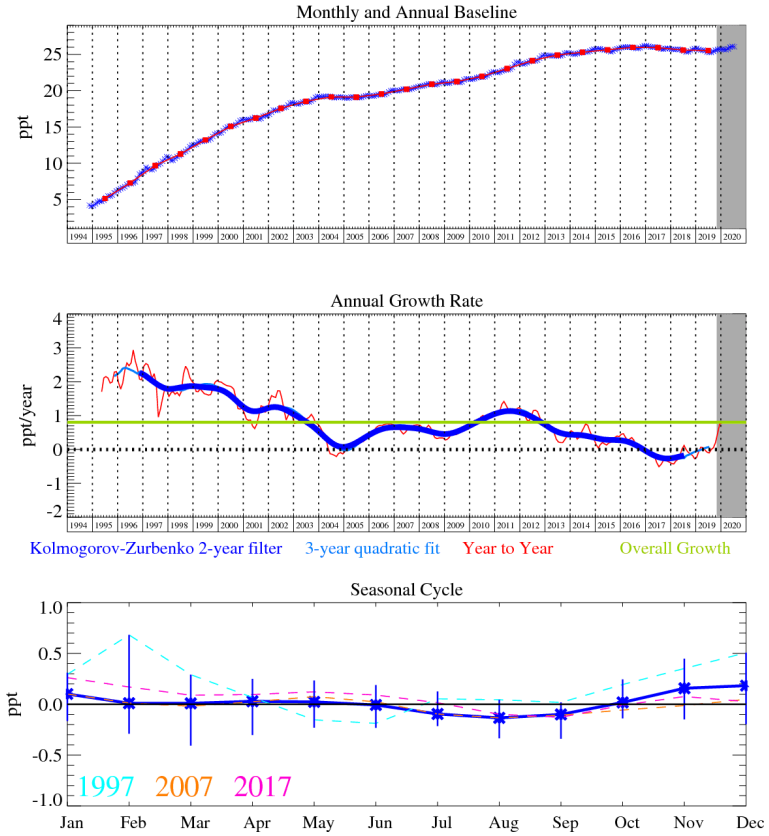

Figure 134: Monthly (blue) and annual (red) Mid-latitude Northern Hemisphere mole fractions (top plot). Annual (blue and red) and overall (green) growth rate (middle plot). Seasonal cycle (de-trended) with year-to-year variability (lower plot). Grey area covers un-ratified provisional data.

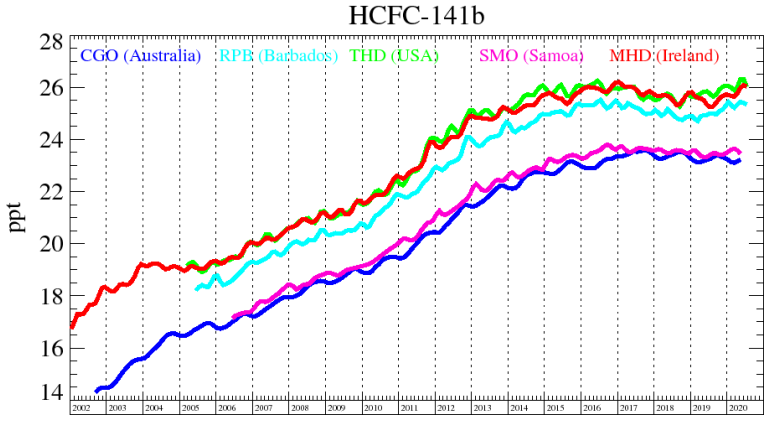

Figure 135: Background mole fractions at 5 AGAGE global stations

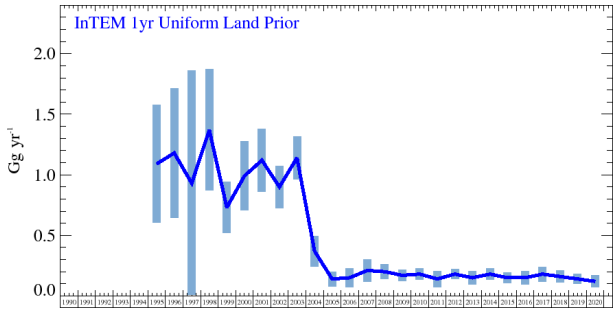

Figure 136: HCFC-141b UK emission estimates (Gg yr^{-1}) from InTEM annual inversion (blue). The uncertainty bars represent 1-σ.

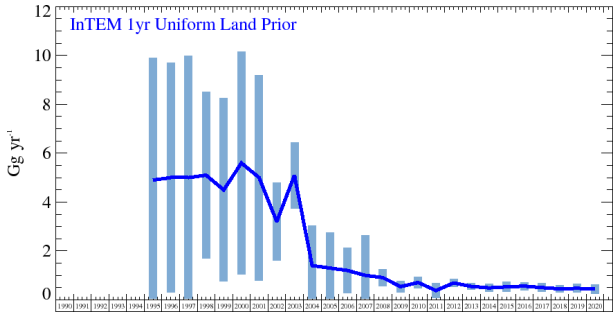

Figure 137: HCFC-141b NWEU emission estimates (Gg yr^{-1}) from InTEM annual inversion (blue). The uncertainty bars represent 1-σ.

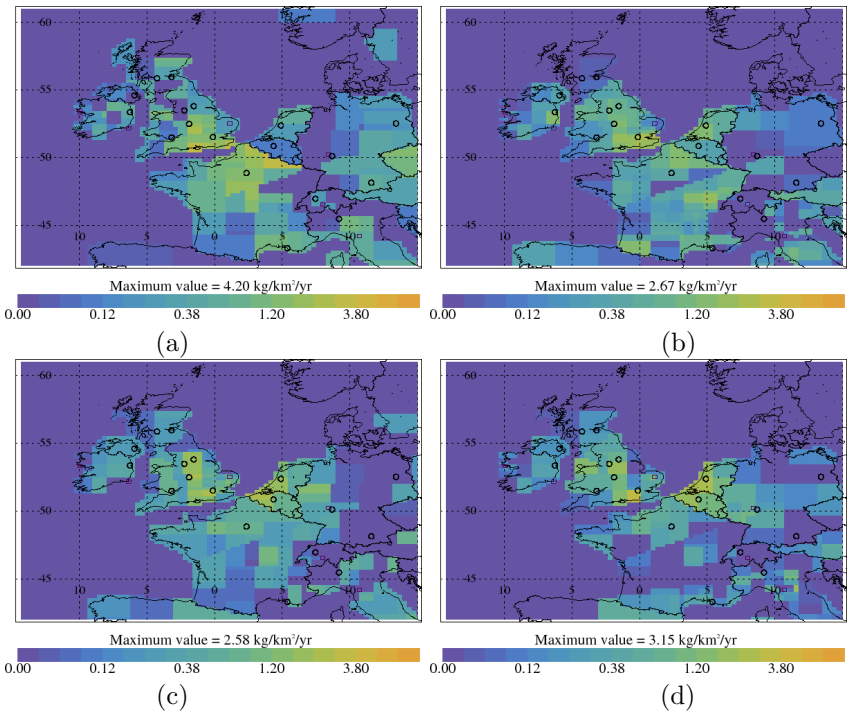

Figure 138: HCFC-141b InTEM emission estimates (kg km^{-2} yr^{-1}) (a) 2008-2010 (b) 2011-2013 (c) 2014-2016 (d) 2017-2019

Table 30: UK and NWEU HCFC-141b emission (Gg yr^{-1}) estimates with 1-σ uncertainty.

Years	UK InTEM 1yr	NWEU InTEM 1yr
1995	1.09 (0.61-1.58)	4.9 (0.0-10.0)
1996	1.18 (0.64-1.71)	5.0 (0.3-9.7)
1997	0.93 (0.00-1.86)	5. (0.-10.)
1998	1.37 (0.87-1.87)	5.1 (1.7-8.5)
1999	0.73 (0.52-0.94)	4.5 (0.7-8.2)
2000	0.99 (0.70-1.27)	5.6 (1.1-10.2)
2001	1.12 (0.86-1.38)	5.0 (0.8-9.2)
2002	0.90 (0.72-1.07)	3.2 (1.6-4.8)
2003	1.14 (0.96-1.31)	5.1 (3.7-6.4)
2004	0.37 (0.25-0.50)	1.4 (0.0-3.3)
2005	0.14 (0.08-0.20)	1.3 (0.0-2.9)
2006	0.15 (0.07-0.23)	1.20 (0.27-2.14)
2007	0.21 (0.12-0.30)	1.0 (0.0-3.3)
2008	0.20 (0.14-0.26)	0.91 (0.57-1.26)
2009	0.17 (0.13-0.22)	0.54 (0.30-0.77)
2010	0.18 (0.13-0.22)	0.71 (0.48-0.94)
2011	0.14 (0.08-0.21)	0.38 (0.07-0.70)
2012	0.18 (0.14-0.22)	0.69 (0.52-0.86)
2013	0.15 (0.09-0.20)	0.55 (0.40-0.69)
2014	0.18 (0.14-0.23)	0.49 (0.33-0.66)
2015	0.15 (0.11-0.20)	0.53 (0.33-0.73)
2016	0.15 (0.10-0.21)	0.56 (0.40-0.72)
2017	0.18 (0.12-0.24)	0.50 (0.32-0.67)
2018	0.16 (0.11-0.21)	0.45 (0.31-0.59)
2019	0.14 (0.10-0.18)	0.47 (0.29-0.64)
2020	0.12 (0.07-0.17)	0.44 (0.25-0.63)

4.34 HCFC-142b

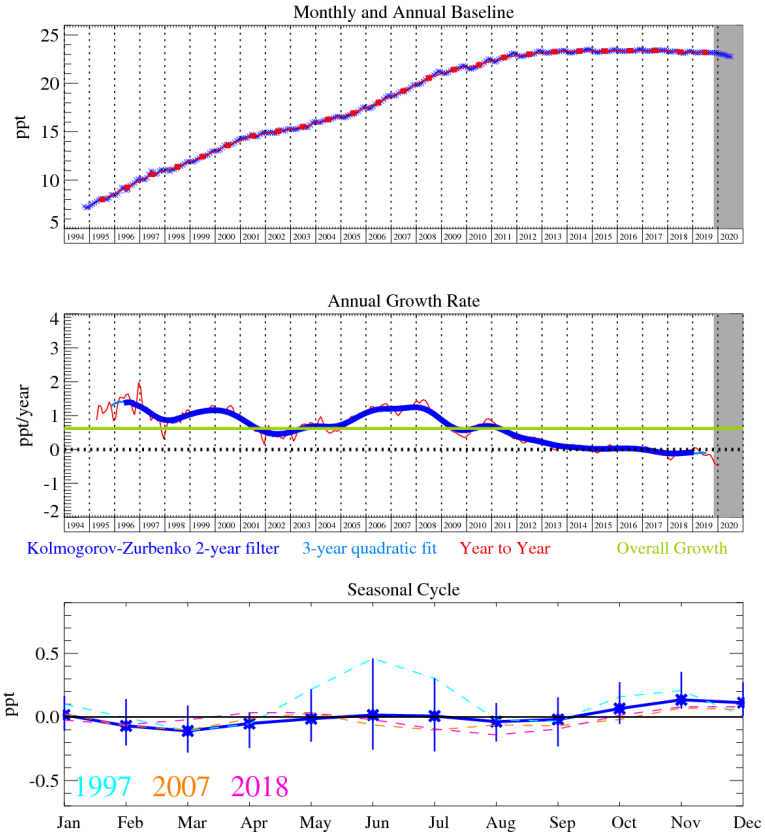

Figure 139: Monthly (blue) and annual (red) Mid-latitude Northern Hemisphere mole fractions (top plot). Annual (blue and red) and overall (green) growth rate (middle plot). Seasonal cycle (de-trended) with year-to-year variability (lower plot). Grey area covers un-ratified provisional data.

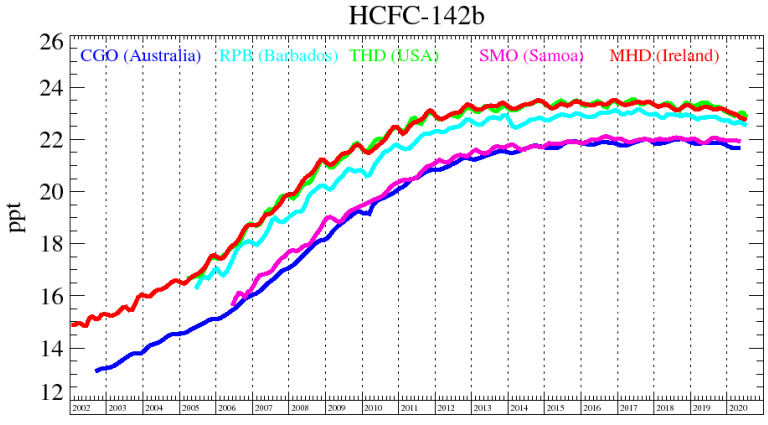

Figure 140: Background mole fractions at 5 AGAGE global stations

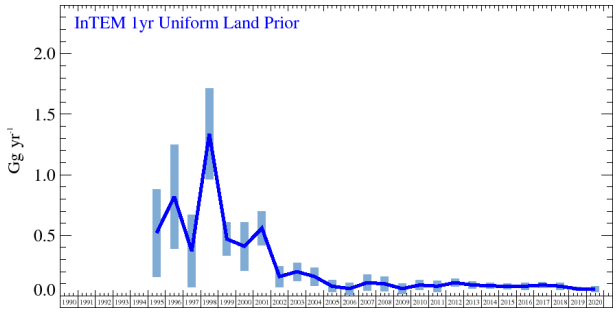

Figure 141: HCFC-142b UK emission estimates (Gg yr^{-1}) from InTEM annual inversion (blue). The uncertainty bars represent 1-σ.

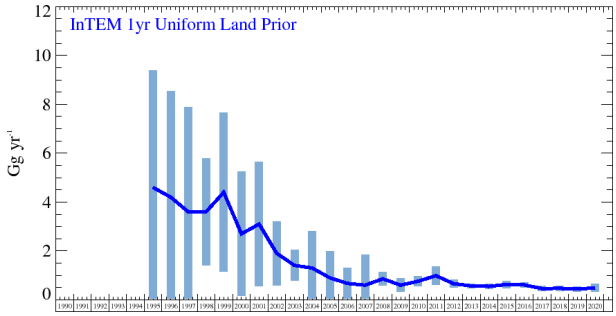

Figure 142: HCFC-142b NWEU emission estimates (Gg yr^{-1}) from InTEM annual inversion (blue). The uncertainty bars represent 1-σ.

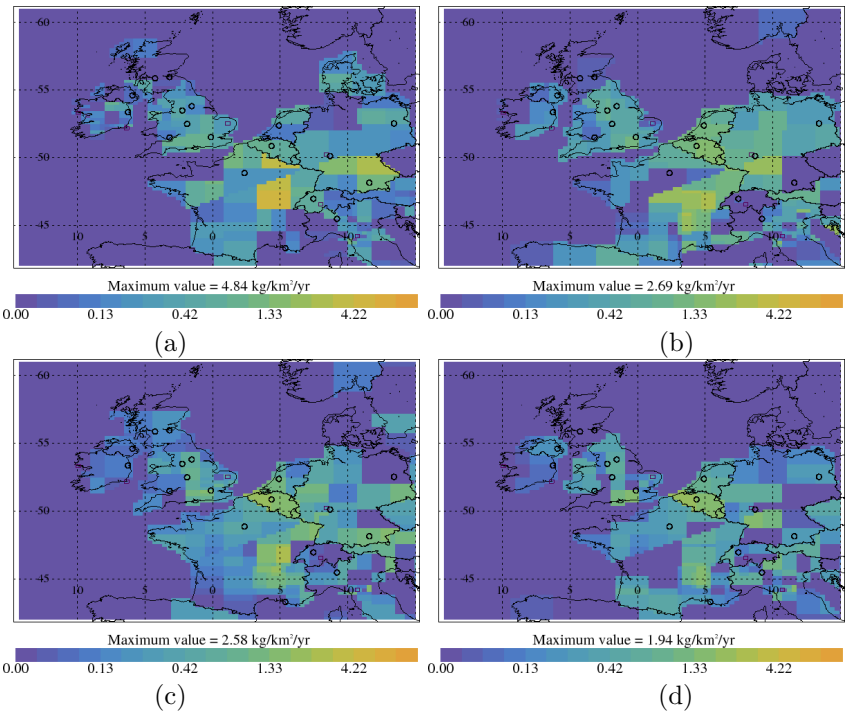

Figure 143: HCFC-142b InTEM emission estimates (kg km^{-2} yr^{-1}) (a) 2008-2010 (b) 2011-2013 (c) 2014-2016 (d) 2017-2019

Table 31: UK and NWEU HCFC-142b emission (Gg yr^{-1}) estimates with 1-σ uncertainty.

Years	UK InTEM 1yr	NWEU InTEM 1yr
1995	0.52 (0.16-0.88)	4.6 (0.0-9.6)
1996	0.82 (0.39-1.25)	4.2 (0.0-8.7)
1997	0.37 (0.07-0.67)	3.6 (0.0-8.6)
1998	1.34 (0.97-1.72)	3.6 (1.4-5.8)
1999	0.47 (0.33-0.60)	4.4 (1.1-7.6)
2000	0.41 (0.21-0.61)	2.7 (0.1-5.2)
2001	0.56 (0.42-0.70)	3.1 (0.6-5.7)
2002	0.16 (0.08-0.25)	1.9 (0.6-3.2)
2003	0.20 (0.12-0.27)	1.41 (0.78-2.03)
2004	0.16 (0.08-0.23)	1.3 (0.0-3.0)
2005	0.08 (0.03-0.13)	0.9 (0.0-2.2)
2006	0.06 (0.01-0.11)	0.67 (0.03-1.32)
2007	0.11 (0.04-0.17)	0.6 (0.0-2.5)
2008	0.10 (0.04-0.16)	0.86 (0.59-1.12)
2009	0.06 (0.02-0.11)	0.60 (0.33-0.88)
2010	0.09 (0.05-0.13)	0.76 (0.55-0.97)
2011	0.08 (0.03-0.12)	0.99 (0.61-1.36)
2012	0.11 (0.08-0.14)	0.66 (0.50-0.83)
2013	0.09 (0.06-0.12)	0.57 (0.48-0.66)
2014	0.08 (0.06-0.11)	0.55 (0.44-0.66)
2015	0.08 (0.05-0.10)	0.63 (0.48-0.78)
2016	0.08 (0.05-0.11)	0.61 (0.50-0.72)
2017	0.09 (0.06-0.11)	0.46 (0.35-0.57)
2018	0.08 (0.05-0.11)	0.47 (0.38-0.57)
2019	0.06 (0.04-0.08)	0.44 (0.34-0.53)
2020	0.06 (0.03-0.08)	0.49 (0.33-0.65)

4.35 Carbon tetrachloride (CCl_4)

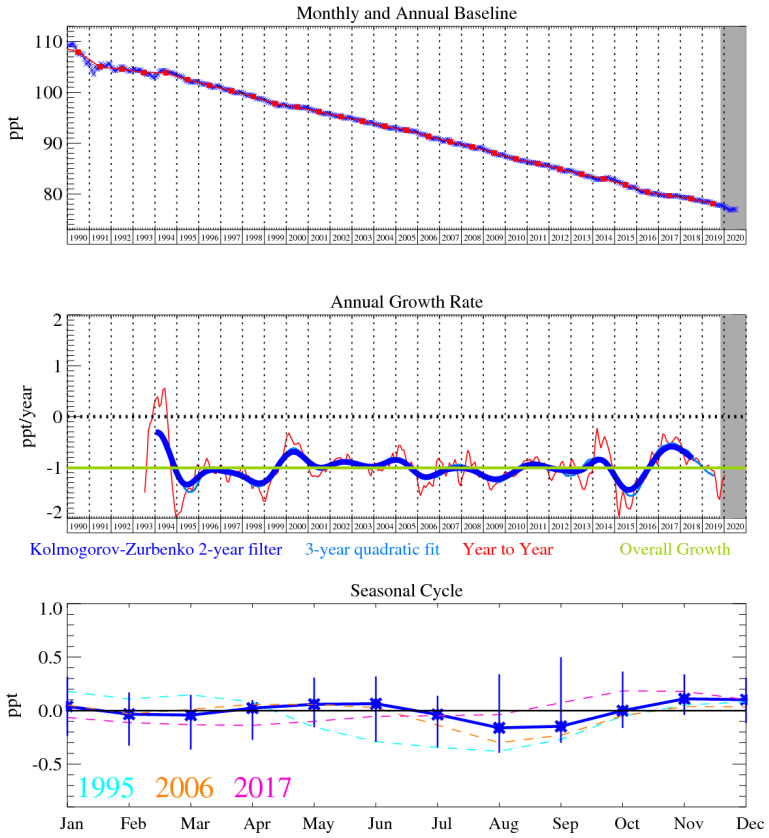

Figure 144: Monthly (blue) and annual (red) Mid-latitude Northern Hemisphere mole fractions (top plot). Annual (blue and red) and overall (green) growth rate (middle plot). Seasonal cycle (de-trended) with year-to-year variability (lower plot). Grey area covers un-ratified provisional data.

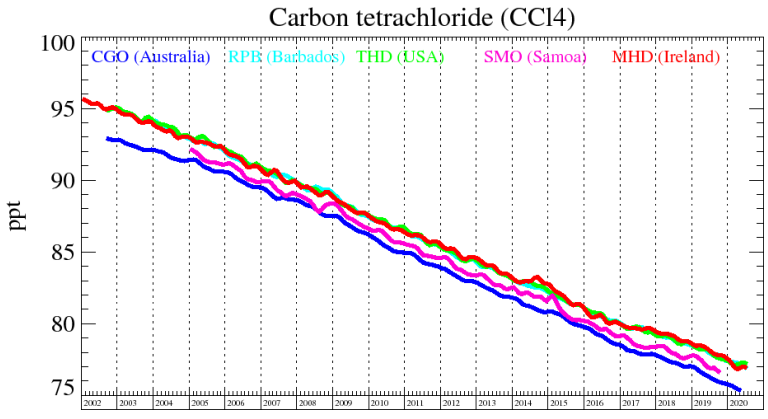

Figure 145: Background mole fractions at 5 AGAGE global stations

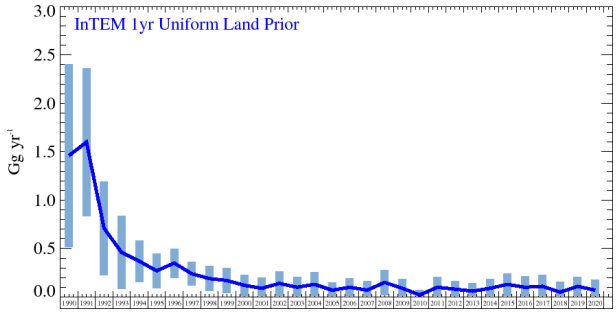

Figure 146: CCl_4 UK emission estimates (Gg yr^{-1}) from InTEM annual inversion (blue). The uncertainty bars represent 1-σ.

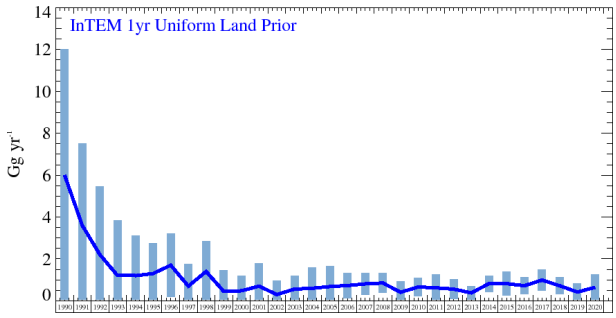

Figure 147: CCl_4 NWEU emission estimates (Gg yr^{-1}) from InTEM annual inversion (blue). The uncertainty bars represent 1-σ.

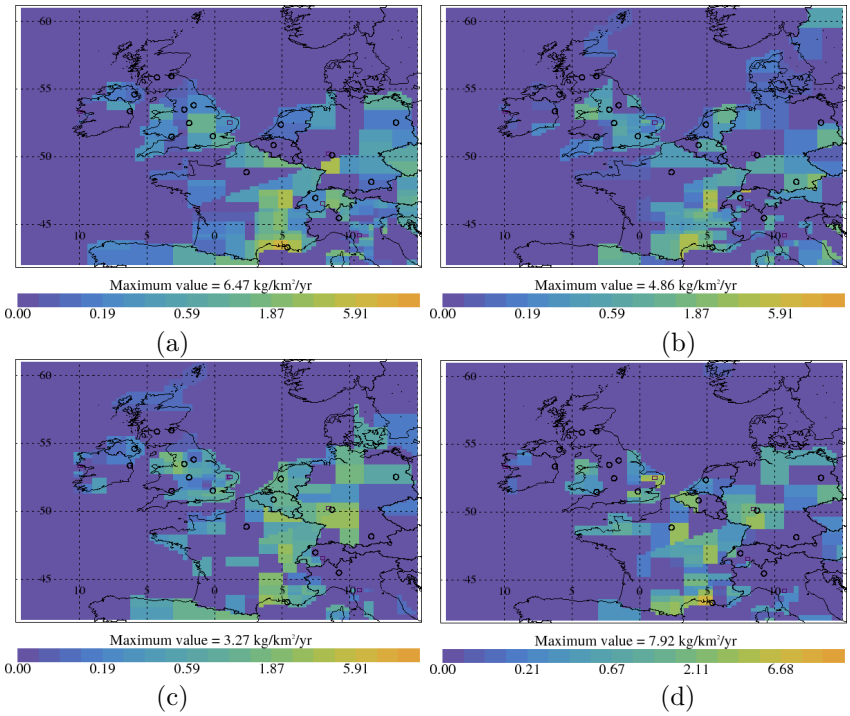

Figure 148: CCl_4 InTEM emission estimates (kg km^{-2} yr^{-1}) (a) 2008-2010 (b) 2011-2013 (c) 2014-2016 (d) 2017-2019

Table 32: UK and NWEU CCl_4 emission (Gg yr^{-1}) estimates with 1-σ uncertainty.

Years	UK InTEM 1yr	NWEU InTEM 1yr
1990	1.46 (0.52-2.41)	6. (0.-12.)
1991	1.60 (0.83-2.36)	3.6 (0.0-7.8)
1992	0.71 (0.22-1.19)	2.2 (0.0-6.5)
1993	0.46 (0.08-0.83)	1.2 (0.0-5.3)
1994	0.37 (0.15-0.58)	1.2 (0.0-3.8)
1995	0.27 (0.09-0.45)	1.3 (0.0-2.9)
1996	0.35 (0.20-0.50)	1.7 (0.2-3.2)
1997	0.24 (0.12-0.36)	0.7 (0.0-2.1)
1998	0.19 (0.06-0.32)	1.4 (0.0-2.9)
1999	0.17 (0.04-0.30)	0.45 (0.00-2.00)
2000	0.12 (0.01-0.23)	0.48 (0.00-1.45)
2001	0.09 (0.00-0.22)	0.7 (0.0-2.2)
2002	0.14 (0.02-0.27)	0.30 (0.00-1.35)
2003	0.10 (0.00-0.21)	0.56 (0.00-1.26)
2004	0.13 (0.00-0.25)	0.60 (0.00-1.99)
2005	0.07 (0.00-0.16)	0.68 (0.00-1.95)
2006	0.10 (0.01-0.20)	0.73 (0.12-1.34)
2007	0.07 (0.00-0.19)	0.81 (0.27-1.34)
2008	0.15 (0.02-0.28)	0.85 (0.39-1.32)
2009	0.09 (0.00-0.19)	0.41 (0.00-1.04)
2010	0.02 (0.00-0.10)	0.66 (0.21-1.11)
2011	0.10 (0.00-0.22)	0.62 (0.00-1.27)
2012	0.08 (0.00-0.17)	0.56 (0.08-1.04)
2013	0.06 (0.00-0.16)	0.38 (0.07-0.69)
2014	0.09 (0.00-0.19)	0.82 (0.43-1.21)
2015	0.13 (0.01-0.24)	0.82 (0.26-1.38)
2016	0.10 (0.00-0.23)	0.72 (0.31-1.12)
2017	0.11 (0.00-0.24)	0.99 (0.48-1.49)
2018	0.05 (0.00-0.22)	0.72 (0.32-1.13)
2019	0.11 (0.01-0.20)	0.42 (0.02-0.83)
2020	0.07 (0.00-0.21)	0.64 (0.03-1.25)

4.36 Methyl Chloroform (CH_3CCl_3)

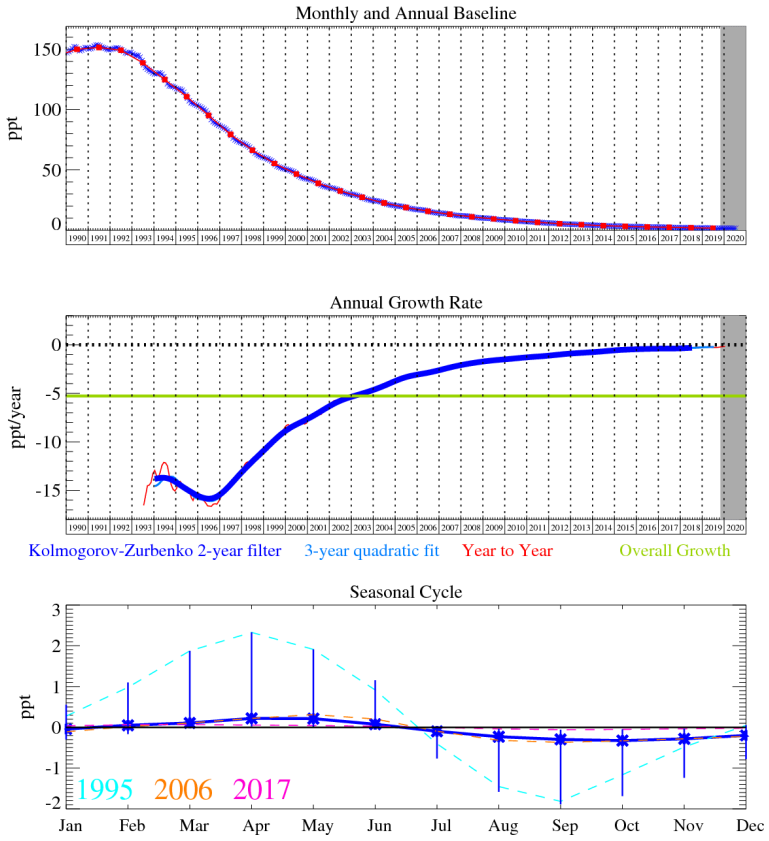

Figure 149: Monthly (blue) and annual (red) Mid-latitude Northern Hemisphere mole fractions (top plot). Annual (blue and red) and overall (green) growth rate (middle plot). Seasonal cycle (de-trended) with year-to-year variability (lower plot). Grey area covers un-ratified provisional data.

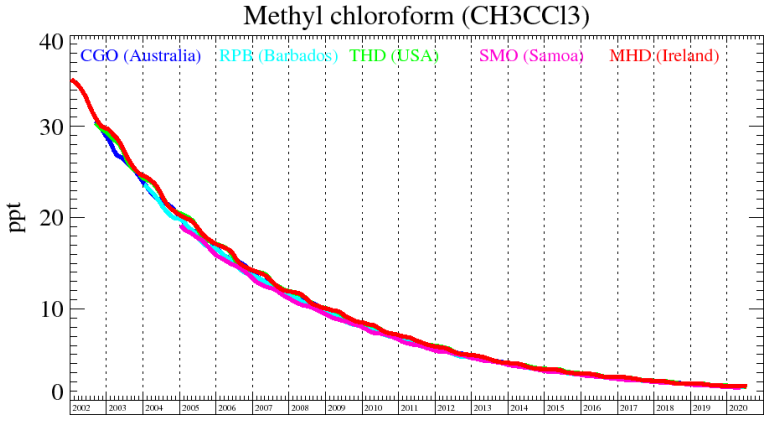

Figure 150: Background mole fractions at 5 AGAGE global stations

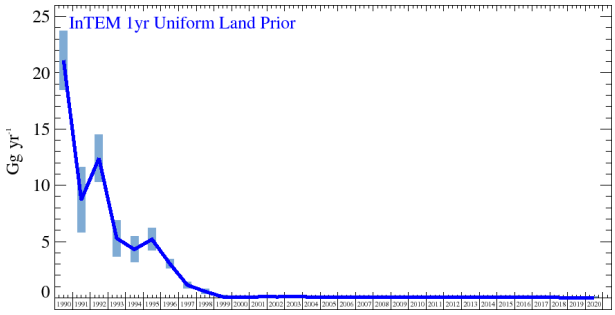

Figure 151: CH_3CCl_3 UK emission estimates (Gg yr^{-1}) from InTEM annual inversion (blue). The uncertainty bars represent 1-σ.

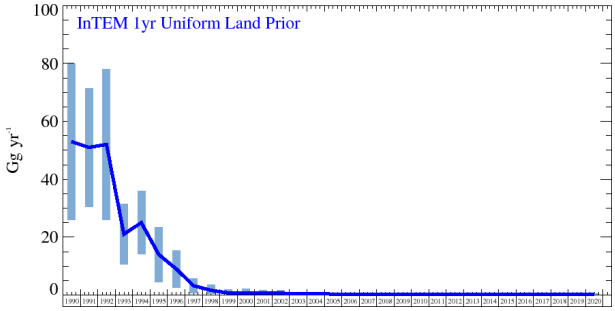

Figure 152: CH_3CCl_3 NWEU emission estimates (Gg yr^{-1}) from InTEM annual inversion (blue). The uncertainty bars represent 1-σ.

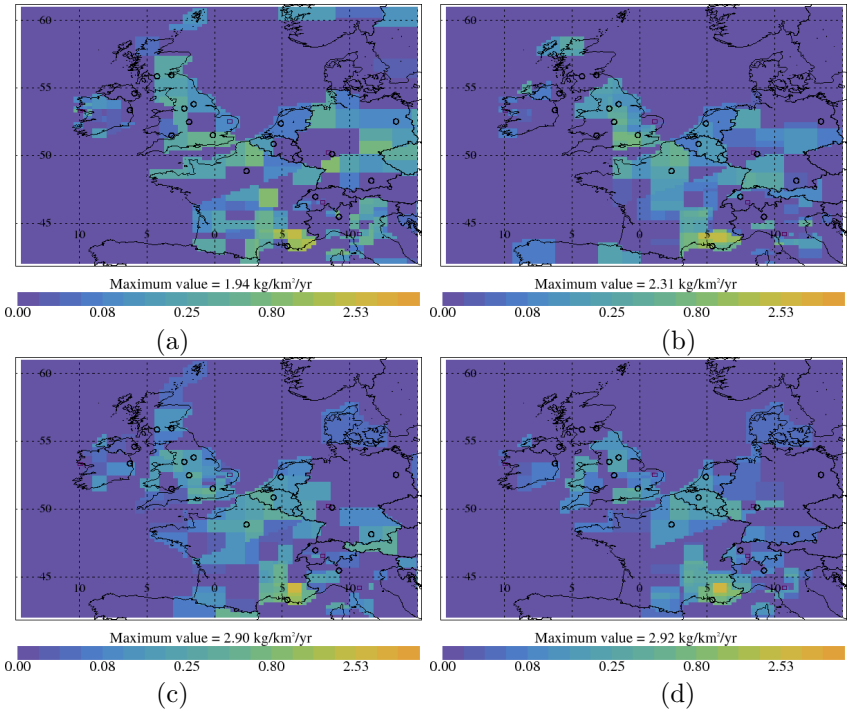

Figure 153: CH_3CCl_3 InTEM emission estimates (kg km^{-2} yr^{-1}) (a) 2008-2010 (b) 2011-2013 (c) 2014-2016 (d) 2017-2019

Table 33: UK and NWEU CH_3CCl_3 emission (Gg yr^{-1}) estimates with 1-σ uncertainty.

Years	UK InTEM 1yr	NWEU InTEM 1yr
1990	21.1 (18.5-23.7)	53. (26.-80.)
1991	8.7 (5.8-11.6)	51. (30.-71.)
1992	12.4 (10.3-14.5)	52. (26.-78.)
1993	5.3 (3.7-6.9)	21. (10.-31.)
1994	4.3 (3.2-5.5)	25. (14.-36.)
1995	5.2 (4.2-6.2)	14. (5.-24.)
1996	3.05 (2.62-3.47)	9.0 (2.-15.)
1997	1.14 (0.85-1.43)	3.2 (0.8-5.7)
1998	0.57 (0.35-0.78)	1.6 (0.0-3.8)
1999	0.09 (0.00-0.28)	0.7 (0.0-2.4)
2000	0.04 (0.00-0.17)	0.8 (0.0-2.5)
2001	0.08 (0.00-0.24)	0.6 (0.0-2.4)
2002	0.08 (0.00-0.22)	0.6 (0.0-2.1)
2003	0.13 (0.01-0.24)	0.49 (0.14-0.83)
2004	0.07 (0.00-0.19)	0.46 (0.10-0.82)
2005	0.08 (0.00-0.17)	0.31 (0.05-0.57)
2006	0.06 (0.00-0.14)	0.33 (0.03-0.62)
2007	0.03 (0.00-0.12)	0.32 (0.08-0.56)
2008	0.07 (0.00-0.17)	0.34 (0.10-0.57)
2009	0.05 (0.00-0.13)	0.18 (0.00-0.42)
2010	0.03 (0.00-0.09)	0.32 (0.18-0.47)
2011	0.05 (0.00-0.10)	0.22 (0.04-0.40)
2012	0.045 (0.021-0.069)	0.20 (0.10-0.29)
2013	0.035 (0.012-0.059)	0.19 (0.13-0.25)
2014	0.040 (0.021-0.059)	0.21 (0.15-0.27)
2015	0.033 (0.015-0.051)	0.17 (0.08-0.25)
2016	0.033 (0.012-0.054)	0.17 (0.11-0.23)
2017	0.032 (0.012-0.052)	0.15 (0.09-0.21)
2018	0.026 (0.010-0.043)	0.13 (0.09-0.17)
2019	0.015 (0.005-0.025)	0.14 (0.10-0.17)
2020	0.018 (0.006-0.031)	0.16 (0.11-0.20)

4.37 Halon Summary

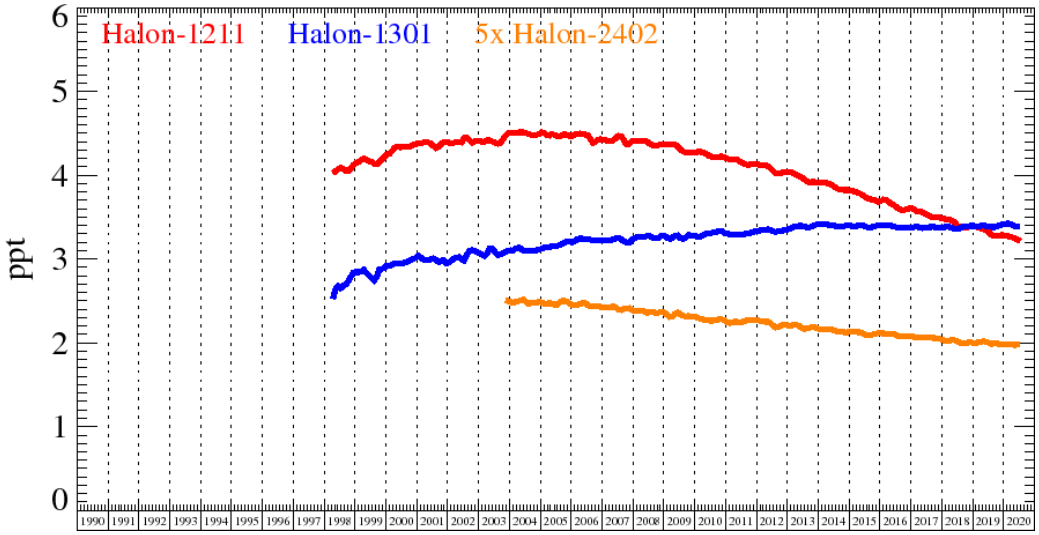

Figure 154: Northern Hemisphere Atmospheric Background Levels of Halons as observed at the Mace Head observing station. Note that for scale purposes the atmospheric mole fractions of Halon-2402 has been multiplied by 5

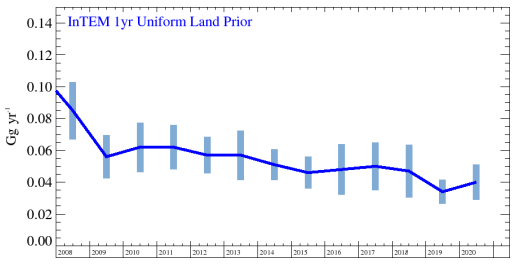

(a) Halon-1211

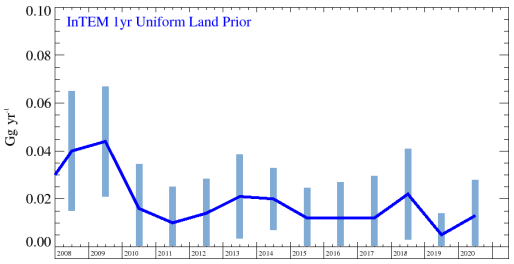

(b) Halon-1301

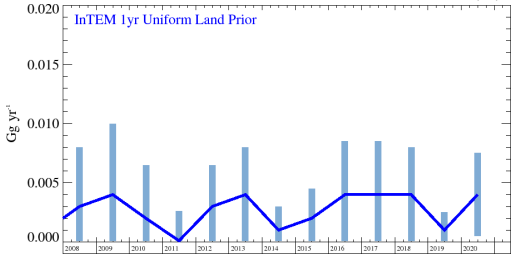

(c) Halon-2402

Figure 155: Halon UK emission estimates (Gg yr^{-1}) from InTEM annual inversion (blue). The uncertainty bars represent 1-σ.

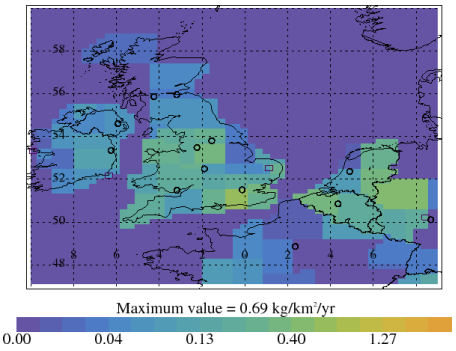

(a) Halon-1211

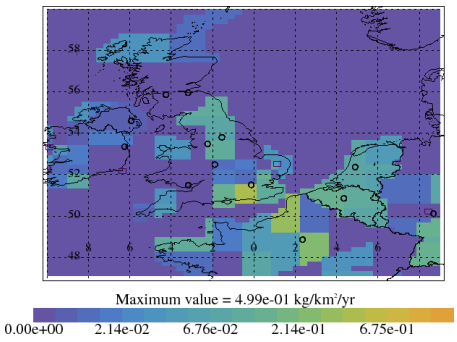

(b) Halon-1301

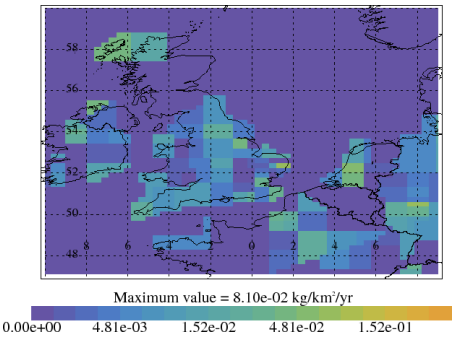

(c) Halon-2402

Figure 156: InTEM Halon emission estimates (kg km^{-2} yr^{-1}). Note each plot has its own scale.

4.38 Halon-1211

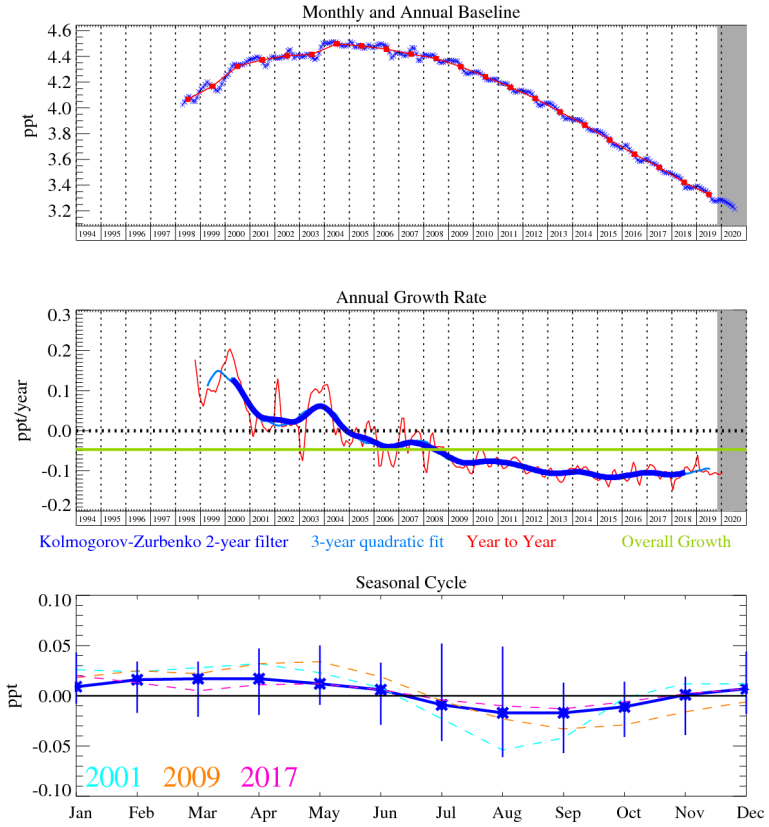

Figure 157: Monthly (blue) and annual (red) Mid-latitude Northern Hemisphere mole fractions (top plot). Annual (blue and red) and overall (green) growth rate (middle plot). Seasonal cycle (de-trended) with year-to-year variability (lower plot). Grey area covers un-ratified provisional data.

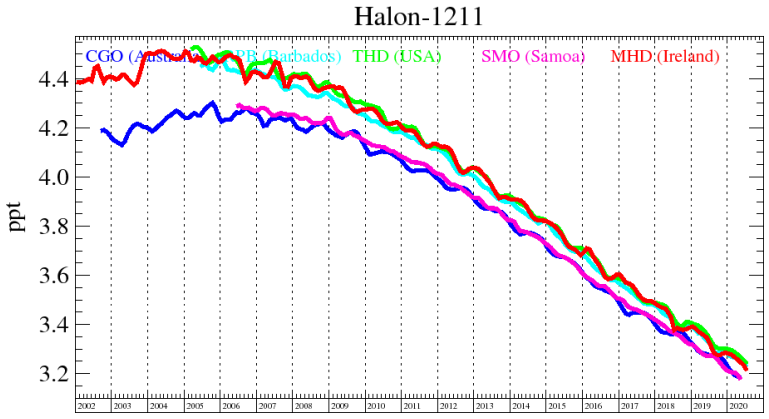

Figure 158: Background mole fractions at 5 AGAGE global stations

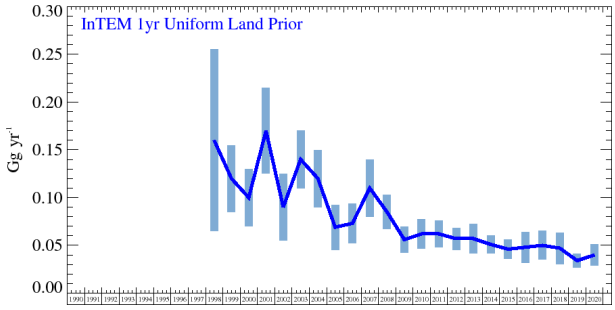

Figure 159: Halon-1211 UK emission estimates (Gg yr^{-1}) from InTEM annual inversion (blue). The uncertainty bars represent 1-σ.

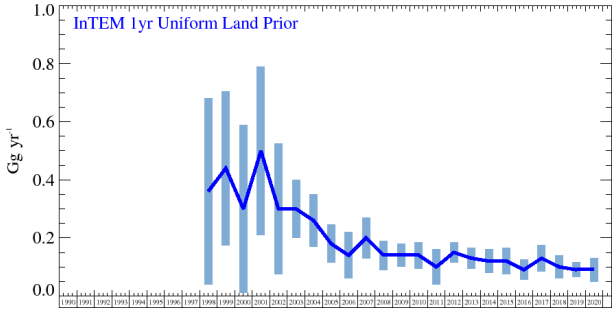

Figure 160: Halon-1211 NWEU emission estimates (Gg yr^{-1}) from InTEM annual inversion (blue). The uncertainty bars represent 1-σ.

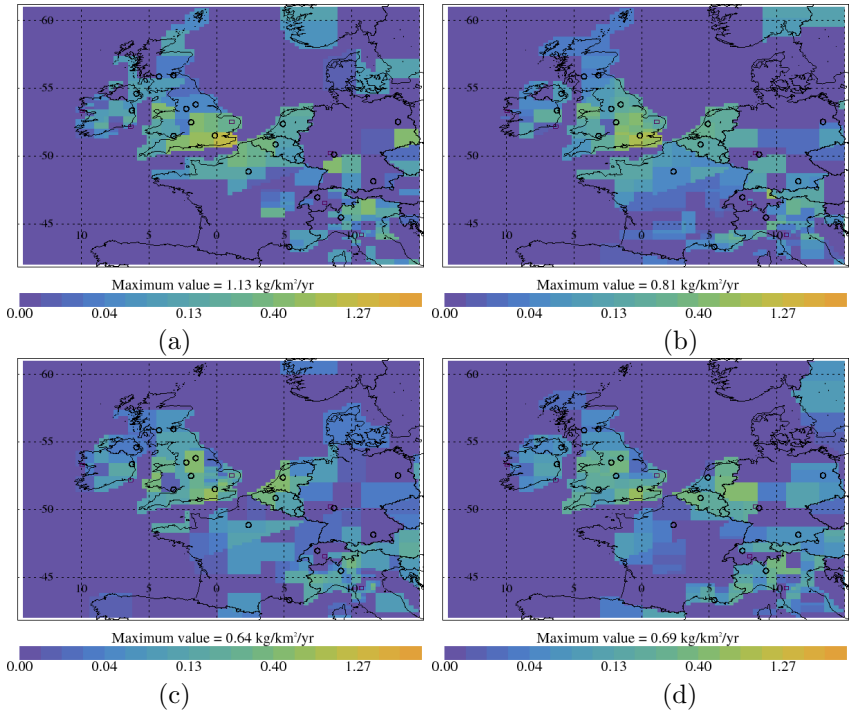

Figure 161: Halon-1211 InTEM emission estimates (kg km^{-2} yr^{-1}) (a) 2008-2010 (b) 2011-2013 (c) 2014-2016 (d) 2017-2019

Table 34: UK and NWEU Halon-1211 emission (Gg yr^{-1}) estimates with 1-σ uncertainty.

Years	UK InTEM 1yr	NWEU InTEM 1yr
1998	0.16 (0.07-0.26)	0.36 (0.04-0.68)
1999	0.12 (0.08-0.15)	0.44 (0.18-0.71)
2000	0.10 (0.07-0.13)	0.30 (0.01-0.59)
2001	0.17 (0.13-0.22)	0.50 (0.21-0.79)
2002	0.09 (0.06-0.13)	0.30 (0.08-0.53)
2003	0.14 (0.11-0.17)	0.30 (0.20-0.40)
2004	0.12 (0.09-0.15)	0.26 (0.17-0.35)
2005	0.069 (0.046-0.093)	0.18 (0.11-0.24)
2006	0.073 (0.053-0.094)	0.14 (0.06-0.22)
2007	0.11 (0.08-0.14)	0.20 (0.13-0.27)
2008	0.085 (0.067-0.103)	0.14 (0.09-0.19)
2009	0.056 (0.043-0.070)	0.14 (0.10-0.18)
2010	0.062 (0.047-0.078)	0.14 (0.10-0.19)
2011	0.062 (0.048-0.076)	0.10 (0.04-0.16)
2012	0.057 (0.046-0.069)	0.15 (0.11-0.18)
2013	0.057 (0.041-0.072)	0.13 (0.10-0.17)
2014	0.051 (0.041-0.060)	0.12 (0.08-0.16)
2015	0.046 (0.036-0.056)	0.12 (0.08-0.17)
2016	0.048 (0.032-0.064)	0.09 (0.05-0.12)
2017	0.050 (0.035-0.065)	0.13 (0.09-0.18)
2018	0.047 (0.031-0.064)	0.10 (0.06-0.14)
2019	0.034 (0.026-0.041)	0.09 (0.07-0.12)
2020	0.040 (0.029-0.051)	0.09 (0.05-0.13)

4.39 Halon-1301

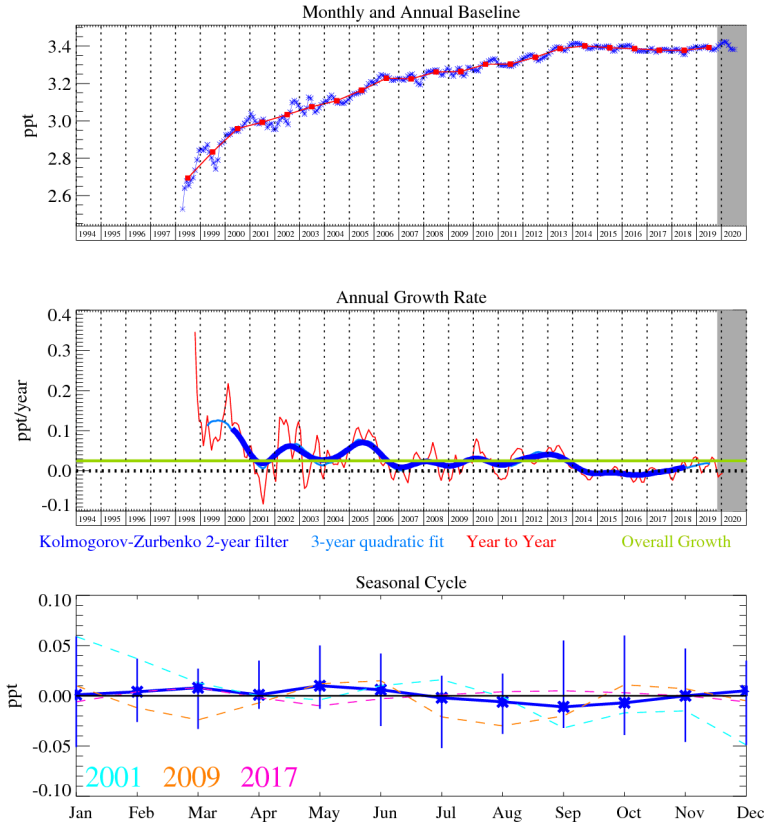

Figure 162: Monthly (blue) and annual (red) Mid-latitude Northern Hemisphere mole fractions (top plot). Annual (blue and red) and overall (green) growth rate (middle plot). Seasonal cycle (de-trended) with year-to-year variability (lower plot). Grey area covers un-ratified provisional data.

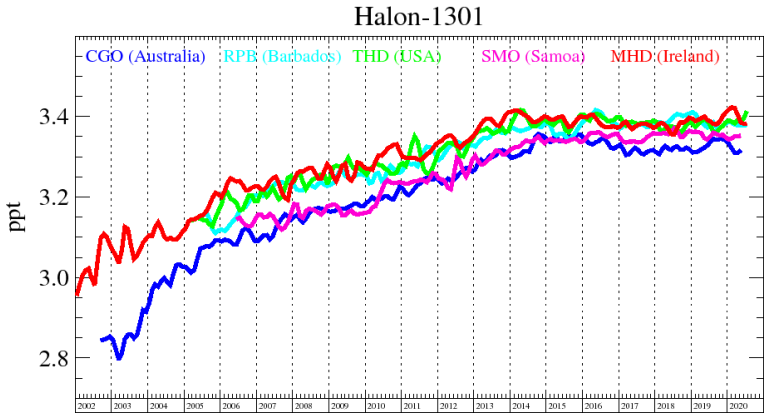

Figure 163: Background mole fractions at 5 AGAGE global stations

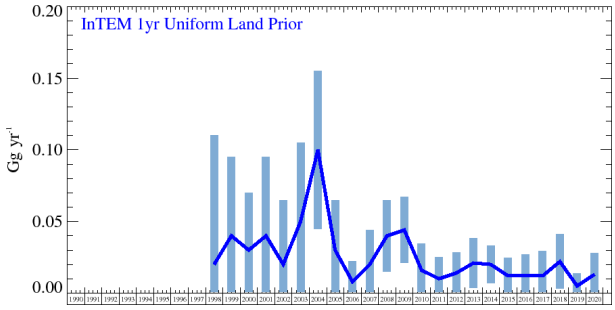

Figure 164: Halon-1301 UK emission estimates (Gg yr^{-1}) from InTEM annual inversion (blue). The uncertainty bars represent 1-σ.

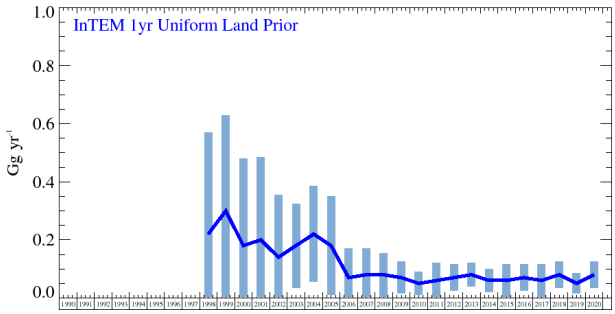

Figure 165: Halon-1211 NWEU emission estimates (Gg yr^{-1}) from InTEM annual inversion (blue). The uncertainty bars represent 1-σ.

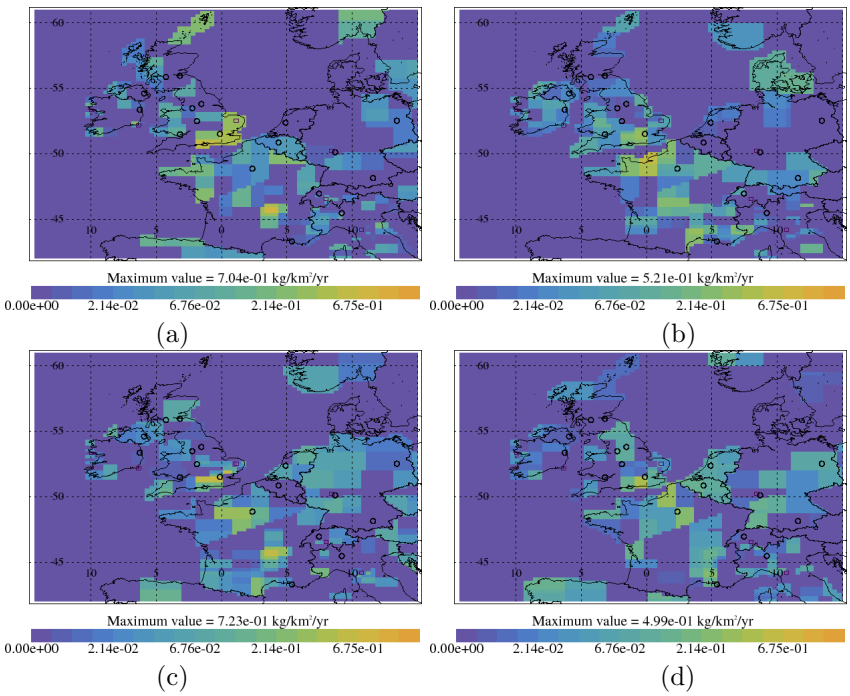

Figure 166: Halon-1301 InTEM emission estimates (kg km^{-2} yr^{-1}) (a) 2008-2010 (b) 2011-2013 (c) 2014-2016 (d) 2017-2019

Table 35: UK and NWEU Halon-1301 emission (Gg yr^{-1}) estimates with 1-σ uncertainty.

Years	UK InTEM 1yr	NWEU InTEM 1yr
1998	0.02 (0.00-0.18)	0.22 (0.00-0.70)
1999	0.04 (0.00-0.11)	0.30 (0.00-0.66)
2000	0.03 (0.00-0.08)	0.18 (0.00-0.60)
2001	0.04 (0.00-0.11)	0.20 (0.00-0.57)
2002	0.02 (0.00-0.09)	0.14 (0.00-0.43)
2003	0.05 (0.00-0.11)	0.18 (0.04-0.33)
2004	0.10 (0.05-0.16)	0.22 (0.06-0.39)
2005	0.03 (0.00-0.07)	0.18 (0.01-0.35)
2006	0.008 (0.000-0.029)	0.07 (0.00-0.20)
2007	0.020 (0.000-0.048)	0.08 (0.00-0.18)
2008	0.04 (0.01-0.06)	0.08 (0.01-0.16)
2009	0.044 (0.021-0.067)	0.07 (0.02-0.13)
2010	0.016 (0.000-0.037)	0.05 (0.01-0.09)
2011	0.010 (0.000-0.030)	0.06 (0.00-0.12)
2012	0.014 (0.000-0.029)	0.07 (0.02-0.11)
2013	0.021 (0.003-0.038)	0.08 (0.04-0.12)
2014	0.020 (0.007-0.033)	0.06 (0.02-0.10)
2015	0.012 (0.000-0.025)	0.06 (0.00-0.11)
2016	0.012 (0.000-0.030)	0.07 (0.02-0.11)
2017	0.012 (0.000-0.035)	0.06 (0.01-0.12)
2018	0.022 (0.003-0.041)	0.08 (0.03-0.12)
2019	0.005 (0.000-0.018)	0.05 (0.01-0.08)
2020	0.013 (0.000-0.030)	0.08 (0.03-0.12)

4.40 Halon-2402

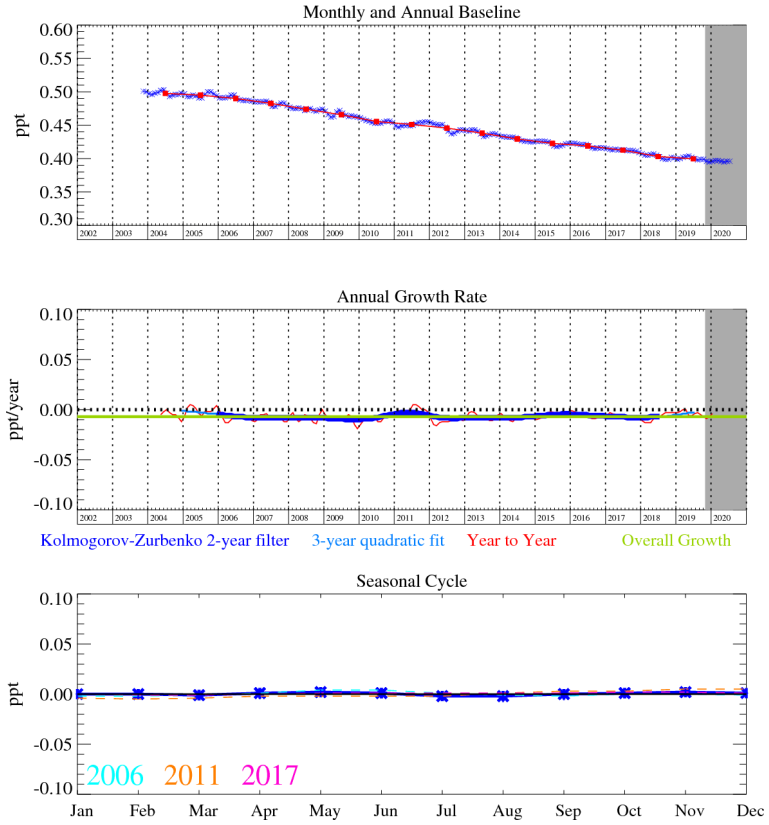

Figure 167: Monthly (blue) and annual (red) Mid-latitude Northern Hemisphere mole fractions (top plot). Annual (blue and red) and overall (green) growth rate (middle plot). Seasonal cycle (de-trended) with year-to-year variability (lower plot). Grey area covers un-ratified provisional data.

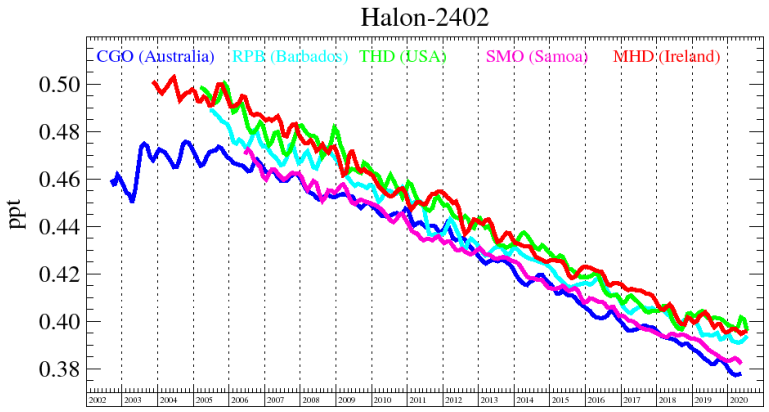

Figure 168: Background mole fractions at 5 AGAGE global stations

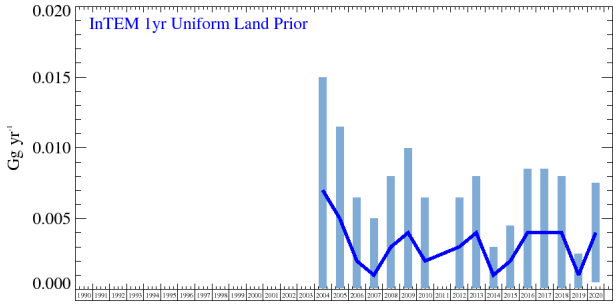

Figure 169: Halon-2402 UK emission estimates (Gg yr^{-1}) from InTEM annual inversion (blue). The uncertainty bars represent 1-σ.

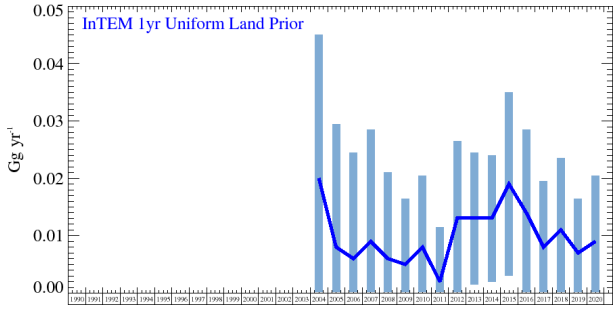

Figure 170: Halon-2402 NWEU emission estimates (Gg yr^{-1}) from InTEM annual inversion (blue). The uncertainty bars represent 1-σ.

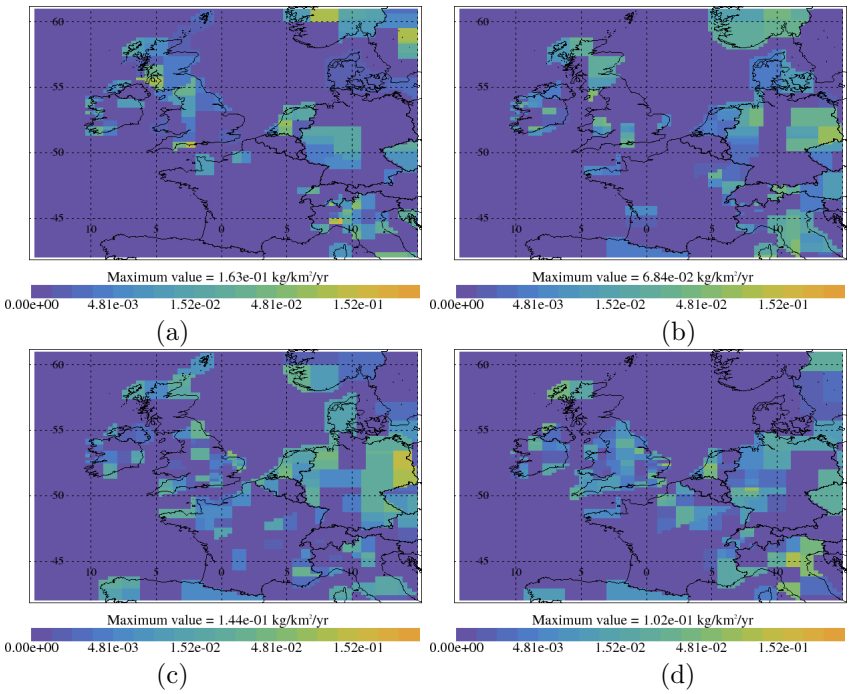

Figure 171: Halon-2402 InTEM emission estimates (kg km^{-2} yr^{-1}) (a) 2008-2010 (b) 2011-2013 (c) 2014-2016 (d) 2017-2019

Table 36: UK and NWEU Halon-2402 emission (Gg yr^{-1}) estimates with 1-σ uncertainty.

Years	UK InTEM 1yr	NWEU InTEM 1yr
2004	0.007 (0.000-0.016)	0.020 (0.000-0.050)
2005	0.005 (0.000-0.013)	0.008 (0.000-0.043)
2006	0.002 (0.000-0.009)	0.006 (0.000-0.037)
2007	0.001 (0.000-0.008)	0.009 (0.000-0.039)
2008	0.003 (0.000-0.010)	0.006 (0.000-0.030)
2009	0.004 (0.000-0.012)	0.005 (0.000-0.023)
2010	0.002 (0.000-0.009)	0.008 (0.000-0.025)
2011	0.000 (0.000-0.005)	0.002 (0.000-0.019)
2012	0.003 (0.000-0.007)	0.013 (0.000-0.027)
2013	0.004 (0.000-0.008)	0.013 (0.001-0.024)
2014	0.001 (0.000-0.004)	0.013 (0.002-0.024)
2015	0.002 (0.000-0.005)	0.019 (0.003-0.035)
2016	0.004 (0.000-0.009)	0.014 (0.000-0.029)
2017	0.004 (0.000-0.009)	0.008 (0.000-0.023)
2018	0.004 (0.000-0.008)	0.011 (0.000-0.025)
2019	0.001 (0.000-0.003)	0.007 (0.000-0.019)
2020	0.004 (0.000-0.007)	0.009 (0.000-0.023)

5 Recent Publications

A list of current publications and presentations resulting from AGAGE and other research are summarized below.

Claxton, T., R. Hossaini, C. Wilson, S. A. Montzka, M. P. Chipperfield, O. Wild, E. M. Bednarz, L. J. Carpenter, S. J. Andrews, S. C. Hackenberg, J. Mühle, D. Oram, S. Park, M.-K. Park, E. Atlas, M. Navarro, S. Schauffler, D. Sherry, M. Vollmer, T. Schuck, A. Engel, P. B. Krummel, M. Maione, J. Arduini, T. Saito, Y. Yokouchi, S. O'Doherty, D. Young, and C. Lunder (2020). "A Synthesis Inversion to Constrain Global Emissions of Two Very Short Lived Chlorocarbons: Dichloromethane, and Perchloroethylene". In: *Journal of Geophysical Research: Atmospheres* 125.12. ISSN: 2169-897X, 2169-8996. DOI: 10.1029/2019JD031818.

Dichloromethane (CH_2Cl_2) and perchloroethylene (C_2Cl_4) are chlorinated very short lived substances (Cl-VSLS) with anthropogenic sources. Recent studies highlight the increasing influence of such compounds, particularly CH_2Cl_2, on the stratospheric chlorine budget and therefore on ozone depletion. Here, a multiyear global-scale synthesis inversion was performed to optimize CH_2Cl_2 (2006–2017) and C_2Cl_4 (2007–2017) emissions. The approach combines long-term surface observations from global monitoring networks, output from a three-dimensional chemical transport model (TOMCAT), and novel bottom-up information on prior industry emissions. Our posterior results show an increase in global CH_2Cl_2 emissions from 637 ± 36 Gg yr-1 in 2006 to 1,171 ± 45 Gg yr-1 in 2017, with Asian emissions accounting for 68% and 89% of these totals, respectively. In absolute terms, Asian CH_2Cl_2 emissions increased annually by 51 Gg yr-1 over the study period, while European and North American emissions declined, indicating a continental-scale shift in emission distribution since the mid-2000s. For C_2Cl_4, we estimate a decrease in global emissions from 141 ± 14 Gg yr-1 in 2007 to 106 ± 12 Gg yr-1 in 2017. The time-varying posterior emissions offer significant improvements over the prior. Utilizing the posterior emissions leads to modeled tropospheric CH_2Cl_2 and C_2Cl_4 abundances and trends in good agreement to those observed (including independent observations to the inversion). A shorter C_2Cl_4 lifetime, from including an uncertain Cl sink, leads to larger global C_2Cl_4 emissions by a factor of ˜1.5, which in some places improves model-measurement agreement. The sensitivity of our findings to assumptions in the inversion procedure, including CH_2Cl_2 oceanic emissions, is discussed.

Derwent, R., D. Parrish, P. G. Simmonds, S. J. O'Doherty, and T. G. Spain (2020). "Seasonal Cycles in Baseline Mixing Ratios of a Large Number of Trace Gases at the Mace Head, Ireland Atmospheric Research Station". In: *Atmospheric Environment* 233, p. 117531. ISSN: 13522310. DOI: 10.1016/j.atmosenv.2020.117531.

A flexible approach for quantifying average long-term changes and seasonal cycles has been applied to the baseline mixing ratios of thirty-two trace gases monitored at the Atmospheric Research Station located at Mace Head, Ireland on the Atlantic Ocean coastline of Europe. Almost all these trace gases exhibit minima in their baseline

seasonal cycles during a two-month period from mid-July to the end of September and maxima during a six-month period between November and May. Relative seasonal cycle amplitudes are largest for those trace gases with the shortest atmospheric lifetimes and smallest for the longest. Robust relationships were found between the timings of the seasonal maxima and minima and their relative amplitudes with the atmospheric lifetimes of the trace gases. These relationships provide a basis for understanding the reasons that the seasonal cycles of a few species (that is, H_2, CCl_4 and the longest-lived gases) deviate significantly; they also have excellent potential as tools to assess global chemistry-transport model performance.

Droste, E. S., K. E. Adcock, M. J. Ashfold, C. Chou, Z. Fleming, P. J. Fraser, L. J. Gooch, A. J. Hind, R. L. Langenfelds, E. Leedham Elvidge, N. Mohd Hanif, S. O'Doherty, D. E. Oram, C.-F. Ou-Yang, M. Panagi, C. E. Reeves, W. T. Sturges, and J. C. Laube (2020). "Trends and Emissions of Six Perfluorocarbons in the Northern Hemisphere and Southern Hemisphere". In: *Atmospheric Chemistry and Physics* 20.8, pp. 4787–4807. ISSN: 1680-7324. DOI: 10.5194/acp-20-4787-2020.

Perfluorocarbons (PFCs) are potent greenhouse gases with global warming potentials up to several thousand times greater than CO_2 on a 100-year time horizon. The lack of any significant sinks for PFCs means that they have long atmospheric lifetimes of the order of thousands of years. Anthropogenic production is thought to be the only source for most PFCs. Here we report an update on the global atmospheric abundances of the following PFCs, most of which have for the first time been analytically separated according to their isomers: c-octafluorobutane (c-C_4F_8), n-decafluorobutane (n-C_4F_{10}), n-dodecafluoropentane (n-C_5F_{12}), n-tetradecafluorohexane (n-C_6F_{14}), and n-hexadecafluoroheptane (n-C_7F_{16}). Additionally, we report the first data set on the atmospheric mixing ratios of perfluoro-2-methylpentane (i-C_6F_{14}). The existence and significance of PFC isomers have not been reported before, due to the analytical challenges of separating them. The time series spans a period from 1978 to the present. Several data sets are used to investigate temporal and spatial trends of these PFCs: time series of air samples collected at Cape Grim, Australia, from 1978 to the start of 2018; a time series of air samples collected between July 2015 and April 2017 at Tacolneston, UK; and intensive campaign-based sampling collections from Taiwan. Although the remote "background" Southern Hemispheric Cape Grim time series indicates that recent growth rates of most of these PFCs are lower than in the 1990s, we continue to see significantly increasing mixing ratios that are between 6 % and 27 % higher by the end of 2017 compared to abundances measured in 2010. Air samples from Tacolneston show a positive offset in PFC mixing ratios compared to the Southern Hemisphere baseline. The highest mixing ratios and variability are seen in air samples from Taiwan, which is therefore likely situated much closer to PFC sources, confirming predominantly Northern Hemispheric emissions for most PFCs. Even though these PFCs occur in the atmosphere at levels of parts per trillion molar or less, their total cumulative global emissions translate into 833 million metric tonnes of CO_2 equivalent by the end of 2017, 23 % of which has been emitted since 2010. Almost two-thirds of the CO_2 equivalent emissions within the last decade are attributable to c-C_4F_8, which currently also has the highest emission rates that continue to grow.

Sources of all PFCs covered in this work remain poorly constrained and reported emissions in global databases do not account for the abundances found in the atmosphere.

Kuyper, B., H. Wingrove, T. Lesch, C. Labuschagne, D. Say, D. Martin, D. Young, M. A. H. Khan, S. O'Doherty, M. T. Davies-Coleman, and D. E. Shallcross (2020). "Atmospheric Toluene and Benzene Mole Fractions at Cape Town and Cape Point and an Estimation of the Hydroxyl Radical Concentrations in the Air above the Cape Peninsula, South Africa". In: *ACS Earth and Space Chemistry* 4.1, pp. 24–34. ISSN: 2472-3452, 2472-3452. DOI: 10.1021/acsearthspacechem.9b00207.

Benzene and toluene, emitted into the atmosphere from a number of common anthropogenic activities, pose a significant human health risk. The mole fractions of toluene and benzene were measured at two urban locations (Foreshore and Potsdam) in Cape Town and one background site at Cape Point, South Africa over the period of July-November 2017. The analysis of the mole fractions of benzene and toluene at two sampling sites in the city of Cape Town gave an indication of the probable anthropogenic sources of the air masses sampled at these sites. We propose that a traffic source dominated at the Foreshore site, while industrial processes dominated at the Potsdam site. The analysis of wind rose plots of benzene and toluene and the elevated mole fractions observed at the remote "clean air" sampling site, Cape Point, suggest that polluted air from Cape Town is the major source of the benzene and toluene mole fractions observed at Cape Point. Hydroxyl (OH) radical concentrations were estimated for Cape Town from the difference in T/B ([toluene]/[benzene]) ratios between Cape Town and Cape Point. The Cape Town OH estimations displayed a mean of (7.2 ± 3.5) × 106 molecules cm^{-3} at the Foreshore site and (9.1 ± 4.4) × 106 molecules cm^{-3} at the Potsdam site, without consideration of dilution reducing to (5.4 ± 3.4) × 106 molecules cm^{-3} for the Foreshore site and (7.4 ± 4.6) × 106 molecules cm^{-3} for the Potsdam site for the period of July-November 2017 when dilution was considered. The estimated Cape Town OH concentrations are on the high side but consistent with the results from other urban studies and may suggest a role for OH recycling following biogenic emissions between Cape Town and Cape Point.

Macdonald, M. L., J. L. Wadham, D. Young, C. R. Lunder, O. Hermansen, G. Lamarche-Gagnon, and S. O'Doherty (2020). "Consumption of CH_3Cl, CH_3Br, and CH_3I and Emission of $CHCl_3$, $CHBr_3$, and CH_2Br_2 from the Forefield of a Retreating Arctic Glacier". In: *Atmospheric Chemistry and Physics* 20.12, pp. 7243–7258. ISSN: 1680-7324. DOI: 10.5194/acp-20-7243-2020.

The Arctic is one of the most rapidly warming regions of the Earth, with predicted temperature increases of 5–7 °C and the accompanying extensive retreat of Arctic glacial systems by 2100. Retreating glaciers will reveal new land surfaces for microbial colonisation, ultimately succeeding to tundra over decades to centuries. An unexplored dimension to these changes is the impact upon the emission and consumption of halogenated organic compounds (halocarbons). Halocarbons are involved in several important atmospheric processes, including ozone destruction, and despite considerable research, uncertainties remain in the natural cycles of some of these compounds. Using flux chambers, we measured halocarbon fluxes across the glacier forefield (the area between the present-day

position of a glacier's ice-front and that at the last glacial maximum) of a high-Arctic glacier in Svalbard, spanning recently exposed sediments (<10 years) to approximately 1950-year-old tundra. Forefield land surfaces were found to consume methyl chloride (CH_3Cl) and methyl bromide (CH_3Br), with both consumption and emission of methyl iodide (CH_3I) observed. Bromoform ($CHBr_3$) and dibromomethane (CH_2Br_2) have rarely been measured from terrestrial sources but were here found to be emitted across the forefield. Novel measurements conducted on terrestrial cyanobacterial mats covering relatively young surfaces showed similar measured fluxes to the oldest, vegetated tundra sites for CH_3Cl, CH_3Br, and CH_3I (which were consumed) and for $CHCl_3$ and $CHBr_3$ (which were emitted). Consumption rates of CH_3Cl and CH_3Br and emission rates of $CHCl_3$ from tundra and cyanobacterial mat sites were within the ranges reported from older and more established Arctic tundra elsewhere. Rough calculations showed total emissions and consumptions of these gases across the Arctic were small relative to other sources and sinks due to the small surface area represented by glacier forefields. We have demonstrated that glacier forefields can consume and emit halocarbons despite their young age and low soil development, particularly when cyanobacterial mats are present.

Michalopoulou, E., D. E. Shallcross, E. Atkins, A. Tierney, N. C. Norman, C. Preist, S. O'Doherty, R. Saunders, A. Birkett, C. Willmore, and I. Ninos (2019). "The End of Simple Problems: Repositioning Chemistry in Higher Education and Society Using a Systems Thinking Approach and the United Nations' Sustainable Development Goals as a Framework". In: *Journal of Chemical Education* 96.12, pp. 2825–2835. ISSN: 0021-9584, 1938-1328. DOI: 10.1021/acs.jchemed.9b00270.

The purpose of this paper is to discuss ways that a chemistry course could reposition itself by adopting interdisciplinary approaches based on systems thinking and the Sustainable Development Goals (SDGs) as overarching frameworks, to give an overview of several challenges that chemistry in higher education is facing, and to discuss how those can be addressed as a result of this repositioning. We will be discussing the need for a new type of scientist, one who has a deep understanding of their own discipline but also an overview of the links with other disciplines and is equipped with skills that will help them contribute to the solutions of a very complex system: the human–environment interaction system. Chemists should be part of what is described by earth systems' science as "the new social contract" between science and society. Finally, we will explore how this can be reflected in the curricula of higher education, and we will present a University of Bristol educational initiative, Bristol Futures, that attempts to address this.

Pugsley, K. L., T. D. J. Knowles, and S. O'Doherty (2018). "Novel Method of Extraction for Radiocarbon Measurements of Atmospheric Carbon Dioxide". In: *Radiocarbon* 61.6, pp. 1867–1877. ISSN: 0033-8222, 1945-5755. DOI: 10.1017/RDC.2019.142.

In this paper, we present the first data from an alternative extraction method for atmospheric $^{14}CO_2$ analysis, based on the direct trapping of whole air samples onto a molecular sieve zeolite (13X) trap, incorporated into a commercially available automated graphitization system. Results are presented for both inter-laboratory comparison samples and an in-house reference standard. The in-house reference was used to calculate the standard

deviation of measurements (2.0‰). This newly developed method will facilitate faster sample processing and therefore lower cost per analysis, critical for scaling up such studies.

Ramonet, M., P. Ciais, F. Apadula, J. Bartyzel, A. Bastos, P. Bergamaschi, P. E. Blanc, D. Brunner, L. Caracciolo di Torchiarolo, F. Calzolari, H. Chen, L. Chmura, A. Colomb, S. Conil, P. Cristofanelli, E. Cuevas, R. Curcoll, M. Delmotte, A. di Sarra, L. Emmenegger, G. Forster, A. Frumau, C. Gerbig, F. Gheusi, S. Hammer, L. Haszpra, J. Hatakka, L. Hazan, M. Heliasz, S. Henne, A. Hensen, O. Hermansen, P. Keronen, R. Kivi, K. Komínková, D. Kubistin, O. Laurent, T. Laurila, J. V. Lavric, I. Lehner, K. E. J. Lehtinen, A. Leskinen, M. Leuenberger, I. Levin, M. Lindauer, M. Lopez, C. L. Myhre, I. Mammarella, G. Manca, A. Manning, M. V. Marek, P. Marklund, D. Martin, F. Meinhardt, N. Mihalopoulos, M. Mölder, J. A. Morgui, J. Necki, S. O'Doherty, C. O'Dowd, M. Ottosson, C. Philippon, S. Piacentino, J. M. Pichon, C. Plass-Duelmer, A. Resovsky, L. Rivier, X. Rodó, M. K. Sha, H. A. Scheeren, D. Sferlazzo, T. G. Spain, K. M. Stanley, M. Steinbacher, P. Trisolino, A. Vermeulen, G. Vítková, D. Weyrauch, I. Xueref-Remy, K. Yala, and C. Yver Kwok (2020). "The Fingerprint of the Summer 2018 Drought in Europe on Ground-Based Atmospheric CO $_2$ Measurements". In: *Philosophical Transactions of the Royal Society B: Biological Sciences* 375.1810, p. 20190513. ISSN: 0962-8436, 1471-2970. DOI: 10.1098/rstb.2019.0513.

During the summer of 2018, a widespread drought developed over Northern and Central Europe. The increase in temperature and the reduction of soil moisture have influenced carbon dioxide (CO_2) exchange between the atmosphere and terrestrial ecosystems in various ways, such as a reduction of photosynthesis, changes in ecosystem respiration, or allowing more frequent fires. In this study, we characterize the resulting perturbation of the atmospheric CO_2 seasonal cycles. 2018 has a good coverage of European regions affected by drought, allowing the investigation of how ecosystem flux anomalies impacted spatial CO_2 gradients between stations. This density of stations is unprecedented compared to previous drought events in 2003 and 2015, particularly thanks to the deployment of the Integrated Carbon Observation System (ICOS) network of atmospheric greenhouse gas monitoring stations in recent years. Seasonal CO_2 cycles from 48 European stations were available for 2017 and 2018. Earlier data were retrieved for comparison from international databases or national networks. Here, we show that the usual summer minimum in CO_2 due to the surface carbon uptake was reduced by 1.4 ppm in 2018 for the 10 stations located in the area most affected by the temperature anomaly, mostly in Northern Europe. Notwithstanding, the CO_2 transition phases before and after July were slower in 2018 compared to 2017, suggesting an extension of the growing season, with either continued CO_2 uptake by photosynthesis and/or a reduction in respiration driven by the depletion of substrate for respiration inherited from the previous months due to the drought. For stations with sufficiently long time series, the CO_2 anomaly observed in 2018 was compared to previous European droughts in 2003 and 2015. Considering the areas most affected by the temperature anomalies, we found a higher CO_2 anomaly in 2003 (+3 ppm averaged over 4 sites), and a smaller anomaly in 2015 (+1 ppm averaged over 11 sites) compared to 2018.

Saunois, M., A. R. Stavert, B. Poulter, P. Bousquet, J. G. Canadell, R. B. Jackson, P. A. Raymond, E. J. Dlugokencky, S. Houweling, P. K. Patra, P. Ciais, V. K. Arora, D. Bastviken, P. Bergamaschi, D. R. Blake, G. Brailsford, L. Bruhwiler, K. M. Carlson, M. Carrol, S. Castaldi, N. Chandra, C. Crevoisier, P. M. Crill, K. Covey, C. L. Curry, G. Etiope, C. Frankenberg, N. Gedney, M. I. Hegglin, L. Höglund-Isaksson, G. Hugelius, M. Ishizawa, A. Ito, G. Janssens-Maenhout, K. M. Jensen, F. Joos, T. Kleinen, P. B. Krummel, R. L. Langenfelds, G. G. Laruelle, L. Liu, T. Machida, S. Maksyutov, K. C. McDonald, J. McNorton, P. A. Miller, J. R. Melton, I. Morino, J. Müller, F. Murguia-Flores, V. Naik, Y. Niwa, S. Noce, S. O'Doherty, R. J. Parker, C. Peng, S. Peng, G. P. Peters, C. Prigent, R. Prinn, M. Ramonet, P. Regnier, W. J. Riley, J. A. Rosentreter, A. Segers, I. J. Simpson, H. Shi, S. J. Smith, L. P. Steele, B. F. Thornton, H. Tian, Y. Tohjima, F. N. Tubiello, A. Tsuruta, N. Viovy, A. Voulgarakis, T. S. Weber, M. van Weele, G. R. van der Werf, R. F. Weiss, D. Worthy, D. Wunch, Y. Yin, Y. Yoshida, W. Zhang, Z. Zhang, Y. Zhao, B. Zheng, Q. Zhu, Q. Zhu, and Q. Zhuang (2020). "The Global Methane Budget 2000–2017". In: *Earth System Science Data* 12.3, pp. 1561–1623. ISSN: 1866-3516. DOI: 10.5194/essd-12-1561-2020.

Understanding and quantifying the global methane (CH_4) budget is important for assessing realistic pathways to mitigate climate change. Atmospheric emissions and concentrations of CH_4 continue to increase, making CH_4 the second most important human-influenced greenhouse gas in terms of climate forcing, after carbon dioxide (CO_2). The relative importance of CH_4 compared to CO_2 depends on its shorter atmospheric lifetime, stronger warming potential, and variations in atmospheric growth rate over the past decade, the causes of which are still debated. Two major challenges in reducing uncertainties in the atmospheric growth rate arise from the variety of geographically overlapping CH_4 sources and from the destruction of CH_4 by short-lived hydroxyl radicals (OH). To address these challenges, we have established a consortium of multidisciplinary scientists under the umbrella of the Global Carbon Project to synthesize and stimulate new research aimed at improving and regularly updating the global methane budget. Following Saunois et al. (2016), we present here the second version of the living review paper dedicated to the decadal methane budget, integrating results of top-down studies (atmospheric observations within an atmospheric inverse-modelling framework) and bottom-up estimates (including process-based models for estimating land surface emissions and atmospheric chemistry, inventories of anthropogenic emissions, and data-driven extrapolations). For the 2008–2017 decade, global methane emissions are estimated by atmospheric inversions (a top-down approach) to be 576 Tg CH_4 yr^{-1} (range 550–594, corresponding to the minimum and maximum estimates of the model ensemble). Of this total, 359 Tg CH_4 yr^{-1} or ∼60 % is attributed to anthropogenic sources, that is emissions caused by direct human activity (i.e. anthropogenic emissions; range 336–376 Tg CH_4 yr^{-1} or 50 %–65 %). The mean annual total emission for the new decade (2008–2017) is 29 Tg CH_4 yr^{-1} larger than our estimate for the previous decade (2000–2009), and 24 Tg CH_4 yr^{-1} larger than the one reported in the previous budget for 2003–2012 (Saunois et al., 2016). Since 2012, global CH_4 emissions have been tracking the warmest scenarios assessed by the Intergovernmental Panel on Climate Change. Bottom-up methods suggest almost 30 % larger global emissions (737 Tg CH_4 yr^{-1}, range 594–881) than

top-down inversion methods. Indeed, bottom-up estimates for natural sources such as natural wetlands, other inland water systems, and geological sources are higher than top-down estimates. The atmospheric constraints on the top-down budget suggest that at least some of these bottom-up emissions are overestimated. The latitudinal distribution of atmospheric observation-based emissions indicates a predominance of tropical emissions ($\sim 65\,\%$ of the global budget, $< 30°$ N) compared to mid-latitudes ($\sim 30\,\%$, 30–60° N) and high northern latitudes ($\sim 4\,\%$, 60–90° N). The most important source of uncertainty in the methane budget is attributable to natural emissions, especially those from wetlands and other inland waters. Some of our global source estimates are smaller than those in previously published budgets (Saunois et al., 2016; Kirschke et al., 2013). In particular wetland emissions are about $35\,\mathrm{Tg\,CH_4\,yr^{-1}}$ lower due to improved partition wetlands and other inland waters. Emissions from geological sources and wild animals are also found to be smaller by $7\,\mathrm{Tg\,CH_4\,yr^{-1}}$ by $8\,\mathrm{Tg\,CH_4\,yr^{-1}}$, respectively. However, the overall discrepancy between bottom-up and top-down estimates has been reduced by only 5 % compared to Saunois et al. (2016), due to a higher estimate of emissions from inland waters, highlighting the need for more detailed research on emissions factors. Priorities for improving the methane budget include (i) a global, high-resolution map of water-saturated soils and inundated areas emitting methane based on a robust classification of different types of emitting habitats; (ii) further development of process-based models for inland-water emissions; (iii) intensification of methane observations at local scales (e.g., FLUXNET-CH_4 measurements) and urban-scale monitoring to constrain bottom-up land surface models, and at regional scales (surface networks and satellites) to constrain atmospheric inversions; (iv) improvements of transport models and the representation of photochemical sinks in top-down inversions; and (v) development of a 3D variational inversion system using isotopic and/or co-emitted species such as ethane to improve source partitioning.

Say, D., B. Kuyper, L. Western, M. A. H. Khan, T. Lesch, C. Labuschagne, D. Martin, D. Young, A. J. Manning, S. O'Doherty, M. Rigby, P. B. Krummel, M. T. Davies-Coleman, A. L. Ganesan, and D. E. Shallcross (2020). "Emissions and Marine Boundary Layer Concentrations of Unregulated Chlorocarbons Measured at Cape Point, South Africa". In: *Environmental Science & Technology* 54.17, pp. 10514–10523. ISSN: 0013-936X, 1520-5851. DOI: 10.1021/acs.est.0c02057.

Unregulated chlorocarbons, here defined as dichloromethane (CH_2Cl_2), perchloroethene (C_2Cl_4), chloroform ($CHCl_3$), and methyl chloride (CH_3Cl), are gases not regulated by the Montreal Protocol. While CH_3Cl is the largest contributor of atmospheric chlorine, recent studies have shown that growth in emissions of the less abundant chlorocarbons could pose a significant threat to the recovery of the ozone layer. Despite this, there remain many regions for which no atmospheric monitoring exists, leaving gaps in our understanding of global emissions. Here, we report on a new time series of chlorocarbon measurements from Cape Point, South Africa for 2017, which represent the first published high-frequency measurements of these gases from Africa. For CH_2Cl_2 and C_2Cl_4, the majority of mole fraction enhancements were observed from the north, consistent with anthropogenically modified air from Cape Town, while for $CHCl_3$ and CH_3Cl, we found evidence for both oceanic and terrestrial sources. Using an inverse method, we estimated emissions for south-western South Africa (SWSA). For each chlorocarbon, SWSA accounted for less than 1% of global emissions. For CH_2Cl_2 and C_2Cl_4, we extrapolated

using population statistics and found South African emissions of 8.9 (7.4-10.4) Gg yr^{-1} and 0.80 (0.64-1.04) Gg yr^{-1}, respectively.

Simmonds, P. G., M. Rigby, A. J. Manning, S. Park, K. M. Stanley, A. McCulloch, S. Henne, F. Graziosi, M. Maione, J. Arduini, S. Reimann, M. K. Vollmer, J. Mühle, S. O'Doherty, D. Young, P. B. Krummel, P. J. Fraser, R. F. Weiss, P. K. Salameh, C. M. Harth, M.-K. Park, H. Park, T. Arnold, C. Rennick, L. P. Steele, B. Mitrevski, R. H. J. Wang, and R. G. Prinn (2020). "The Increasing Atmospheric Burden of the Greenhouse Gas Sulfur Hexafluoride (SF_6)". In: *Atmospheric Chemistry and Physics* 20.12, pp. 7271–7290. ISSN: 1680-7324. DOI: 10.5194/acp-20-7271-2020.

We report a 40-year history of SF_6 atmospheric mole fractions measured at the Advanced Global Atmospheric Gases Experiment (AGAGE) monitoring sites, combined with archived air samples, to determine emission estimates from 1978 to 2018. Previously we reported a global emission rate of $7.3\pm0.6\,Gg\,yr^{-1}$ in 2008 and over the past decade emissions have continued to increase by about 24 % to $9.04\pm0.35\,Gg\,yr^{-1}$ in 2018. We show that changing patterns in SF_6 consumption from developed (Kyoto Protocol Annex-1) to developing countries (non-Annex-1) and the rapid global expansion of the electric power industry, mainly in Asia, have increased the demand for SF_6-insulated switchgear, circuit breakers, and transformers. The large bank of SF_6 sequestered in this electrical equipment provides a substantial source of emissions from maintenance, replacement, and continuous leakage. Other emissive sources of SF_6 occur from the magnesium, aluminium, and electronics industries as well as more minor industrial applications. More recently, reported emissions, including those from electrical equipment and metal industries, primarily in the Annex-1 countries, have declined steadily through substitution of alternative blanketing gases and technological improvements in less emissive equipment and more efficient industrial practices. Nevertheless, there are still demands for SF_6 in Annex-1 countries due to economic growth, as well as continuing emissions from older equipment and additional emissions from newly installed SF_6-insulated electrical equipment, although at low emission rates. In addition, in the non-Annex-1 countries, SF_6 emissions have increased due to an expansion in the growth of the electrical power, metal, and electronics industries to support their continuing development. There is an annual difference of 2.5–5 $Gg\,yr^{-1}$ (1990–2018) between our modelled top-down emissions and the UNFCCC-reported bottom-up emissions (United Nations Framework Convention on Climate Change), which we attempt to reconcile through analysis of the potential contribution of emissions from the various industrial applications which use SF_6. We also investigate regional emissions in East Asia (China, S. Korea) and western Europe and their respective contributions to the global atmospheric SF_6 inventory. On an average annual basis, our estimated emissions from the whole of China are approximately 10 times greater than emissions from western Europe. In 2018, our modelled Chinese and western European emissions accounted for ∼36 % and 3.1 %, respectively, of our global SF_6 emissions estimate.

Stanley, K. M., D. Say, J. Mühle, C. M. Harth, P. B. Krummel, D. Young, S. J. O'Doherty, P. K. Salameh, P. G. Simmonds, R. F. Weiss, R. G. Prinn, P. J. Fraser, and M. Rigby (2020).

"Increase in Global Emissions of HFC-23 despite near-Total Expected Reductions". In: *Nature Communications* 11.1. ISSN: 2041-1723. DOI: 10.1038/s41467-019-13899-4.

Under the Kigali Amendment to the Montreal Protocol, new controls are being implemented to reduce emissions of HFC-23 (CHF3), a by-product during the manufacture of HCFC-22 ($CHClF_2$). Starting in 2015, China and India, who dominate global HCFC-22 production (75% in 2017), set out ambitious programs to reduce HFC-23 emissions. Here, we estimate that these measures should have seen global emissions drop by 87% between 2014 and 2017. Instead, atmospheric observations show that emissions have increased and in 2018 were higher than at any point in history (15.9 ± 0:9 Gg yr^{-1}). Given the magnitude of the discrepancy between expected and observation-inferred emissions, it is likely that the reported reductions have not fully materialized or there may be substantial unreported production of HCFC-22, resulting in unaccounted-for HFC-23 by-product emissions. The difference between reported and observation-inferred estimates suggests that an additional ˜309 Tg CO_2-equivalent emissions were added to the atmosphere between 2015 and 2017.

Wenger, A., K. Pugsley, S. O'Doherty, M. Rigby, A. J. Manning, M. F. Lunt, and E. D. White (2019). "Atmospheric Radiocarbon Measurements to Quantify CO₂ Emissions in the UK from 2014 to 2015". In: *Atmospheric Chemistry and Physics* 19.22, pp. 14057–14070. ISSN: 1680-7324. DOI: 10.5194/acp-19-14057-2019.

Abstract. We present $\Delta^{14}CO_2$ observations and related greenhouse gas measurements at a background site in Ireland (Mace Head, MHD) and a tall tower site in the east of the UK (Tacolneston, TAC) that is more strongly influenced by fossil fuel sources. These observations have been used to calculate the contribution of fossil fuel sources to the atmospheric CO_2 mole fractions; this can be done, as emissions from fossil fuels do not contain $^{14}CO_2$ and cause a depletion in the observed $\Delta^{14}CO_2$value. The observations are compared to simulated values. Two corrections need to be applied to radiocarbon-derived fossil fuel CO_2($ffCO_2$): one for pure $^{14}CO_2$ emissions from nuclear industry sites and one for a disequilibrium in the isotopic signature of older biospheric emissions (heterotrophic respiration) and CO_2 in the atmosphere. Measurements at both sites were found to only be marginally affected by $^{14}CO_2$ emissions from nuclear sites. Over the study period of 2014–2015, the biospheric correction and the correction for nuclear $^{14}CO_2$ emissions were similar at 0.34 and 0.25 ppm $ffCO_2$ equivalent, respectively. The observed $ffCO_2$ at the TAC tall tower site was not significantly different from simulated values based on the EDGAR 2010 bottom-up inventory. We explored the use of high-frequency CO observations as a tracer of $ffCO_2$ by deriving a constant ratio of CO enhancements to $ffCO_2$ ratio for the mix of UK fossil fuel sources. This ratio was found to be 5.7 ppb ppm^{-1}, close to the value predicted using inventories and the atmospheric model of 5.1 ppb ppm^{-1}. The TAC site, in the east of the UK, was strategically chosen to be some distance from pollution sources so as to allow for the observation of well-integrated air masses. However, this distance from pollution sources and the large measurement uncertainty in $^{14}CO_2$ lead to a large overall uncertainty in the $ffCO_2$, being around 1.8 ppm compared to typical enhancements of 2 ppm.

Western, L. M., Z. Sha, M. Rigby, A. L. Ganesan, A. J. Manning, K. M. Stanley, S. J. O'Doherty,

D. Young, and J. Rougier (2020). "Bayesian Spatio-Temporal Inference of Trace Gas Emissions Using an Integrated Nested Laplacian Approximation and Gaussian Markov Random Fields". In: *Geoscientific Model Development* 13.4, pp. 2095–2107. ISSN: 1991-9603. DOI: 10.5194/gmd-13-2095-2020.

We present a method to infer spatially and spatio-temporally correlated emissions of greenhouse gases from atmospheric measurements and a chemical transport model. The method allows fast computation of spatial emissions using a hierarchical Bayesian framework as an alternative to Markov chain Monte Carlo algorithms. The spatial emissions follow a Gaussian process with a Matérn correlation structure which can be represented by a Gaussian Markov random field through a stochastic partial differential equation approach. The inference is based on an integrated nested Laplacian approximation (INLA) for hierarchical models with Gaussian latent fields. Combining an autoregressive temporal correlation and the Matérn field provides a full spatio-temporal correlation structure. We first demonstrate the method on a synthetic data example and follow this using a well-studied test case of inferring UK methane emissions from tall tower measurements of atmospheric mole fraction. Results from these two test cases show that this method can accurately estimate regional greenhouse gas emissions, accounting for spatio-temporal uncertainties that have traditionally been neglected in atmospheric inverse modelling.

6 Bibliography

Arnold, T., A. J. Manning, J. Kim, S. Li, H. Webster, D. Thomson, J. Mühle, R. F. Weiss, S. Park, and S. O'Doherty (2018). "Inverse Modelling of CF_4 and NF_3 Emissions in East Asia". In: *Atmospheric Chemistry and Physics* 18.18, pp. 13305–13320. ISSN: 1680-7324. DOI: 10.5194/acp-18-13305-2018 (cit. on p. 17).

Ciais, P., C. Sabine, G. Bala, L. Bopp, V. Brovkin, J. Canadell, A. Chhabra, R. DeFries, J. Galloway, M. Heimann, C. Jones, C. Le Quéré, R. B. Myneni, S. Piao, and P. Thornton (2013). "Carbon and Other Biogeochemical Cycles". In: *Climate Change 2013 - The Physical Science Basis*. Cambridge: Cambridge University Press, pp. 465–570. ISBN: 978-1-107-41532-4. DOI: 10.1017/CBO9781107415324.015 (cit. on pp. 22, 27).

Crutzen, P. J. (1970). "The Influence of Nitrogen Oxides on the Atmospheric Ozone Content". In: *Quarterly Journal of the Royal Meteorological Society* 96.408, pp. 320–325. ISSN: 00359009, 1477870X. DOI: 10.1002/qj.49709640815 (cit. on p. 27).

Cunnold, D. M., L. P. Steele, P. J. Fraser, P. G. Simmonds, R. G. Prinn, R. F. Weiss, L. W. Porter, S. O'Doherty, R. L. Langenfelds, P. B. Krummel, H. J. Wang, L. Emmons, X. X. Tie, and

E. J. Dlugokencky (2002). “In Situ Measurements of Atmospheric Methane at GAGE/AGAGE Sites during 1985–2000 and Resulting Source Inferences”. In: *Journal of Geophysical Research* 107.D14. ISSN: 0148-0227. DOI: 10.1029/2001JD001226 (cit. on p. 22).

Dlugokencky, E. J., L. Bruhwiler, J. W. C. White, L. K. Emmons, P. C. Novelli, S. A. Montzka, K. A. Masarie, P. M. Lang, A. M. Crotwell, J. B. Miller, and L. V. Gatti (2009). “Observational Constraints on Recent Increases in the Atmospheric CH_4 Burden”. In: *Geophysical Research Letters* 36.18. ISSN: 0094-8276. DOI: 10.1029/2009GL039780 (cit. on p. 22).

Dlugokencky, E. J., S. Houweling, L. Bruhwiler, K. A. Masarie, P. M. Lang, J. B. Miller, and P. P. Tans (2003). “Atmospheric Methane Levels off: Temporary Pause or a New Steady-State?” In: *Geophysical Research Letters* 30.19, p. 1992. ISSN: 0094-8276. DOI: 10.1029/2003GL018126 (cit. on p. 22).

Frankenberg, C., I. Aben, P. Bergamaschi, E. J. Dlugokencky, R. van Hees, S. Houweling, P. van der Meer, R. Snel, and P. Tol (2011). “Global Column-Averaged Methane Mixing Ratios from 2003 to 2009 as Derived from SCIAMACHY: Trends and Variability”. In: *Journal of Geophysical Research* 116.D4, p. D04302. ISSN: 0148-0227. DOI: 10.1029/2010JD014849 (cit. on p. 22).

Ganesan, A. L., S. Schwietzke, B. Poulter, T. Arnold, X. Lan, M. Rigby, F. R. Vogel, G. R. Werf, G. Janssens-Maenhout, H. Boesch, S. Pandey, A. J. Manning, R. B. Jackson, E. G. Nisbet, and M. R. Manning (2019). “Advancing Scientific Understanding of the Global Methane Budget in Support of the Paris Agreement”. In: *Global Biogeochemical Cycles* 33.12, pp. 1475–1512. ISSN: 0886-6236, 1944-9224. DOI: 10.1029/2018GB006065 (cit. on p. 22).

Griffis, T. J., X. Lee, J. M. Baker, M. P. Russelle, X. Zhang, R. Venterea, and D. B. Millet (2013). “Reconciling the Differences between Top-down and Bottom-up Estimates of Nitrous Oxide Emissions for the U.S. Corn Belt”. In: *Global Biogeochemical Cycles* 27.3, pp. 746–754. ISSN: 08866236. DOI: 10.1002/gbc.20066 (cit. on p. 27).

Hmiel, B., V. V. Petrenko, M. N. Dyonisius, C. Buizert, A. M. Smith, P. F. Place, C. Harth, R. Beaudette, Q. Hua, B. Yang, I. Vimont, S. E. Michel, J. P. Severinghaus, D. Etheridge, T. Bromley, J. Schmitt, X. Faïn, R. F. Weiss, and E. Dlugokencky (2020). “Preindustrial $^{14}CH_4$ Indicates Greater Anthropogenic Fossil CH_4 Emissions”. In: *Nature* 578.7795, pp. 409–412. ISSN: 0028-0836, 1476-4687. DOI: 10.1038/s41586-020-1991-8 (cit. on p. 22).

Manning, A. J., S. O'Doherty, A. R. Jones, P. G. Simmonds, and R. G. Derwent (2011). "Estimating UK Methane and Nitrous Oxide Emissions from 1990 to 2007 Using an Inversion Modeling Approach". In: *Journal of Geophysical Research: Atmospheres* 116.D2, p. D02305. ISSN: 2156-2202. DOI: 10.1029/2010JD014763 (cit. on p. 17).

McNorton, J., C. Wilson, M. Gloor, R. J. Parker, H. Boesch, W. Feng, R. Hossaini, and M. P. Chipperfield (2018). "Attribution of Recent Increases in Atmospheric Methane through 3-D Inverse Modelling". In: *Atmospheric Chemistry and Physics* 18.24, pp. 18149–18168. ISSN: 1680-7324. DOI: 10.5194/acp-18-18149-2018 (cit. on p. 22).

Monteil, G., S. Houweling, E. J. Dlugockenky, G. Maenhout, B. H. Vaughn, J. W. C. White, and T. Rockmann (2011). "Interpreting Methane Variations in the Past Two Decades Using Measurements of CH_4 Mixing Ratio and Isotopic Composition". In: *Atmospheric Chemistry and Physics* 11.17, pp. 9141–9153. ISSN: 1680-7324. DOI: 10.5194/acp-11-9141-2011 (cit. on p. 22).

Myhre, G., D. T. Shindell, F.-M. Bréon, W. Collins, J. Fuglestvedt, J. Huang, D. Koch, J.-F. Lamarque, D. Lee, B. Mendoza, T. Nakajima, A. Robock, G. Stephens, T. Takemura, and H. Zhang (2013). "Anthropogenic and Natural Radiative Forcing". In: *Climate Change 2013 - The Physical Science Basis. Contribution of Working Group I to the Fifth Assessment Report of the Intergovernmental Panel on Climate Change*. Cambridge: Cambridge University Press, pp. 659–740. ISBN: 978-1-107-41532-4. DOI: 10.1017/CBO9781107415324.018 (cit. on pp. 21, 22).

Nisbet, E. G., E. J. Dlugokencky, M. R. Manning, D. Lowry, R. E. Fisher, J. L. France, S. E. Michel, J. B. Miller, J. W. C. White, B. Vaughn, P. Bousquet, J. A. Pyle, N. J. Warwick, M. Cain, R. Brownlow, G. Zazzeri, M. Lanoisellé, A. C. Manning, E. Gloor, D. E. J. Worthy, E.-G. Brunke, C. Labuschagne, E. W. Wolff, and A. L. Ganesan (2016). "Rising Atmospheric Methane: 2007-2014 Growth and Isotopic Shift". In: *Global Biogeochemical Cycles* 30.9, pp. 1356–1370. ISSN: 08866236. DOI: 10.1002/2016GB005406 (cit. on p. 22).

Nisbet, E. G., R. E. Fisher, D. Lowry, J. L. France, G. Allen, S. Bakkaloglu, T. J. Broderick, M. Cain, M. Coleman, J. Fernandez, G. Forster, P. T. Griffiths, C. P. Iverach, B. F. J. Kelly, M. R. Manning, P. B. R. Nisbet-Jones, J. A. Pyle, A. Townsend-Small, A. al-Shalaan, N. Warwick, and G. Zazzeri (2020). "Methane Mitigation: Methods to Reduce Emissions, on the Path to the Paris Agreement". In: *Reviews of Geophysics* 58.1. ISSN: 8755-1209, 1944-9208. DOI: 10.1029/2019RG000675 (cit. on p. 22).

Nisbet, E. G., M. R. Manning, E. J. Dlugokencky, R. E. Fisher, D. Lowry, S. E. Michel, C. L. Myhre, S. M. Platt, G. Allen, P. Bousquet, R. Brownlow, M. Cain, J. L. France, O. Hermansen, R. Hossaini, A. E. Jones, I. Levin, A. C. Manning, G. Myhre, J. A. Pyle, B. H. Vaughn, N. J. Warwick, and J. W. C. White (2019). "Very Strong Atmospheric Methane Growth in the 4 Years 2014–2017: Implications for the Paris Agreement". In: *Global Biogeochemical Cycles* 33.3, pp. 318–342. ISSN: 0886-6236, 1944-9224. DOI: 10.1029/2018GB006009 (cit. on p. 22).

Prather, M. J., J. Hsu, N. M. DeLuca, C. H. Jackman, L. D. Oman, A. R. Douglass, E. L. Fleming, S. E. Strahan, S. D. Steenrod, O. Amund Søvde, I. S. A. Isaksen, L. Froidevaux, and B. Funke (2015). "Measuring and Modeling the Lifetime of Nitrous Oxide Including Its Variability". In: *Journal of Geophysical Research: Atmospheres*, 2015JD023267. ISSN: 2169-8996. DOI: 10.1002/2015JD023267 (cit. on p. 27).

Ravishankara, A. R., J. S. Daniel, and R. W. Portmann (2009). "Nitrous Oxide (N_2O): The Dominant Ozone-Depleting Substance Emitted in the 21st Century". In: *Science* 326.5949, pp. 123–125. ISSN: 0036-8075, 1095-9203. DOI: 10.1126/science.1176985 (cit. on p. 27).

Rigby, M., R. G. Prinn, P. J. Fraser, P. G. Simmonds, R. L. Langenfelds, J. Huang, D. M. Cunnold, L. P. Steele, P. B. Krummel, R. F. Weiss, S. O'Doherty, P. K. Salameh, H. J. Wang, C. M. Harth, J. Mühle, and L. W. Porter (2008). "Renewed Growth of Atmospheric Methane". In: *Geophysical Research Letters* 35.22. ISSN: 0094-8276. DOI: 10.1029/2008GL036037 (cit. on p. 22).

Rigby, M., S. A. Montzka, R. G. Prinn, J. W. C. White, D. Young, S. O'Doherty, M. F. Lunt, A. L. Ganesan, A. J. Manning, P. G. Simmonds, P. K. Salameh, C. M. Harth, J. Mühle, R. F. Weiss, P. J. Fraser, L. P. Steele, P. B. Krummel, A. McCulloch, and S. Park (2017). "Role of Atmospheric Oxidation in Recent Methane Growth". In: *Proceedings of the National Academy of Sciences*, p. 201616426. ISSN: 0027-8424. DOI: 10.1073/PNAS.1616426114 (cit. on p. 22).

Saunois, M., A. R. Stavert, B. Poulter, P. Bousquet, J. G. Canadell, R. B. Jackson, P. A. Raymond, E. J. Dlugokencky, S. Houweling, P. K. Patra, P. Ciais, V. K. Arora, D. Bastviken, P. Bergamaschi, D. R. Blake, G. Brailsford, L. Bruhwiler, K. M. Carlson, M. Carrol, S. Castaldi, N. Chandra, C. Crevoisier, P. M. Crill, K. Covey, C. L. Curry, G. Etiope, C. Frankenberg, N. Gedney, M. I. Hegglin, L. Höglund-Isaksson, G. Hugelius, M. Ishizawa, A. Ito, G. Janssens-Maenhout, K. M. Jensen, F. Joos, T. Kleinen, P. B. Krummel, R. L. Langenfelds, G. G. Laruelle, L. Liu, T. Machida, S. Maksyutov, K. C. McDonald, J. McNorton, P. A. Miller, J. R. Melton, I. Morino, J. Müller, F. Murguia-Flores, V. Naik, Y. Niwa, S. Noce, S. O'Doherty, R. J. Parker, C. Peng, S. Peng, G. P. Peters, C. Prigent, R. Prinn, M. Ramonet, P. Regnier, W. J. Riley,

J. A. Rosentreter, A. Segers, I. J. Simpson, H. Shi, S. J. Smith, L. P. Steele, B. F. Thornton, H. Tian, Y. Tohjima, F. N. Tubiello, A. Tsuruta, N. Viovy, A. Voulgarakis, T. S. Weber, M. van Weele, G. R. van der Werf, R. F. Weiss, D. Worthy, D. Wunch, Y. Yin, Y. Yoshida, W. Zhang, Z. Zhang, Y. Zhao, B. Zheng, Q. Zhu, Q. Zhu, and Q. Zhuang (2020). "The Global Methane Budget 2000–2017". In: *Earth System Science Data* 12.3, pp. 1561–1623. ISSN: 1866-3516. DOI: 10.5194/essd-12-1561-2020 (cit. on p. 22).

Schaefer, H., S. E. M. Fletcher, C. Veidt, K. R. Lassey, G. W. Brailsford, T. M. Bromley, E. J. Dlugokencky, S. E. Michel, J. B. Miller, I. Levin, D. C. Lowe, R. J. Martin, B. H. Vaughn, and J. W. C. White (2016). "A 21st-Century Shift from Fossil-Fuel to Biogenic Methane Emissions Indicated by $^{13}CH_4$". In: *Science* 352.6281, pp. 80–84. ISSN: 0036-8075, 1095-9203. DOI: 10.1126/science.aad2705 (cit. on p. 22).

Schwietzke, S., O. A. Sherwood, L. M. P. Bruhwiler, J. B. Miller, G. Etiope, E. J. Dlugokencky, S. E. Michel, V. A. Arling, B. H. Vaughn, J. W. C. White, and P. P. Tans (2016). "Upward Revision of Global Fossil Fuel Methane Emissions Based on Isotope Database". In: *Nature* 538.7623, pp. 88–91. ISSN: 0028-0836, 1476-4687. DOI: 10.1038/nature19797 (cit. on p. 22).

Turner, A. J., C. Frankenberg, and E. A. Kort (2019). "Interpreting Contemporary Trends in Atmospheric Methane". In: *Proceedings of the National Academy of Sciences* 116.8, pp. 2805–2813. ISSN: 0027-8424, 1091-6490. DOI: 10.1073/pnas.1814297116 (cit. on p. 22).

Turner, P. A., T. J. Griffis, X. Lee, J. M. Baker, R. T. Venterea, and J. D. Wood (2015). "Indirect Nitrous Oxide Emissions from Streams within the US Corn Belt Scale with Stream Order". In: *Proceedings of the National Academy of Sciences* 112.32, pp. 9839–9843. ISSN: 0027-8424, 1091-6490. DOI: 10.1073/pnas.1503598112 (cit. on p. 27).

WMO (2018). *WMO Greenhouse Gas Bulletin: The State of Greenhouse Gases in the Atmosphere Based on Global Observations through 2017*. Tech. rep. 14. https://library.wmo.int/doc_num.php?explnum_id=5455: World Meteorological Organization, Global Atmosphere Watch (cit. on p. 27).

Worden, J. R., A. A. Bloom, S. Pandey, Z. Jiang, H. M. Worden, T. W. Walker, S. Houweling, and T. Röckmann (2017). "Reduced Biomass Burning Emissions Reconcile Conflicting Estimates of the Post-2006 Atmospheric Methane Budget". In: *Nature Communications* 8.1. ISSN: 2041-1723. DOI: 10.1038/s41467-017-02246-0 (cit. on p. 22).

7 Acknowledgements

- Empa, Switzerland for the use of Jungfraujoch (JFJ) observations
- ISAC-CNR, Italy for the use of Monte Cimone (CMN) observations
- Irish EPA for the use of Carnsore Point (CSP) observations
- TNO, The Netherlands, for the use of the Cabauw (CBW) CH_4 observations.
- University of East Anglia and NERC for the use of CH_4 observations from the Weybourne Atmospheric Observatory (WAO).
- University of Frankfurt, Germany, for the use of Taunus (TOB) observations of HFCs and PFCs.
- AGAGE (NASA) for their support of the global atmospheric GHG and O_3-depleting network.

8 Nomenclature

ACTRIS:	Aerosols, Clouds and Trace gases Research Infrastructure
AGAGE:	Advanced Global Atmospheric Gases Experiment
ANSTO:	Australian Nuclear Science and Technology Organisation
BEIS:	Department of Business, Energy and Industrial Strategy, UK
BSD:	Bilsdale tall tower observatory, North Yorkshire, UK
CBW:	Cabauw tall tower observatory, The Netherlands
CFC:	Chlorofluorocarbon
CMN:	Monte Cimone observatory, Italy
CSP:	Carnsore Point observatory, Ireland
DA:	Devolved Administration of the UK
DARE-UK:	Detection and Attribution of Regional greenhouse gas Emissions in the UK
DECC:	Deriving Emissions related to Climate Change Network
ECMWF:	European Centre for Medium-range Weather Forecasting
EDGAR:	Emission Database for Global Atmospheric Research
ERA-5:	ECMWF Re-Analysis meteorology, version 5
ERA-Interim:	ECMWF Re-Analysis meteorology, Interim version
EU:	European Union
GAGE:	Global Atmospheric Gases Experiment
GAUGE:	Greenhouse gAs UK and Global Emissions
GCMD:	Gas Chromatography Multi-Detector
GCMS:	Gas Chromatography Mass Spectrometry
GHG:	GreenHouse Gas

GHGI:	GreenHouse Gas Inventory
GWP_{100}:	Global Warming Potential over a 100 year time-horizon
HCFC:	Hydrochlorofluorocarbon
HFC:	Hydrofluorocarbon
HFD:	Heathfield tall tower observatory, West Sussex, UK
HUGS	HUb for Greenhouse gas data Science
ICOS:	Integrated Carbon Observation System
InTEM:	Inversion Technique for Emission Modelling
IPCC:	Intergovernmental Panel on Climate Change
JFJ:	Jungfraujoch research station, Switzerland
magl:	Metres above ground level
MHD:	Mace Head research station, Ireland
NAEI:	National Atmospheric Emissions Inventory
NAME:	Numerical Atmospheric dispersion Modelling Environment
NASA:	National Aeronautics and Space Administration
NERC:	Natural Environment Research Council
NH:	Northern Hemisphere
NIR:	National Inventory Report
NOAA:	National Oceanic and Atmospheric Administration
NOAA-ESRL:	NOAA Earth System Research Laboratories
NPL:	National Physical Laboratory
NWEU:	North West Europe (IRL,UK,FRA,BEL,NLD,LUX,DEU)
PFC:	Perfluorocarbon
RGL:	Ridge Hill tall tower observatory, Herefordshire, UK
SH:	Southern Hemisphere
TAC:	Tacolneston tall tower observatory, Norfolk, UK
TOB:	Taunus observatory, Germany
TTA:	Angus tall tower observatory, Scotland, UK
UNFCCC:	United Nations Framework Convention on Climate Change
WAO:	Weybourne Atmospheric Observatory, Norfolk, UK